Biomarkers of Anti-Angiogenic Therapy in Breast Cancer

Thesis submitted by

Shaveta Mehta
St Hugh's College

For the degree of

Doctor of Philosophy

Supervisor: Professor Adrian L. Harris

Abstract

Shaveta Mehta
St Hugh's College
University of Oxford

D.Phil
Hilary Term
April 2013

The hunt for biomarkers for anti-VEGF agent bevacizumab is ongoing since last decade with no success. Identifying robust biomarkers for stratifying patients and for monitoring response is important for the future use of bevacizumab in breast cancer. Dynamic contrast-enhanced magnetic resonance imaging (DCE-MRI) analysis and genome wide gene expression analysis are two promising approaches to understand the molecular mechanisms and search for biomarker of anti-angiogenic therapy.

Firstly, with the retrospective pilot study, a close link between DCE-MRI findings and the molecular mechanisms assisting cancer survival and metastasis was established.

Secondly, the prospective window of opportunity study conducted using single cycle of bevacizumab given before neoadjuvant chemotherapy and by performing detailed pharmacodynamic analyses with DCE-MRI and gene expression before and two weeks after bevacizumab had shown a wide variation in responses to bevacizmab both at genomic and imaging level. A close link between changes in DCE-MRI and the changes in gene expression profile was further established suggesting DCE-MRI has potential to serve as non-invasive biomarkers of antiangiogenic therapy. Tumours with high baseline values of forward transfer constant K^{trans} showed the maximum response as assessed by DCE-MRI after bevacizumab. By performing biopsy after single cycle of bevacizumab, the changes in genes related to immune response, metabolism and cell signalling were observed that gives a useful insight into mechanisms governing response and resistance to bevacizumab. Also the certain gene expression changes observed with post bevacizumab biopsies, such as down regulation of endothelial cell specific molecule-1 (ESM1), cyclin E1 (CCNE1) and up regulation of pyruvate dehydrogenase kinase 1 (PDK1), cyclic GMP-inhibited phosphodiesterase B (PDE3B) could be helpful in decision-making about future therapy with bevacizumab at an early stage. This study has suggested that using bevacizumab in combination with other targeted agents could overcome resistance.

Acknowledgements

First and foremost, my utmost gratitude to Professor Adrian Harris, whose sincerity, patience, guidance and encouragement I will never forget. Professor Harris has been my inspiration as I hurdle all the obstacles in the completion of this research work.

I am highly indebted to Nick Hughes and Francesca Buffa for their indispensable assistance right from early days of protocol development and guiding me through the complicated MRI analyses and bioinformatics analyses.

My thanks and appreciations also go to the clinical and research staff especially research nurses, surgeons, breast care nurses, data managers particularly Marian Taylor and Kulwinder Kaur, for their precious help and strenuous work in the clinical study, and Dr Rosie Adams for support in MRI analyses and carrying out biopsies.

I would like to reserve a special thanks for my collaborators at Mount Vernon Cancer Centre especially Dr Andreas Makris, Sonia Li for enrolling patients at their centre Dr Anwar Padhani and Jane Taylor for providing invaluable guidance in MRI analyses.

All the members of the Harris' laboratory have been extremely helpful. In particular, Helen Sheldon, Simon Wigfield, Alan McIntyre, Elena Favaro, Harriet Gee, Ji-Liang, Russell Leek, and Simon Lord: you all have been great help and pleasure to work with. Thanks to Helen Turley and Adrian Jubb for the immunohistochemistry work.

I thank Roche Ltd and Liz Hamilton in particular, for their financial support and insightful scientific discussions.

Finally, I am grateful to all the patients who participated in this study.

I wishes to express gratitude to my beloved family, my children, parent-in-laws, my brother for their understanding & endless love, and to my friends Rekha and Vishwas Wadekar who were always there to boost me. A special thank to Vipin for his unconditional love, patience and understanding. Thank-you for being there for me, I could have never done it without you.

This thesis is dedicated to my parents who gave me the strength to plod on despite my constitution wanting to give up. They dedicated all their lives to make sure I am successful at every venture of my life.

Table of Contents

List of Figures

List of Tables

List of Abbreviations

3 D	Three-dimensional
5 FU	Fluorouracil
AE	Adverse events
AJCC	American Joint Committee on Cancer
ASR	Age standardised rate
BI-RADS	Breast Imaging-Reporting and Data System Atlas
BOLD	Blood oxygenation level dependent
BV	Bevacizumab
CA	Contrast agent
CHF	Congestive heart failure
CR	Complete response
CRUK	Cancer Research UK
CSC	Cancer stem cell
CVA	Cerebrovascular accident
DAB	2, 3-diaminobenzidine
DCE-MRI	Dynamic contrast enhanced magnetic resonance imaging
DCIS	Ductal carcinoma in situ
DEPC	Diethylpyrocarbonate
DNA	Deoxyribonucleic acid
DW	Diffusion weighted
ECOG	Eastern Cooperative Oncology Group
EDTA	Ethylene diamine tetra acetic acid
EES	Extra-vascular extra-cellular space
ER	Oestrogen receptor
FC	Fold change
FDA	Food and Drug Administration
FDR	False discovery rate
FFPE	Formalin fixed paraffin embedded
FOV	Field of view
G-CSF	Granulocyte colony-stimulating factor
Gd-DTPA	Gadopentetate dimeglumine
HER2	Human epidermal growth factor receptor 2
HR	Hazard ratio
HRT	Hormone replacement therapy
I.V.	Intravascular
IAUGC 60	Initial (60s) area under the gadolinium curve
IHC	Immunohistochemistry
KEGG	Kyoto Encyclopaedia of Genes and Genomes
k_{ep}	Rate constant from EES to plasma
K^{trans}	Transfer constant from plasma to EES
LABC	Locally advanced breast cancer
LCIS	Lobular carcinoma in situ
MBC	Metastatic breast cancer

mL	Milli-litre
µL	Micro-litre
MRI	Magnetic resonance imaging
MVD	Micro vessel density
n	Number
NAC	Neo-adjuvant chemotherapy
NaOH	Sodium hydroxide
NEF	Non-enhancing fraction
NEX	number of excitations
NRES	National Research Ethics Services
NRP	Neuropilin
NYHA	New York Heart Association
ORR	Overall response rate
OS	Overall survival
PANTHER	Protein ANalysis THrough Evolutionary Relationships
pCR	Pathological complete response
PD	Progressive disease
PDGF	Platelet derived growth factor
PDW	Proton density weighted
PFS	Progression free survival
PICR	Paterson Institute for Cancer Research
PK	Pharmacokinetic
PLGF	Placental growth factor
PLVAP	Plasmalemma vesicle associated protein
PR	Progesterone receptor
PR	Partial response
qRT-PCR	Quantitative real-time polymerase chain reaction
RECIST	Response Evaluation Criteria In Solid Tumours
RIN	RNA integrity number
RNA	Ribonucleic acid
ROI	Region of interest
RPS	Relapse free survival
SAM	Significance Analysis for Microarrays
SD	Stable disease
SOP	Standard operating procedure
TE	Echo time
TR	Repetition time
v_e	Fractional volume of EES
VEGF	Vascular endothelial growth factor
VEGFR	Vascular endothelial growth factor receptor
VOI	Volume of interest
WHO	World Health Organisation

CHAPTER ONE

1 Introduction and Objectives

1.1 Breast cancer

Cancer is the one of the leading causes of mortality and morbidity in the world. The age standardised rate (ASR) per 100,000 persons per year is 180.8 and the ASR for mortality is 105.6 from all the cancers (Globocan 2008). In 2008 an estimated 8 million deaths were attributed to cancer. Globally, breast cancer is the second leading cause of cancer death and is the most common cancer affecting women worldwide. In 2008, it was estimated that 1.38 million women worldwide were diagnosed with breast cancer, accounting for around a tenth (10.9%) of all new cancers and nearly a quarter (23%) of all female cancer cases (Globocan 2008).

In the UK, breast cancer is by far the most common female cancer accounting for 31% of all cancer cases in women. The lifetime risk of being diagnosed with breast cancer is 1 in 8 for women in the UK. In the UK, in 2008 almost 47,700 women were diagnosed with breast cancer, which are approximately 130 women a day (Benson and Jatoi 2012).

In the last ten years following the discontinuation of hormone replacement therapy (HRT) there has been a decline in the incidence of breast cancer in females in the developed world (Benson and Jatoi 2012). Although female breast cancer incidence rates in the UK have increased by 3.6% but fortunately, death rates from breast cancer have been decreasing; this decrease is probably the result of earlier detection and improved treatment modalities (Berry, Cronin et al. 2005).

Among presenting patients, 3–6 % already have metastatic disease; a further 50 – 70% of patients with initially localized breast cancer will suffer a systemic relapse. Approximately 75% of the relapses occur within the first 5 years, but can occur up to 30 years later (Levin 2008).

1.2 Breast cancer classifications

1.2.1 Histopathological classification

There are various types of breast cancer categorized by the way the cells appear under the microscope. The WHO has classified breast cancer into different histological types (Tavassoli 2003), the common histopathological types are:

1. Ductal carcinoma (70-80%): tumours that resemble the breast ducts.
2. Lobular carcinoma (5-10%): tumours that resemble the breast lobules.

In some cases, invasive breast carcinoma is preceded by an earlier, 'pre-cancerous' condition known as ductal carcinoma in situ (DCIS) or lobular carcinoma in situ (LCIS).

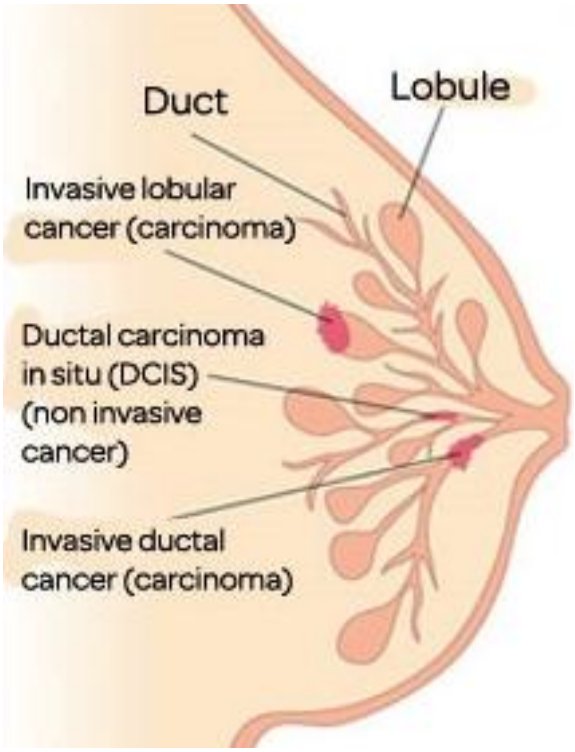

Figure-1.1: Common pathological types of breast cancer (taken from www.breastcancercare.org.uk)

1.2.2 Classification based on receptor status

Cells have receptors on their surface and in their cytoplasm and nucleus. Chemical messengers such as hormones bind to receptors, and this causes changes in the cell. Breast cancer cells may or may not have many different types of receptors, the three most important in the present classification are: oestrogen receptor (ER), progesterone receptor (PR), and HER2/neu. Cells are classified as ER positive (ER+), ER negative (ER-), PR positive (PR+), PR negative (PR-), HER2 positive (HER2+), and HER2 negative (HER2-) based on the status of these receptors. Cells with none of these receptors are called basal- like or triple negative.

1.2.3 Molecular intrinsic subtypes of breast cancer

With the recent advancement in techniques, genomic studies have identified five breast cancer intrinsic subtypes (Table 1.1). These include luminal A, luminal B, triple negative/ basal like, HER2 enriched and claudin-low (Perou, Sorlie et al. 2000; Sorlie, Perou et al. 2001; Prat, Parker et al. 2010) and a normal intrinsic breast type group. These subtypes differ markedly in prognosis and in the therapeutic targets they express (Eroles, Bosch et al. 2012) e.g. luminal A tumours have the best prognosis of all breast cancer subtypes and basal-like breast cancer have a poor prognosis.

Table-1.1: Molecular intrinsic subtypes of breast cancer.

Subtype	Features	Prevalence (approximate)
Luminal A	ER+ and/or PR+, HER2- and low Ki67	40%
Luminal B	ER+ and/or PR+, HER2+ (or HER2- with high Ki67)	20%
Triple negative/ Basal-like	ER-, PR-, HER2-, cytokeratin 5/6 + and/or EGFR+ and high grade	15-20%
HER2 enriched	ER-, PR-, HER2+	10-15%
Claudin low type (Prat, Parker et al. 2010; Prat and Perou 2011)	Non-basal triple-negative breast cancers with low to absent expression of epithelial cell-cell adhesion genes (claudin 3, 4 and 7, E-cadherin), differentiated luminal cell surface markers (EpCAM and MUC1) and enrichment for epithelial-to-mesenchymal transition markers, immune response genes and cancer stem cell-like features (CD44+/CD24-, high ALDH1A1)	Uncommon

1.3 Angiogenesis and breast cancer

Angiogenesis, the formation of new blood vessels from existing vasculature, plays an essential role in tumour growth, invasion and metastasis (Folkman 1971). Tumours require persistent new blood vessels for growth and spread, and acquire these by co-option of neighbouring blood vessels, capillary sprouting from existing vessels and new vessel formation from endothelial precursor cells. Angiogenesis is not only responsible for the growth of the primary tumour; it is also associated with systemic dissemination of tumour cells (Carmeliet and Jain 2000). A balance between pro-angiogenic and anti-angiogenic factors regulates angiogenesis. The disruption of the normal balance has been called the 'angiogenic switch' and is necessary for tumours to grow beyond a volume of about $1mm^3$ (Baeriswyl and Christofori 2009).

1.3.1 Vascular endothelial growth factor

Vascular endothelial growth factor (VEGF) is one of the key factors responsible for regulation of angiogenesis. VEGF stimulates quiescent endothelial cells to divide and form new blood vessels; tumour endothelial cells may divide as rapidly as every 7–10 days, as opposed to the normal time of approximately every 10 years. Binding of VEGF to its receptors begins the signalling cascade that regulates cellular events, including endothelial cell mitogenesis and migration, induction of proteinases leading to remodelling of the extracellular matrix, increased vascular permeability, maintenance and survival of newly formed blood vessels, enhanced chemotaxis and homing of bone-marrow progenitors to 'prepare' an organ for subsequent metastasis (Rapisarda and Melillo 2012).

The proteins belonging to the VEGF family can mediate a variety of biological effects, including endothelial cell mitogenesis and migration, induction of proteinases leading to remodelling of the extracellular matrix, increased vascular permeability, and maintenance of survival of newly formed blood vessels (Ferrara, Houck et al. 1992).

1.3.2 VEGF ligands and angiogenesis signaling

The VEGF family is encoded by seven genes including VEGF-A, B, C, D, E and placenta growth factor (PLGF)-1, 2 (Ferrara and Davis-Smyth 1997; Kowanetz and Ferrara 2006). These VEGF ligands specifically bind to each of their receptors. These receptors have an extracellular immunoglobulin (Ig)-like domain, a transmembrane region and an intracellular tyrosine-kinase domain. All VEGFA isoforms bind both VEGFR1 (FLT1) and VEGFR2 (FLK1). Binding affinity of VEGFA to FLT1 is higher as compared to FLK1 but it induces weaker tyrosine-kinase activity in FLT1 (Fischer, Mazzone et al. 2008). PLGF1 and 2, and VEGFB isoforms bind only VEGFR1. VEGF-E binds VEGFR-2. VEGFC and VEGFD bind both VEGFR2 and VEGFR3. Two co-receptor proteins in the cell membrane, neuropilin (NRP)-1 and NRP-2, interact with VEGFR proteins to increase the affinity of the latter for their ligands (Neufeld, Kessler et al. 2002). They differ from VEGFR proteins in not having intracellular signalling domains (Hicklin and Ellis 2005; Shibuya 2006). VEGFR1 binds VEGFA, VEGFB, and PLGF homo-dimers and is required for normal angiogenesis and haematopoiesis. VEGFR2 binds VEGF-A, C, D, and E homodimers and is the primary mediator of the physiological effects of VEGFA in angiogenesis, including micro-vascular permeability, endothelial cell proliferation, invasion,

migration, and survival. VEGFR3 preferentially binds VEGFC and VEGFD. Mutations of the VEGFR3 tyrosine kinase domain are seen in human lymphoedema. VEGFR3 expression has been correlated with transient lymphangiogenesis in wound healing and may modulate VEGFR2 signalling in maintaining vascular integrity (Casanovas, Hicklin et al. 2005). Higher affinity and weak tyrosine-kinase activity of VEGFA to VEGFR1 have led to the development of a model in which VEGFR1 acts as a decoy receptor and modulates angiogenesis through its ability to sequester VEGFA, and thereby reduces signaling through FLK1. VEGFR1 in this way functions as a negative regulator of angiogenesis, by binding VEGF and preventing it's binding to VEGFR2.

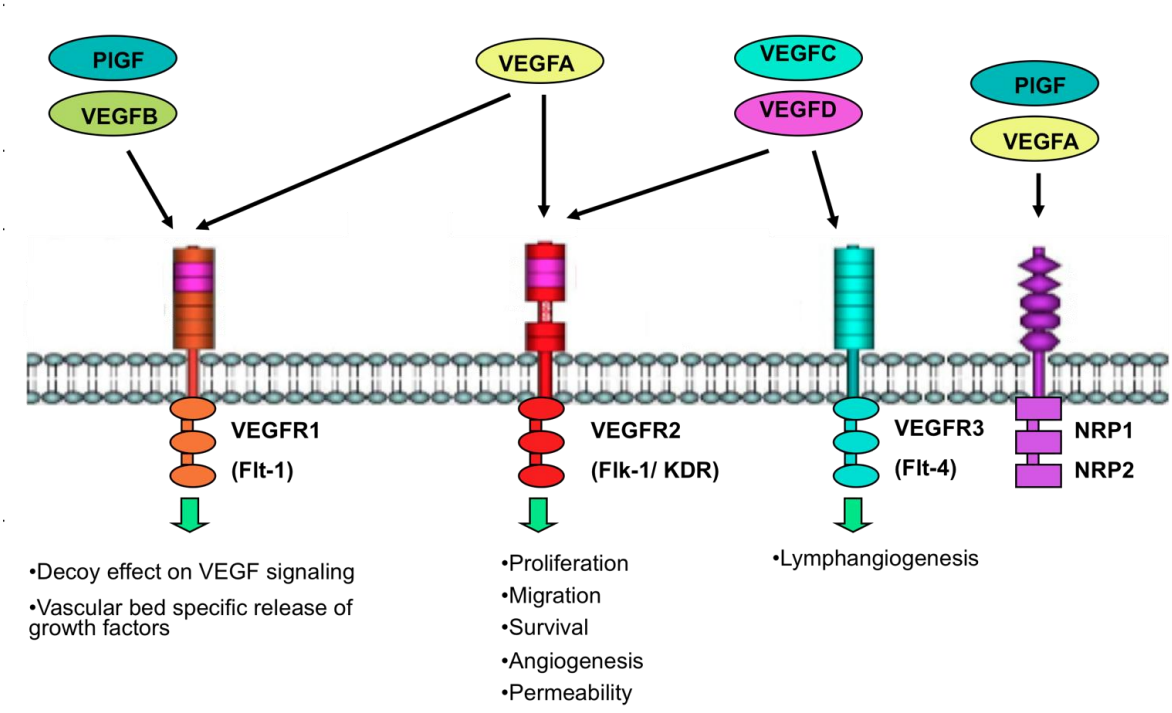

Figure–1.2: VEGF ligands and receptors on endothelial cells

1.3.3 Role of angiogenesis in breast cancer

Angiogenesis is of key importance in the process of tumour progression in a number of tumour types including breast cancer. Preclinical studies have confirmed that angiogenesis also plays a central role in breast cancer carcinogenesis and metastatic potential (Weidner, Semple et al. 1991; Chu, Lee et al. 1995). Over expression of VEGF has been observed in breast cancer, and is associated with worse overall survival (OS) and relapse free survival (RPS) in both node negative and node positive breast cancer (Gasparini 2000; Banerjee, Dowsett et al. 2007). VEGF is likely to be critical in initial phase of tumour growth. Breast cancer biopsies have shown that VEGF is produced as the major pro-angiogenic factor in early stage disease. The tumour micro-vessel density (MVD) of breast cancers is known to be predictive of bone marrow micro-metastases, recurrence and overall survival (Weidner, Folkman et al. 1992; Fox, Leek et al. 1997).

Owing to a critical role in cancer growth and metastasis, tumour related angiogenesis has become an attractive therapeutic target (Gasparini and Harris 1995). As VEGF is a key mediator of angiogenesis, inhibiting the VEGF pathway has been considered one of the most potent approaches in the treatment of cancer including breast cancer.

1.4 Bevacizumab (rhuMAb- VEGF, AVASTIN)

Bevacizumab is a recombinant humanized monoclonal antibody to VEGF composed of human IgG1 framework regions and antigen-binding complementary determining regions from a murine monoclonal antibody

(muMAb VEGFA.4.6.1) that blocks the binding of human VEGF to its receptors. Bevacizumab has a molecular mass of approximately 149 kDa and is glycosylated.

1.4.1 Mechanism of action of bevacizumab

Bevacizumab recognizes all isoforms of VEGF. Bevacizumab binds to VEGF and thereby inhibits the binding of VEGF to its receptors, Flt1 (VEGFR1) and KDR (VEGFR2), on the surface of endothelial cells. Neutralising the biological activity of VEGF reduces the vascularisation of tumours, thereby inhibiting tumour growth. It does not recognize other peptide growth factors tested (fibroblast growth factor, epidermal growth factor, hepatocyte growth factor, platelet-derived growth factor and nerve growth factor). It may exert a direct anti-angiogenic effect by binding to and clearing VEGF from the tumour environment. Additional anti-tumour activity may be obtained via the effects of bevacizumab on tumour vasculature, interstitial pressure and blood vessel permeability, providing rationale for enhanced chemotherapy delivery to tumour cells (Tong, Boucher et al. 2004; Jain 2005).

In summary, the main accepted mechanisms of action of bevacizumab are:

1) Regression of existing tumour microvasculature (Gerber and Ferrara 2005).
2) Normalization of surviving mature tumour vasculature (Gerber and Ferrara 2005; Jain 2005).
3) Inhibition of vessel re-growth and neo-vascularisation as an effect with continuous treatment (Gerber and Ferrara 2005).

1.4.2 Side-effects of bevacizumab

Unlike chemotherapy that causes cytotoxic effects, anti-VEGF drugs typically cause vascular adverse reactions. Side effects observed in patients receiving bevacizumab therapy include: hypertension, proteinuria, bleeding, thromboembolism, wound-healing complications, gastrointestinal perforation, and reversible posterior leukoencephalopathy syndrome (Table-1.2). Although, importantly, studies thus far show that bevacizumab does not increase chemotherapy-related toxicities.

Table-1.2: Toxicities associated with bevacizumab treatment

Toxicity	Incidence	Details
Hypertension	22 -- 32%	Dose-dependent increased risk
Proteinuria	21 -- 63%	Dose-dependent increased risk
Haemorrhage	30.40%	Most commonly epistaxis
Wound healing	13%	Seen in patients having surgery during bevacizumab treatment
Thromboembolism	11.90%	
Gastrointestinal perforation	0.90%	Risk varies with bevacizumab dose and tumour type
Reversible leukoencephalopathy syndrome	N/a	Symptoms: seizure, headache, confusion, loss of vision

1.4.3 Pharmacokinetics

The pharmacokinetic data for bevacizumab are available from eight clinical trials in patients with solid tumours. In all clinical trials, bevacizumab was administered as an IV infusion either as a single-agent or in combination with various anti-neoplastic agents. The rate of infusion was based on tolerability, with initial infusion duration of 90 minutes. Bevacizumab concentration–time profiles were well described using a two-compartment model. Of all the

covariates tested, body weight and sex showed the highest correlation with bevacizumab pharmacokinetics. Bevacizumab clearance and volume of the central compartment (Vc) increased with increasing body weight. For the typical patient, bevacizumab clearance was 0.206L/day and the central volume of distribution 2.66L. After adjusting for body weight, bevacizumab clearance was 26% faster, and Vc was 22% larger in men than in women.

The distribution half-life is 1.4 days and the elimination half-life is 20 days, with a predicted time to steady state of 100 days. Bevacizumab pharmacokinetics is linear within the range of 1-10 mg/kg/week. Consistent with those for other IgG1, the pharmacokinetics of bevacizumab was characterized by slow clearance and a long terminal half-life, which enables administration every 2–3 weeks. 15mg/kg has been used as a standard dose for breast cancer, on a 3 weekly cycle.

1.5 Bevacizumab in breast cancer

Bevacizumab has been tested in various Phase II and III studies in combination with chemotherapy as first line or second line therapy in advanced breast cancer and also in neoadjuvant setting recently. The results of main phase III trials has been summarised below.

1.5.1 First-line bevacizumab studies in metastatic breast cancer

Three randomized phase III studies (Miller 2003; Miller, Wang et al. 2007; Miles, Chan et al. 2010; Robert, Dieras et al. 2011) evaluating the impact of adding bevacizumab to chemotherapy in the first-line treatment of HER2-

negative metastatic breast cancer (MBC) have reported positive results in terms of overall response rate (ORR) and progression-free survival (PFS).

The Eastern Cooperative Oncology Group (ECOG) (E2100) (Miller 2003; Miller, Wang et al. 2007) demonstrated the benefit of adding bevacizumab to paclitaxel in first-line therapy for MBC. In this trial women with locally recurrent or metastatic breast cancer were randomized to receive paclitaxel (90mg/m^2 on days 1, 8 and 15 of a 4-week cycle) with or without bevacizumab (10mg/kg/2weekly). The addition of bevacizumab was associated with significantly higher response rate (28% vs14%; P<0.0001) and significantly longer PFS (11 months vs. 6 months; P<0.001).

The AVADO (Avastin and docetaxel) trial (Miles, Chan et al. 2010) was a three-arm trial comparing docetaxel as a single agent with docetaxel and bevacizumab at two dose levels: 7.5mg/kg and 15mg/kg in HER2 negative locally recurrent or MBC. All drugs were administered at 3 weeks intervals. They have shown that combination of bevacizumab 15 mg/kg, but not 7.5 mg/kg, with docetaxel showed superior median PFS to placebo plus docetaxel in stratified analysis (with placebo 8.1 months; with 7.5mg/kg, 9.0 months [HR 0.80; P = 0.045]; and with 15mg/kg, 10.0 months [HR 0.67; P<0.001]). Response rates in patients with measurable disease at baseline also increased with bevacizumab 15 mg/kg (46% [placebo] v 55% [7.5 mg/kg; P=0.07] and 64% [15 mg/kg; P<0.001]).

In the RIBBON (Regimens in Bevacizumab for Breast Oncology)-1 trial

(Robert, Dieras et al. 2011), patients were randomized either to receive or not to receive bevacizumab with first-line chemotherapy regimen, as were favored by the treating medical oncologist. The data were analyzed in two distinct chemotherapy groups: “anthracycline-based” or “taxane-based” chemotherapy with or without bevacizumab. A significant improvement in both response rate and PFS was reported when bevacizumab was added to each chemotherapy regimen. However, overall survival was not improved.

1.5.2 Second line bevacizumab studies in metastatic breast cancer

In the AVF2119g study (Miller, Chap et al. 2005); bevacizumab was used in combination with capecitabine (Xeloda, Roche-Genentech) as second-line treatment for patients previously treated with anthracycline-taxane therapy. Patients with breast cancer refractory to anthracyclines and taxanes were randomized to receive capecitabine (2,500 mg/m^2 daily for 2 weeks of a 3-week cycle) with or without bevacizumab (15 mg/kg/ 3 weekly). The addition of bevacizumab significantly increased response rates (19.8% vs. 9.1%; P=0.001) and had an acceptable safety profile.

In the RIBBON-2 trial (Brufsky, Hurvitz et al. 2011) women with HER2-negative disease that progressed after first-line therapy were randomly assigned to receive chemotherapy according to the choice of the treating oncologist with or without bevacizumab. With subsequent disease progression, bevacizumab could be added to the third-line regimen. A 2:1 randomization was used to assign 225 women to the control arm and 459 to chemotherapy with bevacizumab. PFS favored the bevacizumab-treated patients (5.1 months vs.

7.2 months; P=0.007). No improvement in OS was observed, and no unique toxicity profile was identified.

1.5.3 Neoadjuvant bevacizumab trials

The results of two large neoadjuvant trials have recently been published. Both the National Surgical Adjuvant Breast and Bowel Project (NSABP) B-40 (Bear, Tang et al. 2012) and the GeparQuinto (GBG44) (von Minckwitz, Eidtmann et al. 2012) were designed to evaluate whether the addition of bevacizumab to chemotherapy would increase the rates of pathologic complete response (pCR) in women with early stage HER2-negative breast cancer.

Both of these trials reported that the addition of bevacizumab to chemotherapy significantly and moderately increases pCR rate (34.5% *vs*. 28.2%, P=0.02) in the breast by the NSABP B-40 trial, and in the breast and nodes (18.4% *vs*. 14.9%, P=0.04) by the GeparQuinto study. NSABP B-40, also reported that the effect of bevacizumab was more pronounced in the hormone-receptor–positive subset (15.1% without bevacizumab vs. 23.2% with bevacizumab, P=0.007), with a weaker effect in the hormone-receptor–negative subset (47.1% without bevacizumab vs. 51.5% with bevacizumab, P=0.34). Conversely the GeparQuinto trial reported a more pronounced effect in triple negative breast cancers (the pCR rate 9.3% vs. 27.9%; P=0.003). Both of these trials reported significant increase in pCR in high grade tumours.

1.5.4 Approval status of bevacizumab in breast cancer

On February 22, 2008, the FDA granted accelerated approval for bevacizumab (Avastin®, made by Genentech) to be used in combination with paclitaxel (Taxol®) for the treatment of patients who have not received chemotherapy for metastatic HER2-negative breast cancer. This was based on two phase III clinical trials (AVF2119g, E2100) (Miller 2003; Miller, Chap et al. 2005; Miller, Wang et al. 2007) However, the FDA revoked the approval of the breast cancer indication for bevacizumab used in combination with paclitaxel in November 2011 citing that the combination has not been shown to be safe or effective. The addition of bevacizumab increased toxic effects such as grade 3 or 4 neuropathy, infection, fatigue and cerebrovascular ischemia. Furthermore, as shown above the subsequent phase 3 clinical trials i.e. AVADO and RIBBON-1, have not verified the benefits shown in E2100. Nonetheless bevacizumab is still approved by different regulatory agencies across several countries (e.g. EU, Australia) as a standard antiangiogenic drug for the treatment of first-line advanced breast cancer.

1.6 Biomarkers of anti-angiogenic therapy in breast cancer

Bevacizumab is the most commonly used anti-angiogenic agent in breast cancer clinical trials. To date thousands of women have been enrolled or received bevacizumab in these clinical trials. Several biomarkers like polymorphism in VEGF pathways (Schneider, Wang et al. 2008; Schneider, Shen et al. 2012; Miles, de Haas et al. 2013), genetic markers like VEGFA amplification (Schneider, Gray et al. 2013), delta like ligand 4 (DLL4), VEGF-C, and neuropilin-1 expression (Jubb, Miller et al. 2011), circulating markers like

short VEGFA isoforms (Miles, de Haas et al. 2013) VEGFA expression (Jayson GC 2011), soluble vascular endothelial growth factor receptor 1 (sVEGFR1) (Tolaney SM 2012), infiltrating myeloid cells (Shojaei, Wu et al. 2007; Ferrara 2010; Lu, Kujawski et al. 2012) Imaging biomarkers, like changes in forward rate constant (K^{trans}) on DCE-MRI analysis (O'Connor, Jackson et al. 2012) have been proposed in breast cancer studies.

Currently, there are no proven biomarkers of efficacy of anti-VEGF therapy (Jubb and Harris 2010; Gyanchandani and Kim 2013; Lambrechts, Lenz et al. 2013). These biomarkers are urgently needed to validate the mechanistic hypothesis, to identify responsive patients and to predict efficacy of regimens that include anti-VEGF agents. The discovery of the biomarkers for anti-angiogenic therapies such as bevacizumab would enable these highly effective agents to be offered to patients based on expression of biomarker or change at an early stage to decide about further continuation of treatment. This would offer significant cost savings, as well as reducing the number of patients who experience the side effects of anti-angiogenic therapy without any of the clinical benefits (Jubb and Harris 2010).

The vast majority of anti-angiogenic drugs are investigated in end-stage patients for whom biopsies are not available, and in which multiple mechanisms of resistance to cellular stress are likely to have developed (Schneider et al 2005). The conventional line of testing poses a significant problem to angiogenesis inhibitors, because it is unlikely that this type of drug will have an effect in those patients. A large tumour burden may produce large

quantities of angiogenic factors, which locally may overwhelm the angiogenesis inhibitor and even if angiogenesis was effectively reduced, cells may be able to withstand the hypoxic acidic environment, resulting in a lack of clinical benefit to the patient.

A way to assess anti-angiogenesis agents in early stage disease is to use the drugs in short term neoadjuvant therapy, as first line treatment, with a detailed investigation of mechanistic pathways in a pre-treatment biopsy and analysis of relation of these to pharmacodynamic endpoints which are potentially clinically relevant endpoints (Generali, Berruti et al. 2011). There are few trials reported in literature in which bevacizumab has been used in early breast cancer patients and have provided some valuable information on potential biomarkers and mechanism of angiogenesis.

Preliminary data from a phase II trial of neoadjuvant docetaxel with or without bevacizumab in locally advanced breast cancer indicates that the combination is well tolerated and effective in reducing tumour perfusion assessed by DCE-MRI and serum e-selectin levels (Overmoyer B 2004).

Wedam SB et al. (Wedam, Low et al. 2006), have studied the effect of neoadjuvant bevacizumab and chemotherapy (e.g. Doxorubicin and docetaxel) on markers of angiogenesis (e.g. CD31, ki67, MVD, VEGF, pVEGFR2) and vascular permeability (k21), assessed by DCE-MRI, in previously untreated patients with locally advanced or inflammatory breast cancer. A decrease in k21 and phosphorylated VEGFR2 was seen following first cycle of

bevacizumab, indicating an inhibitory effect of bevacizumab on VEGFR activation and vascular permeability.

Denduluri N et al. (Denduluri, Yang et al. 2007), have studied circulating biomarkers of bevacizumab activity in patients with breast cancer. Twenty-one patients with breast cancer underwent neoadjuvant treatment with bevacizumab for 1 cycle followed by 6 cycles of bevacizumab, chemotherapy, and filgrastim. Soluble vascular cell adhesion molecule (sVCAM-1), soluble VEGF receptor-2 (sVEGFR-2), and plasma VEGF levels were assessed as potential biomarkers of therapy with bevacizumab. Tumour samples were evaluated for VEGFR-2 mutations before and after bevacizumab. This study concluded that sVCAM-1 and sVEGFR-2 values increased significantly, by a median of 180.5 ng/mL ($P<0.0001$) and 1927 ng/mL respectively ($P=0.0003$) after the first cycle of treatment with bevacizumab only

Yang et al. (Yang, Steinberg et al. 2008), have analysed the angiogenic tumour markers (VEGFA, CD31, pVEGFR2 (Y996), pVEGFR2 (Y951), PDGFRβ, MVD, Ki67, apoptosis, grade) at baseline by immunohistochemistry, in a study of twenty patients with inflammatory breast cancer and one with locally advanced breast cancer that received one cycle of bevacizumab followed by six cycles of bevacizumab plus docetaxel-doxorubicin before surgery. They have reported that the higher level of baseline CD31, PDGFRβ, and VEGF were significantly associated with response to bevacizumab followed by bevacizumab plus chemotherapy.

In another neoadjuvant randomized phase II study (Baar, Silverman et al. 2009), 49 patients with inoperable breast cancer received 2 cycles of preoperative docetaxel 35mg/m^2 i.v. weekly for 6 weeks, followed by a 2-week break or docetaxel with bevacizumab 10 mg/kg i.v. every other week for a total of 16 weeks. Plasma and serum markers of endothelial damage, DCE-MRI and tumour micro-vessel density were assessed before treatment and at the end of each preoperative cycle. They have shown that bevacizumab plus docetaxel caused a greater increase in vascular endothelial growth factor ($P<0.0001$) and VCAM-1 ($P=0.069$), and a greater reduction in tumour perfusion by DCE-MRI compared with docetaxel alone. Clinical outcomes of inoperable breast cancer were predicted by changes in VCAM-1 and E-selectin.

1.7 Rationale for the study

Two key challenges for these new generations of anti-neoplastic agents are to determine the mechanism of response and to identify the group of patients most likely to show a clinical benefit. As these drugs become increasingly expensive, a significant reduction in treatment cost could come from the therapeutic selection of those patients that would probably get a significant benefit with anti-angiogenic agents.

The hypothesis that I wanted to test was that gene array analysis and analysis of key markers related to angiogenic/ molecular pathways might be predictive of those patients that show a pharmacodynamic response to bevacizumab in their primary tumour as assessed by DCE-MRI. I also proposed that the

changes after two weeks of therapy with bevacizumab, assessed by gene array analysis and selected marker studies, would correlate with the changes induced in MRI. The value of this approach was that we would have a much more extensive understanding of the factors associated with baseline differences between patients in the DCE-MRI results, and may be able to predict those patients most likely to show short term response, as assessed by DCE-MRI. It could non-invasively guide the likely therapeutic value of antiangiogenic therapy for individual patients and help in deciding further treatment management.

Early in the treatment, there was a window of opportunity to give antiangiogenic agent for between 2-4 weeks with biopsies and pharmacodynamic endpoints without affecting standard patient treatment. As little is known about the determinants of response to bevacizumab and this study could enable a comprehensive analysis to understand the mechanisms governing response and resistance that could further enhance our understanding of the biomarkers of response and resistance to antiangiogenic therapy. I decided to use bevacizumab for this clinical study as it is a specific anti-VEGFA agent and is the most common antiangiogenic agent used so far in clinical practice with a known toxicity profile. The two main techniques used to assess response to bevacizumab in this study were: Dynamic contrast enhanced magnetic resonance imaging and genome wide gene expression array using the Affymetrix platform.

1.7.1 Dynamic contrast enhanced MRI (DCE-MRI)

DCE-MRI is a form of MRI that makes use of low molecular weight paramagnetic contrast agents (e.g. Gd-DTPA). Following injection of the contrast agent (CA), serial T1-weighted MR scans were performed in order to image the passage of the CA. It gives rise to characteristic enhancement patterns in the region of a tumour which reflect the state of the tumour vasculature (vessel permeability, blood flow, volume of extra vascular extracellular space) (Turkbey, Thomasson et al. 2009). In regions of tumour vasculature, contrast agent can leak into the extravascular extracellular space (EES) that gives rise to a rapid increase in the MR signal. Contrast agent then diffuses back into the blood plasma, resulting in a gradual decrease in the MR signal. Pharmacokinetic (PK) models can be used to quantify the rate constants (K^{trans}, k_{ep}) governing this process (Fig 1). K^{trans} represents the volume transfer constant between plasma and the EES (units: min^{-1}) whereas k_{ep} represents the rate constant between EES and plasma (units: min^{-1}) and v_e represents volume of EES per unit volume of tissue.

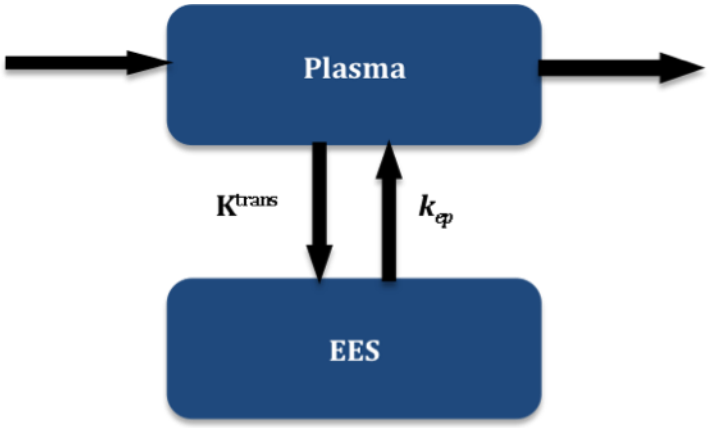

Figure-1.3: Physiological basis of DCE-MRI. EES- Extravascular extracellular space; K^{trans} - transfer constant from plasma to EES; k_{ep} - rate constant from EES to plasma; v_e - fractional volume of the EES.

DCE-MRI parameters quantify changes in micro vascular physiology, therefore, can serve as a non-invasive imaging biomarker of tumour angiogenesis (Furman, Kelcz et al. 2002; Degani, Chetrit et al. 2003; Leach, Brindle et al. 2005; O'Connor, Jackson et al. 2007; Padhani, Liu et al. 2009). DCE-MRI can be used to reliably detect and characterize the effects of angiogenesis inhibitors in phase-I trials (Raatschen, Simon et al. 2008). DCE-MRI has previously demonstrated a significant reduction in physiological parameters that reflect changes in angiogenesis following neoadjuvant bevacizumab treatment in inflammatory and locally advanced breast cancer (Wedam, Low et al. 2006; Thukral, Thomasson et al. 2007; Baar, Silverman et al. 2009).

Most trials and investigator-led studies using DCE-MRI to assess antiangiogenic agents and vascular-targeting agents have used changes in either the area under the contrast agent concentration–time curve at 60 or 90 seconds post-injection (IAUC60 and IAUC90, respectively) or the volume transfer constant (K^{trans}) or variations in these parameters as imaging end points. These are the composite parameters influenced by blood flow, vessel surface area and vessel permeability (O'Connor and Jayson 2012).

In addition to DCE-MRI, a blood oxygenation level dependent (BOLD) scan can be performed at same time (prior to administration of the contrast agent) to assess the oxygenation status of red blood cells in perfused regions, and a diffusion-weighted (DW) MRI scan to assess cellularity (Li and Padhani 2012). Together, these scans can be used to characterise the spatial patterns of

angiogenesis across the full extent of the tumour, to quantify the perfusion characteristics of the tumour (in terms of flows and permeability), and to assess any drug-induced changes in tissue oxygenation and cellularity.

1.7.2 Gene expression arrays

A comprehensive characterization of all of the genomic modifications associated with the cancer is critical for the understanding of the origins of tumour process, and for finding the targets of therapeutic interventions. The utilization of high-density nucleic acid microarrays is one of the most effective approaches to identifying these key molecular events. Whole-genome expression profiling can reveal complex molecular pathways, which are involved in cancer and could be useful in identifying markers for therapeutic response.

The Affymetrix Gene Chip® Human Genome U133 Plus 2.0 array (HG-U133 Plus 2.0) is one microarray comprised of 1,300,000 unique oligonucleotide features covering over 47,000 transcripts and variants, which in turn, represent approximately 39,000 of the best characterized human genes.

With approximately four probes per exon and roughly 40 probes per gene, the Gene Chip® Human Exon 1.0 ST array enables two complementary levels of analysis, gene expression and alternative splicing. Multiple probes per exon enable "exon-level" analysis and allow distinguishing between different isoforms of a gene. This exon-level analysis on a whole-genome scale opens

the door to detecting specific alterations in exon usage that may play a central role in disease mechanism and aetiology. The second level is "gene-level" expression analysis, in which multiple probes on different exons are summarized into an expression value of all transcripts from the same gene. Exon arrays provide the most comprehensive coverage of the genome, including empirically supported and predicted transcribed sequences, enabling the discovery of previously unidentified novel events.

1.8 Objectives

The main objectives of this study were:

1) To assess the correlation of baseline MRI parameters with gene expression array in breast cancer patients.
2) To investigate the early changes in clinical parameters and DCE-MRI parameters after a single cycle of bevacizumab in a chemotherapy naïve breast cancer population.
3) To assess the early changes in gene expression in response to bevacizumab therapy.
4) To analyse the correlation of baseline and changes in MRI parameters with baseline gene expression and changes on bevacizumab therapy.
5) To identify clinically useful biomarkers to identify patients most likely to respond to bevacizumab.

CHAPTER TWO

2 Materials and Methods

2.1 Study designs and patient selection criteria

2.1.1 Retrospective study

This retrospective study included newly diagnosed primary breast cancer patients who were referred to Department of Medical Oncology for neoadjuvant chemotherapy between April 2001 to Dec 2008 (Ethical approval no. C01.237).

A.Selection criteria

The patients with histology proven invasive ductal carcinoma of the breast who had a formalin fixed paraffin embedded (FFPE) core biopsy sample taken prior to treatment and had a baseline DCE-MRI scan done within 0-14 days prior to commencing neoadjuvant chemotherapy were considered for this study.

All the clinical data were collected for these patients from the breast cancer database at the Department of Oncology, Churchill Hospital, Oxford. For any missing data, the patient file notes were checked to get as much information as possible. The follow up data was collected for these patients until April 2012.

2.1.2 Prospective study

A.Study design

A prospective two-centre, Phase II, non-randomised, open label investigator-led window of opportunity study was conducted from Aug 2008 until Nov 2010. This study was sponsored by the Oxford Radcliffe Hospitals NHS Trust (ORH/PID/5575) and was approved by National Research Ethics Services (NRES) UK. (Oxford REC no. - 08/H0604/69). Two centres involved were

Cancer and Haematology Centre, Churchill Hospital Oxford and Mount Vernon Cancer Centre, Northwood, Middlesex.

B.Target population

In this study, the newly diagnosed previously untreated breast cancer patients who were deemed fit for neoadjuvant chemotherapy were enrolled based on following selection criteria.

C.Selection criteria

I. Inclusion criteria

1) Female patients.
2) Age ≥ 18 years.
3) ECOG performance status of 0-1.
4) Histology proven breast cancer.
5) Tumours greater than 3 cm in diameter or locally advanced breast cancer (LABC). LABC will be defined as stage IIB, IIIA, IIIB, and IIIC tumours as per 2002 American Joint Committee on Cancer (AJCC) guidelines on breast cancer staging (Singletary, Allred et al. 2002).
6) No prior treatment for breast cancer.
7) All women of child-bearing age (i.e. unless postmenopausal, having had no menstrual period ≥1 yr) must have a negative pregnancy test performed within 7 days before treatment with bevacizumab. They should be using effective contraception during the study and for a period of 6 months following administration of bevacizumab.
8) Written (signed and dated) informed consent and be capable of co-operating with protocol.

9) Haematological and biochemical indices within the ranges shown below.

Lab Test	Value required
Haemoglobin (Hb)	≥9.0 g/dL
Platelet count	≥100 x 10/L
Absolute Neutrophil count	≥1.5 x 10/L
Serum bilirubin	≤1.5 x upper normal limit
Alanine amino-transferase (ALT)	≤2.5 x upper limit of normal unless due to tumour in which case up to 5 x upper limit of normal was permissible
Serum creatinine	≤1.25 x upper limit of normal
Urine dipstick for proteinuria	≤2+
International normalised ratio (INR)	< 1.5
Partial prothrombin time (PTT or aPTT)	< 1.5 x upper limit of normal

II. Exclusion criteria

A patient was not considered eligible for the trial if any of the following criteria apply:

1) Radiotherapy, major surgery, significant traumatic injury, endocrine therapy, immunotherapy, chemotherapy or experimental therapy during four weeks prior to starting or during trial.
2) Minor surgery including insertion of indwelling catheter within 24 hours prior to bevacizumab infusion.
3) Current or recent (within 10 days of bevacizumab) use of aspirin (> 325 mg/day) or clopidogrel (> 75 mg/day)

4) Current or recent (within 10 days of bevacizumab) use of full-dose oral or parenteral anticoagulants or thrombolytic agent for therapeutic purposes. Prophylactic use of anticoagulants is allowed.
5) History or evidence of inherited bleeding diathesis or coagulopathy with the risk of bleeding.
6) Uncontrolled hypertension (systolic >150 mmHg and/or diastolic >100 mmHg).
7) Clinically significant (i.e. active) cardiovascular disease for example CVA (≤6 months before enrolment), myocardial infarction (MI) (≤6 months before enrolment) unstable angina, CHF NYHA Class ≥II study, Cardiac arrhythmias requiring anti-arrhythmic therapy (beta-blockers or digoxin) are permitted.
8) Non-healing wound, active peptic ulcer or bone fracture.
9) History of abdominal fistula, diagnosed with tracheo-oesophageal fistula or any grade 4 non – gastrointestinal fistula, gastrointestinal perforation or intra-abdominal abscess within 6 months of enrolment.
10) Treatment with any other investigational agent, or participation in another clinical trial within 28 days prior to enrolment
11) Known hypersensitivity to bevacizumab and any of its excipients.
12) Other psychological, social or medical condition, physical examination finding or a laboratory abnormality that the Investigator considers would make the patient a poor trial candidate or could interfere with protocol compliance or the interpretation of trial results.

D.Study procedures

As summarised in Figure - 2.1, patients were given information about the study at their first clinic appointment to discuss neoadjuvant chemotherapy. The patients who were interested to participate in the study were seen the following day for consent, physical examination and screening blood tests as per the protocol along with the diagnostic DCE-MRI breast scan performed on the same day. The patients who met the eligibility criteria were enrolled in the study and had research DCE-MRI scan on the following day followed by research core biopsies. Bevacizumab infusion was given at least 24 hours after baseline core biopsies. Blood samples for pharmacodynamic assessment were performed on the day of bevacizumab therapy before starting infusion. Any adverse event(s) (AE) experienced since the previous visit were assessed and recorded along with any new or changes to concomitant medications. Patients received bevacizumab infusion after taking blood samples and recording observations e.g. blood pressure, pulse, temperature etc. A single dose of bevacizumab (15mg/kg) was given by intravenous infusion over 90 minutes. Commercial packs of bevacizumab (RO 487-6646 -marketed as Avastin), were used in this study. Roche Products (UK) Ltd provided participating pharmacy departments (Oxford and Mount Vernon) with bevacizumab free of charge for use in this study. Observation including blood pressure, pulse and temperature were checked again after infusion. Patients were observed for an hour post infusion for any acute reaction. Patients were discharged home on the same day if there was no acute reaction and observations were within normal limits. Total duration of stay in hospital was about 2-3 hours if no acute reaction occurred to bevacizumab.

The patients were seen two weeks after bevacizumab infusion for recording any adverse events, physical examination, checking observations, repeat research DCE-MRI scan, core biopsies and blood samples for pharmacodynamic assessments as per protocol. Following this patients were considered off study and were commenced on neoadjuvant chemotherapy with 3 cycles of 5FU, epirubicin and cyclophosphamide [FEC100], followed by 3 cycles of docetaxel 100mg/m^2, all with filgrastim [G-CSF] support.

Patients were deemed to have successfully completed the study if they had successfully undergone both pre- and post-bevacizumab core biopsies together with the corresponding MRI scans.

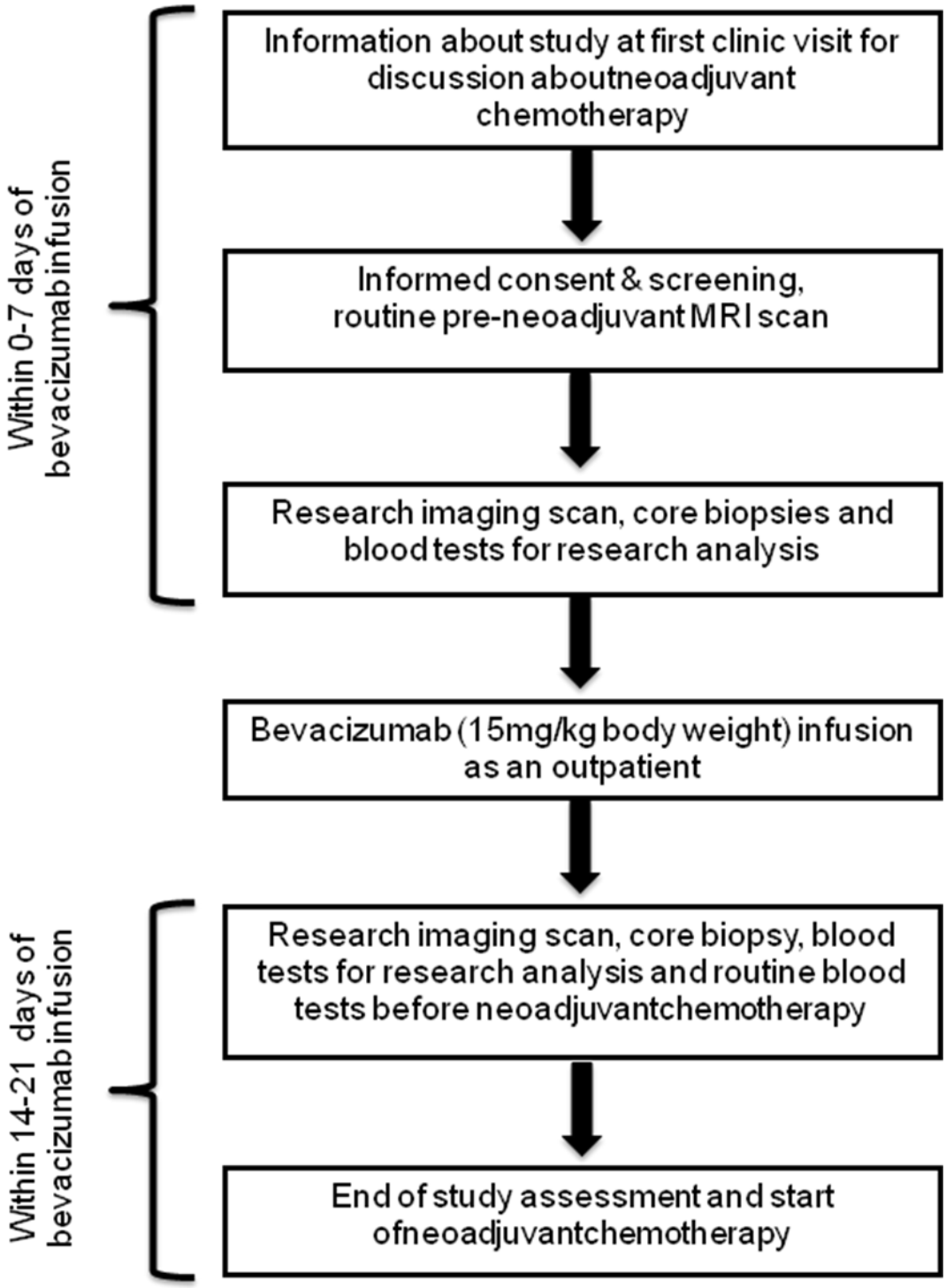

Figure-2.1: Flow diagram showing overview of study procedure

2.2 Dynamic contrast-enhanced (DCE) MRI

2.2.1 Scanning protocol

Scanning protocol for both the retrospective and prospective studies were as follows: -

A.Retrospective study

DCE-MRI data was collected for the diagnostic scan of the patients. Patients were scanned on a GE 1.5 T scanner at the John Radcliffe Hospital or the Churchill Hospital, Oxford. In summary, scanning protocol was as follows:

Following injection of the contrast agent, Gadopentetate dimeglumine (Gd-DTPA; dose 0.1mmol/kg body weight), serial T1 weighted scans were acquired using a 3D fast spoiled gradient echo (FSPGR) pulse sequence. Imaging field of view (FOV) included full volumes of both breasts. Average voxel dimensions were 1.3 mm x 1.3 mm x 3 mm and volume acquisition time was ~60 seconds. For DCE-MRI scans performed at the Churchill, the acquisition parameters were as follows: TE/TR = 4.2/10.6 ms, flip angle = 35°, number of frequency/phase encoding lines = 256/256, NEX = 1, bandwidth = 139.53 kHz. For DCE-MRI scans performed at the JR, the acquisition parameters were as follows: TE/TR = 4.2/8.8 ms, flip angle = 10°, number of frequency/phase encoding lines = 256/256, NEX = 1, bandwidth = 244.14 kHz. Variable flip angle sequences were available for 27 patients only, using flip angles of 3° and 10° for the Churchill scans, and 3° and 17° for the John Radcliffe scans.

B.Prospective study

The MRI protocol was designed to image multiple aspects of the tumour pathophysiology and to enable the imaging FOV to be matched as closely as possible between the pre- and post-bevacizumab scans for each patient. First of all, a localizer sequence was performed followed by axial and coronal T2-weighted scans. Next, a DW sequence was performed in the axial plane using b-values of 0, 100, and 700 s/mm^2 and a FOV of 340 mm x 340 mm (slice thickness = 5.6 mm, TE/TR = 114.5/5650 ms, reconstruction matrix = 256 x 256, NEX = 5). The diffusion-weighted images were then used to identify the location of the tumour and to set up the FOV for the subsequent "positional scan". This consisted of a 3D gradient echo sequence (slice thickness = 5 mm, TE/TR = 4.2/10.1 ms, flip angle = 35°, reconstruction matrix = 256 x 256) that was performed in the sagittal plane and was used to select eight central tumour slices for all subsequent sequences. In case of the post-bevacizumab MRI scan, the positional scan was used to identify the eight slices that provided the best overall match to those slices selected in the pre-bevacizumab scan.

Having set up the FOV using eight central tumour slices (slice thickness = 5 mm, reconstruction matrix = 256 x 256) selected from the positional scans, then R2* scan, variable flip angle and dynamic contrast-enhanced MRI scans were performed, all in the sagittal plane. Specifically, the R2* scan consisted of a multi-gradient echo sequence with echo times of 4.8, 14.3, 23.8, 33.4, and 61.9 ms (TR = 100 ms, flip angle = 40°, bandwidth = 41.67 kHz). For native T1 mapping prior to the DCE scan, we performed a variable flip angle sequence

using flip angles of 2° and 8° (Oxford scans), or a single proton-density weighted (PDW) sequence with a flip angle of either 2° or 3° (Mount Vernon scans).

T1-weighted DCE-MRI scans were performed using either a FAME sequence (Oxford scans) with extended dynamic range (EDR) and zero-fill interpolation processing (ZIP x 2), or a VIBE sequence (Mount Vernon scans). All DCE-MRI scans were acquired with a temporal resolution of 5.4 seconds over a period of 8 minutes (TE/TR = 1.5/4.2 ms, flip angle = 18°, number of frequency/phase encoding lines = 256/128, NEX = 1, bandwidth = 41.67 kHz). At the start of the 6th dynamic volume, 0.1 mmol per kg body weight of contrast agent was injected intravenously using a power injector at a rate of 3 mL/s (Oxford scans) or 4 mL/s (Mount Vernon scans), followed by a chasing bolus of 40 mL saline. Gadoteridol (Gd-HP-DO3A, ProHance, Bracco) was used for patients scanned at Oxford, and gadopentetate dimeglumine (Gd-DTPA, Magnevist, Bayer-Schering) for patients scanned at Mount Vernon.

Following the DCE-MRI scan, a final “book-end” T1 mapping sequence was performed that was identical to the pre-contrast T1 mapping sequence (i.e. variable flip angle for Oxford scans, proton density weighted for Mount Vernon scans).

In order to characterise the extent of anti-angiogenic change due to bevacizumab, the perfusion imaging and diffusion sequences were repeated at 14-21 days post bevacizumab infusion.

2.2.2 Regions of Interest (ROI)

For the retrospective as well as for the prospective study the ROI annotations were performed by an experienced radiologist (Dr Rosie Adams). A spline-based ROI tool (Figure-2.2) was used to annotate the boundary of the tumour (if present) on each slice of the early post-contrast subtraction volume (120 secs). Entire tumour volume was delineated for each scan.

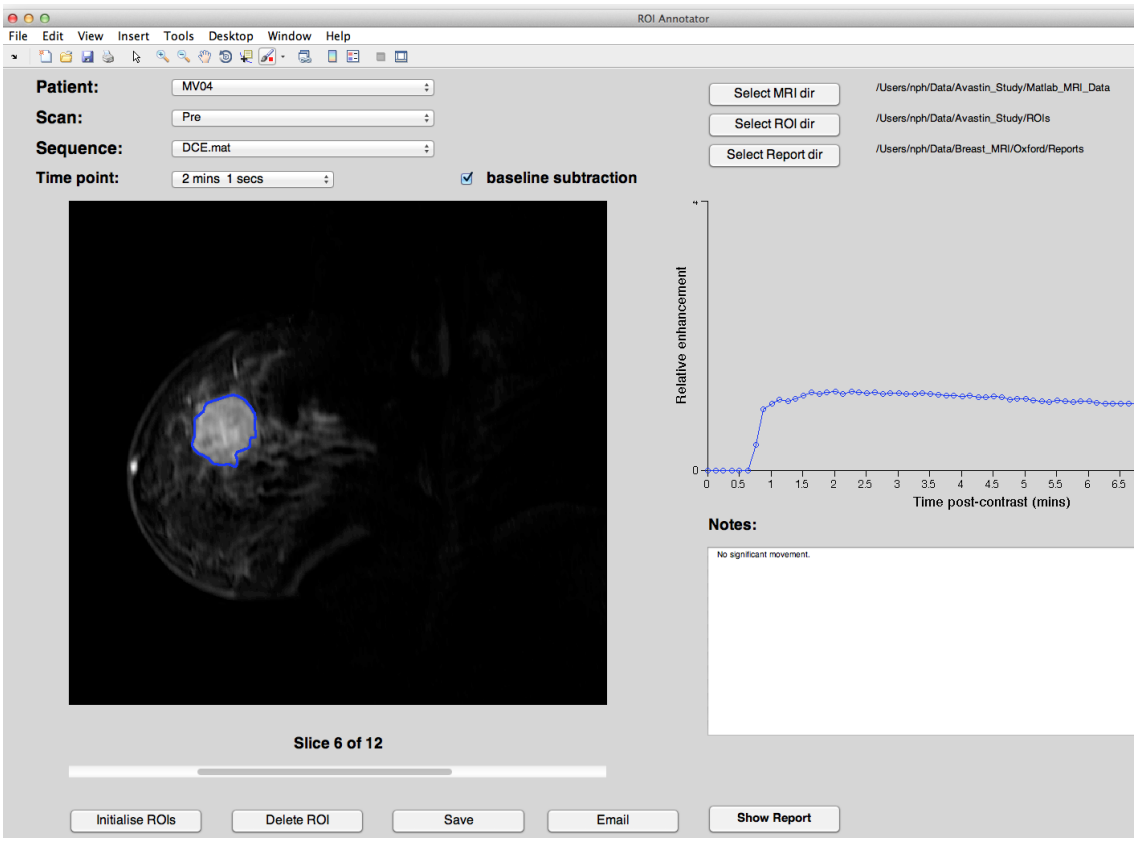

Figure-2.2: Annotation of ROI using spline based tool.

After combining ROIs of entire volume of tumour the 3-dimensional (3D) images of the tumour were constructed (Figure- 2.3).

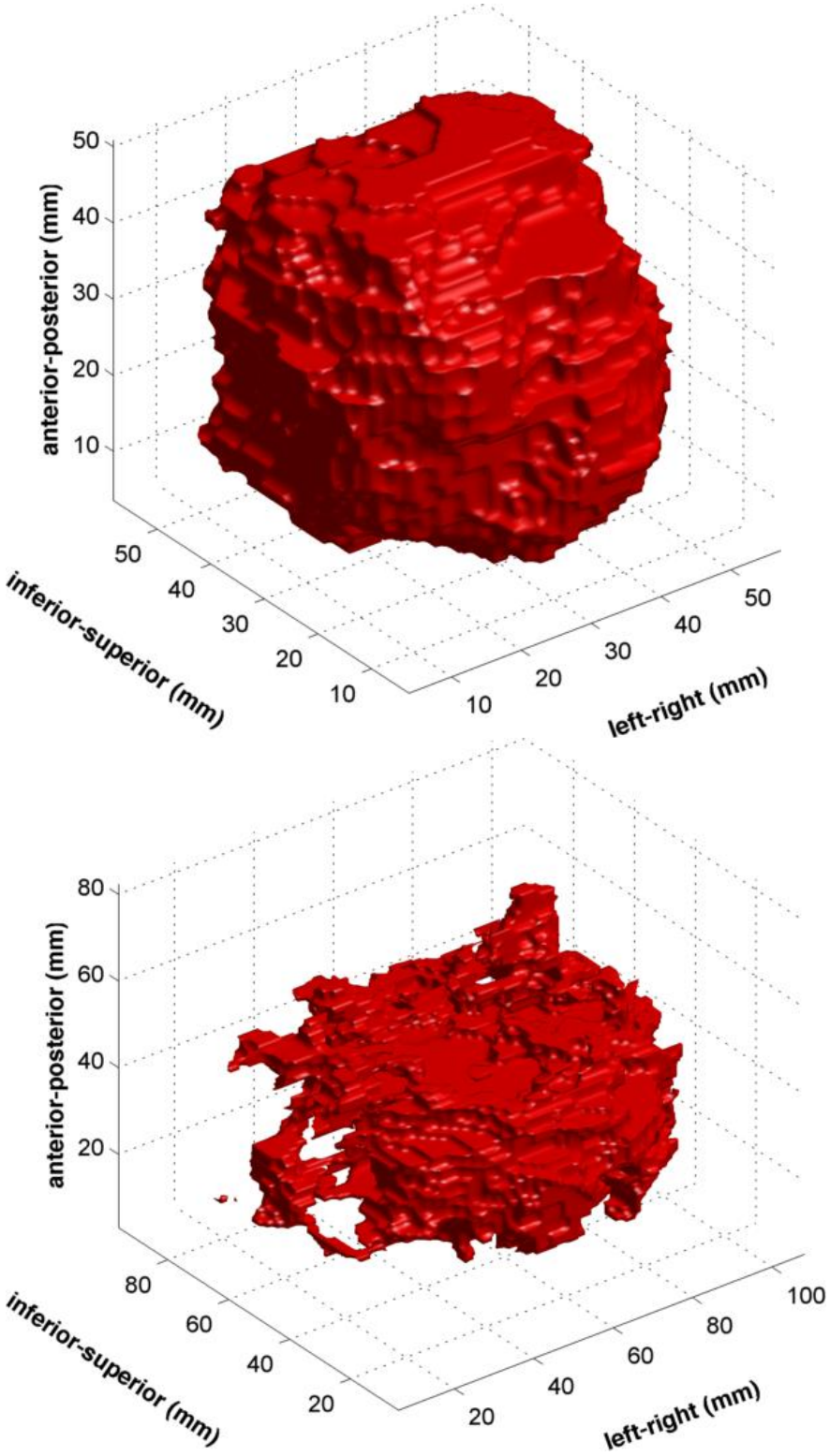

Figure-2.3: Construction of three-dimensional image for each tumour after combining tumour ROI

From these 3D images, the tumour morphology information was collected according to standard Breast Imaging-Reporting and Data System Atlas (BI – RADS) lexicon which was developed by the American College of Radiology to provide a standardised lexicon to describe the morphological and enhancement kinetics features of breast lesions. (American College of Radiology, Breast Imaging-Reporting and Data System Atlas (BI-RADS® Atlas). 2003; Erguvan-Dogan, Whitman et al. 2006) (Figure - 2.4(a), (b), (c))

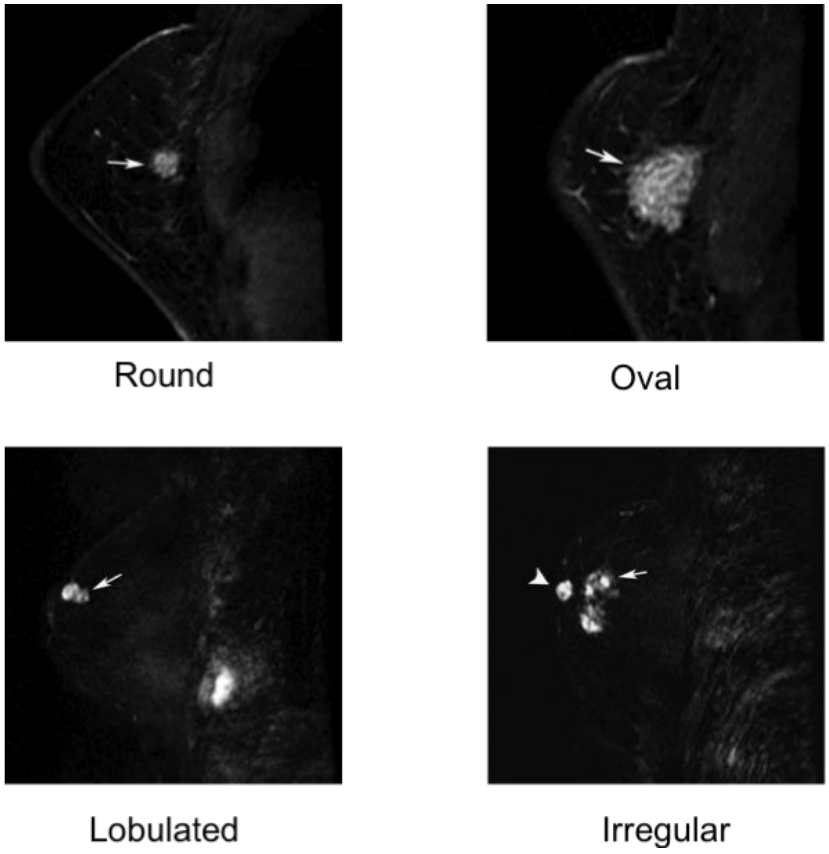

Figure-2.4(a): BI-RADS Morphological descriptors: Shape

Round- Spherical or ball-shaped

Oval- Elliptical or egg-shaped

Lobulated- Undulating contour

Irregular- Uneven shape (not round, oval, or lobulated)

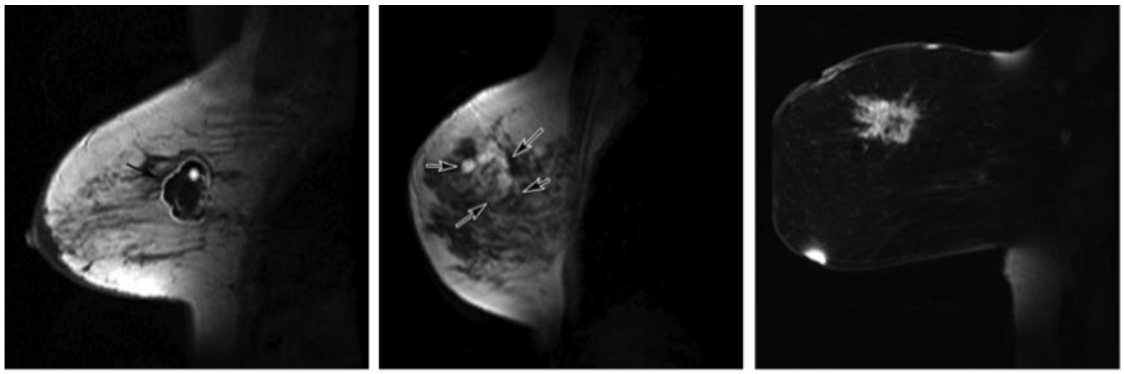

Figure-2.4(b): BI-RADS morphological descriptors: Margin

Smooth- Well demarcated and well defined

Irregular- Uneven margin can be round or jagged (not smooth or spiculated)

Spiculated- Characterized by radiating lines

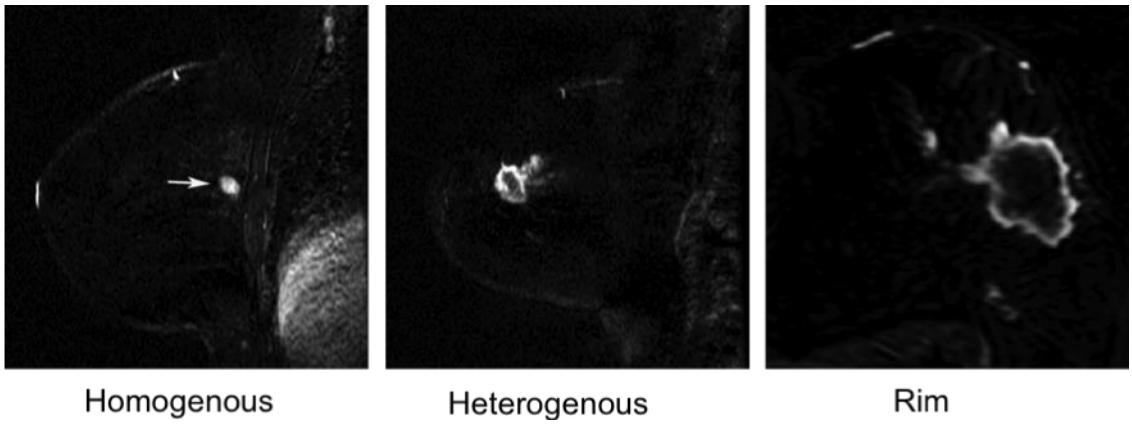

Figure-2.4(c): BI-RADS morphological descriptors: Enhancement characteristics

Homogenous- Confluent uniform enhancement

Heterogeneous- Non-specific mixed enhancement

Rim- Enhancement pronounced in the periphery of the mass

2.2.3 Pharmacokinetic modelling

This work was performed by Dr Nick Hughes (Postdoctoral Fellow, Molecular Imaging Program, Stanford University).

In summary, pharmacokinetic modelling based on the Tofts' model (Tofts, Brix et al. 1999) (Figure- 2.5) with a population-based arterial input function (modified Fritz-Hansen)(Fritz-Hansen, Rostrup et al. 1996) was used to model the contrast agent concentration time course at each tumour voxel. The resulting fitted model was then used to quantify the volume transfer constant K^{trans} (units min $^{-1}$), the rate constant k_{ep} (units min $^{-1}$) and the fractional volume of the extravascular extracellular space v_e on a voxel-wise basis within each 3D tumour ROI.

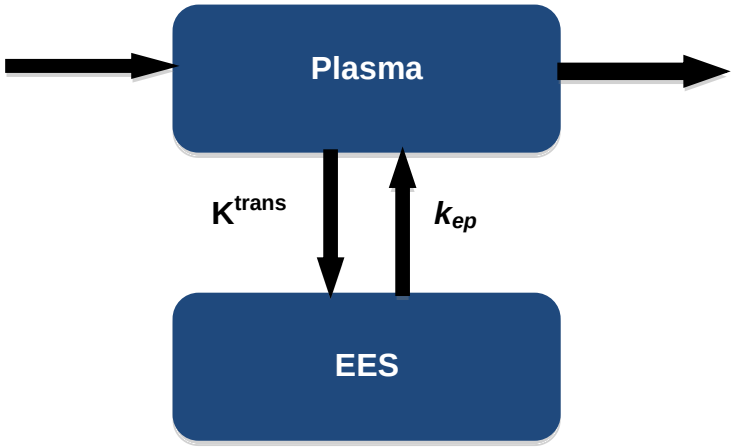

Figure-2.5: Overview of Tofts' Model for Pharmacokinetic analysis of DCE-MRI. EES- Extravascular extracellular space; K^{trans} - transfer constant from plasma to EES; k_{ep} - rate constant from EES to plasma; v_e - fractional volume of the EES

Along with these parameters for prospective study, non- pharmacokinetic parameters were also estimated. These included Initial Area under the Gadolinium Contrast Agent Concentration curve at 60 secs post-injection (IAUGC60) (Walker-Samuel, Leach et al. 2006) on a voxel-wise basis and non-enhancing fraction (NEF) (O'Connor, Jayson et al. 2007) i.e. fraction of all tumour voxels that do not show significant enhancement (defined as no statistically significant difference in the MR signal values between the pre-contrast values and the post-contrast values up to 60 secs post-injection).

2.2.4 Summary of PK parameters for analysis

For summarisation, in both retrospective and prospective study, median of the PK parameters was calculated from the voxel by voxel values over entire tumour ROI. Median was used instead of mean as median is more robust to outliers.

In addition to this for prospective study, total K^{trans} was also calculated.

$$\text{Total } K^{trans} = \sum_{i} \left\{ K_i^{trans} \right\}$$

Total K^{trans} takes into account tumour volume that might be more biological significant especially in understanding the mechanism of response to antiangiogenic therapy by integrating biomarkers.

2.3 Sample collection, processing and storage

2.3.1 Retrospective study

For all the eligible patients, the initial diagnostic core biopsy blocks were collected from the Department of Pathology, Oxford along with their corresponding diagnostic H&E slides. Dr Russell Leek (Pathologist) scored the amount of invasive tumour present in each H&E slide. The blocks with >10% invasive tumour was used for RNA extraction.

2.3.2 Prospective study

At both centres, an experienced radiologist obtained the ultrasound guided core biopsies using 14 gauge core biopsy needles with a 22mm throw from the margin of tumours. Fresh samples collected directly in RNAlater® (Applied Biosystems/ Ambion, Warrington, UK) to be used for gene expression analysis and another sample on biopsy cassettes that were immediately immersed in 50mLs of 10% Formalin in standard biopsy pot for Immunohistochemistry analysis.

I. Sample processing and storage

a) For gene expression analysis

Fresh biopsy samples were left in RNAlater® for 24hrs at 4°C and then removed and kept frozen at -80°C. All samples were shipped on dry ice to Weatherall Institute of Molecular medicine, John Radcliffe hospital, Oxford, in batches of 5 patient's samples and stored at -80°C till RNA extraction.

b) For Immunohistochemistry analysis

Sample collected in formalin at both centres were shipped within 24-72 hrs to the Department of Pathology John Radcliffe Hospital, Oxford. All samples were processed within 7 days of collection to render formalin-fixed paraffin-embedded blocks. FFPE blocks were stored at room temperature at Nuffield department of clinical lab sciences till needed for immunohistochemical analysis.

2.4 RNA extraction and Nucleic acid quantification

2.4.1 Retrospective study

From FFPE core biopsies, 5-6 Sections of 10μm thickness were cut using a microtome (Leica, Milton Keynes, UK).

RNA extraction was performed using Recover-all Total Nucleic Acid Isolation kit (Ambion, Cambridgeshire, UK) as per the manufacturer's instructions, with the exception of an initial protease digestion of 16 hours rather than 4 hours at 50°C (Figure-2.6).

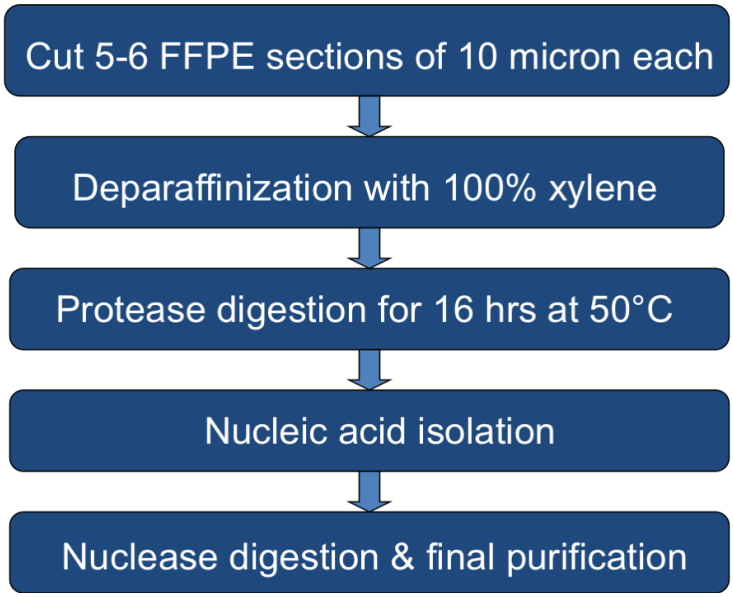

Figure-2.6: Overview of Recover All™ total nucleic acid isolation procedure

2.4.2 Prospective study

From the RNA Later fixed fresh frozen core biopsy samples, were extracted total RNA by following Departmental SOP (SOP/LAB/GF/006/01) with some modifications. This involved homogenisation; RNA extraction and RNA clean up along with DNAse treatment. A detail of the procedure followed is as mentioned below:

a) Homogenisation

For homogenisation protocol followed was as below:

1) Thaw cryovials containing samples at room temperature.
2) Once thawed tip sample onto sterile plastic Petri dish or remove sample from cryovials using sterile forceps.
3) Cut as small as possible using a sterile scalpel.
4) Add 1mL Tri®Reagent RNA isolation reagent (Sigma-Aldrich, Dorset, England) for each 50mg of sample, rounding up to nearest 50mg.
5) Pre-wash the homogenisation probes (Ultra-Turrax T8, Fisher Scientific, Leicestershire, UK) with 2 x 10 seconds bursts in 1M NaOH to inhibit RNases. Wash probes again with Diethylpyrocarbonate (DEPC) treated water then place each probe in a separate sterile tube until use.
6) Homogenise samples in Tri reagent on ice with 3 x 5 seconds bursts from the homogeniser. Repeat if sample not fully dispersed.
7) Remove sample from 50mL tube into a 1.5mL microfuge tubes, 1mL per tube.
8) Freeze aliquots in -80°C freezer or continue with RNA extraction procedure.

b) RNA extraction

For RNA extraction protocol followed was as below:

1) Thaw homogenate at room temperature. Once thawed store the homogenate for 5 minutes at room temperature to permit the complete dissociation of nucleoprotein complexes.
2) Add 0.2 mL of chloroform (BDH, UK) per 1 mL of Tri®Reagent used and shake the tubes vigorously for 15 seconds.
3) Leave at room temperature for 15 minutes
4) Centrifuge at 12000g for 15 minutes at 4°C.
5) Transfer the top colourless layer to another RNase free microfuge tube (taking care not to disturb the DNA at the interphase, leaving some sample if necessary).
6) Add 0.5 mL isopropanol and mix by inversion.
7) Leave at room temperature for 10 minutes to allow precipitation of the RNA.
8) Centrifuge at 20000g for 10 minutes at 4°C.
9) Remove supernatant by aspirating with a 1mL pipette without disturbing RNA pellet.
10) Wash the pellet by vortexing with 1 mL of 75% ethanol.
11) Centrifuge at 12000g for 5 minutes at 4°C.
12) Remove supernatant by aspirating with a 1 mL pipette and centrifuge again for 1 minute and remove residual supernatant by aspirating with a 200μl pipette.
13) Briefly air-dry the pellet for 5-10 minutes. It is important not to over-dry the RNA pellet as this will greatly decrease its solubility.

14) Dissolve RNA pellet in 30-50 μL DEPC-treated water. Gently flick the tube to ensure mixing and place immediately on ice.

c) RNA cleanup and DNAse treatment

After this, the samples were divided in 2 aliquots (10-30 μL each) depending on the RNA yield as assessed by Nanodrop machine. One aliquot was stored at -80°C for micro RNA assessments later on and other aliquot of RNA sample was cleaned and on column DNAse treated using manufacturer's protocol of RNeasy® mini kit (QIAGEN Group, West Sussex, UK) After cleaning, RNA concentrations were again assessed and samples stored at -80°C till shipment to CRUK, Gene Chip facility, Paterson Institute for Cancer Research (PICR), Manchester.

Nucleic acid quantification

From FFPE as well as fresh samples, RNA quality and quantity were confirmed using the Nano-Drop ND-1000 spectrophotometer (Thermo Scientific, Surrey, UK). Briefly, a fresh sample of distilled water was used to blank the ND-1000 before use, and then 1.0 μl sample of RNA read using setting RNA-40. A260/ 280 ratios were used for checking RNA quality. Absorbance at 260 nm (n260) was used to calculate RNA yield as follows:

RNA concentration (μg/ mL) = n260 x 40 x dilution

RNA samples were also checked on Agilent 2100 Bioanalyzer (Agilent Technologies, Santa Clara, USA) to provide total RNA and mRNA data with RNA integrity numbers (RIN) as per manufacturer's instructions using RNA 6000 Nano-chip (Agilent Technologies, Santa Clara, USA).

2.5 Gene expression arrays

For FFPE samples (retrospective study) Affymetrix Gene Chip® Human Genome U133 Plus 2.0 Array (HG-U133 Plus 2.0) was used and for fresh samples (prospective study) Affymetrix Gene Chip® Human Exon 1.0 ST Array was used. All array work was performed at CRUK, Gene Chip Facility, PICR, Manchester, UK. In summary protocol used was as follows:

2.5.1 Retrospective study

To generate amplified cDNA from FFPE-derived total RNA for gene expression analysis they were then amplified using the NuGEN WT-Ovation FFPE RNA Amplification System V2 (NuGEN Technologies, Inc, US) (Figure-2.7)

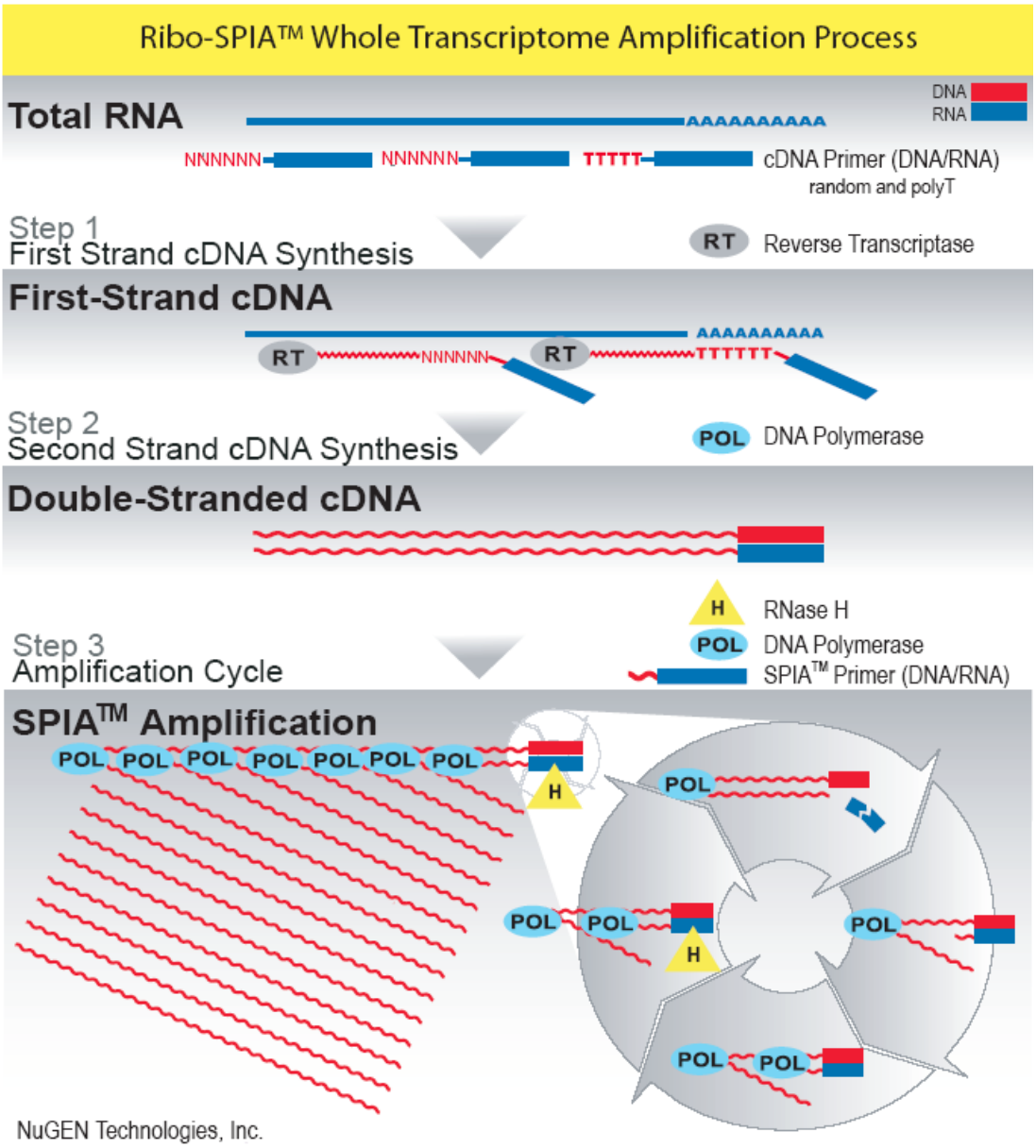

Figure-2.7: Ribo-SPIA RNA Amplification Process used in the WT-Ovation™ FFPE System V2

After that 5 µg of cDNA was biotin labelled and fragmented using the NuGEN Encore Biotin Module. This is a two-step procedure; the first step is a combined chemical and enzymatic fragmentation process that yields single-stranded cDNA products in the 50 to 100 base ranges. In the second step, this fragmented product is labelled via enzymatic attachment of a biotin-labelled nucleotide to the 3-hydroxyl end of the fragmented cDNA generated in the first

step. The resulting fragmented and labelled single-stranded cDNA target generated with the Encore Biotin Module was then hybridised to Human genome U133 plus 2 arrays using the standard Affymetrix protocols (http://www.affymetrix.com/support/technical/manual/expression_manual.affx).

In summary, this involved preparation of NuGEN cocktail, hybridisation and scanning which was performed in the Affymetrix Gene Chip Scanner 3000 system with Autoloader. Data collection and management was performed in the Affymetrix Gene Chip Operating Software (GCOS).

2.5.2 Prospective study

After initial quality and quantity checks, RNA samples were amplified using the NuGEN Pico WTA kit (NuGEN Technologies, Inc, US) to produce amplified cDNA. Sense transcript cDNA (ST- cDNA) was then generated using the NuGEN WT-Ovation™ Exon Module Version 1.0 (NuGEN Technologies, Inc, US). 3µg of amplified cDNA used for this purpose. ST-cDNA was then Biotin labelled and fragmented using the NuGEN Encore™ Biotin Module (NuGEN Technologies, Inc, US) as mentioned above for FFPE samples, before being hybridised to Human Exon array 1.0 ST arrays using the standard Affymetrix protocols.
(http://www.affymetrix.com/support/technical/manual/expression_manual.affx).

In summary, this involved NuGEN Exon Cocktail preparation, NuGEN Exon Hybridisation and scanning which was performed in the Affymetrix Gene Chip

Scanner 3000 system with Autoloader. Data collection and management was performed in the Affymetrix Gene Chip Operating Software (GCOS).

2.6 Gene expression analysis

This work was performed by experienced bioinformatician Dr Francesca Buffa. The gene expression analysis of the retrospective study was performed by Dr Laura Winchester under the supervision of Dr Francesca Buffa.

2.6.1 Gene expression array processing

Retrospective study

Affymetrix U133 plus 2 CEL files were processed using gCRMA (Wu JZ 2002) quantile normalised and logged base 2.

Prospective study

Only core probes were considered initially and analysis focus was gene-level expression of known genes. Signals were estimated using IterPLIER. This is a variation of PLIER that iteratively discards probes that do not correlate well with the overall gene-level signal.

(http://media.affymetrix.com/support/technical/technotes/plier_technote.pdf)

Gene-level signals were also estimated using RMA (Irizarry, Ooi et al. 2003) and key results were similar. Data were quantile normalised and logged base 2. Data were then filtered using data above background p-values to removes low intensity signals which could produce low trust/misleading results. All processing was performed in R using Bio-conductor packages. Annotation was performed using Affymetrix services, NetAffx™ (http://www.affymetrix.com/analysis/index.affx) via R.

2.6.2 Gene expression: Statistical analyses

For the prospective study, pre- and post-samples for each patient were paired. A permutation based paired t-test method was used which was corrected for heteroscedasticity of gene expression distributions (Tusher, Tibshirani et al. 2001). Local false discovery is estimated (Tibshirani and Efron 2002) and cluster transcripts with false discovery rate <5% are extracted. The differential expression analyses before and after treatment was performed at the single gene level and at metagene level (phenotype and pathway activation changes). A specific breast cancer hypoxia signature (Buffa, Harris et al. 2010), proliferation signature (Desmedt, Haibe-Kains et al. 2008), angiogenesis signature (Masiero, Simoes et al. 2013) and a recently published anti-VEGF signature (Genentech Inc., South San Francisco, CA, US) (Bais, Singh et al 2011) were used to analyse the effect of bevacizumab on these important pathways. Genes in the signatures were re-annotated to arrays using Affymetrix annotation services (NetAffx). In each sample, the expression distribution of these genes was considered and the median expression of the gene expression was calculated when summarisation score was needed. Gene signature summary expression scores were estimated as described previously (Buffa, Camps et al. 2011).

Statistical analyses were performed in R 2.11.1 and PAWS 18. Statistical tests comparing gene expression, signatures and other variables before and after treatment were t-test, Wilcox test and modified t-test as in Significance Analysis of Microarrays (Tusher, Tibshirani et al. 2001; Storey and Tibshirani

2003). All these tests were paired. Local false discovery and Q-values were computed and the threshold for considering a gene significant was 5%, unless otherwise stated. Pearson's product-moment and Spearman rank correlation analyses were performed to study the association of genes with clinical variables, IHC results and MRI parameters. Hierarchical clustering with optimisation of the number of clusters was used as implemented in PAWS 18 (Two Step algorithm). To determine the number of independent clusters, the Balanced Iterative Reducing and Clustering using Hierarchies (BIRCH) (Zhang, Ramakrishnan et al. 1996) method was used together with a Bayes information criterion.

Biological processes and pathway analyses were performed using Genecodis 3.0 (Nogales-Cadenas, Carmona-Saez et al. 2009; Tabas-Madrid, Nogales-Cadenas et al. 2012). Gene set analyses were performed using the Bioconductor implementation of the gene set enrichment algorithm by Subramanian et al (Subramanian, Tamayo et al. 2005); pathway tested for enrichment were all the Biocarta pathways (http://www.biocarta.com/) and the aforementioned signatures; all pathway and signature genes were annotated to Ensembl using biomart (http://www.biomart.org/). All bioinformatics analyses except from the two-step clustering were performed in R (http://cran.r-project.org/).

2.7 Real-time quantitative polymerase chain reaction (qRT-PCR)

To confirm the gene expression results, the quantitative real-time PCR (qRT-PCR) from both retrospective and prospective study samples were performed using the same cDNA as used for the affymetrix gene expression array work performed at PICR, Manchester. From the prospective clinical study samples, cDNAs were diluted to a concentration of 10ng/µL, but for the retrospective FFPE samples cDNA concentration used was 5 ng/µL due to constraints in sample amounts.

For each gene of interest (see Table- 2.1 and 2.2) primers were designed using Roche Applied Sciences assay designing tool (https://www.roche-applied-science.com/sis/rtpcr/upl/index.jsp?id=uplct_030000).

Heat shock 90kDa protein 1 beta (HSPCB), Ubiquitin C (UBC) and Ribosomal protein L13a (RPL13A) were used as housekeeping genes in the prospective study and in the retrospective study only HSPCB was used as a housekeeping gene due to the large variation in expression of RPL13A and UBC.

Table-2.1: Details of primer sequences for genes of interest (Retrospective study)

Gene Symbol	Gene Name	Primer sequence	Probe ID
HSPCB	Heat shock 90kDa protein 1 beta	L: AGCCTACGTTGCTCACTATTACG R: GAAAGGCAAAAGTCTCCACCT	55
SLC31A2	Solute carrier family 31 (copper transporters) member 2	L: TGACTCGGAGCGAGGAGA R: CTGTATCTGAGAAGATGAAATGC	81
IGF2R	Insulin-like growth factor 2 receptor	L: TCTCCAGTGGACTGCCAAGT R: GTGCTTAGGCCAGTCAGGTC	20
SGK1	Serum/ glucocorticoid regulated kinase1	L: TTTCCAAAGAGGGGTTCTCC R: TGGCATGATTACATGGCTCT	2
PDK1	Pyruvate dehydrogenase kinase isozyme 1	L: CACCAAGACCTCGTGTTGAG R: ACGTGATATGGGCAATCCAT	20
IL6R	Interleukin 6 receptor	L: TGTATTGAAGAGGGTTGTTTTCC R: GGATGTATACCTGTGTACGCTGA	26
CD44	CD44 molecule (Indian blood group)	L: CAACAACACAAATGGCTGGT R:CTGAGGTGTCTGTCTCTTTCATCT	40
SLC16A1	Solute carrier family 16 member1 (monocarboxylic acid transporter1)	L: GTGACCATTGTGGAATGCTG R: CATGTCATTGAGCCGACCTA	49
EIF2AK2	Eukaryotic translation initiation factor 2-alpha kinase 2	L: GGGAAAACGAAACTGAGAACC R: TCCAGGAAGGCAAACTGAAT	50
ALDH1A3	Aldehyde dehydrogenase 1 family member A3	L: TGGTGGCTTTAAAATGTCAGG R: TATTCGGCCAAAGCGTATTC	53

Table-2.2: Details of primer sequences for genes of interest (Prospective study)

Gene Symbol	Gene Name	Primers for PCR	Probe ID
HSPCB	Heat shock 90kDa protein 1 beta	L: AGCCTACGTTGCTCACTATTACG R:GAAAGGCAAAAGTCTCCACCT	55
UBC	Ubiquitin C	L: AGGCAAAGATCCAAGATAAGGA R: GGACCAAGTGCAGAGTGGAC	11
RPL13A	Ribosomal protein L13a	L: CAGCGGCTGAAGGAGTACC R: GGTGGCCAGTTTCAGTTCTT	60
ESM1	Endothelial cell-specific molecule1	L: CATGGATGGCATGAAGTGTG R: GTGCCGTAGGGACAGTCTTT	30
SULF1	Sulfatase 1	L: CAGACAGCCTGTGAACAACC R: ATTCGAAGCTTGCCAGATGT	29
CCNE1	Cyclin E1	L: GGCCAAAATCGACAGGAC R: GGGTCTGCACAGACTGCAT	36
SPRY4	Sprouty homolog 4 (Drosophila)	L: CCTGCAGCTCCTCAAAGG R:TGACTGAGTTGGGAGTCAAGG	19
FLT-1	Fms-related tyrosine kinase1	L: CCACTCCCTTGAACACGAG R: GTCGCCTTACGGAAGCTCT	85
PDK1	Pyruvate dehydrogenase kinase, isozyme1	L: CACCAAGACCTCGTGTTGAG R: ACGTGATATGGGCAATCCAT	20
PDE3B	Phospho-diesterase 3B, cGMP-inhibited	L:AACAATGGTATAAGCCTCATTATCAA R: CGAGCCTCATTTAGCACTGA	10
VEGFA	Vascular endothelial growth factor A	L: CCTTGCTGCTCTACCTCCAC R: CCACTTCGTGATGATTCTGC	29
PPARG	Peroxisome proliferator-activated receptor gamma	L:GACAGGAAAGACAACAGACAAATC R: GGGGTGATGTGTTTGAACTTG	7
ANGPTL4	Angiopoietin-like 4	L:GACAAGAACTGCGCCAAGA R: GCCGTTGAGGTTGGAATG	75
PIK3IP1	Phosphoinositide-3-kinase interacting protein1	L:GCTCCTAGCAGAAGCCTATGG R: TCTGGTCCTCCCGGTACA	75
CTLA4	Cytotoxic T-lymphocyte-associated protein 4	L: TTCATCCCTGTCTTCTGCAA R: AGTGGCTTTGCCTGGAGAT	40
PIK3CG	Phosphoinositide 3 kinase, catalytic, gamma polypeptide	L: CCTCAACCATGAAGGAAACC R: GGCAGTTGTCCTCTCTCAGC	78

A master mix of each gene was prepared (see Table- 2.3) using specific primers (Invitrogen, Paisley, UK), SensiMix Probe (Bioline, London, UK), Nuclease free water and specific probe from the Roche Universal probe Library (Roche applied Sciences, UK). 2ng of cDNA was added per reaction and each cDNA was analysed in triplicate for each gene.

Table-2.3: Components of Master-mix for each gene

Component	Volume per reaction
SensiMix	5 µl
Forward Primer (10 µM)	0.5 µl
Reverse Primer (10 µM)	0.5 µl
Probe	0.125 µl
Nuclease-free water	1.875 µl

PCR reactions were prepared in 384 well plates by CAS-1200 Liquid Handling System (Corbett Robotics, Qiagen, UK). RT-PCR reactions were run in the 7900HT Real Time PCR System (Applied Biosystems, UK)

Results were analysed using $\Delta\Delta$ CT method with normalisation to relevant housekeeping gene(s). The housekeeping genes used in this study were identified as those which had the least variation from analysis of the affymetrix whole genome expression analysis (Table-2.4). Data for each gene was normalised to the average expression of the pre-treatment samples.

Table-2.4: Genes analysed to search for housekeeping genes

Name	Cluster ID	FC_summ	min_summ	t_test	Ref Seq
ACTB	3036924	6.96	5.28	0.06	NM_001101
RPL11	2325192	3.41	8.78	0.73	NM_001199802
TBP	2937984	4.74	4.58	0.24	NM_003194
HMBS	3351841	2.18	4.54	0.83	NM_000190
HPRT1	3991698	4.70	5.37	0.50	NM_000194
HSPCB	2908474	2.41	10.56	0.18	NM_007355
SDHA	2798538	6.27	3.08	0.84	NM_004168
UBC	3476741	1.55	11.20	0.53	NM_021009
GUSB	3053691	4.99	5.87	0.07	NM_000181

2.8 Immunohistochemistry

From the prospective study FFPE samples, IHC for carbonic anhydrase 9 (CA-9), hypoxia inducible factor 1 alpha subunit (HIF-1α), vascular endothelial growth factor A (VEGFA), vascular endothelial growth factor receptor 2 (VEGFR2/KDR) tumour, KDR vessel, proliferation marker (Ki67), and plasmalemma vesicle-associated protein (PLVAP) were performed by Dr Helen Turley (Oxford) / Dr Adrian Jubb (Genentech).

In summary, 4 µm tissue Sections of FFPE blocks (both pre bevacizumab and post bevacizumab) were mounted onto slides. After dewaxing, all slides underwent antigen retrieval. In brief, antigen retrieval was performed in target

retrieval solution (Dako, Carpinteria, CA, USA) using a Decloaking Chamber (Biocare Medical, Concord, CA, USA). For HIF-1α this involved steaming under pressure at 15 psi for 3 minutes in a buffer of Tris EDTA (pH 9.0; Sigma, St. Louis, MO). Sections were incubated for 16h at 4ºC with the primary antibody at 1µg/mL. Bound antibody was labelled with Novolink polymer (Leica Microsystems, Bannockburn, IL, USA), visualised using 2, 3-diaminobenzidine (DAB) chromogen and counterstained with haematoxylin.

Antibodies used for VEGF (clone VG1 ABCAM) (Turley, Scott et al. 1998; Boddy, Fox et al. 2005), HIF-1α (clone 54, BD Transduction Laboratories, San Jose, CA, USA), carbonic anhydrase 9 (CA-9) (clone M75, a gift from Professors S Pastorekova and J Pastorek, Institute of Virology, Slovak Academy of Sciences, Bratislava, Slovak Republic) (Pastorekova, Zavadova et al. 1992; Loncaster, Harris et al. 2001), vascular endothelial growth factor receptor 2 (VEGFR2/ KDR) (Cell Signalling 55B11 Ab) (Smith, Baker et al. 2010) and for proliferation marker (ki67) (SP6 antibody, 1:200, rabbit monoclonal, Neomarkers, Thermo Fisher Scientific, Kalamazoo, MI, USA) (Fodor, Hutchins et al. 2012). For PLVAP, the anti-human PLVAP monoclonal antibody (MAb; 10D4.1.2) was used at 10 µg/mL concentration (Strickland, Jubb et al. 2005). Validation of all antibodies has been previously undertaken and published by our group or Genentech using cells transfected with the relevant targets (Pastorekova, Zavadova et al. 1992; Turley, Scott et al. 1998; Loncaster, Harris et al. 2001; Boddy, Fox et al. 2005; Strickland, Jubb et al. 2005; Smith, Baker et al. 2010; Fodor, Hutchins et al. 2012).

Staining was scored by Dr Adrian Jubb. For CA-9 and HIF-1α cytoplasmic and nuclear staining was used and the percentage of positive cells was scored as a continuous variable. For VEGFA and VEGFR2/ KDR cytoplasmic and membranous tumour immunoreactivity was scored with an H score i.e. 1x% cells scored 1 + 2x% cells score 2 + 3x% cells scored 3, which gives a continuous score on scale of 0-300. For KDR, vessel endothelial immunoreactivity was also scored as intensity (0=none, 1=weak, 2=moderate, 3=strong). For Ki67 - Tumour cell nuclear immunoreactivity was scored as the percentage of Ki67 positive cells in each sample. For PLVAP – vessel endothelial cell immunoreactivity was scored using an automated algorithm performed on scanned slide images as a percentage of the total tumour area.

2.9 Statistical methods

As mentioned in subsequent chapters, changes in gene expression median score at the single gene level for some specific genes and in the median scores of gene signatures, changes in MRI parameters, changes in immunohistochemistry parameters scores after bevacizumab were analysed using a paired non-parametric method (Wilcoxon-signed rank test). The correlation analyses between gene expression scores, MRI parameters, clinical variables, IHC parameters scores were also performed using non-parametric methods (Spearman test for continuous variables, Mann-Whitney test or Kruskal-wallis for categorical variables). Graphpad PRISM version 4.0c and R version 2.13.0 were used for these analyses.

CHAPTER THREE

3 Correlation of DCE-MRI and Gene Expression in a Retrospective study of Primary Breast cancer patients treated with Neo-adjuvant Chemotherapy

3.1 Introduction

Magnetic Resonance Imaging (MRI) is a commonly used imaging technique in the management of breast cancer for diagnosis, staging and monitoring response to chemotherapy (Chen, Mehta et al. 2007; Ah-See, Makris et al. 2008; Chen, Feig et al. 2008; Turkbey, Thomasson et al. 2009). The use of DCE-MRI techniques can also allow evaluation of anatomical and physiological characteristics simultaneously. There are several studies that show detailed analysis of DCE-MRI characteristics could have predictive value in assessment of responses to neoadjuvant chemotherapy in breast cancer (Li, Makris et al. 2011; Dongfeng, Daqing et al. 2012; Li and Padhani 2012; Marinovich, Sardanelli et al. 2012).

Genome wide gene expression profiling also has been widely used for predicting response to chemotherapy (van 't Veer, Dai et al. 2002; Zembutsu, Suzuki et al. 2009; Straver, Glas et al. 2010; Kolacinska, Fendler et al. 2012). Furthermore, there are several studies highlighting that informative RNA expression analysis could be derived from archived FFPE samples (Coudry, Meireles et al. 2007; Penland, Keku et al. 2007). Studies have shown that gene expression derived from these FFPE samples could be used to predict response to chemotherapy (Gianni, Zambetti et al. 2005; Chang, Makris et al. 2008; Sadi, Wang et al. 2011). However, to date, little work has been reported to correlate the gene expression with MRI features especially in breast cancer patients (Yamamoto, Maki et al. 2012).

Several studies have recently introduced novel methods for correlating unique features of tumour morphology and physiology through non-invasive imaging with specific patterns of gene expression on a genome-wide scale, thereby introducing the field of “radio-genomics” (Rutman and Kuo 2009). Radio-genomic studies correlating imaging features to global gene expression patterns in hepatocellular carcinoma and glioblastoma multiforme have shown that the global genomic activity of tumours can be extracted from imaging (Kuo, Gollub et al. 2007; Diehn, Nardini et al. 2008). However, despite the possibility of detailed noninvasive characterisations by modern MR breast imaging techniques, only one pilot study published after completion of this work has evaluated whether imaging can capture the gene expression profiles of breast cancer (Yamamoto, Maki et al. 2012).

In view of these issues, I decided to do a pilot study by retrospectively collecting the data of breast cancer patients treated with neoadjuvant chemotherapy in our department, between 2001- 2008, for whom DCE-MRI and core biopsy samples were available at baseline. The main aim of this study was to determine whether routine low temporal resolution DCE-MRI imaging could potentially reveal correlations with the genomic diversity in breast cancer as assessed by genome wide expression analysis using archived FFPE samples.

3.2 Study summary

The newly diagnosed primary breast cancer female patients who were referred to the Department of Medical Oncology, Churchill hospital, Oxford, for neoadjuvant chemotherapy from April 2001 to Dec 2008 were considered for this study. Based on selection criteria (as mentioned in Chapter 2, Section 1) a total of seventy-two patients were initially identified for this study. However, nine patients were subsequently excluded due to the lack of adequate tissue for analysis and two patients due to poor quality MRI. Sixty-one patients were considered eligible for final analysis (Figure-3.1).

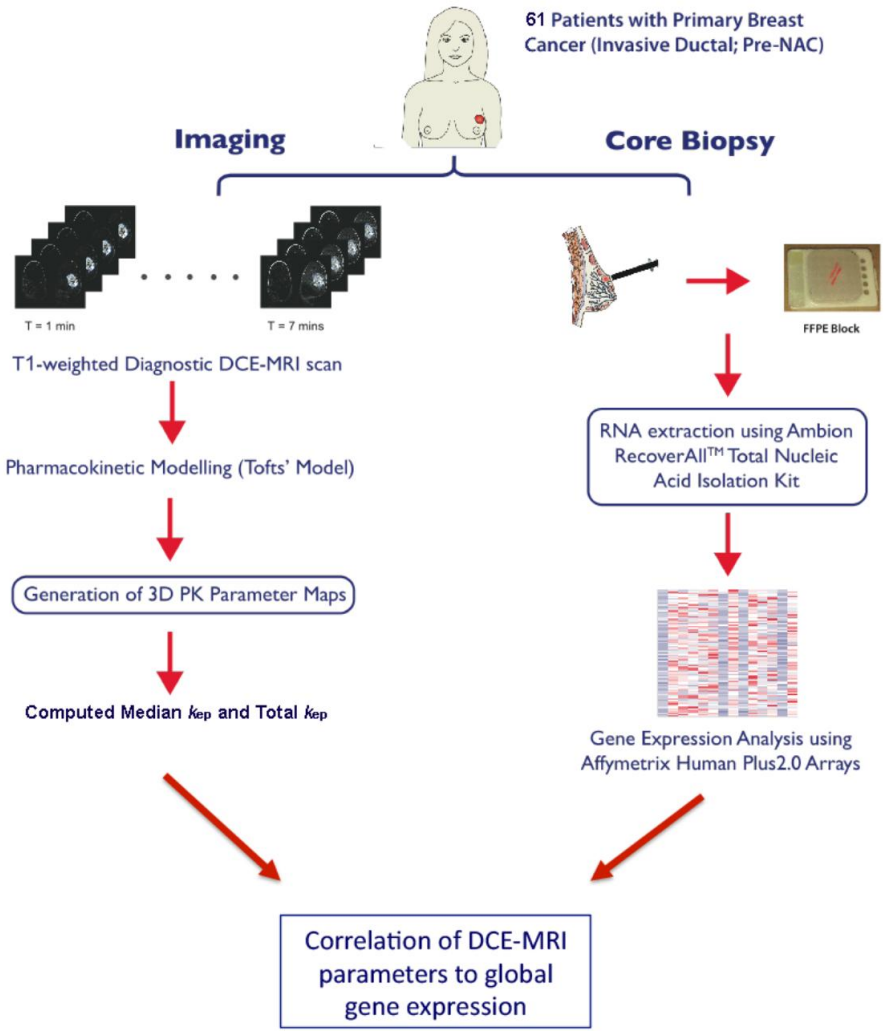

Figure-3.1: Summary of study procedures

3.3 Patient characteristics

All were female breast cancer patients with ductal subtype of cancer. Median age was 44 years. 23/61 patients were HER2 receptor positive, 51/61 were positive for ER and 41/61 were positive for PR. 8 patients were triple receptor negative. Median maximum diameter was 60 mm as per clinical assessment, and on MRI assessment the median volume of tumour was 38.5 cm^3. Patient received chemotherapy every three weeks for a total of 6 cycles. For assessing the initial response to chemotherapy, interim MRI was done after 3 cycles of chemotherapy. Interim MRI response was available for 49/61 patients. As assessed by interim MRI scans, using RECIST criteria (Eisenhauer, Therasse et al. 2009) only 8 patients had complete response. There was a variation in the chemotherapy regimen over these years; however, the first 3 chemotherapy cycles were with a FEC (5-Flourouracil, epirubicin and cyclophoshamide) regimen for all the patients but with different epirubicin doses (please see details in Table- 3.1). Although 23 patients were HER2 positive in this study data set, trastuzumab was given only to 18 patients (not given to patients before November 2004). 18 patients had lumpectomy and 41 patients had mastectomy, one patient had inoperable tumour and data not available for one patient. After surgery, 6 patients had complete pathological response and 6 patients had near to complete pathological response with scattered cells only either in the breast mass or lymph nodes. Follow-up data was collected until April 2012. Out of 61 patients, 15 had relapsed and 11 patients were dead, all deaths were due to cancer related causes (Please see Table- 3.1 for summary).

Table-3.1: Summary of Patient characteristics

Median Age (Range)	44 yrs (22-66 yrs)
Histology	Ductal (n=61)
Receptor status	HER 2 (Positive 23, negative 38) ER (Positive 51, negative 10) PR (Positive 41, negative 20) Triple negative (8)
Median max. diameter at baseline (Clinical measurement) (Range)	60 mm (30mm-140mm)
Median Tumour volume at baseline MRI (Range)	38.5 cm^3 (7.8cm^3-240.2 cm^3)
Inflammatory breast cancers	n=3
Lymph node status at baseline[1]	N0 (n=29), N1 (n= 23), N2 (n=6), N3 (n=2), n/a (n=1)
Chemotherapy[2,3]	FEC (60) x6 (n=8), FEC (60) x 4 (n=1) FEC (75) x 6 (n=6), FEC (75) x 4 (n=1) FEC (75) x 4+ Dtx (75) x 4 (n=14) FEC (75) x 4+ Dtx (75) x 4+ Tzb (n=8) FEC (100) x3+ Dtx (100) x 3 (n=13) FEC (100) x6 +Tzb (n=1) FEC (100) x3+ Dtx (100) x3 +Tzb (n=9)
Interim MRI response after 3 cycles of chemotherapy (RECIST)	CR (n=8), PR (n=35), SD (n=5), PD (n=1)
Surgery	Mastectomy (n=41) Lumpectomy (n=18) Not done (n=1), n/a (n=1)
Number of Lymph nodes (final pathology)	0 (n=30), 1-3 (n=21), >4 (n=8), n/a (n=2)
Complete Pathological response (pCR)	pCR (n=6) and near to pCR[4] (n=6)
Follow-up	Relapse (n=15), Dead (n=11)

1. N defined as per AJCC 2002 breast cancer staging (Singletary, Allred et al. 2002).
2. FEC (60/ 75/ 100): 5FU, Epirubicin (60mg/m^2 or 75 mg/m^2 or 100mg/m^2) and Cyclophosmide; Dtx (75): Docetaxel 75 mg/m^2; Tzb: Trastuzumab
3. 'x' followed by number signified number of cycles of chemotherapy.
4. Near to pCR means only scattered cells in the final pathology

3.4 DCE-MRI analysis

Using the BI-RAD system (2003; Erguvan-Dogan, Whitman et al. 2006), the most common shape observed was irregular (41/61), most of the tumours had an irregular margin (43/ 61) and were heterogeneously enhanced with contrast in MRI assessments (33/ 61) (see Table- 3.2 for details).

Table-3.2: MRI characteristics based on BI-RADS classification

BI-RADS classification		No. of patients
Shape	Irregular	41
	Lobulated	17
	Oval	3
Margin	Irregular	43
	Smooth	15
	Spiculated	3
Enhancement characteristics	Heterogeneous	33
	Homogeneous	16
	Rim	12

3.4.1 Pharmacokinetic analysis DCE-MRI data

Pharmacokinetic analysis was done using Toft's model (Tofts, Brix et al. 1999) (details as mentioned in Chapter 2, Section 2). Only the low temporal resolution diagnostic scans were available for these patients. We simulated 10,000 enhancement curves at a temporal resolution of 1 sample / minute and investigated the accuracy with which the different PK parameters could be estimated. Our simulations showed that the "washout" rate constant k_{ep} (units:

min^{-1}) could be reliably estimated from the low temporal resolution scans in the retrospective data set (Figure - 3.2).

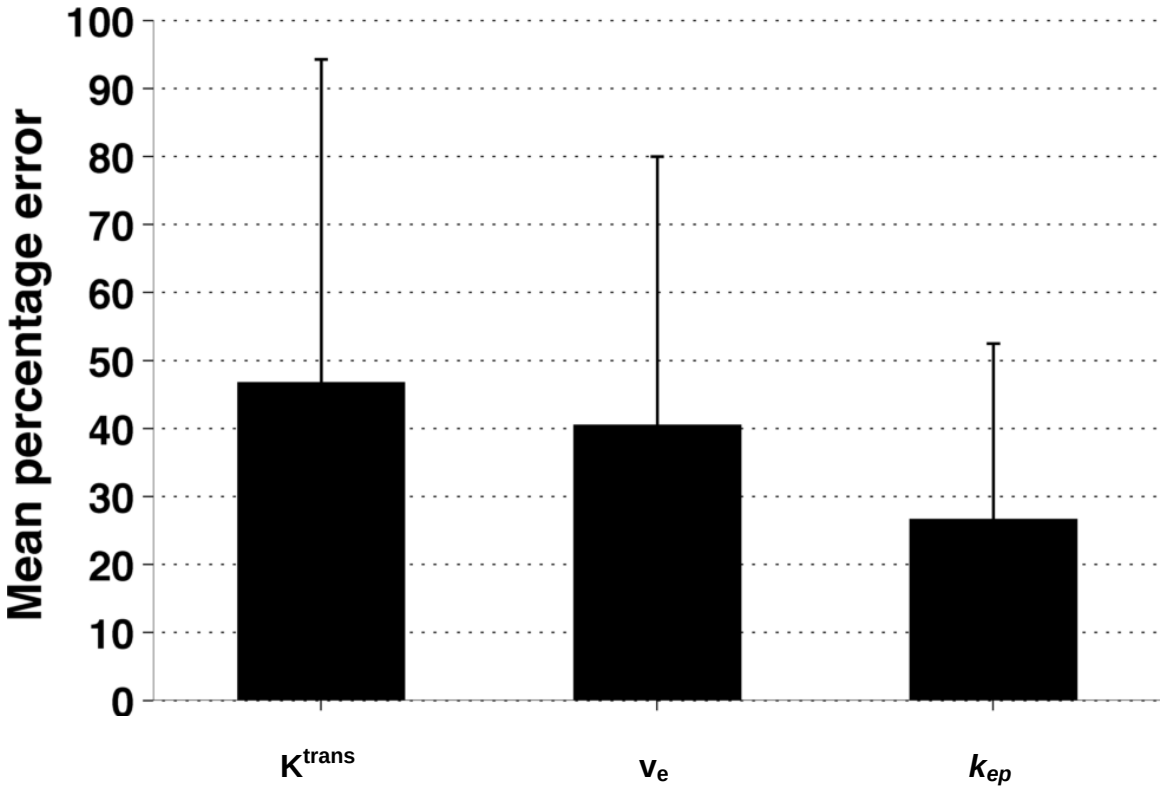

Figure-3.2: Graph showing mean percentage error vs. PK parameters (mean±SD). Mean percentage error was significantly lower for k_{ep} in comparison to K^{trans} and v_e for this study data set.

3.4.2 Three-dimensional pharmacokinetic maps

After calculating the k_{ep} of each voxel 3D PK maps were generated to understand the inter-tumoural as well as intra-tumoural variation in the wash out rate constant k_{ep}. A wide variation in the k_{ep} was noted among different voxels over the entire tumour (Figure-3.3).

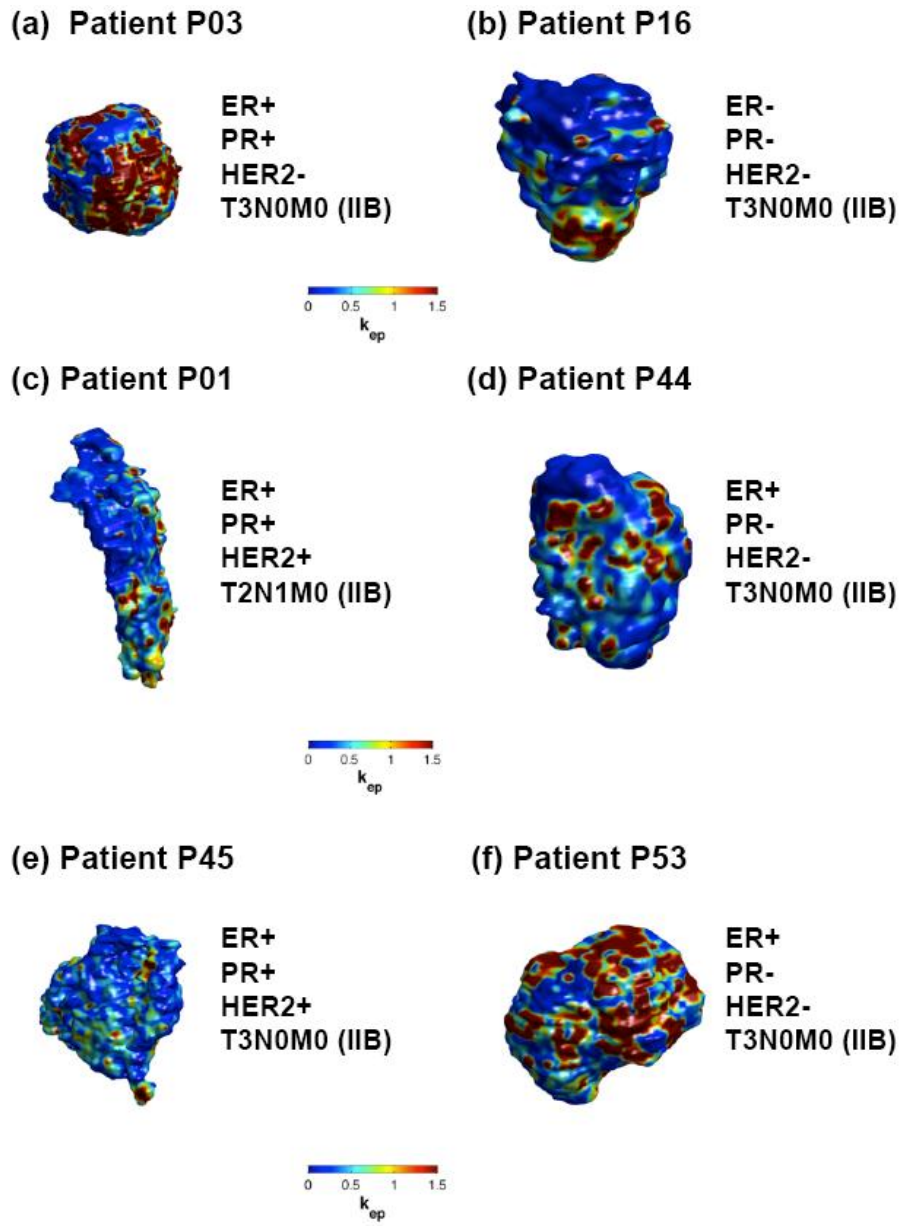

Figure-3.3: Three-dimensional PK mapping of tumour k_{ep} over the entire tumour. Inter-tumoural as well as intra-tumoural variation was noted in $k_{ep.}$ ER, PR and HER2 status of each tumour were shown along with their stage at presentation.

3.4.3 Summarisation of PK analysis

To summarise the DCE-MRI PK analysis data, median k_{ep} was computed over the entire tumour volume of interest (VOI). Similarly, as seen with PK maps a wide variation in the median k_{ep} (median= 0.585, range = 0.87 to 1.85) was noted among these patients (Figure- 3.4).

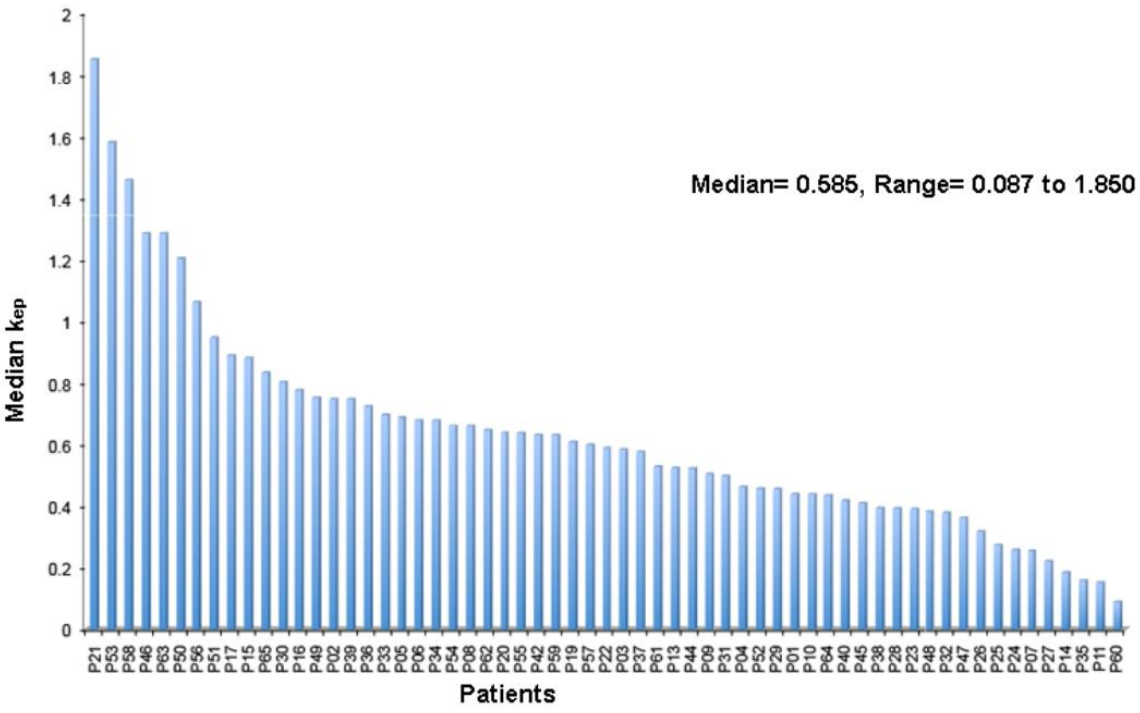

Figure-3.4: Waterfall plot showing the variation in median k_{ep} over all the study patients.

3.5 Relationship between PK parameters and BI-RADS classification

Interestingly, the median k_{ep} level in patients with a lobulated shape tumour was significantly higher than those with an irregular shape (Mann-Whitney test, P= 0.005). Similarly, tumours with a smooth margin had significantly higher median k_{ep} than those with an irregular margin (Mann-Whitney test, P= 0.01). Also the median k_{ep} levels in patients with homogenously enhancing tumours were significantly higher than those with heterogeneous and rim-enhancement (Kruskal-Wallis test, P=0.02; Dunn's Multiple Comparison Test; Homo vs. Hetero (P<0.05), Rim vs. Hetero (P>0.05), Homo vs. Rim (P>0.05)) (Figure-3.5).

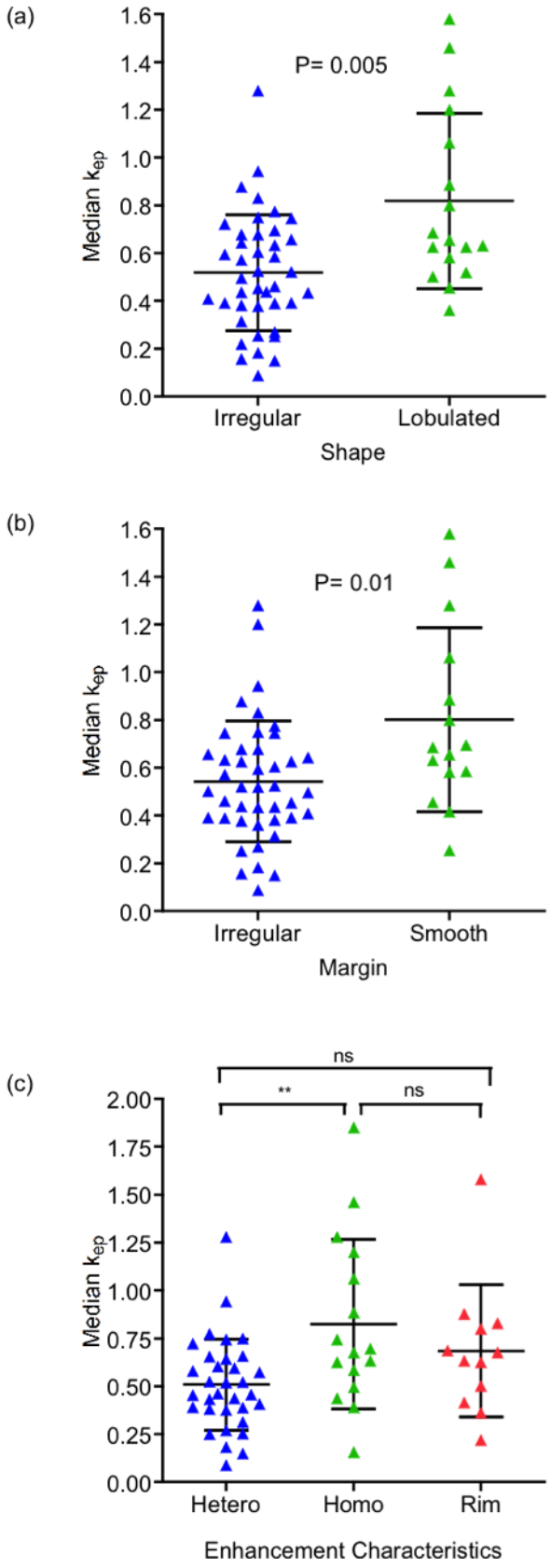

Figure-3.5: Relationship of median k_{ep} and BI-RADS classification.
(a) Shape (b) Margin (c) Enhancement characteristics.
(Error bars show mean± SD)

3.6 Relationship between PK parameters and the clinical/ pathological prognostic factors in breast cancer

We were interested to establish whether there was any difference in median k_{ep} in terms of different subtypes based on receptor status (ER/ PR/ HER2 status) and other clinical and pathological prognostic factors (age, grade, size of tumour, stage at presentation) in breast cancer. Interestingly, a weak but significant positive correlation between the age of patients and median k_{ep} (Spearman r= 0.33, P= 0.009) was observed i.e. the older the patients the higher was the median k_{ep} (Figure-3.6).

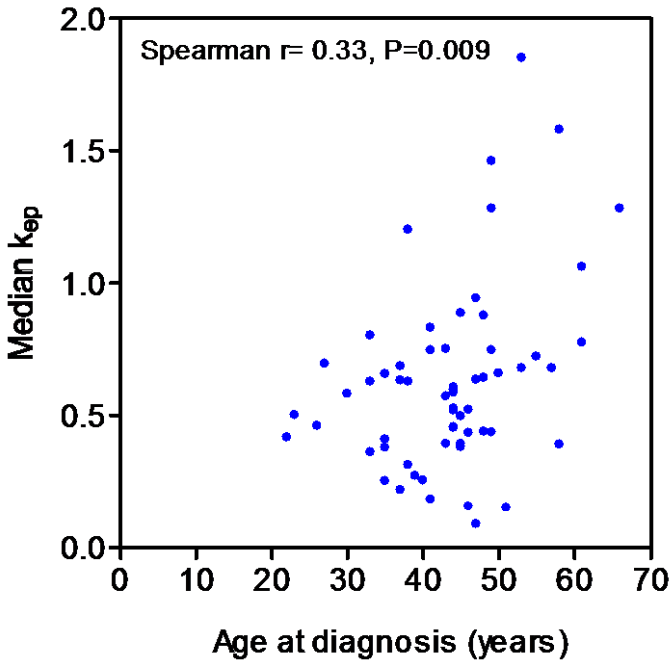

Figure-3.6: Correlation of age at diagnosis with median k_{ep}

There was no significant difference in median k_{ep} in subgroups of patients based on ER status (Mann-Whitney test, P=0.37), HER2 status (Mann-Whitney test, P= 0.34), or tumour volume as measured by MRI (Spearman r = - 0.12, P= 0.35) or stage at presentation (Mann-Whitney test, P= 0.42).

It is well known that PR is an oestrogen-regulated gene, and its synthesis in normal and cancer cells requires oestrogen and ER (Cui, Schiff et al. 2005). Further analysis was done to assess difference in median k_{ep} in ER+PR+ (n= 40), ER+PR- (n=11) and ER-PR- (n= 9) subgroups. As expected, there was only one patient with ER-PR+ status so she was not included in the analyses. Interestingly, median k_{ep} was significantly higher in ER+PR- group in comparison to ER+PR+ group (P=0.003, Kruskal-Wallis test, P<0.01, Dunn's multiple comparison test) (Figure- 3.7).

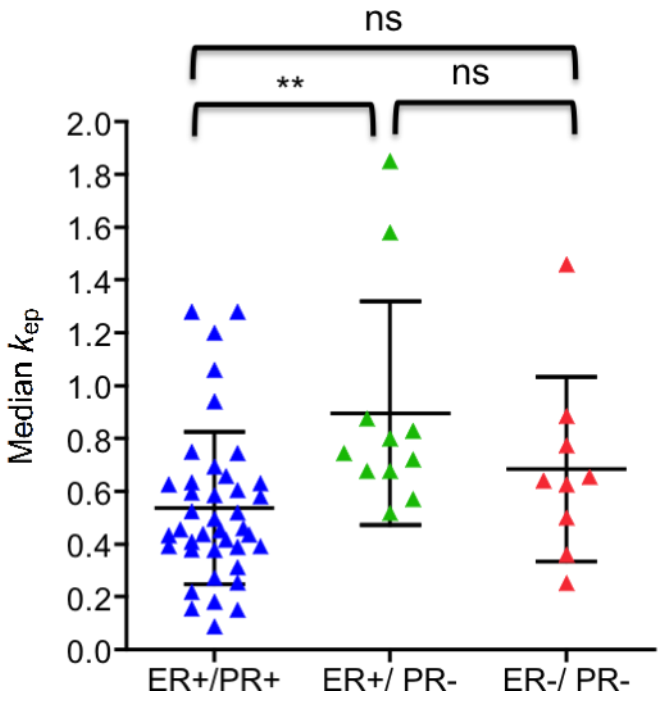

Figure-3.7: Median k_{ep} vs. receptor status. Significantly higher median k_{ep} in ER+PR- (n=11) in comparison to ER+PR+ (n=40) and ER-PR- (n=9). (** denotes P<0.01, ns = P>0.05, Dunn's multiple comparison test (Kruskal-Wallis test) (Graphs show mean ± SD for each group)

On further analysis, we observed borderline significantly higher median k_{ep} in triple negative patients (n=8) in comparison to ER+PR+ patients (n=40) (Mann-Whitney test, P=0.05) (Figure- 3.8)

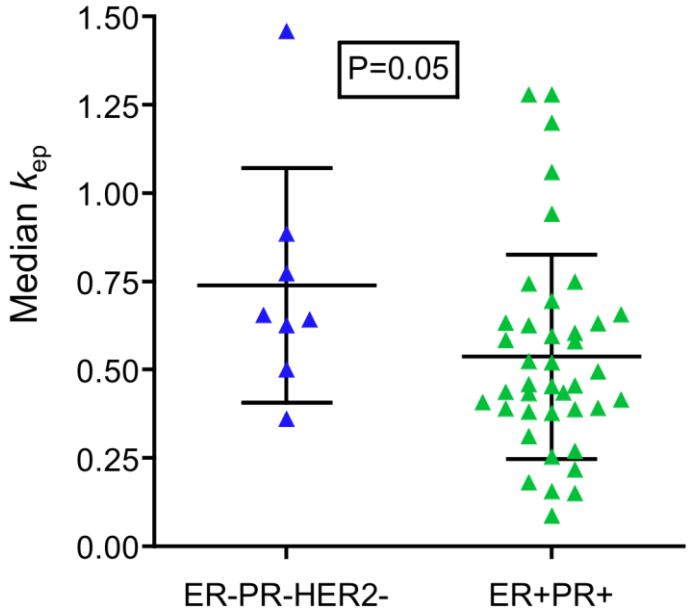

Figure-3.8: Difference in median k_{ep} in triple negative (ER-PR-HER2-) vs. luminal group (ER+PR+). Error bars show mean ± SD; P-value with Mann-Whitney test.

3.7 Prognostic significance of median k_{ep}

As mentioned above, there were wide variations in chemotherapy regimens, however, for all the patients, the first 3 cycles were with a FEC regimen although with different doses of epirubicin. Analyses were done to see if there was any association of median k_{ep} with interim MRI responses (available for 49 patients), which were assessed using RECIST criteria after 3 cycles of chemotherapy. There was no significant difference observed in median k_{ep} between different groups (CR (n=8) vs. PR (n=35) vs. SD (n=5)) based on MRI responses (Kruskal-Wallis test, P= 0.26). Only one patient had PD so she was excluded from the analysis.

Apart from this, association with final pathological responses after 6 cycles of chemotherapy was also assessed. For study purposes patients were classified

as good pathological responders (n=12) vs. others (n=47). Patients in the good pathological response group included pCR (n=6) and near to pCR (n=6) i.e. patients with only scattered cells on final histology. As mentioned before, pathological response data was available for 59 patients. There was no significant difference in median k_{ep} among patients based on the pathological responses (good pathological response vs. others) (Mann-Whitney test, P= 0.12).

3.8 Assessment of quality and quantity of RNA from FFPE samples

From FFPE core biopsies, there was sufficient yield of good quality RNA from 63 FFPE core biopsy samples but 2 of these samples failed in quality checks at PICR, Manchester, so a total of 61 patients was included for array work using the Affymetrix Human U133 Plus2.0 array (whole genome array) platform. The median RNA concentration was 84 ng/μL (range 0.95- 332 ng/μL), the median A260/280 ratio was 2.07 (range 1.90-2.39) and median RIN value was 2.3 (range 1.0-5.4) (Figure-3.9).

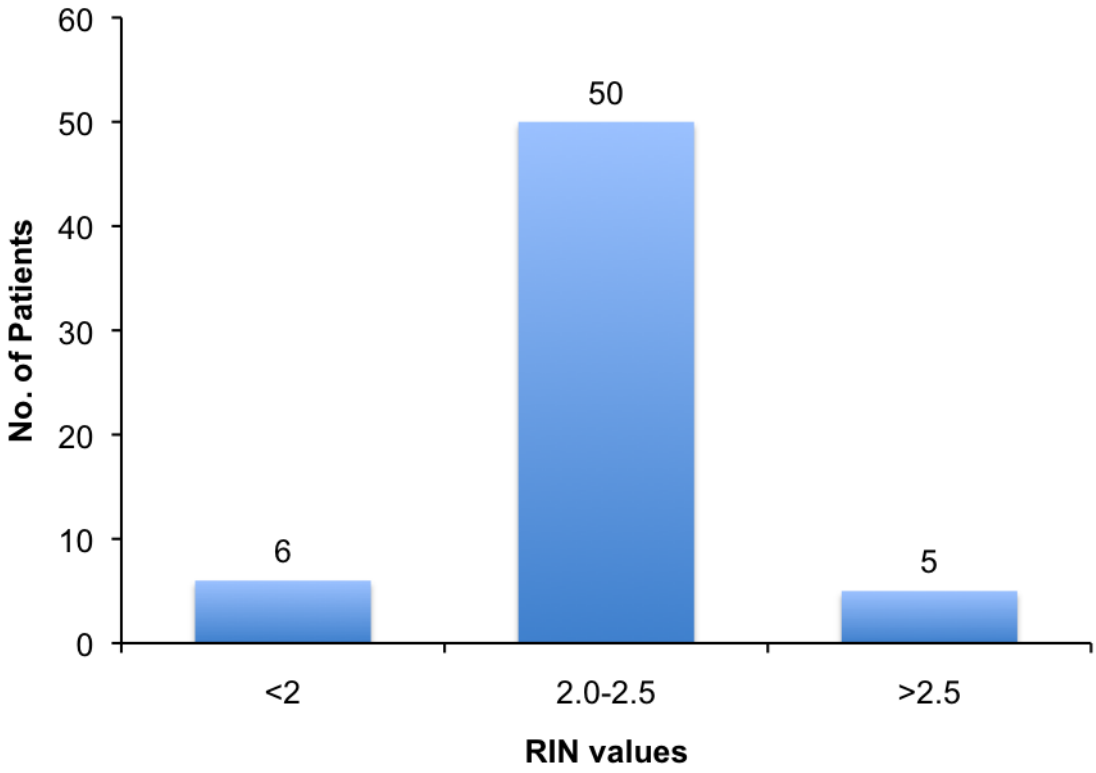

Figure-3.9: Histogram showing number of patients with corresponding RNA integrity number (RIN)

3.9 Gene expression analysis

Gene expression work was performed at PICR, Manchester using Affymetrix Human U133 Plus2.0 array (whole genome array) platform. (Please see Chapter 2, Section 5 for details). Gene expression analysis was conducted by an experienced bio-informatician Dr Laura Winchester under the supervision of Dr Francesca Buffa. In summary, normalisation and pre-processing of array data was done to remove probe sets not showing significant variation across the samples (for details see Chapter 2, Section 6). There were 15,000 genes after pre-processing.

3.9.1 Quality checks and validation of gene expression data

As FFPE degradation is known to happen over the time, quality checks were done on the array data. The initial clustering analysis showed S26 as an outlier with low presence score of 0.119 (Figure- 3.10)

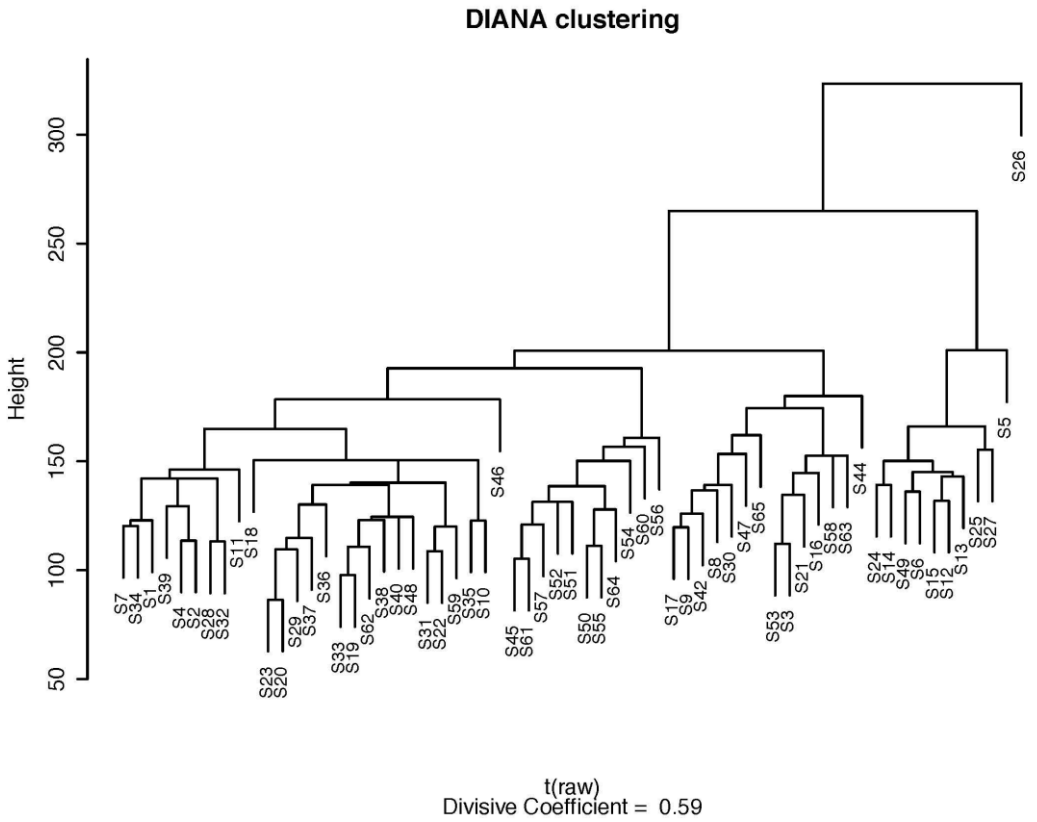

Figure-3.10: Hierarchical clustering using divisive analysis (Diana). The divisive coefficient (DC) indicates the strength of the clustering structure found by the algorithm. Divisive clustering starts with all the samples in a single cluster group and then partitions by dissimilarity among sample expression.

Standardisation and Significance Analysis for Microarrays (SAM) was done with and without S26 and there was no significant difference observed so we decided to proceed with the original list of 61 patients as before including S26.

To further check the reliability of the gene array data generated from FFPE samples, we calculated the correlation between ESR1 gene expression (using

probe set 205225_at) and ER score known from pathological data and similarly for ERBB2 gene expression (using probe set 216836_s_at) and known HER2 scores from clinical data. Highly significant correlations were noted between the gene expression values and the known pathological IHC scores for both of these receptors (Spearman r= 0.87, P<2.2e-16 between probe and core biopsy ER score and Spearman r= 0.75, P=4.7e-12 between probe and core biopsy HER2 score) (Figure- 3.11).

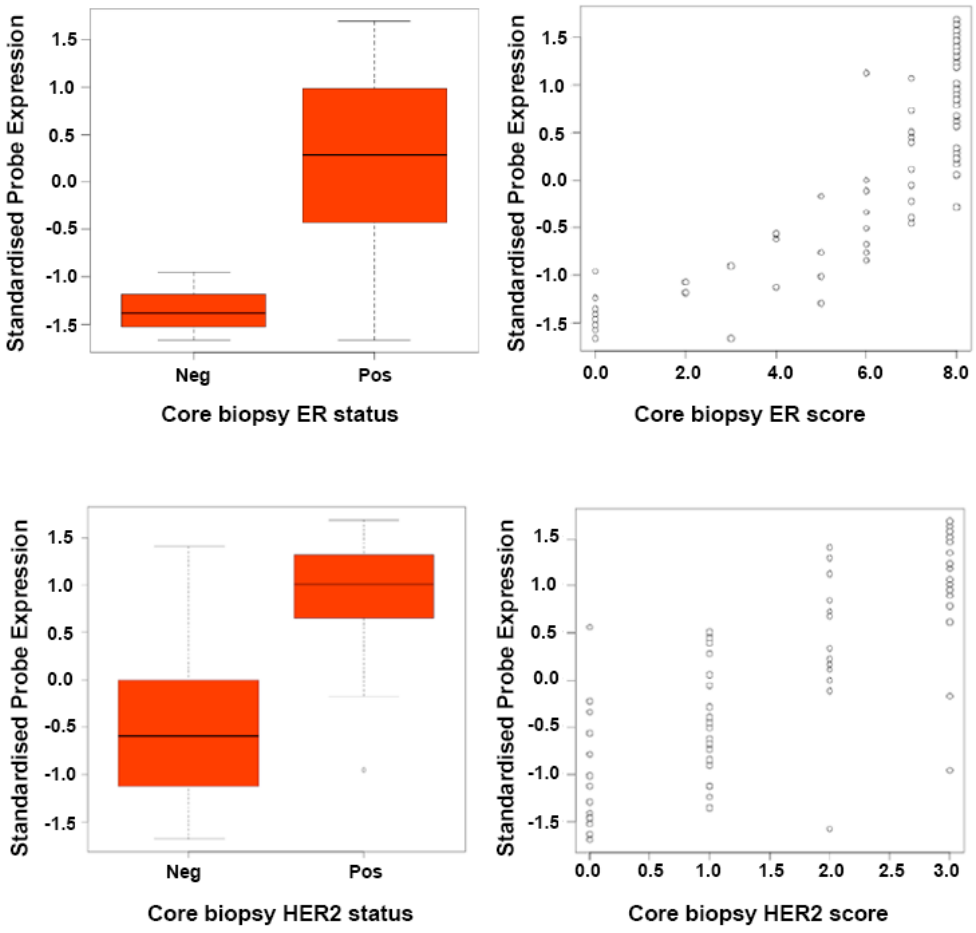

Figure-3.11: Correlation of expression of ER and HER2 probes vs. clinical classification as assessed by immunohistochemistry.
Probe used for ER: 205225_at. Significant correlation between probe and core ER score: Spearman rho= 0.87117, P-value < 2.2e-16,
Probe used for HER2: 216836_s_at. Significant correlation between probe and core HER2 score: Spearman rho = 0.7470048, P-value = 4.736e-12.

3.10 Correlation of gene expression with DCE-MRI pharmacokinetic parameters

After quality checks, the permutations test based ¨Significance Analysis for Microarrays" (SAM) (http://www-stat.stanford.edu/~tibs/SAM/) was used to determine which genes (if any) were significantly correlated with median k_{ep}. Setting the False Discovery Rate to 5% resulted in 328 genes that were significantly positively correlated with median k_{ep} (Table- 3.3, Figure- 3.12, Appendix 3.1) i.e. the higher the median $k_{ep,}$ the higher was the expression of these genes at baseline. There were no significant negatively correlated genes.

Table-3.3: Top 20 genes whose expression at baseline was significantly positively correlated with median k_{ep} at baseline.

Gene Symbol	Gene Title	Numerator (r) [1]	Q value [2] (%)	Chr [3]	Entrez Gene
SLC31A2	Solute carrier family 31 (copper transporters) member 2	0.62	0.00	chr9q31-q32	1318
IGF2R	Insulin-like growth factor 2 receptor	0.58	0.00	chr6q26	3482
UBE2J1	Ubiquitin-conjugating enzyme e2 j1	0.55	0.00	chr6q15	51465
MTO1	Mitochondrial translation optimization 1 homolog	0.54	0.00	chr6q13	25821
BCLAF1	Bcl2-associated transcription factor 1	0.54	0.00	chr6q22-q23	9774
TRAPPC10	Trafficking protein particle complex 10	0.54	0.00	chr21q22.3	7109
CALR	Calreticulin	0.53	0.00	chr19p13.3-p13.2	811
LGMN	Legumain	0.53	0.00	chr14q32.1	5641
SGK1	Serum/glucocorticoid regulated kinase 1	0.52	0.72	chr6q23	6446
NUS1	Nuclear undecaprenyl pyrophosphate synthase 1 homolog	0.52	0.72	chr6q22.1	116150
EIF2S1	Eukaryotic translation initiation factor 2 subunit 1 alpha 35KDa	0.51	0.72	chr14q23.3	1965
HDAC2	Histone deacetylase 2	0.51	0.72	chr6q21	3066
ASCC3	Activating signal cointegrator 1 complex subunit 3	0.51	0.72	chr6q16	10973
RIPK2	Receptor-interacting serine-threonine kinase 2	0.51	0.72	chr8q21	8767
TRMT11	Trna methyltransferase 11 homolog	0.50	0.72	chr6q11.1-q22.33	60487
MTHFD1L	Methylenetetrahydrofolate dehydrogenase (nadp+ dependent) 1-like	0.50	0.72	chr6q25.1	25902
RNF8	Ring finger protein 8	0.50	0.72	chr6p21.3	9025
LYN	V-yes-1 yamaguchi sarcoma viral related oncogene homolog	0.49	0.72	chr8q13	4067
RPF2	Ribosome production factor 2 homolog	0.49	0.72	chr6q21	84154
CDT1	Chromatin licensing and dna replication factor 1	0.49	0.72	chr16q24.3	81620

1. Numerator: Correlation of gene probe expression with median k_{ep} values.
2. Q-value: Lowest False Discovery Rate at which the gene is called significant.
3. Chr: Chromosomal location of the gene probe.

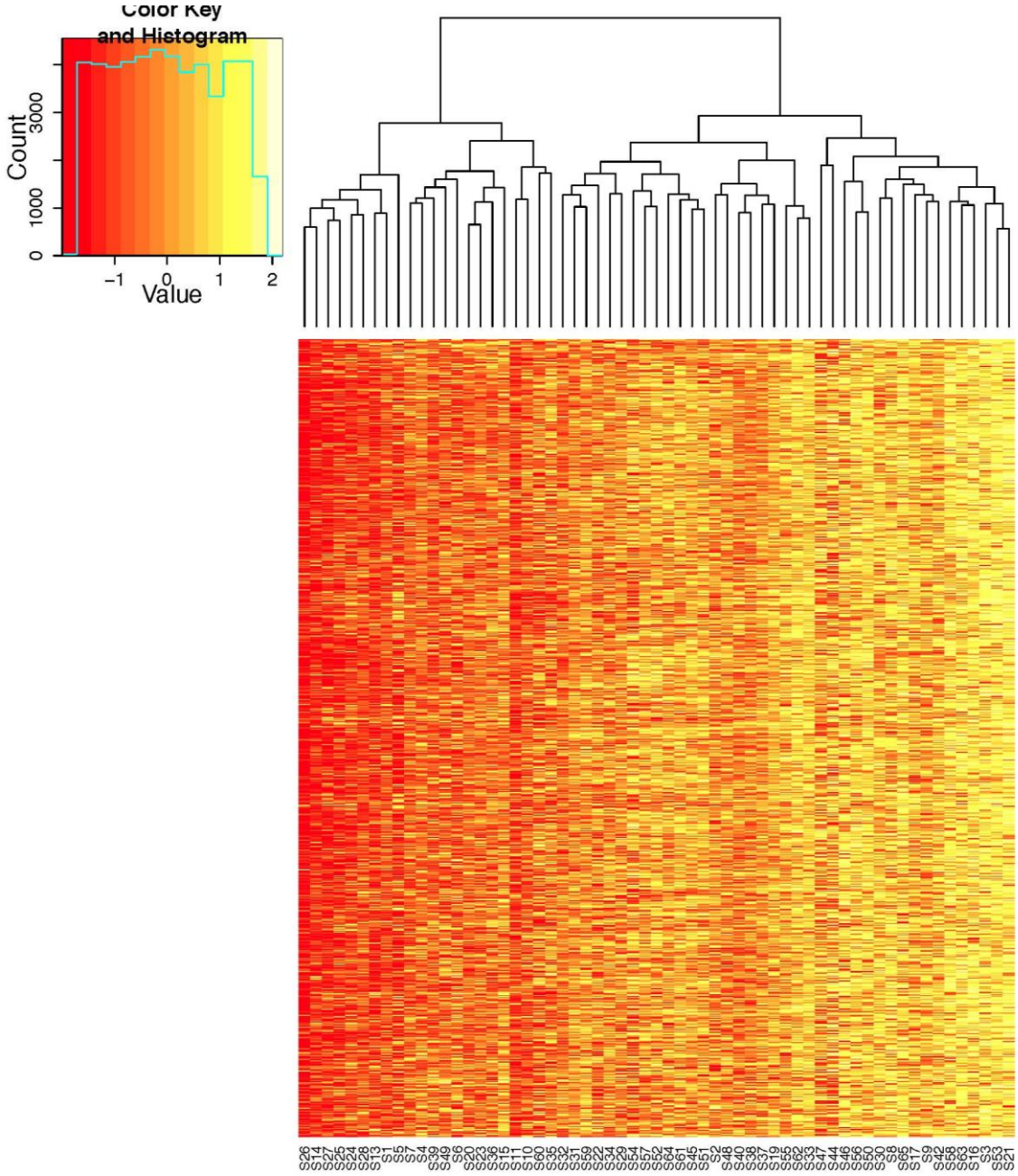

Figure-3.12: Heatmap showing genes positively correlated with median k_{ep}. Each row represents a gene and each column represents a patient. Color reflects expression value for each gene. Yellow= low expression; red= high expression.

Although on visual inspection of this heatmap, there appears to be clustering of patients in different groups. But, after comparison of the groups to clinical/ pathological prognostic factors, there was no clear pattern between the subgroups.

3.11 Validation by qRT-PCR

From the 328 genes positively correlated with median k_{ep}, 9 interesting genes were further validated by qRT-PCR (Table-3.4, Figure-3.13). As mentioned previously (Chapter 2, Section 7) samples of the same cDNA as used for the gene expression work, were used for this validation experiment with qRT-PCR. Heat shock protein 90kDa alpha (cytosolic), class B member 1 (HSPCB) was used as a house keeping gene and the relative expression of each gene of interest was calculated (see Chapter 2, Section 7 for details).

Table-3.4: Details of genes validated by qRT-PCR

Gene Title	Gene Symbol	Numerator (r)[1]	Q-value[2] (%)	Entrez Gene	Chromosome Location
Solute carrier family 31 (copper transporters) member 2	SLC31A2	0.62	0.00	1318	chr9q31-q32
Insulin-like growth factor 2 receptor	IGF2R	0.58	0.00	3482	chr6q26
Serum/glucocorticoid regulated kinase 1	SGK1	0.52	0.72	6446	chr6q23
Pyruvate dehydrogenase kinase isozyme 1	PDK1	0.46	0.72	5163	chr2q31.1
Interleukin 6 receptor	IL6R	0.45	0.72	3570	chr1q21
CD44 molecule (Indian blood group)	CD44	0.42	1.06	960	chr11p13
Solute carrier family 16 member 1 (monocarboxylic acid transporter 1)	SLC16A1	0.40	1.99	6566	chr1p12
Eukaryotic translation initiation factor 2-alpha kinase 2	EIF2AK2	0.39	2.27	5610	chr2p22-p21
Aldehyde dehydrogenase 1 family member A3	ALDH1A3	0.38	2.27	220	chr15q26.3

1. Numerator (r) : Correlation of gene probe expression to median k_{ep} values
2. Q value- Lowest False Discovery Rate at which the gene is called significant.

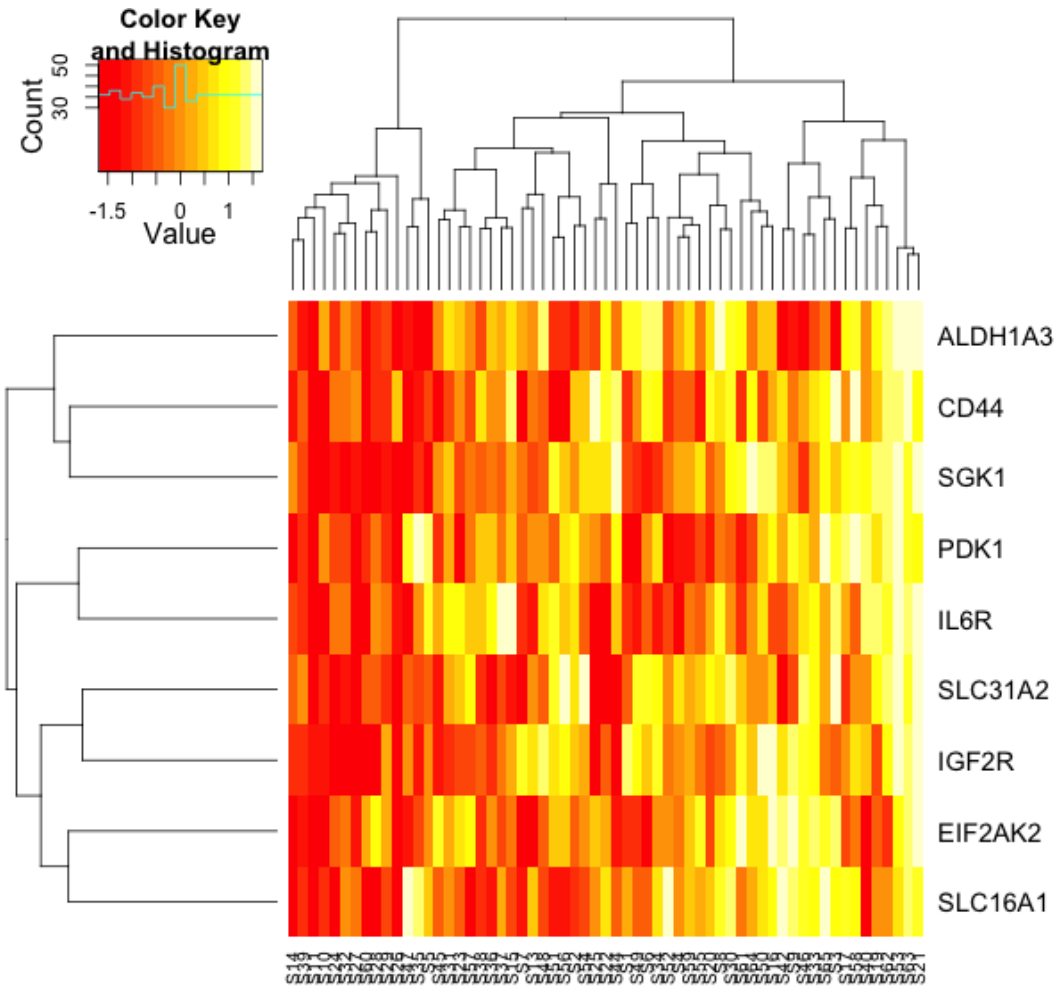

Figure-3.13: Heatmap of genes validated by qRT-PCR. Each row represents a gene and each column represents a patient. Color reflects expression value for each gene.

There was significant correlation observed between the expression value for ALDH1A3, SLC31A2, PDK1 and SLC16A1 as measured by qRT-PCR in comparison to expression values assessed by gene expression analysis by using Affymetrix, Human Plus 2.0 U133 array platform (Figure- 3.14). But there was no significant relationship observed between expression values of other genes as assessed by qRT-PCR and array platform (Table 3.5).

Table-3.5: Validation of gene expression by qRT-PCR.
(Gene symbols are arranged in alphabetical order)

Genes	**Array vs. PCR** Spearman r (P-value)
ALDH1A3	**0.53 (<0.0001)**
CD44	-0.05 (0.77)
EIF2AK2	0.05 (0.72)
IGF2R	0.04 (0.75)
IL6R	0.25 (0.06)
PDK1	**0.50 (<0.0001)**
SGK1	0.25 (0.11)
SLC16A1	**0.69 (<0.0001)**
SLC31A2	**0.42 (0.001)**

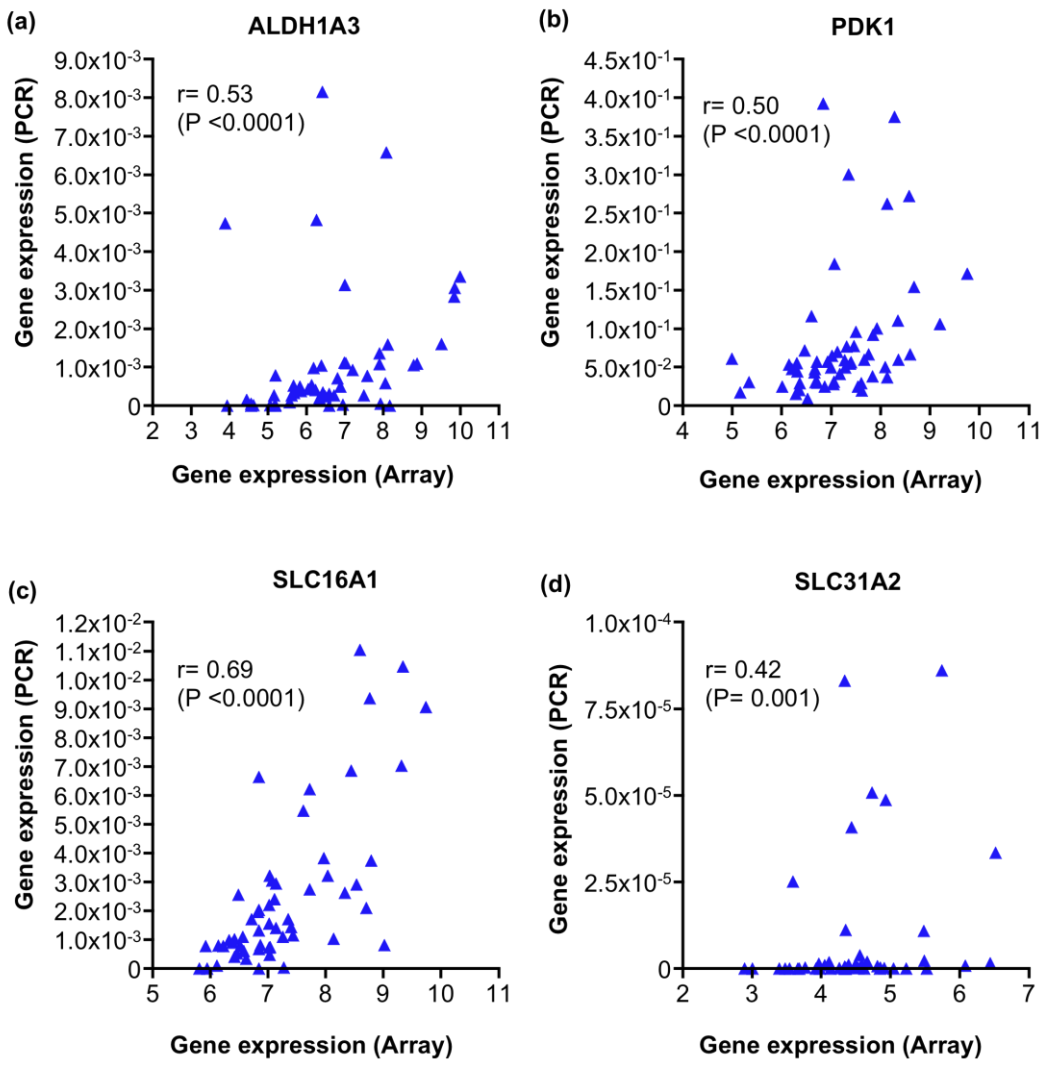

Figure-3.14: Correlation between gene expression as measured by Affymetrix Human Plus 2.0 array vs. qRT-PCR.
Spearman coefficient r (P value)

3.12 Relationship between genes of interest at baseline and clinical/ pathological prognostic factors in breast cancer

As shown previously in Figure- 3.11, there was wide variation in gene expression observed among patients. Further univariate analysis was done to see if there was any difference in gene expression in subgroups based on the known clinical and pathological prognostic factors in breast cancer. Variables considered were ER/ HER2 status, initial tumour volume as assessed by MRI and age at presentation (Table- 3.6). Interestingly the expression of IGF2R, PDK1 and SLC16A1 was significantly higher in ER negative (n=10) as compared to ER positive patients (n=51) (Mann-Whitney test, P=0.04, P= 0.003, P=0.006 respectively) (Figure- 3.15).

Progesterone receptor (PR) is well known to be influenced by oestrogen and ER, further analysis was done to see if there was any difference in three groups based on these two receptors i.e. ER+PR+ (n= 41) versus ER+PR- (n=11) and ER-PR- (n=9). As there was only one patient with ER-PR+ status she was not included in the analysis. The expression of CD44 and ALDH1A3 was significantly higher in ER+PR- group in comparison to the ER+PR+ group (Kruskal- Wallis test, P= 0.008, Dunn multiple comparison test P<0.01 and P= 0.04, Dunn's multiple comparison test P<0.05 respectively) (Figure3.16).

The expression of SLC16A1 was significantly higher in HER2- patients in comparison to HER2+ patients (Mann-Whitney test, P= 0.004).

The expression of PDK1 and SLC16A1 were significantly higher in the triple negative group (ER-PR-HER2-) of patients (n=8) in comparison to others (n= 53) (Mann-Whitney test P= 0.003 and 0.001 respectively) (Figure-3.17).

Table-3.6: Comparison of gene expression in different subpopulations of patients based on their receptor status

Genes	ER+ vs. ER- [1*]	ER+PR+ vs. ER+PR- vs. ER-PR- [2 ‡]	HER2+ vs. HER2- [3*]	ER-PR-HER2- vs. others [4*]
ALDH1A3	0.86	**0.04**	0.77	0.45
CD44	0.84	**0.01**	0.32	0.29
EIF2AK2	0.88	0.98	0.73	0.42
IGF2R	**0.04**	0.07	0.18	0.08
IL6R	0.87	0.2	0.9	0.79
PDK1	**0.003**	**0.001**	0.5	**0.003**
SGK1	0.45	0.16	0.81	0.13
SLC16A1	**0.01**	**0.01**	**0.004**	**0.001**
SLC31A2	0.4	0.58	0.31	0.84

* Columns showing P-value, Mann-Whitney test.
‡ Columns showing P-value, Kruskal-Wallis test.
1. ER: Oestrogen Receptor, ER+ (n=51), ER - (n=10)
2. ER+/PR+ (n=40), ER+PR- (n=11), ER-PR- (n= 9).
3. HER2: Human Epidermal Growth Factor Receptor 2, HER2+ (n= 23), HER2 - (n=38).
4. ER-PR-HER2- (n= 8), others (n= 53).

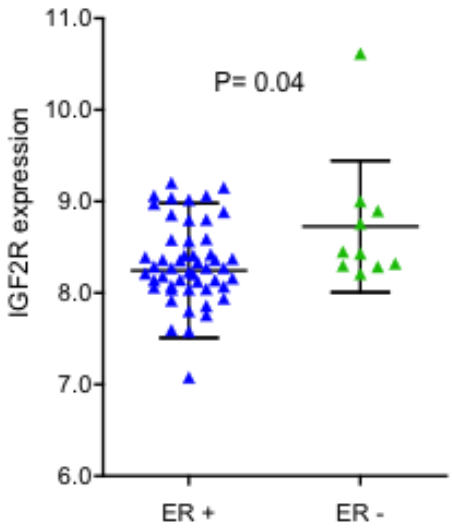

Figure-3.15: IGF2R expression in ER+ vs. ER- Error bars show mean±SD; P-value, Mann-Whitney test.

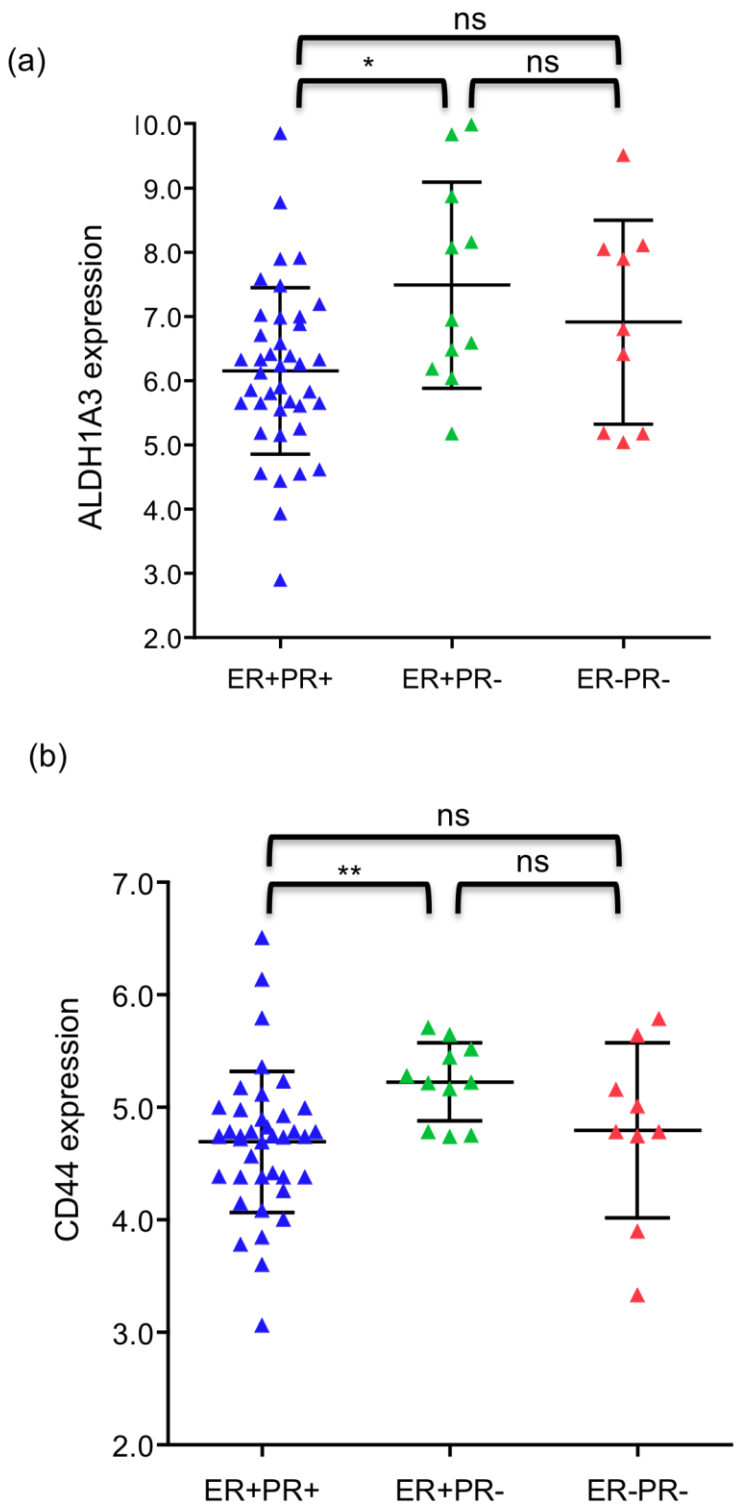

Figure-3.16: Gene expression versus receptor status (a) ALDH1A3 expression in ER+PR+ vs. ER+PR- vs. ER-PR- patients (b) CD44 expression in ER+PR+ vs. ER+PR- vs. ER-PR- Kruskal-Wallis test, Dunn's multiple comparison test (* = P <0.05, ** = P<0.01, ns = P>0.05).

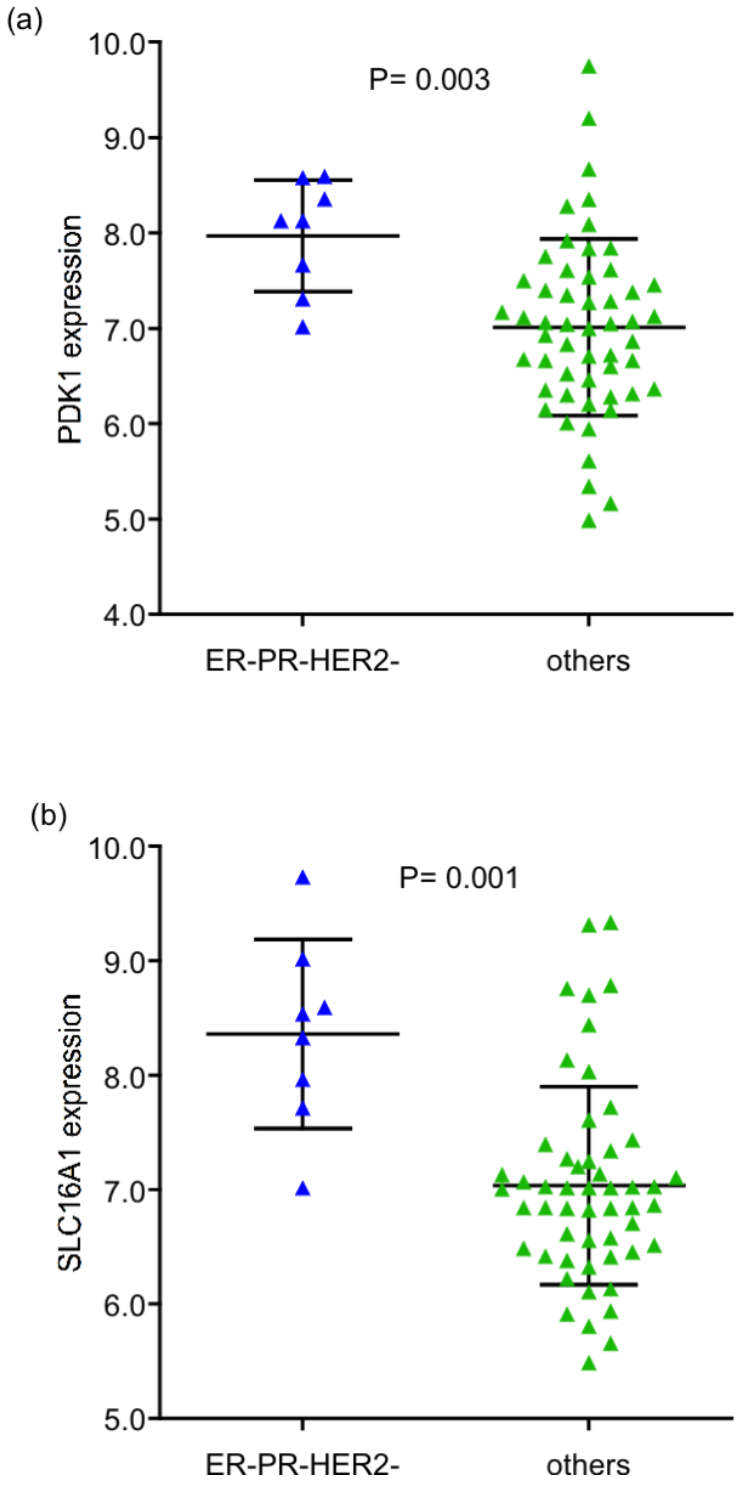

Figure-3.17: (a) PDK1 and (b) SLC16A1 expression in triple negatives versus others. Mann-Whitney test, P-value; Error bars show mean±SD.

On further analysis, there was weak but significant positive correlation noted between the age of patients and expression of ALDH1A3 and SLC31A2 (Spearman r = 0.30, P= 0.02 and r= 0.29, P= 0.02, respectively). This indicated that the higher the age of the patients, the greater was the expression of ALDH1A3 and SLC31A2 (Figure- 3.18). There was no relationship observed between gene expression at baseline with tumour volume at baseline.

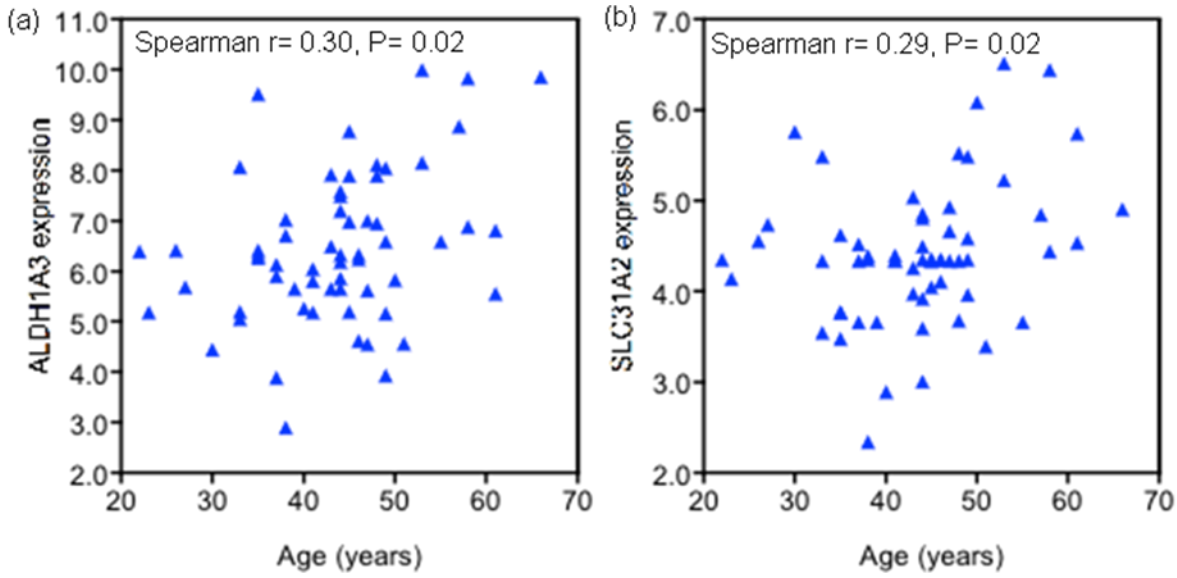

Figure-3.18: Association of ALDH1A3 and SLC31A2 expression at baseline with age of the patient at diagnosis.

3.13 Prognostic significance of baseline expression of genes

We were interested to see if the expression of any of these genes at baseline has any prognostic significance for locally advanced breast cancer patients undergoing neoadjuvant chemotherapy. For this difference between genes expression at baseline was assessed between different groups based on interim MRI responses after 3 cycles of chemotherapy and final pathological responses after 6 cycles of chemotherapy. As mentioned before, interim MRI responses after 3 cycles of chemotherapy (assessed using RECIST criteria)

were available for 49 patients and final pathological responses after 6 cycles of chemotherapy (good pathological response vs. others) were available for 59 patients.

There was no significant difference observed in baseline gene expression between different groups (CR/ PR/ SD) based on MRI responses. Interestingly, the baseline gene expression of ALDH1A3 was significantly higher in the good pathological responder group (n=12) in comparison to others (n= 47) (Mann-Whitney test, P= 0.02) (Figure- 3.19).

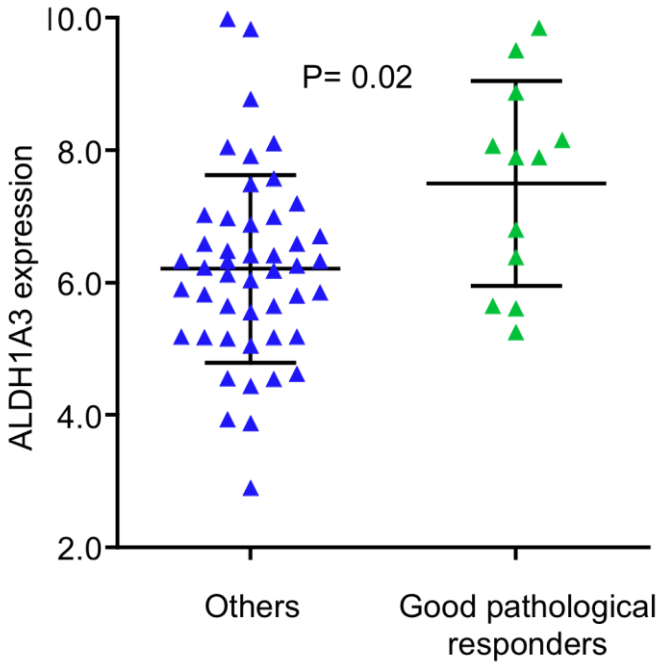

Figure-3.19: Association of baseline ALDH1A3 with pathological response after 6 cycles of neoadjuvant chemotherapy.
Good pathological responders (n=12), others (n=47); P-value, Mann Whitney test; Error bars show mean±SD.

3.14 Gene Signature analysis

A number of research groups, including our own, have previously published "metagenes" also called "signatures". These are lists of genes involved in specific pathways. For the purpose of this study, Hypoxia (Buffa, Harris et al. 2010), Proliferation (Desmedt, Haibe-Kains et al. 2008) and angiogenesis signatures (Masiero, Simoes et al. 2013) were considered. To investigate the relationship between the median k_{ep} and each of these gene signatures, corresponding median metagene scores were computed from the gene array data for each tumour.

Interestingly, a highly significant positive correlation was noted between the median hypoxia score with median k_{ep} (Spearman r=0.41, P=0.001) and a weak but positive correlation between median proliferation score and median k_{ep} (Spearman r=0.29, P=0.02) (Figure-3.20). The hypoxia signature comprised genes derived from analysis of an independent breast cancer data set (Buffa, Harris et al. 2010) and among these; genes related to proliferation were excluded to obtain the hypoxia score. There was no significant relationship observed between median angiogenesis score and median k_{ep} (Spearman r= 0.11, P=0.38).

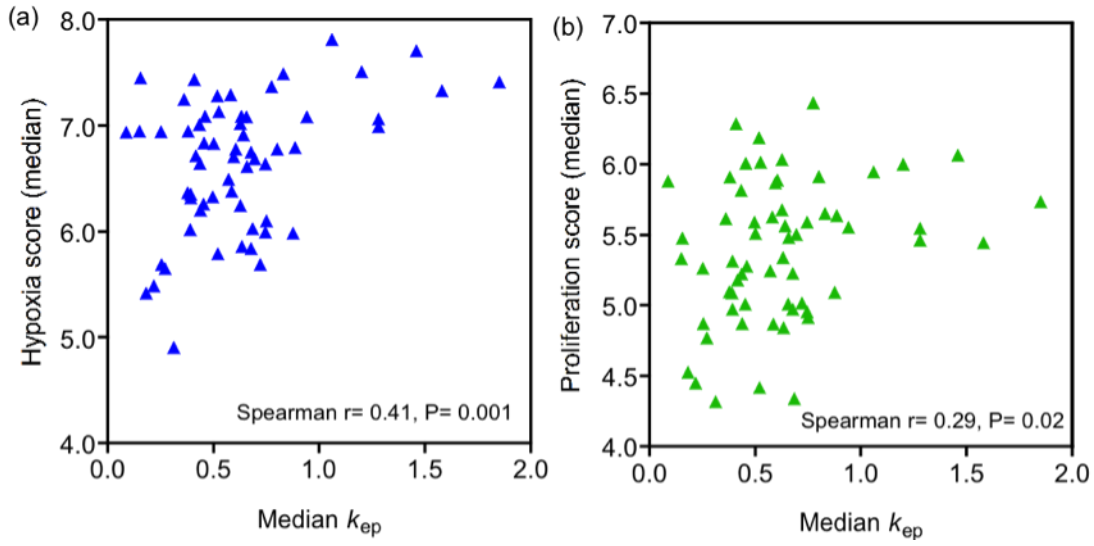

Figure-3.20: Correlation of hypoxia and proliferation gene signatures with median k_{ep} at baseline.

3.15 Biological processes and pathway analysis

Biological processes and pathways were evaluated using Genecodis 3.0 (Tabas-Madrid, Nogales-Cadenas et al. 2012). The most significant biological processes were the *cytokine mediated signalling pathways*; interferon *mediated signalling pathways and regulation of apoptosis* (Figure- 3.21, Table- 3.7).

The most significant pathways using the KEGG database were *protein processing in endoplasmic reticulum* and *antigen processing and presentation* (Figure- 3.22, Table- 3.8).

(a)

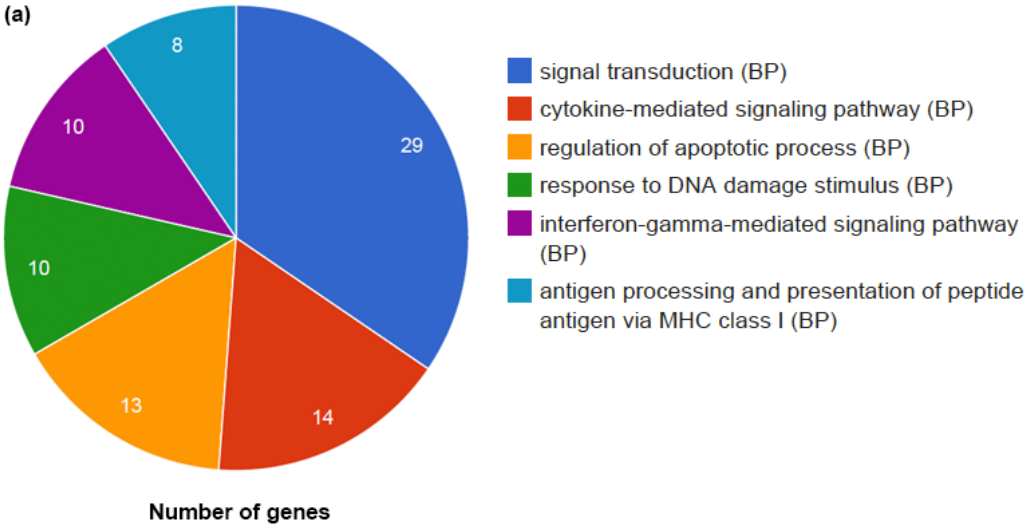

(b)

Annotations	No. of genes	Hyp*
GO:0019221: Cytokine-mediated signaling pathway (BP)	14	1.77E-06
GO:0060333: Interferon-gamma-mediated signaling pathway (BP)	10	2.42E-06
GO:0042981: Regulation of apoptotic process (BP)	13	2.41E-05
GO:0006974: Response to DNA damage stimulus (BP)	10	9.50E-05
GO:0002474: Antigen processing and presentation of peptide antigen via MHC class I (BP)	8	0.0003
GO:0007165: Signal transduction (BP)	29	0.0004

Figure-3.21: Significant biological processes from genes positively correlated with median k_{ep}. (a) Pie chart showing number of genes involved in each biological process from the list of positively correlated genes to median k_{ep}. (b) Table showing annotations of each biological process arranged by order of significance. 'No. of genes'- Number of genes involved in each biological process out of genes showing significant positive correlation to median k_{ep}. Hyp*- Hypergeometric P-value corrected by FDR method.

Table-3.7: Lists of genes involved in significant biological processes. Gene symbols arranged alphabetically.

Annotations	Gene Symbols
GO:0019221: Cytokine-mediated signalling pathway	B2M, CCR1, CD44, GBP2, HLA-A, HLA-B, HLA-C, HLA-DRA, HLA-DRB1, HLA-E, IFNAR2, IFNGR1, IL6R, STAT1
GO:0060333: Interferon-gamma-mediated signalling pathway	B2M, CD44, GBP2, HLA-A, HLA-B, HLA-C, HLA-DRA, HLA-DRB1, HLA-E, IFNGR1
GO:0042981: Regulation of apoptotic process	BEX2, C19orf2, CALR, CARD16, CSTB, DAPK1, IFIH1, IL6R, LYN, PEA15, PSMB1, SGK1, VCP
GO:0006974: Response to DNA damage stimulus	SGK1, OBFC2A, MNDA, ATR, VCP, LYN, MCTS1, APTX, DTX3L, RAD1
GO:0002474: Antigen processing and presentation of peptide antigen via MHC class I	B2M, CALR, ERAP1, HLA-A, HLA-B, HLA-C, HLA-E, PSMB1
GO:0007165: Signal transduction	APOL3, ARHGAP18, ATF6, ATP2C1, DAPK1, DEK, DEPDC1, HBS1L, HIF1A, IFNGR1, IGF2R, IQGAP3, LITAF, LYN, MTSS1L, MYO10, OPTN, PPP2R5E, RAP2A, RASA2, RASSF4, RCAN1, RHEB, RIPK2, RSU1, TANK, TLE1, TLR2, TRIM38

(a)

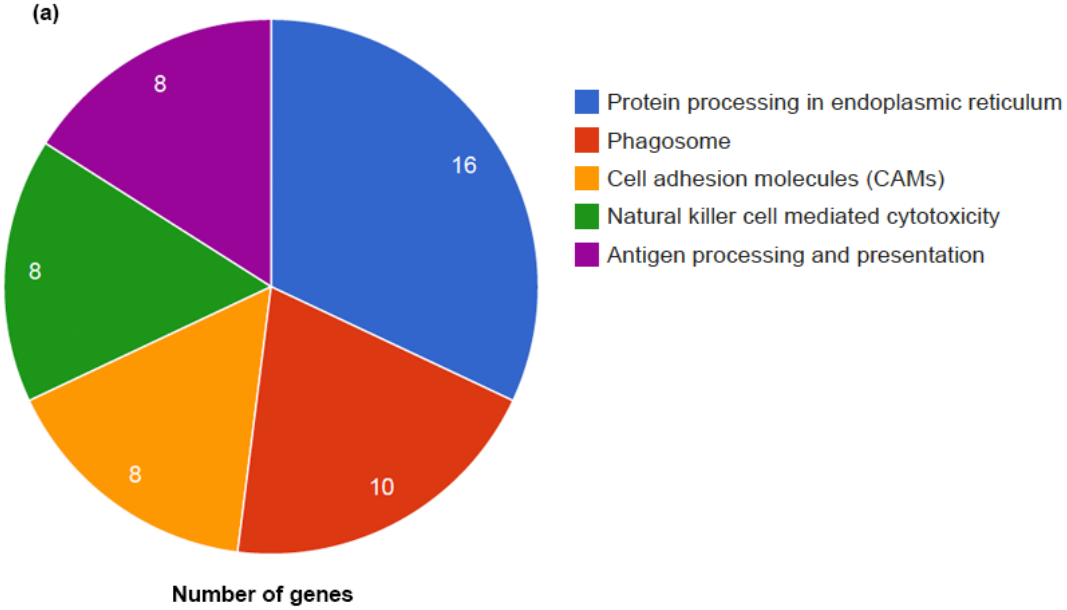

(b)

Annotations	No. of genes	Hyp*
(KEGG) 04141: Protein processing in endoplasmic reticulum	16	3.0E-10
(KEGG) 04612: Antigen processing and presentation	8	3.4E-06
(KEGG) 04145: Phagosome	10	3.1E-05
(KEGG) 04514: Cell adhesion molecules (CAMs)	8	3.2E-04
(KEGG) 04650: Natural killer cell mediated cytotoxicity	8	3.2E-04

Figure-3.22: Significant KEGG pathways from genes positively correlated with median k_{ep}. (a) Pie chart showing number of genes involved in each pathway from the list of genes showing positive correlation with median k_{ep}. (b) Table showing annotations of each pathway arranged by order of significance. 'No. of genes'- Number of gene involved in each pathway out of the genes showing positive correlation to median k_{ep}. Hyp*- Hypergeometric P-value corrected by FDR method.

Table-3.8: Lists of genes involved in significant KEGG pathways.
Gene symbols arranged alphabetically.

Annotations	Gene Symbols
(KEGG) 04141: Protein processing in endoplasmic reticulum	ATF6, CALR, CRYAB, DNAJA1, EDEM3, EIF2AK1, EIF2AK2, EIF2S1, HYOU1, SEC61B, SEC63, UBE2D1, UBE2J1, UGGT1, VCP, YOD1
(KEGG) 04612: Antigen processing and presentation	B2M, CALR, HLA-A, HLA-B, HLA-C, HLA-DQA1, HLA-DRB1, LGMN
(KEGG) 04145: Phagosome	CALR, CLEC7A, DYNC1H1, HLA-A, HLA-B, HLA-C, HLA-DQA1, HLA-DRB1, SEC61B, TLR2
(KEGG) 04514: Cell adhesion molecules (CAMs)	CD58, F11R, HLA-A, HLA-B, HLA-C, HLA-DQA1, HLA-DRB1, ITGA6
(KEGG) 04650: Natural killer cell mediated cytotoxicity	HLA-A, FCER1G, HLA-B, SYK, HLA-C, BID, IFNGR1, IFNAR2

3.16 Discussion

While it is often assumed that areas of high contrast enhancement and / or washout on dynamic MRI scans comprise areas of increased angiogenesis and tumour activity, the molecular pathways that govern this phenotype are poorly understood.

This pilot study has successfully shown that quantitative and physiologically relevant information can be extracted from diagnostic low temporal resolution DCE-MRI scans and archived FFPE samples, which can be helpful in understanding the biology of the tumour and potentially in the development of biomarkers for personalised therapy in breast cancer.

The pharmacokinetic parameter k_{ep} that governs the washout of contrast agent from the tumour extravascular extracellular space (EES) to plasma, is considered more robust than the other parameters since it is not dependent on the T1 values of the tissue (Choyke, Dwyer et al. 2003; Li, Padhani et al. 2011). The analysis done in this study showed that k_{ep} can be estimated reliably from the low temporal resolution diagnostic DCE-MRI scans that are routinely performed.

Breast tumours are well known to be heterogeneous based on a number of pathological studies (Shipitsin, Campbell et al. 2007; Polyak 2011). With the help of three dimensional pharmacokinetic maps we have shown non-invasively the uneven distribution of blood vessels within and in between different tumour lesions, referred to as tumour “heterogeneity”, that might be

related to differences in biology of different subtypes. Although there was no difference observed in median k_{ep} values in ER- patients in comparison to ER+ patients, we did find that median k_{ep} was significantly higher in patients with ER+PR- tumours than ER+PR+ or ER-PR- tumours. PR is well known to be an oestrogen-regulated gene, and its synthesis in normal and cancer cells requires oestrogen and ER (Cui, Schiff et al. 2005). Thus PR reflects the combined effect of ER and growth factors (Daniel, Hagan et al. 2011). ER+ PR- tumours are known to be highly proliferative and more aggressive than ER+PR+ tumours (Arpino, Weiss et al. 2005). Similar to other studies, there was a marginally significant higher median k_{ep} was observed in triple negative patients in comparison to ER+PR+ group (Li, Padhani et al. 2011; Koo, Cho et al. 2012). The higher median k_{ep} values in ER+PR- and triple negative cancers may reflect the rapid return of contrast medium into the vasculature that may render the tumour more hypoxic leading to hypoxia induced adaptation by post-translational and transcriptional changes that promote cell survival and metastasis. The detailed genomic analysis discussed below suggests this important biological correlation.

Several studies have reported (Ah-See, Makris et al. 2008; Pickles, Manton et al. 2009; Dongfeng, Daqing et al. 2012) that baseline MRI parameters can predict outcome of neoadjuvant chemotherapy in breast cancer. There was no such relationship observed in this study. This might be due to the differences in the MRI protocol used in the study and the associated analysis methods (semi quantitative analysis methods for the kinetic curve pattern that were used in previous studies) or due to definition of clinical responders e.g. in study by Ah-

See et al (Ah-See, Makris et al. 2008) the responder group consisted of complete as well as partial responders.

As reported previously in the literature (Ribeiro-Silva, Zhang et al. 2007; Abdueva, Wing et al. 2010; Kibriya, Jasmine et al. 2010; Budczies, Weichert et al. 2011) we also observed that reliable information can be extracted from the gene expression analysis of degraded RNA from stored FFPE samples.

In breast cancer, only a few studies in the literature have reported on the relationship of MRI characteristics with molecular pathways in preclinical or clinical studies. Preclinical studies performed in murine tumours have shown that the expression of ribosomal proteins was greatly increased in high enhancement and washout regions, implying increased protein translation and consequently increased cellular activity (Costouros, Lorang et al. 2002). Similar to our study, Yamamoto et al. have reported that the MRI phenotypes correlate with immune-related genes such as STAT1, IF144 and IF16 (Yamamoto, Maki et al. 2012). However, in that study only 10 patients were included for radiogenomic analysis and complex MRI phenotypes were used which were not very clearly defined.

In this study, by analysing the whole genome wide gene expression patterns from biopsy samples from 61 patients, not only the genes related to interferon signalling pathways were identified, as shown by Yamomata et al. (Yamamoto, Maki et al. 2012) but several other interesting genes which were positively correlated with the baseline median k_{ep} i.e. the higher the median k_{ep} at

baseline, the higher the expression of these genes at baseline. These included copper transporter like solute carrier family31member2 (SLC31A2) (Wee, Weinstein et al. 2013); monocarboxylic acid transporter-1 i.e. SLC16A1 (solute carrier family 16, member 1 (Pinheiro, Sousa et al. 2011); cancer stem cell (CSC) related genes such as CD44, aldehyde dehydrogenase family 1 member A3 (ALDH1A3), and integrin alpha-6 (ITGA6) (Ali, Dawson et al. 2011); hypoxia regulated genes such as hypoxia inducible factor 1a (HIF1a) (Generali, Berruti et al. 2006; Patiar and Harris 2006); kinases such as eukaryotic translation initiation factor2-alpha kinases (EIF2AK2, EIF2AK1) (Dey, Tameire et al. 2013) and pyruvate dehydrogenase kinases (PDK1, PDK3) (Kim, Gao et al. 2007; Sutendra, Dromparis et al. 2012); genes involved in metabolism such as insulin like growth factor receptor 2 (IGF2R) (Harris and Westwood 2012), serum/glucocorticoid regulated kinase1 (SGK1) (Hall, Kim et al. 2012) and genes related to immune functions such as signal transducer and activator of transcription 1 (STAT1) (Khodarev, Roizman et al. 2012), interferon gamma receptor 1 (IFNGR1) and interleukin 6 receptor (IL6R). All these genes are known to play an important role in tumour growth and survival under stress - especially in highly proliferative breast tumours.

For example, the SLC31A2 gene that encodes copper ion solute carrier transporter CTR2 was the most significantly correlated gene to median k_{ep} in this study. Increased levels of CTR2 have been postulated to result in poor prognosis in breast cancer and resistance to platinum based chemotherapies (Wee, Weinstein et al. 2013). In addition, knock-down of one of the three SLC

genes has shown increased paclitaxel susceptibility in breast cancer (Njiaju, Gamazon et al. 2012).

Also, among the significantly positively correlated genes to median k_{ep} were translational regulator genes like EIF2S1, EIF2AK2 and EIF2AK1. These genes are known to regulate phosphorylation of eIF2α that in turn results in translational up-regulation of ATF4, i.e. the main transcriptional regulator of the cellular hypoxic response to the Unfolded Protein Response (UPR) and activates genes that promote restoration of normal endoplasmic reticulum function and survival under hypoxia (Rzymski, Milani et al. 2009; Dey, Tameire et al. 2013).

The significantly higher expression of stem cell markers CD44 and ALDH1A3 was observed in ER+PR- patients in comparison to others. As discussed above these tumours are known to be highly proliferative and more aggressive (Arpino, Weiss et al. 2005) and high expression of stem cells markers goes with the high proliferative nature of tumour. Significantly higher expression of PDK1 and SLC16A1 was noted in triple negative patients in comparison to others in this study. The up-regulation of PDK1 which is an important regulator of PI3K/AKT signalling pathway (Umemura, Yoshida et al. 2007) and up-regulation of MCT1/SLC16A1 is already known to be associated with poor prognostic variables such as basal-like subtype and high grade tumours (Pinheiro, Albergaria et al. 2010; Pinheiro, Sousa et al. 2011). As discussed above median k_{ep} was also higher in this subgroup of the patients.

Furthermore, a significant positive correlation of gene signatures related to hypoxia and proliferation with median k_{ep} was also noted in this study.

We observed a weak but significant correlation of baseline ALDH1A3 and SLC16A1 with the age of the patients. Also, baseline ALDH1A3 expression was significantly higher in patients showing complete pathological response after chemotherapy.

The results of this study, illustrate how functional imaging modalities such as DCE-MRI can be combined with gene expression profiling to provide insight into molecular targets that may have important therapeutic implications in breast cancer. We found that locally advanced breast cancers with high vascular permeability and/or blood flow, as quantified by the washout parameter median k_{ep} were also more hypoxic. The gene expression analyses showed gene involved in pathways such as immune response angiogenesis, a shift to glycolytic metabolism, the expression of ABC transporters and the cancer stem cell genes that play an important role in cell survival through adaptive processes, thereby accelerating cancer progression.

These results suggested that locally advanced breast cancers with high vascular permeability and/or blood flow may benefit from therapies directed at one or more of these molecular targets. Furthermore, by this pilot study, we have successfully shown that functional imaging with DCE-MRI may be helpful as a non-invasive means of selecting and monitoring therapy against these targets.

CHAPTER FOUR

4 Clinical and DCE-MRI analysis of Prospective Neoadjuvant Bevacizumab study in Primary Breast Cancer

4.1 Introduction

Currently, there are no proven biomarkers of efficacy of anti-VEGF therapy. These biomarkers are urgently needed to identify responsive patients and to predict efficacy of bevacizumab in breast cancer (Banerjee, Dowsett et al. 2007; Quesada, Medina et al. 2007).

The conventional phase I design of trials poses a significant problem for effective biomarkers of angiogenesis inhibitors. In advanced stages patients may have multiple mechanisms of resistance to cellular stress (Schneider and Miller 2005). One way to assess anti-angiogenesis agents is to use the drugs in short-term neoadjuvant therapy, as first line treatment, with detailed pharmacodynamic assessments.

The pharmacokinetic analysis of DCE-MRI scans can provide valuable information about angiogenesis of breast cancer (Buckley, Drew et al. 1997; Leach 2001; Su, Cheung et al. 2003; Ikeda, Nishimura et al. 2004). Significant reduction in DCE-MRI parameters reflecting reduced angiogenesis, such as inflow transfer rate constant and in the backflow extravascular- extracellular rate constant, has been shown previously following neoadjuvant bevacizumab treatment in inflammatory and locally advanced breast cancer (Wedam, Low et al. 2006; Thukral, Thomasson et al. 2007; Baar, Silverman et al. 2009).

We however conducted a window-of-opportunity study in newly diagnosed locally advanced breast cancer patients using a single cycle of bevacizumab

given before standard neoadjuvant chemotherapy with detailed pharmacodynamic assessments using dynamic contrast-enhanced magnetic resonance imaging (DCE-MRI), core biopsies for gene expression arrays and immunohistochemistry analysis at baseline and 2 weeks after bevacizumab. In comparison to other studies done previously (Wedam, Low et al. 2006; Baar, Silverman et al. 2009), the key features of this study were the detailed pharmacodynamic analysis with multiparameteric DCE-MRI scans along with human genome wide gene expression analysis with Affymetrix Exon 2.0 arrays and analysis of the circulating markers at baseline and two weeks after bevacizumab only. This study was designed to complete in 2-3 weeks window period before starting neoadjuvant chemotherapy to avoid undue delays in definitive chemotherapy treatment of patients.

In this chapter, the clinical and the DCE-MRI results of this study are described.

4.2 Study summary

A total of 47 previously untreated locally advanced primary breast cancer patients were enrolled between July 2008 and November 2010 based on selection criteria (as mentioned in Chapter 2, Section 1). This study was approved by NRES, UK (Oxford REC no. 08/H0604/69). Written consent was obtained from all patients prior to enrolment in the study.

As mentioned in Chapter 2, Section 2, at baseline, patients received a routine DCE-MRI staging scan which is performed in all breast cancer patients who receive neoadjuvant chemotherapy for tumour sizing, localisation and staging. On the next day a research DCE-MRI scan was performed. This was a high temporal resolution T1-weighted scan to image 8-12 slices taken through the central tumour region only. Core biopsies and blood samples were then collected, immediately following this each patient received a single infusion of bevacizumab (15mg/kg). Two weeks after bevacizumab a post-treatment research MRI scan was performed, and core biopsies and blood samples were collected (Figure-4.1). At this stage patients were considered out of clinical trial and they underwent a standard course of neoadjuvant chemotherapy as per standard clinical practise with FECx3 followed by docetaxel x 3 +/- trastuzumab. This is a combination regimen of 5FU 600mg/m^2, epirubicin 100mg/m^2 and cyclophosphamide 600mg/m^2 for 3 cycles at 3-week intervals, followed by docetaxel 100mg/m^2 for 3 cycles at 3-week intervals +/- trastuzumab 6mg/kg (depending on HER2 status). Surgery was performed after neoadjuvant chemotherapy wherever indicated as per standard management for the patient.

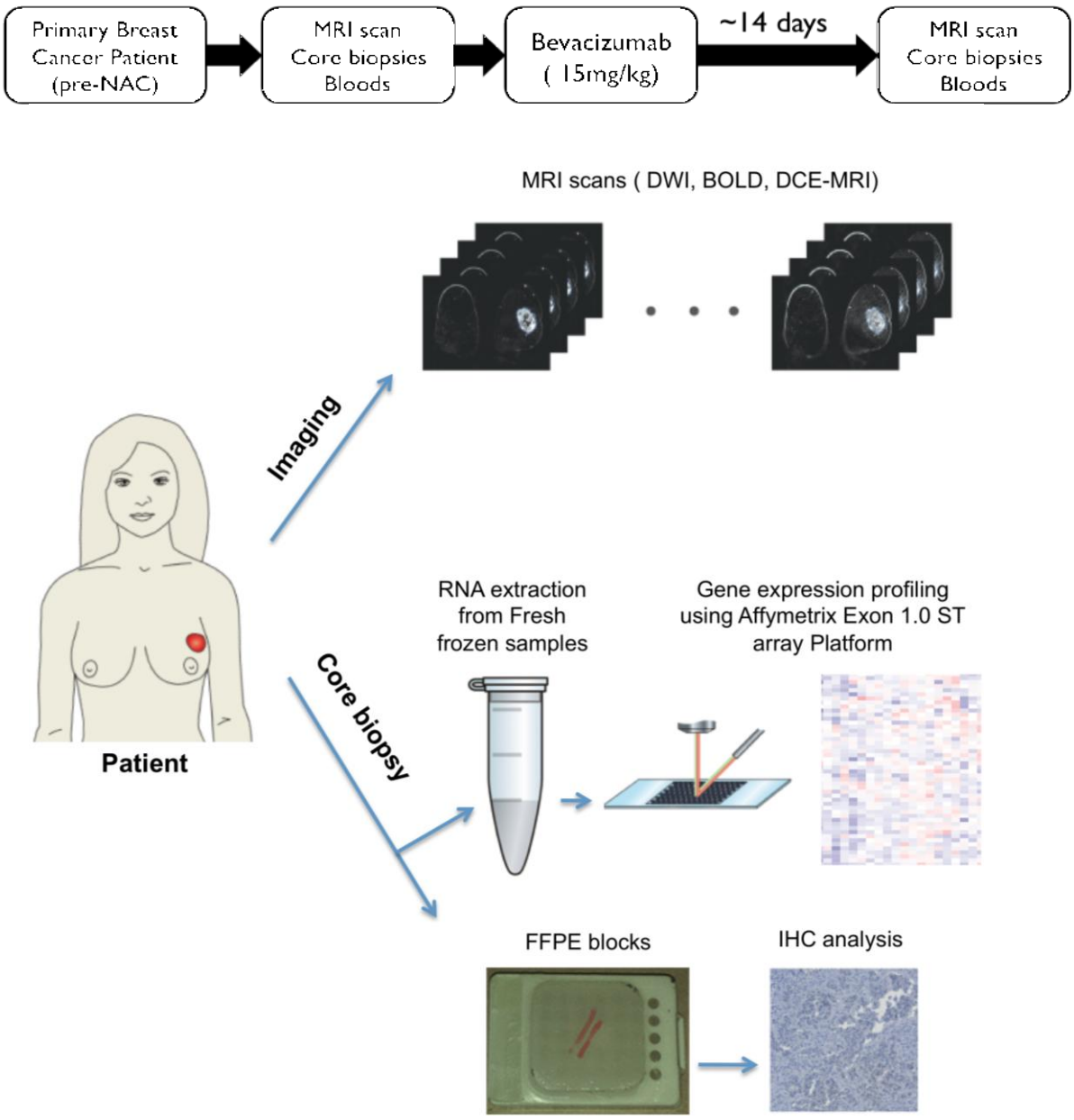

Figure-4.1: Summary of clinical study. NAC- neoadjuvant chemotherapy, MRI- Magnetic resonance imaging, DWI- Diffusion weighted imaging, BOLD- Blood oxygen level dependent scan, DCE-MRI- Dynamic contrast enhanced MRI, FFPE- Formalin fixed paraffin embedded, IHC- Immunohistochemistry.

Of the 47 patients (Oxford, n=30 and MVH, n=17) enrolled in the study, 41 had both good quality MRI scans and core biopsies, pre- and post- bevacizumab therapy and were considered suitable for subsequent comparative analysis (Figure-4.2: CONSORT diagram summarising patient recruitment).

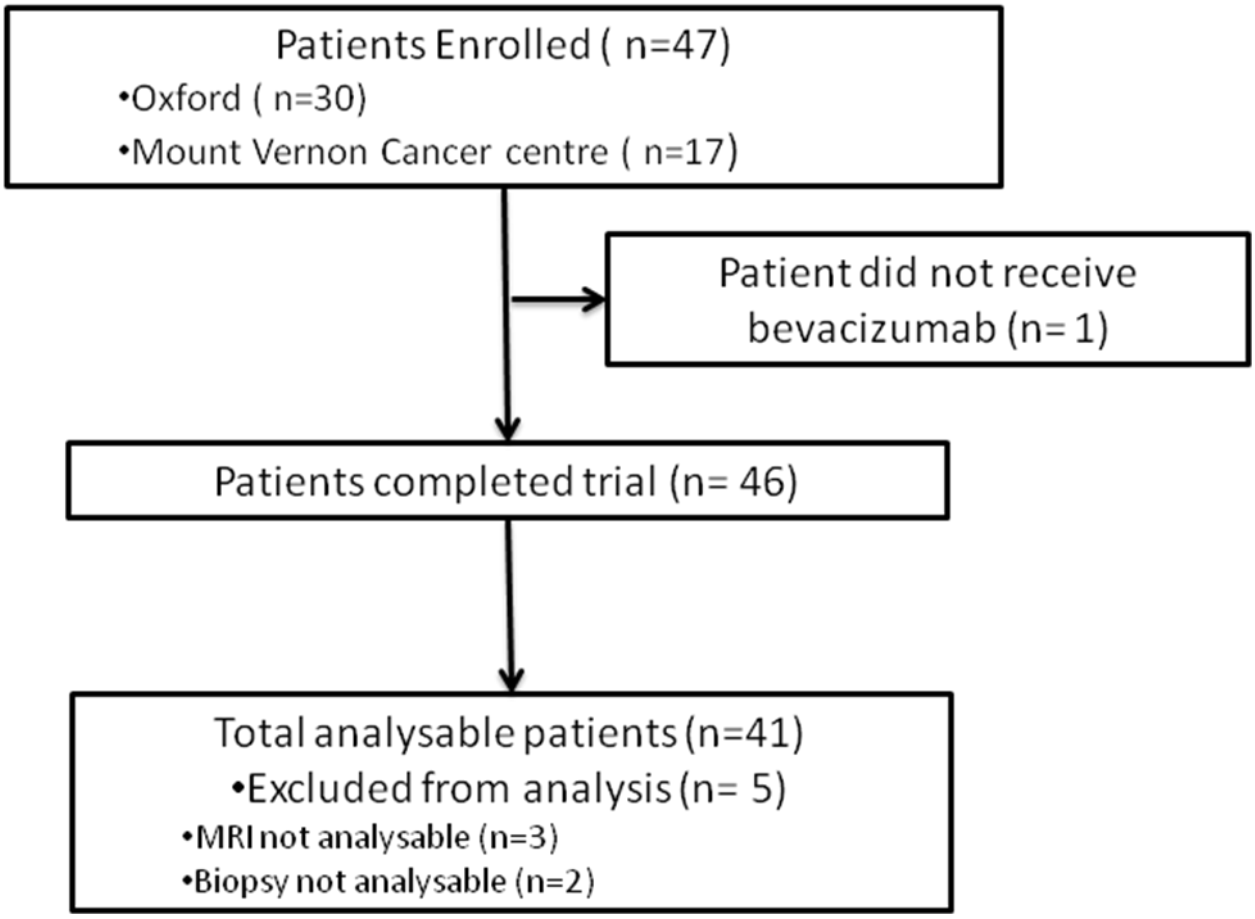

Figure-4.2: CONSORT diagram showing the clinical trial recruitment.

For this research work, only the ductal subtype was considered for analysis (n=36). In this chapter, the clinical and DCE-MRI analysis results of these patients are discussed. DCE-MRI data was available for 35 patients.

4.3 Patient characteristics

All 36 patients were female with a median age of 47 years (range 34-76 years); median size of breast mass (maximum diameter measured clinically) was 50 mm (range 20-100 mm). 19/36 patients had a right-sided breast tumour mainly involving right outer (upper/ lower) quadrants (n=12). The most common stage of presentation was stage IIB (n=15) followed by IIIA (n=13). 6 patients clinically had breast erythema at their initial presentation. Out of these 36 patients, 26 were ER positive and 9 patients were HER2 positive. 5 patients were triple receptor negative. All patients received neoadjuvant chemotherapy as per local protocol at both sites (Oxford and Mount Vernon Cancer Centre). 36% patients (n=13) had good pathological response after neoadjuvant chemotherapy. This includes 6 patients (classified as pCR) with no viable tumour seen either in breast or in lymph nodes and 7 patients who had only few scattered cells in final histological examination of either breast mass or lymph nodes after chemotherapy (classified as near to pCR) (see Table-4.1 for details).

Table-4.1: Patients characteristics

Sex	Female (n=36)
Median Age (range)	47 years (34-76 years)
Side of breast mass (Right/ Left)	19 / 17
Menopausal status	Premenopausal (n=25), Postmenopausal (n=11)
Median size (maximum diameter) of breast mass (range)	50 mm (20-100mm)
Erythema (Pre-bevacizumab)	6 patients
Initial Stage at Presentation[1]	IIA (n= 2), IIB (n=15), IIIA (n=13), IIIB (n=4), IIIC (n=2)
Lymph nodes status[1] (Pre- bevacizumab)	N0(n=6), N1(n= 23), N2(n=5), N3(n=2)
Grade	Grade 2 (n=15), Grade 3 (n=21)
Receptor Status	ER positive (n=26) negative(n=10) PR Positive (n=20) negative (n=16) HER2 positive (n=09) negative (n= 27) Triple Negative (n=5)
Pathological response (post NAC) [2]	pCR (n=6) / near to pCR (n= 7), PR (n= 19), no/ minimal (n= 2), n/a (n=2)

1. As per AJCC 2002 breast cancer staging (Singletary, Allred et al. 2002)
2. Pathological responses: pCR- Complete pathological response, Near to pCR - only scattered cells in the final pathology, PR- Partial response

4.4 Assessment of clinical response

Patients were examined at baseline and two weeks after dosing with bevacizumab. Clinical response was assessed qualitatively by clinical examination to see any physical changes in the breast mass and quantitatively by measuring the maximum dimension of the palpable tumour using a vernier calliper. Although, there was no significant change in clinically measureable maximum dimension of tumour (P=0.14), there was a marked reduction in breast erythema observed two weeks after a single cycle of bevacizumab in 4 out of 6 patients who had an erythematous breast mass at initial presentation (Figure- 4.3).

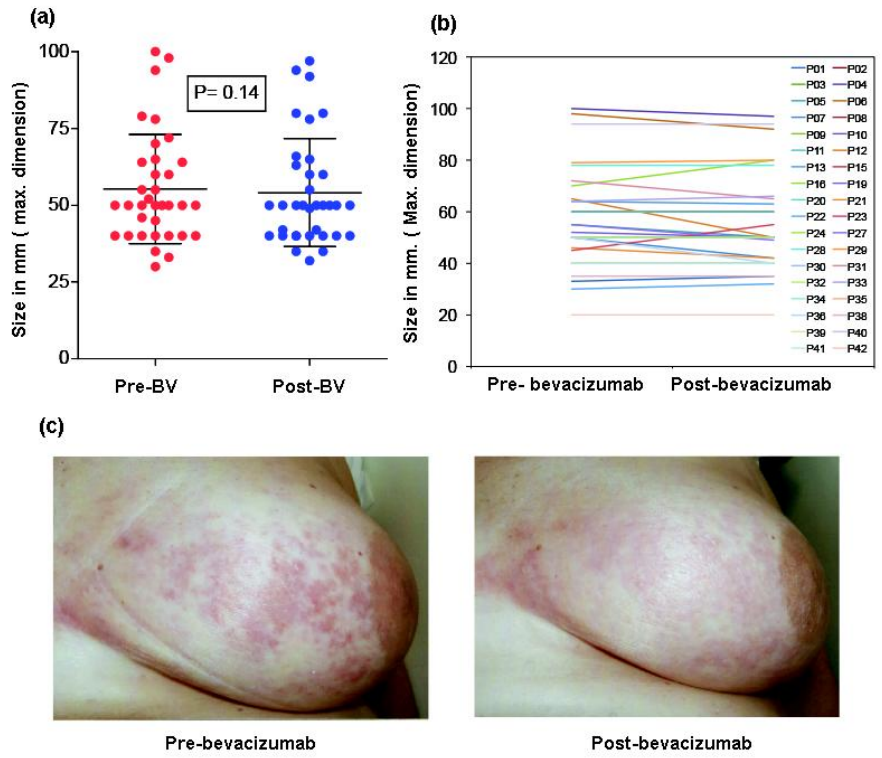

Figure-4.3: Clinical response two weeks after one cycle of bevacizumab. (a) Plot showing clinically no significant change in size (error bars show mean± SD), BV- bevacizumab. (b) Line plot showing patient-by-patient change in maximum dimension after bevacizumab. (c) Marked reduction in erythema two weeks after bevacizumab.

4.4.1 Side-effects of bevacizumab

Two weeks after the single dose of bevacizumab, the side effects were reported as per Common Terminology Criteria for Adverse Events (CTCAE v3.0) (http://ctep.cancer.gov). Only a few patients reported grade 1/2 toxicities. These were: headache (n=5), tiredness (n=5), bleeding from the PICC line (peripherally inserted central catheters) site (n=4), hypertension defined as >150/100 mm of Hg (n=1), flu-like symptoms (n=2) and allergic reaction (n=1). Only 1 patient had grade 3 hypertension requiring a change in antihypertensive during treatment. There was no proteinuria noted on urine dipstick after bevacizumab.

4.5 Baseline MRI parameters analyses

As mentioned previously (Chapter 2, Section 2), pre-bevacizumab DCE-MRI images were classified using the BI-RADS classification (2003; Erguvan-Dogan, Whitman et al. 2006). The most common shape observed was 'Round/ Oval' (18/ 35) and most tumours had 'Irregular' margin (26/35) (Table-4.2).

Table- 4.2: Pre-bevacizumab BI-RADS Classification

BI-RADS classification (Pre-bevacizumab)		Number of patients
Shape	Irregular	16
	Round/ Oval	18
	Lobulated	1
Margins	Irregular	26
	Smooth	4
	Spiculated	5

4.6 Assessment of DCE-MRI pharmacokinetic parameters

To understand the effect of bevacizumab on tumour vascularity, DCE-MRI scans were analysed using a standard two-compartment pharmacokinetic model (Tofts model) (Tofts, Brix et al. 1999). Specifically, for every tumour voxel, estimates of the forward transfer constant K^{trans}, the reverse rate constant k_{ep}, and v_e, the fractional volume of the extravascular extracellular space were computed. To summarise the voxel-wise pharmacokinetic parameters for each scan, the median as well as total K^{trans}, k_{ep}, and v_e values for the region of interest were computed. In addition, non-pharmacokinetic parameters – the Initial Area Under the Gadolinium Concentration Curve at 60 seconds ($IAUGC_{60}$) and the fraction of non-enhancing voxels (NEF), were also analysed at baseline and two weeks after a single dose of bevacizumab (details mentioned in Chapter 2, Section 2).

The baseline values of the different DCE-MRI parameters are summarised in Table-4.3.

Table-4.3: Summary of Pre- bevacizumab DCE-MRI parameters

MRI parameters (pre-bevacizumab)		**Median (range)**
Pharmacokinetic parameters	Median K^{trans}	0.38 (0.11-1.54)
	Median k_{ep}	0.79 (0.38-3.82)
	Median v_e	0.48 (0.21-0.85)
	Total K^{trans}	3420 (775-52900)
	Total k_{ep}	7920 (2180-14600)
	Total v_e	5070 (745- 43000)
Non-pharmacokinetic parameters	Median IAUGC60	0.066 (0.015-0.225)
	NEF	0.014 (0-0.195)

1. K^{trans}: Transfer constant from plasma to EES
2. k_{ep} : Rate constant from EES to plasma
3. v_e : Fractional volume of EES
4. IAUGC60: Initial area under the gadolinium curve at 60 seconds post-contrast injection
5. NEF: Non-enhancing fraction i.e. fraction of all tumour voxels that do not show significant enhancement

4.7 Correlation of baseline DCE-MRI parameters with BI-RADS classifications

We were interested to see if there was any association of BI-RADS classifications specifically the shape and margin of tumour, with the baseline DCE-MRI parameters. Interestingly, irregular shape tumours had significantly higher total K^{trans}, total k_{ep} and total v_e in comparison to round/oval shaped tumours (Mann-Whitney test, P=0.008, P=0.01, P= 0.002 respectively) (Table-4.4, Figure- 4.4 a, c, e). To check whether the highly significant relationship was because of one extreme case, the analysis was done after excluding outliers. As expected, the significant relationship still exists even after exclusion of the two outliers (Figure- 4.4 b, d, f).

There was no significant relationship observed with other DCE-MRI parameters. Also there was no association observed between the margin of tumour and DCE-MRI parameters.

Table-4.4: Relationship of baseline DCE-MRI parameters with shape of tumour

Baseline DCE-MRI parameters	**Shape of tumour (Irregular vs. Round vs. Oval)** P values (Mann-Whitney test)	**Margin (Irregular vs. Others)** P values (Mann-Whitney test)
Median K^{trans}	0.49	0.46
Median k_{ep}	0.57	0.61
Median v_e	0.11	0.33
Total K^{trans}	**0.008**	0.38
Total k_{ep}	**0.01**	0.41
Total v_e	**0.002**	0.53
Median IAUGC60	0.18	0.21
NEF	0.59	1.00

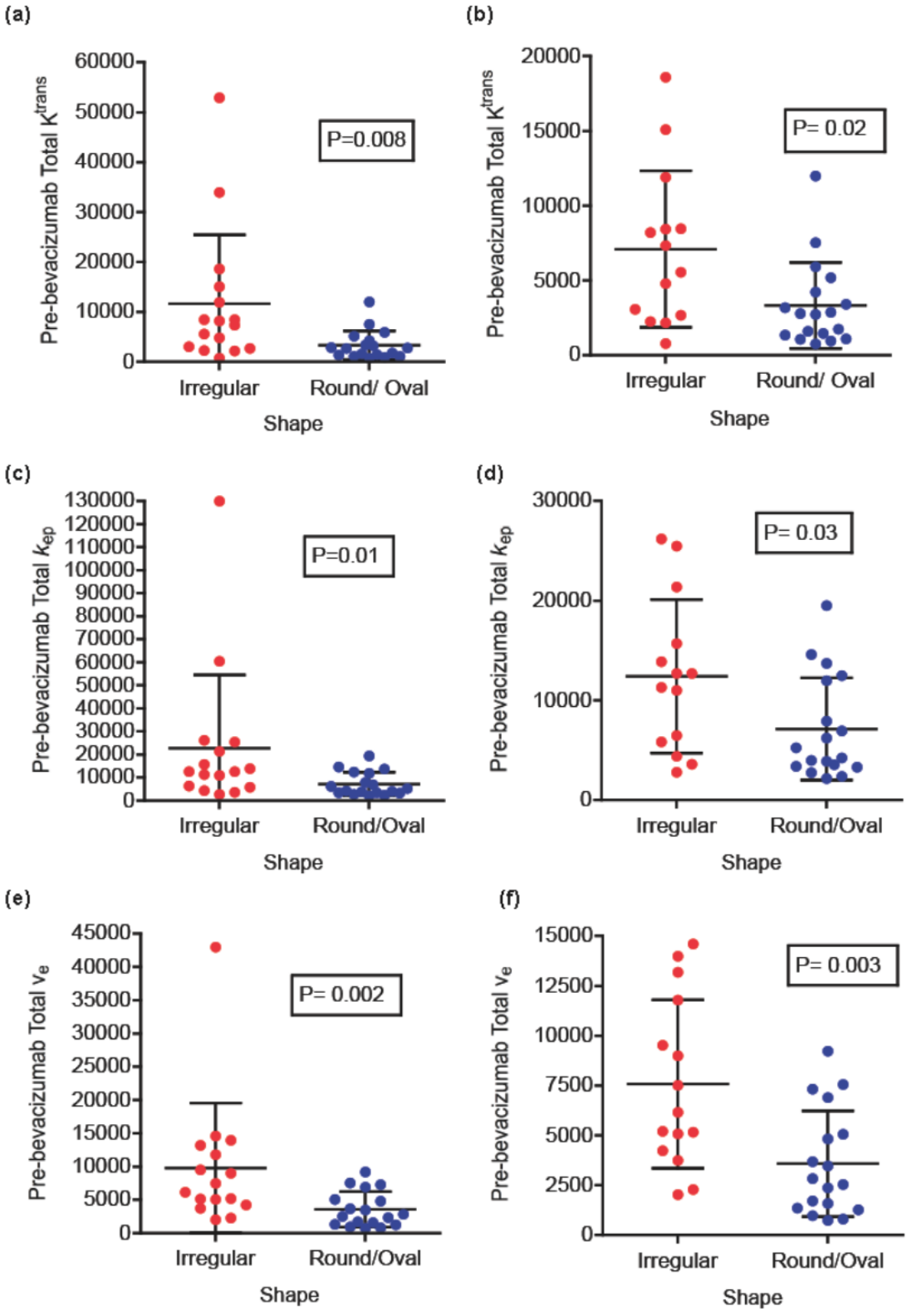

Figure-4.4: Correlation of baseline DCE-MRI PK parameters with shape of tumour. Plots (a), (c), (e) show significantly higher values of total K^{trans}, total k_{ep} and total v_e respectively, in irregular shape tumours considering all the patients. Plots (b), (d), (f) show results after exclusion of outliers; Error bars show mean±SD in each plot; P-values, Mann-Whitney test.

4.8 Relationship of baseline DCE-MRI parameters with the prognostic factors in breast cancer.

The association of baseline DCE-MRI parameters (median K^{trans}, total K^{trans}, median k_{ep}, median, v_e, median IAUGC60, NEF) with prognostic factors in breast cancer (ER, PR, HER2, grade, initial size included both clinically measured as well as tumour volume as assessed by MRI, and age at presentation) was assessed. There was no significant correlation observed between DCE-MRI parameters and most of the prognostic factors (Table-4.5, 4.6) except as expected, there was a significant association of baseline total K^{trans}, total k_{ep} and total v_e with size/ volume of tumour (Table- 4.6).

Table-4.5: Relationship of baseline DCE-MRI parameters with receptor status

DCE-MRI Parameters	ER+ vs. ER- [1*]	ER+PR+ vs. ER+PR- vs. ER-PR- [2‡]	HER2+ vs. HER2 - [3*]	ER-PR-HER2- vs. others [4*]
Median K^{trans}	0.08	0.22	0.50	0.14
Median k_{ep}	0.22	0.29	0.31	0.44
Median v_e	0.67	0.72	0.93	0.69
Total K^{trans}	0.52	0.58	0.35	0.41
Total k_{ep}	0.51	0.38	0.36	0.47
Total v_e	0.73	0.6	0.41	0.69
Median IAUGC60	0.38	0.59	0.50	0.18
NEF	0.58	0.4	0.45	0.33

* Columns showing P values (Mann-Whitney test)

‡ Columns showing P value (Kruskal-Wallis test)

1. ER+ (n= 25), ER- (n= 10)
2. ER+PR+ (n= 18), ER+PR- (n=7), ER-PR- (n=9), only one patient was ER-PR+ not included in analysis.
3. HER2+ (n= 9), HER2- (n= 26)
4. ER-PR-HER2- (n=5), Others (n=30)

Table-4.6: Relationship of baseline DCE-MRI parameters with other prognostic factors

DCE-MRI Parameters	Grade 2 vs. Grade 3 [1*]	Size (clinical) ‡	Tumour volume (MRI) ‡
Median K^{trans}	0.99	0.03 (0.87)	0.16 (0.37)
Median k_{ep}	0.95	-0.16 (0.35)	-0.12 (0.49)
Median v_e	0.94	0.29 (0.09)	0.29 (0.09)
Total K^{trans}	0.78	0.52 (0.001)	0.85 (<0.0001)
Total k_{ep}	0.57	0.51 (0.002)	0.87 (<0.0001)
Total v_e	0.93	0.63 (<0.0001)	0.94 (<0.0001)
Median IAUGC60	0.88	0.22 (0.20)	0.37 (0.03)
NEF	0.49	-0.01 (0.94)	-0.30 (0.08)

* Column showing P-Value, Mann-Whitney test.
‡ Column showing Spearman coefficient r (P-value)
1) Grade 2 (n= 14), Grade 3 (n=21).

4.9 Assessment of changes in DCE-MRI parameters in response to bevacizumab

DCE-MRI analysis was done at baseline and 2 weeks after a single cycle of bevacizumab. There was a significant reduction observed in the tumour volume as assessed by MRI (P=0.0005, Wilcoxon-signed rank test) (Figure-4.5).

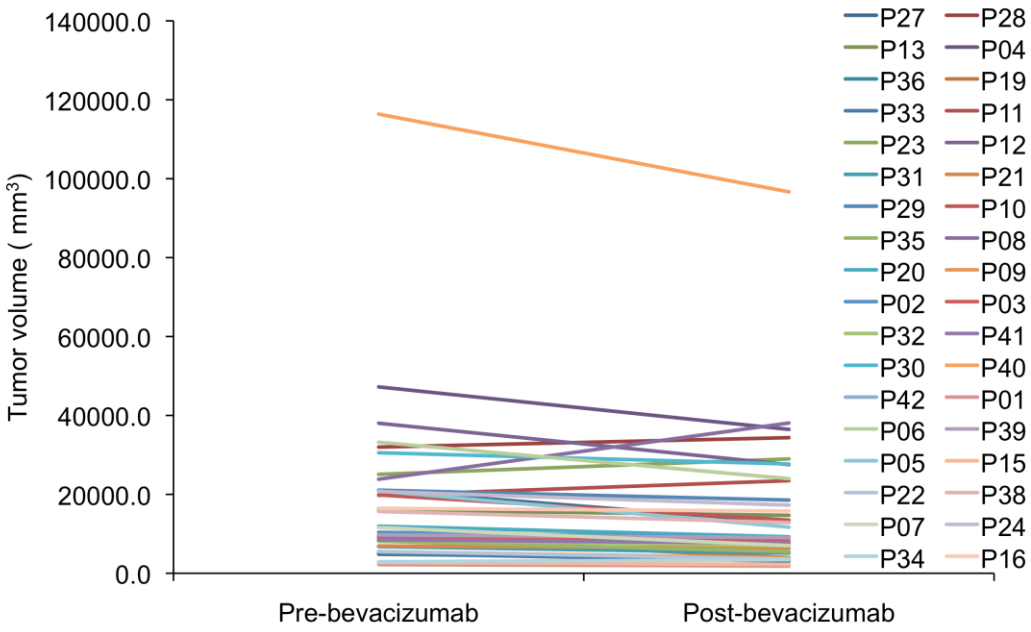

Figure-4.5: Significant reduction in tumour volume as measure by MRI two weeks after single cycle of bevacizumab. (P= 0.0005, Wilcoxon-signed rank test)

From pharmacokinetic analysis of DCE-MRI, a significant reduction was observed on average across all patients of median K^{trans} (P<0.0001), total K^{trans} (P<0.0001), median k_{ep} (P<0.0001), total k_{ep} (P=0.002) and $IAUGC_{60}$ (P<0.0001), along with a significant increase in NEF (P<0.0001), but there was no significant change in median or total v_e (P=0.88, P=0.44 respectively) (Figure-4.6, 4.7). The whole study population (n=35) was considered for this analysis.

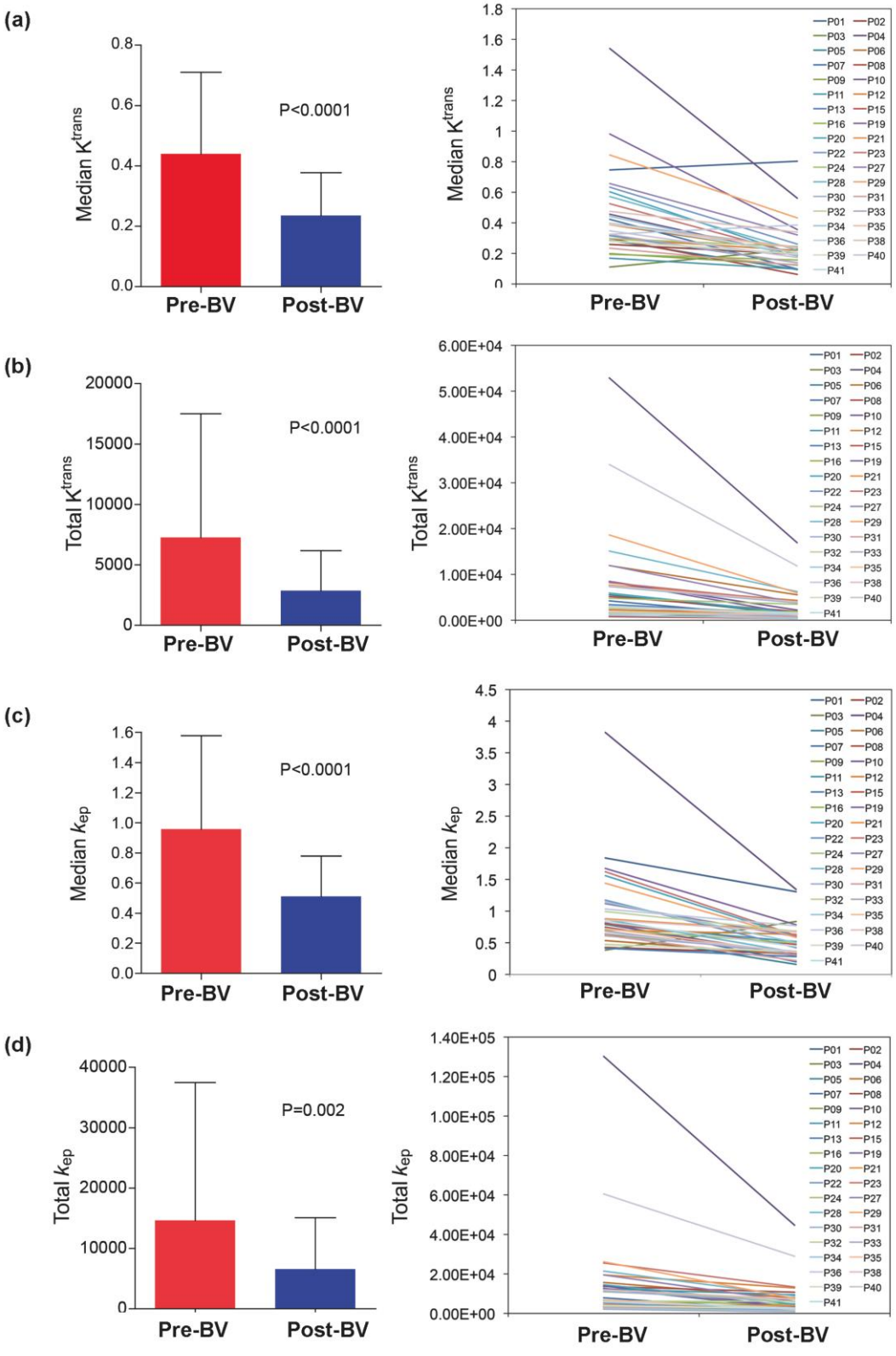

Figure-4.6: Plots showing significant reduction of DCE-MRI parameters after bevacizumab. Specifically, there was reduction of (a) Median K^{trans}, (b) Total K^{trans}, (c) Median $k_{ep,}$ (d) Total k_{ep}. Left panel shows mean± SD of each parameter across all the patients both pre and post bevacizumab (BV), right panel shows patient by patient changes in each parameter (P- value, Wilcoxon-rank test).

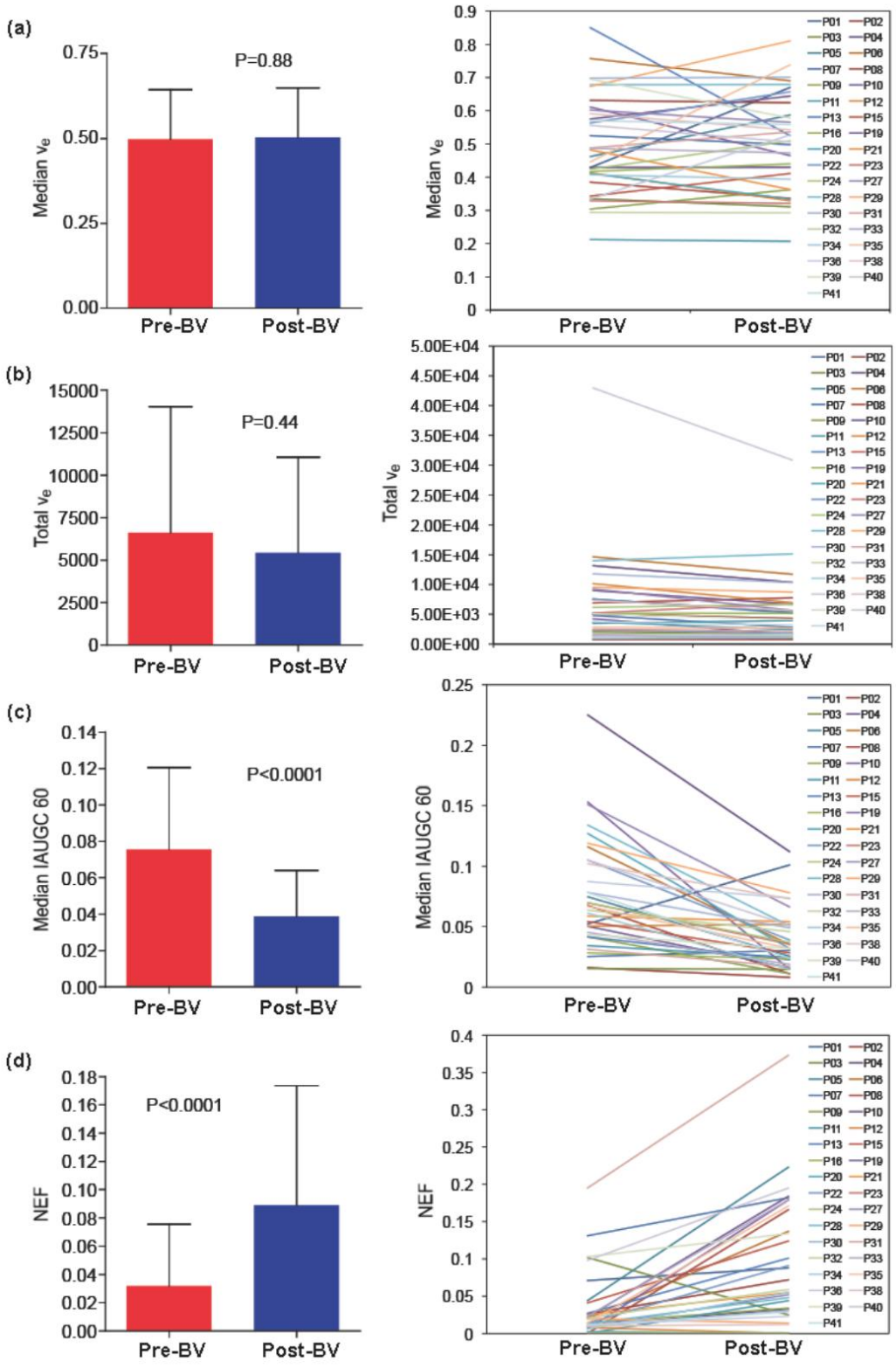

Figure-4.7: Plots showing changes of DCE-MRI parameters after bevacizumab. Specifically, there was no significant reduction of (a) Median v_e, (b) Total v_e, but there was a significant reduction of (c) Median IAUGC60, (d) NEF. Left panel shows mean± SD of each parameter across all the patients both pre and post bevacizumab (BV), right panel shows patient by patient changes in each parameter (P-value, Wilcoxon-rank test).

Although globally across all patients, there was a significant change observed in most of the DCE-MRI parameters (except v_e) after bevacizumab (Figure 4.6, 4.7) there was a wide variation observed across patients in response to bevacizumab. For example, there was significant variation observed in percentage change in median K^{trans} ranging from 104% to -79% (Figure 4.8). Similar responses were noted considering other DCE-MRI parameters On further analysis, the imaging patterns of response, assessed visually by 3 independent observers and then consensus together from parametric maps of K^{trans}, varied from no significant change in spatial K^{trans} values after bevacizumab to a highly significant reduction in K^{trans} values across the complete tumour mass (examples are shown in Figure 4.9 to 4.13).

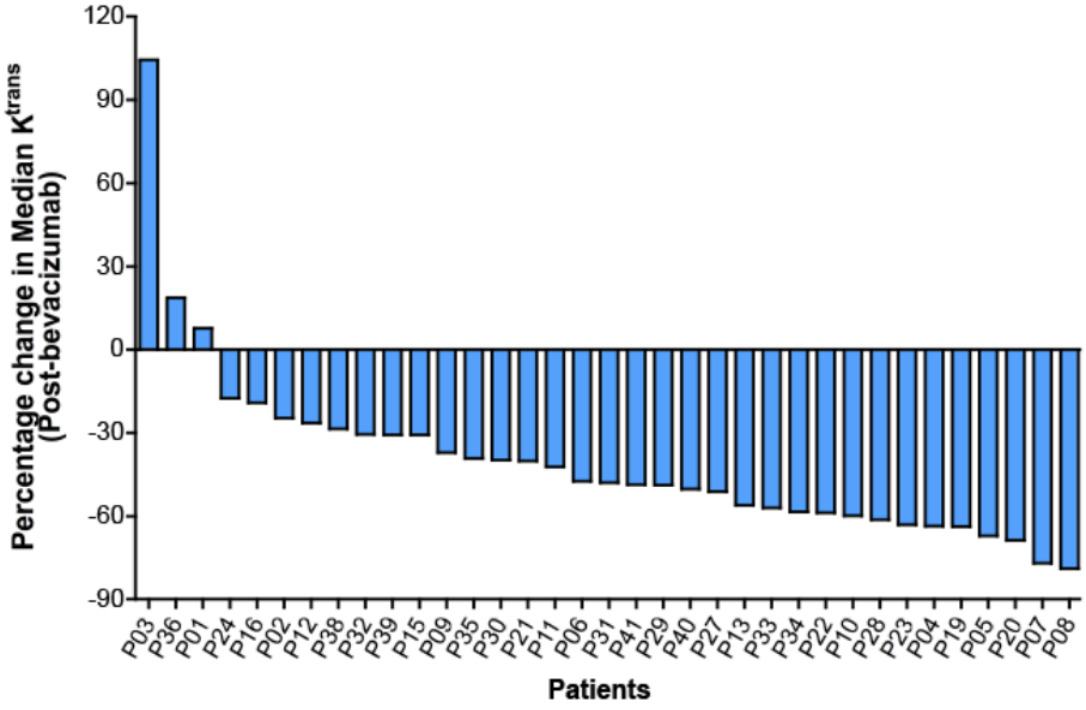

Figure-4.8: Waterfall plot showing percentage change in median K^{trans} across all the patients in response to bevacizumab.

Patient- P03 K^{trans} maps

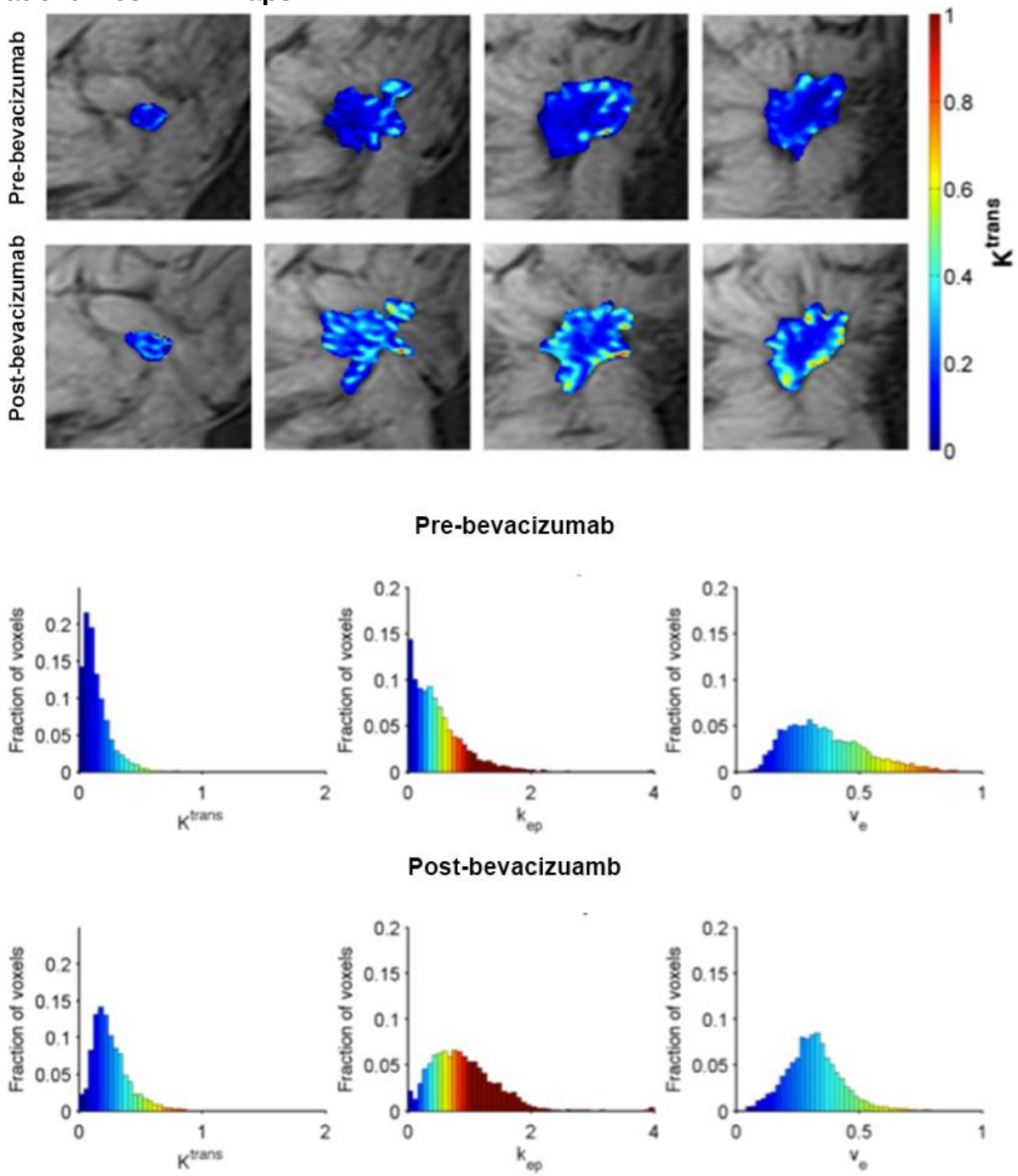

Figure-4.9: Parametric K^{trans} map for patient P03 [Ductal carcinoma, ER+ PR- Her2+, Grade 2, Stage IIA (T2N0M0)]. Color-coding is on scale from blue to red depicts proportionate increase in K^{trans}.
Top: Parametric maps of tumour K^{trans} overlaid on the pre-contrast T1-weighted image for 4 central tumour slices.
Bottom: Histograms of voxel-wise K^{trans}, k_{ep} and v_e values taken over 4 central tumour slices. Histograms showing shift towards right in both K^{trans} and k_{ep} with no significant difference in v_e depicting increase in fraction of voxels with higher values of K^{trans} and k_{ep} after bevacizumab. For v_e there was no significant difference observed.

Patient- P38 K^{trans} maps

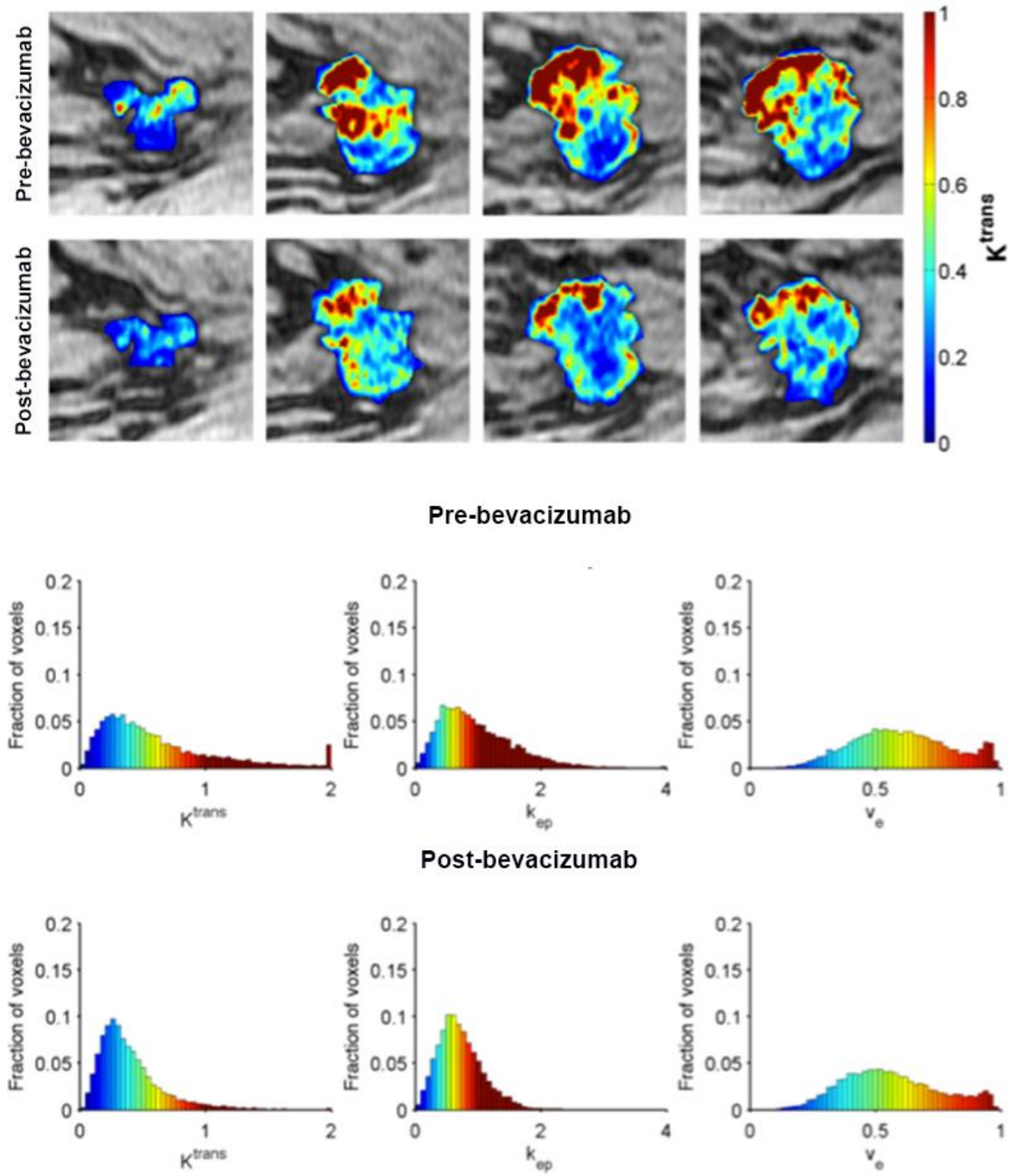

Figure-4.10: Parametric K^{trans} map for patient P38 [Ductal carcinoma, ER+ PR+ HER2-, Grade 3, Stage IIIA (T2N2aMx)]. Color-coding is on scale from blue to red depicts proportionate increase in K^{trans}.
Top: Parametric maps of tumour K^{trans} overlaid on the pre-contrast T1-weighted image for 4 central tumour slices.
Bottom: Histograms of voxel-wise K^{trans}, k_{ep} and v_e values taken over 4 central tumour slices. Histograms showing shift towards left in both K^{trans} and k_{ep} with no significant difference in v_e depicting decrease in fraction of voxels with higher values of K^{trans} and k_{ep} after bevacizumab. For v_e there was no significant difference observed.

Patient- P11 K^{trans} maps

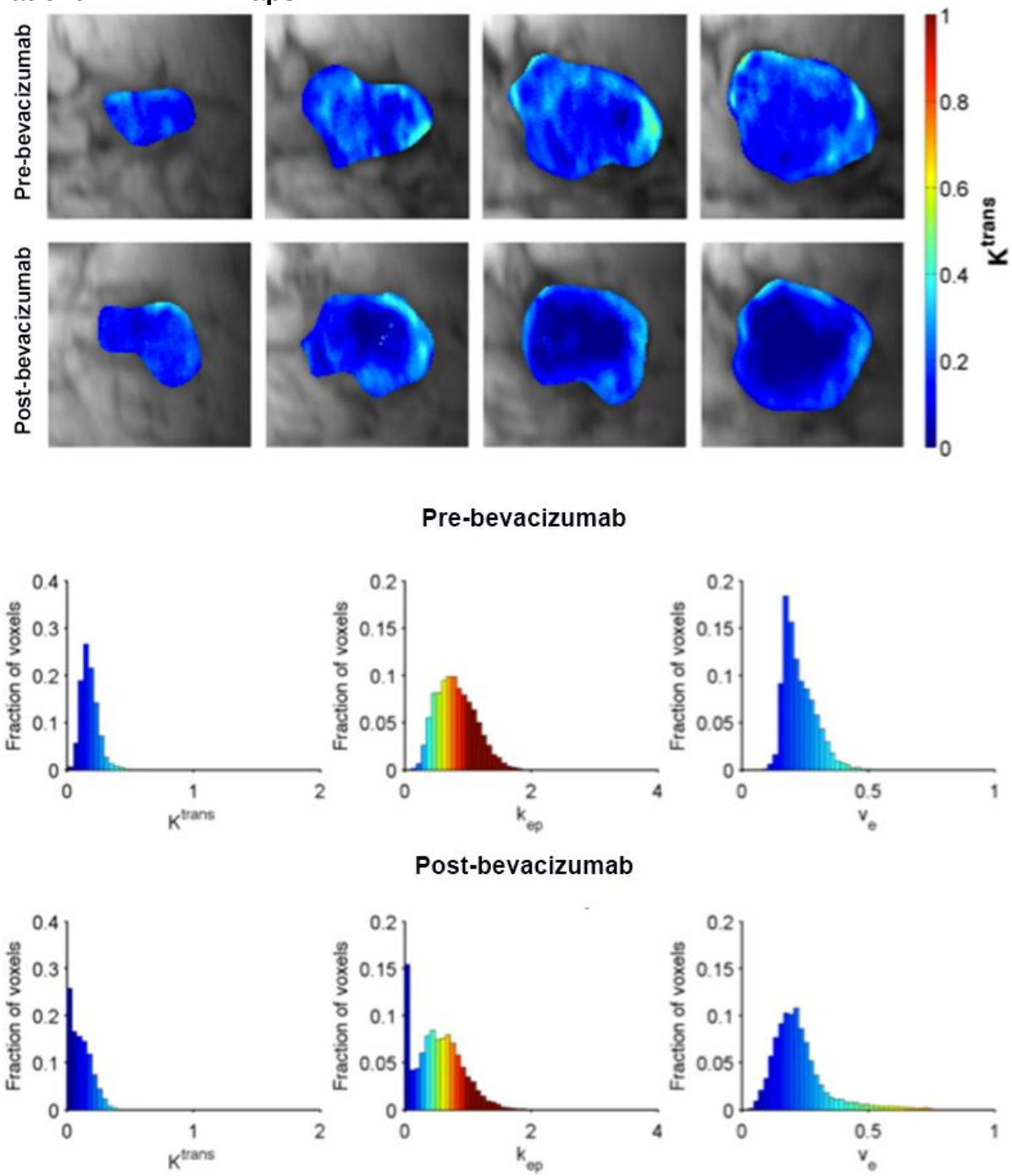

Figure-4.11: Parametric K^{trans} map for patient P11 [Ductal carcinoma, ER-PR- HER2-, Grade 2, Stage IIB (T2N1M0)]. Color-coding is on scale from blue to red depicts proportionate increase in K^{trans}.
Top: Parametric maps of tumour K^{trans} overlaid on the pre-contrast T1-weighted image for 4 central tumour slices.
Bottom: Histograms of voxel-wise K^{trans}, k_{ep} and v_e values taken over 4 central tumour slices. Histograms showing shift towards left in both K^{trans} and k_{ep} with no significant difference in v_e depicting decrease in fraction of voxels with higher values of K^{trans} and k_{ep} after bevacizumab. For v_e there was no significant difference observed.

Patient- P05 K^{trans} maps

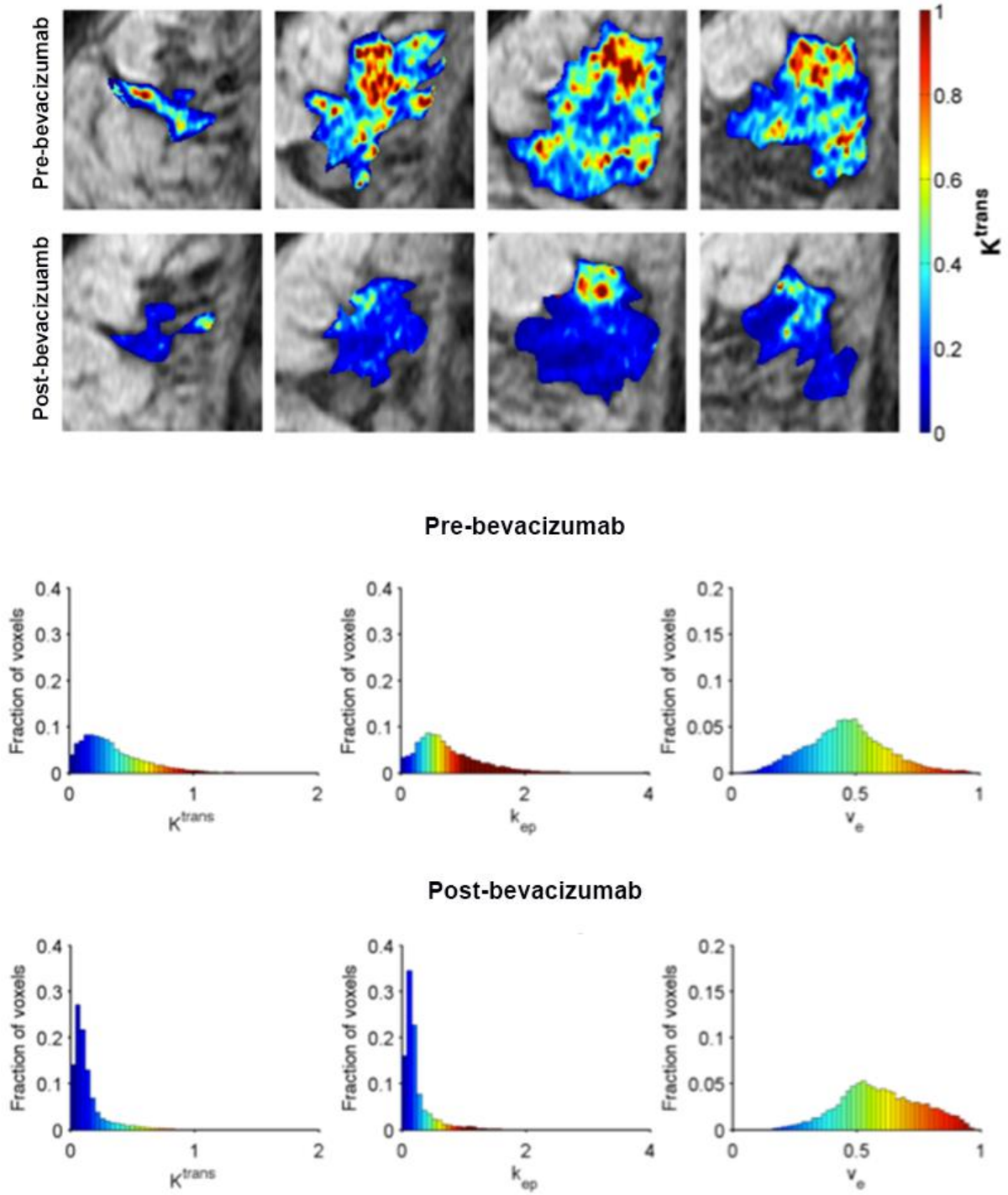

Figure-4.12: Parametric K^{trans} map for patient P05 [Ductal carcinoma, ER+ PR- HER2-, Grade 3, Stage IIIA (T3N2M0)]. Color-coding is on scale from blue to red depicts proportionate increase in K^{trans}.
Top: Parametric maps of tumour K^{trans} overlaid on the pre-contrast T1-weighted image for 4 central tumour slices.
Bottom: Histograms of voxel-wise K^{trans}, k_{ep} and v_e values taken over 4 central tumour slices. Histograms showing shift towards left in K^{trans} and k_{ep} but not for v_e depicting significant decrease in fraction of voxels with higher values of K^{trans} and k_{ep} after bevacizumab. For v_e there was an increase in number of voxels with higher values of v_e.

Patient- P08 K^{trans} maps

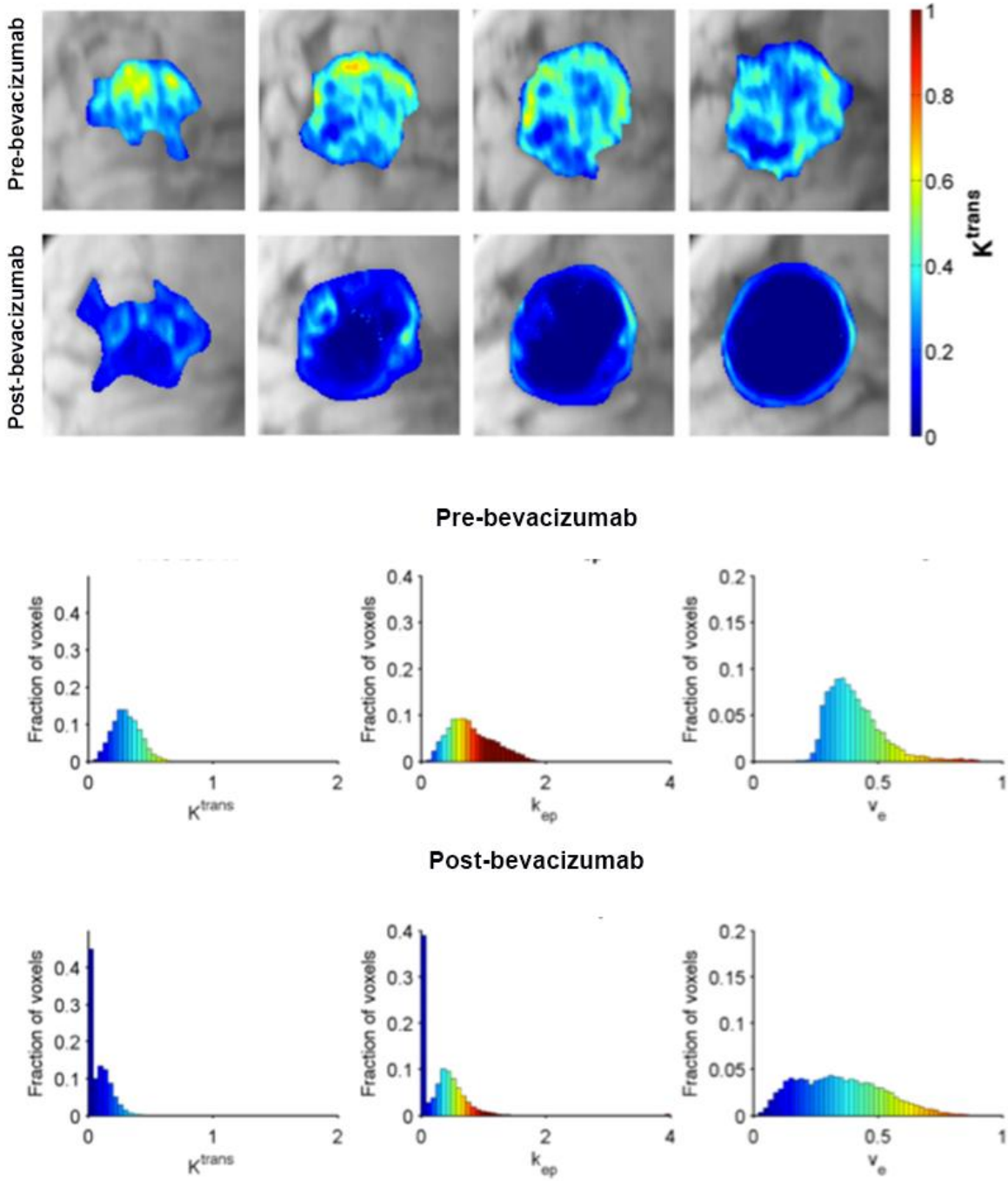

Figure-4.13: Parametric K^{trans} map for patient P08. [Ductal carcinoma, ER-PR+ HER2-, Grade 3, Stage IIB (T2N1M0)]. Color-coding is on scale from blue to red depicts proportionate increase in K^{trans}.
Top: Parametric maps of tumour K^{trans} overlaid on the pre-contrast T1-weighted image for 4 central tumour slices.
Bottom: Histograms of voxel-wise K^{trans}, k_{ep} and v_e values taken over 4 central tumour slices. Histograms showing shift towards left in K^{trans}, k_{ep} and v_e depicting significant decrease in fraction of voxels with higher values of K^{trans} and k_{ep} after bevacizumab. For v_e also there was a marked increase in number of voxels with lower values of v_e.

4.10 Assessment of changes in DCE-MRI parameters in subgroup of patients based on receptor status

Two recent neoadjuvant bevacizumab trials have shown variable response to bevacizumab along with chemotherapy in different subgroup of patients based on their receptor status (Bear, Tang et al. 2012; von Minckwitz, Eidtmann et al. 2012). In view of this, to this study data was analysed to see whether any specific subgroup of patients based on their receptor status showed a difference in reduction of their DCE-MRI parameters two weeks after single cycle of bevacizumab.

There was no significant difference observed in the absolute changes or the percentage changes of median K^{trans}, total K^{trans}, median k_{ep}, total k_{ep} or median IAUGC60 among sub-groups based on pre-bevacizumab receptor status of patients (Table- 4.7).

Table-4.7: Changes in DCE-MRI parameters in different subgroups of patients based on their receptor status

DCE-MRI parameters		ER+ vs. ER- [1*]	ER+PR+ vs. ER+PR- vs. ER-PR- [2‡]	HER2+ vs. HER2 - [3*]	ER-PR-HER2- vs. others [4*]
Median K^{trans}	Absolute change	0.66	0.77	0.21	0.31
	Percentage change	0.89	0.63	0.2	0.21
Total K^{trans}	Absolute change	0.67	0.57	0.39	0.41
	Percentage change	0.92	0.88	0.44	0.27
Median k_{ep}	Absolute change	0.67	0.82	0.83	0.31
	Percentage change	0.92	0.58	0.71	0.19
Total k_{ep}	Absolute change	0.37	0.35	0.46	0.38
	Percentage change	0.43	0.80	0.78	0.47
Median $IAUGC_{60}$	Absolute change	0.92	0.39	0.84	0.18
	Percentage change	0.27	0.34	0.77	0.27

* Columns showing P values (Mann-Whitney test)

‡ Columns showing P value (Kruskal-Wallis test)

1. ER+ (n= 25), ER- (n= 10)
2. ER+PR+ (n= 18), ER+PR- (n=7), ER-PR- (n=9), only one patient was ER-PR+ not included in analysis.
3. HER2+ (n= 9), HER2- (n= 26)
4. ER-PR-HER2- (n=5), Others (n=30)

4.11 Change in DCE-MRI parameters after one cycle of bevacizumab as a function of pre-bevacizumab values

These analyses were done to assess the association of significantly changing PK parameters with the corresponding pre-bevacizumab values. Interestingly, a strong negative correlation was observed between absolute change in median K^{trans}, median k_{ep} and total K^{trans} with the corresponding pre-bevacizumab values (Spearman r= -0.75 (P<0.0001), -0.77 (P<0.0001) and -0.97 (P<0.0001) respectively). In contrast, a weaker negative correlation was observed between the percentage changes with baseline values (Specifically, spearman r= -0.49 (P=0.003), -0.38 (P=0.02), -0.48 (P=0.003) for median K^{trans}, median k_{ep} and total K^{trans} respectively). A similar relationship was observed for absolute change in total k_{ep} (Spearman r= - 0.88, P=0.003), but the percentage change in total k_{ep} was not significantly related to the pre-bevacizumab total k_{ep} (Spearman r= -0.28, P=0.10) (Figure- 4.14, 4.15).

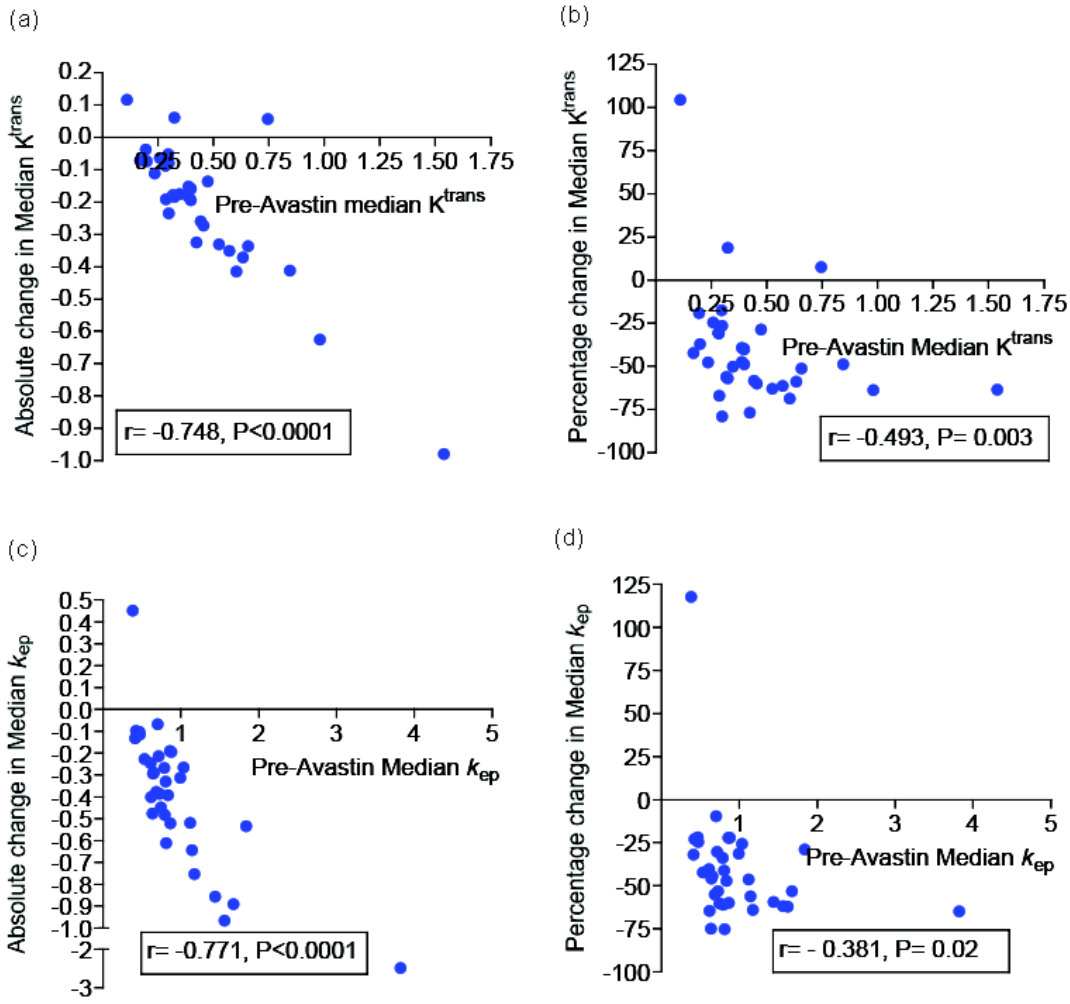

Figure-4.14: Changes of median PK parameters as function of baseline values (n=35**).** Significant negative correlation of (a) Absolute change in median K^{trans}, (b) Percentage change in median K^{trans}, (c) Absolute change in median k_{ep}, (d) Percentage change in median k_{ep} with corresponding pre-bevacizumab values.

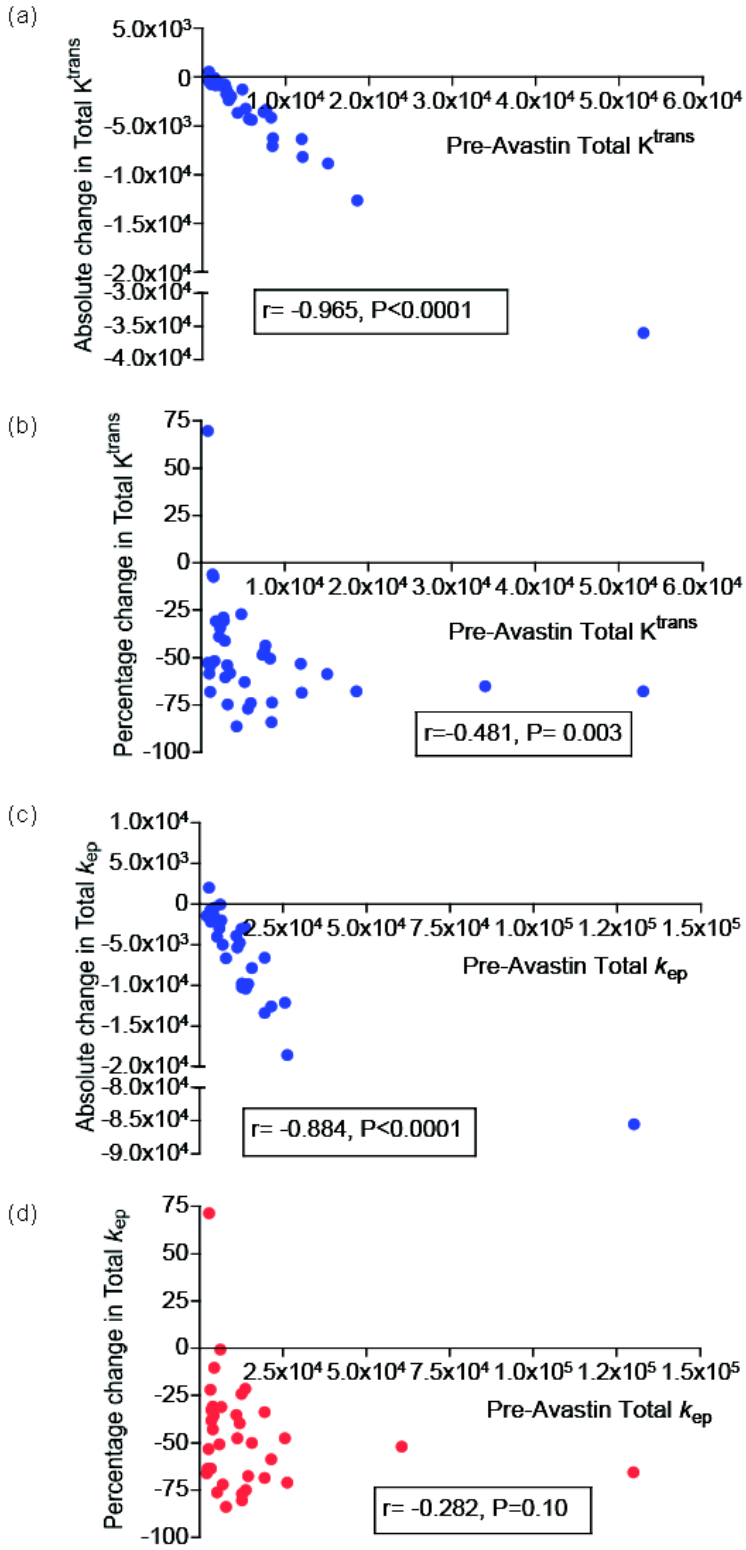

Figure-4.15: Changes of total PK parameters as function of baseline values (N=35). Plot showing negative correlation of (a) Absolute change in total K^{trans}, (b) Percentage change in total K^{trans}, (c) Absolute change in total k_{ep}, (d) Percentage change in total k_{ep} with corresponding pre-bevacizumab values.

4.12 Assessment of final pathological response as a function of the baseline DCE-MRI

This analysis was performed to understand if baseline DCE-MRI parameters were correlated with the final pathological response after neoadjuvant chemotherapy. There was no significant difference noted in the pre-bevacizumab values of DCE-MRI parameters (median K^{trans}, total K^{trans}, median k_{ep}, total k_{ep} or median IAUGC60) among good pathological responders vs. others as assessed in surgical specimens after 6 cycles of neoadjuvant chemotherapy (Table- 4.8).

Table-4.8: Final pathological responses as function of baseline DCE-MRI parameters

DCE-MRI parameters (Pre-bevacizumab)	**Good pathological responders[1] vs. Others [2]** (P-value, Mann-Whitney test)
Median K^{trans}	0.62
Total K^{trans}	0.90
Median k_{ep}	0.45
Total k_{ep}	0.70
Median IAUGC60	0.056

1. Good pathological responders: Complete/ near complete pathological response (n=13)
2. Others: Includes PR (n=18), no response (n=2), not available (n=2)

4.13 Assessment of final pathological response as function of changes in DCE-MRI parameters after bevacizumab

Antiangiogenic therapies may prune the abnormal leaky tumour blood vessels, leading to transient normalisation of the vessels (Jain 2005), which in turn could result in better drug delivery to tumours and eventually better response to chemotherapy. To investigate this hypothesis, additional analysis was performed to assess whether the changes in DCE-MRI parameters two weeks after the single cycle of bevacizumab were predictive of the final pathological responses after neoadjuvant chemotherapy.

There was no significant difference observed between the absolute or percentage changes of different parameters considering good pathological responders versus others (Table- 4.9).

Table-4.9: Final pathological responses as function of changes in DCE-MRI parameters after bevacizumab

DCE-MRI parameters		Good pathological responders[1] vs. others [2] (P-value, Mann-Whitney test)
Median K^{trans}	Absolute change	0.30
	Percentage change	0.95
Total K^{trans}	Absolute change	0.82
	Percentage change	0.55
Median k_{ep}	Absolute change	0.30
	Percentage change	0.48
Total k_{ep}	Absolute change	0.38
	Percentage change	0.10
Median IAUGC60	Absolute change	0.11
	Percentage change	0.10

1. Good pathological responders: Complete/ near complete pathological response (n=13)
2. Others: Includes PR (n=18), no response (n=2), not available (n=2)

4.14 Discussion

Bevacizumab is the most commonly used anti-angiogenic drug in clinical practice (Ignoffo 2004; Rossari, Metzger-Filho et al. 2012; Wu and Staton 2012). In the specific case of breast cancer, the development and validation of novel biomarkers for the prediction of patient response to bevacizumab therapy is an area of particular importance given that none of the clinical studies to date have shown an overall survival benefit (Miller 2003; Miller, Chap et al. 2005; Miller, Wang et al. 2007; Miles, Chan et al. 2010; O'Shaughnessy, Miles et al. 2010; Smith, Pierga et al. 2010; Mortimer, Zonder et al. 2012; Rossari, Metzger-Filho et al. 2012). DCE-MRI has the potential to be used as non-invasive marker of angiogenesis and can be used to monitor the effects of antiangiogenic drugs (Wedam, Low et al. 2006; Padhani, Liu et al. 2009; O'Connor, Jackson et al. 2012), and as such is a potentially powerful tool for understanding and predicting response to neo-adjuvant bevacizumab therapy in primary breast cancer.

Anti-vascular drugs are believed to cause minimal cytotoxic effects and minimal changes in tumour size (Ellis, Rosen et al. 2006). In this study, no significant change in tumour size was noted on clinical assessment two weeks after bevacizumab. However, a considerable change in tumour volume as measured by MRI was observed, although detailed interpretation is difficult since our DCE-MRI research scans had a limited field of view and did not always contain the entire tumour mass (only 6 central slices were imaged during each acquisition). Other studies have also reported reduction in size with antiangiogenic agents (Karrison, Maitland et al. 2007; O'Connor, Carano

et al. 2009; O'Connor and Jayson 2012) but not after only a single cycle of bevacizumab as observed in this study. As reported previously (Wedam, Low et al. 2006) marked reduction in erythema of skin overlying breast tumours was observed in this study.

There were concerns reported in other studies regarding the side effects particularly hypertension and proteinuria (Mortimer, Zonder et al. 2012; Rossari, Metzger-Filho et al. 2012) but there were no significant grade 3/4 side effects noted due to bevacizumab in this study probably because of the short duration of therapy.

The relationship of BIRADS classification to DCE-MRI parameters has not been extensively reported (Tozaki 2004; Tse, Chaiwun et al. 2007). Interestingly, we observed that the irregular tumours that are known to be highly malignant were also significantly more vascular at baseline than the round or oval tumours as shown by the significantly higher values of PK parameters (K^{trans} and k_{ep}).

As reported previously in other neoadjuvant bevacizumab breast cancer studies (Wedam, Low et al. 2006; Baar, Silverman et al. 2009), this study also demonstrated that systemic bevacizumab therapy markedly alters the perfusion kinetics of the tumour vasculature, as manifested by significant reductions in the DCE-MRI parameters (K^{trans}, k_{ep}, $IAUGC_{60}$) across the majority of the study population. Interestingly, we noted marked heterogeneity of response across patients, as illustrated by variation in the changes in DCE-

MRI parameters, e.g. change in median K^{trans} ranges from 104% to -79% after single cycle of bevacizumab only. There was no significant difference observed in absolute or percentage change in MRI parameters based on ER /PR/ HER2 status, grade or size of tumour at baseline. This might be due to lack of power of this study for detailed subgroup analysis based on receptor status.

Interestingly, we observed that the absolute change in the median as well as total K^{trans} and k_{ep} values after single cycle of bevacizumab were significantly negatively correlated with the corresponding baseline values. In other words, for higher pre-treatment K^{trans} / k_{ep} values, a greater decrease was observed after bevacizumab. This might have important clinical implications for selecting patients for bevacizumab therapy at baseline. Hayes et al (Hayes, Padhani et al. 2002) have reported previously similar effects after a single cycle of neoadjuvant chemotherapy especially for responders (Kendall's T = -0.72 (P = 0.002). One could argue that these effects may be due in part to regression to the mean, A good way to test for a regression to the mean effect is to average multiple baseline readings in order to reduce noise, then look at the correlation between the averaged baseline measurement and the change after therapy from the averaged baseline measurement (Barnett, van der Pols et al. 2005). The values that were artifactually high or low from a single baseline reading would thus be corrected after averaging multiple readings, which would reduce any regression to the mean trend. This analysis was performed by using the diagnostic MRIs (for the Oxford patients only, n= 14) as a second baseline measurement (since they were performed 24 hours prior to the pre-bevacizumab research scan), and then calculated the diagnostic median K^{trans}

and k_{ep} and averaged these with the corresponding research measurements. With the averaged measurements, a similar trend was still evident for both K^{trans} and k_{ep} (Figure- 4.16 a, b).

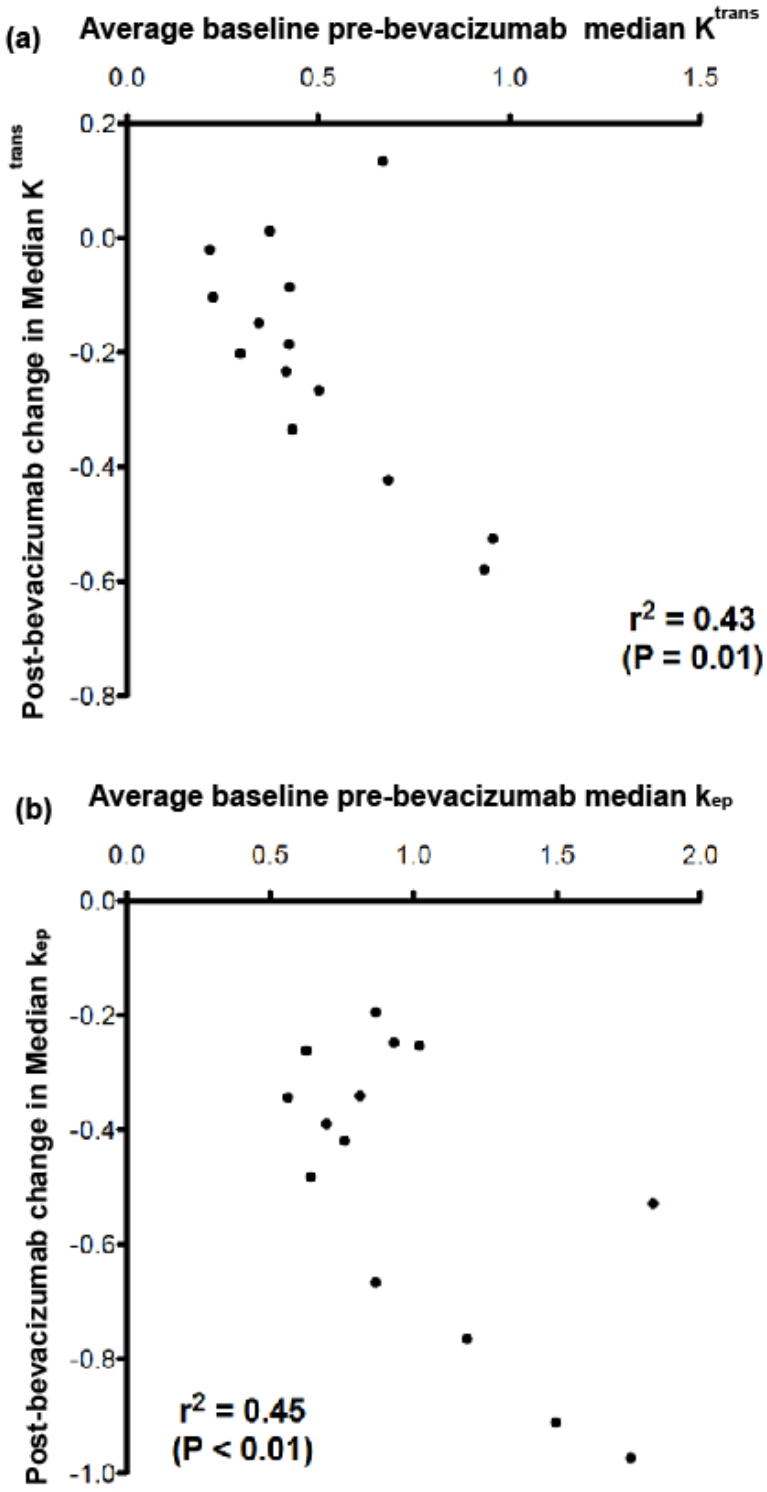

Figure-4.16: Correlation between average baseline PK parameters vs. change in PK parameters after bevacizumab. Averaged computed from diagnostic and research MRI scans.

Although this study was not designed to analyse this, we were interested to see the clinical implications of the significant reduction in DCE-MRI parameters after a single cycle of bevacizumab as observed in this study. Does this change translate into better pathological response due to reduced permeability (transient normalization of vessels) (Tong, Boucher et al. 2004; Jain 2005) and could bevacizumab increase the delivery of the first cycle of chemotherapy, enabling an improved response on subsequent cycles? Alternatively, could it worsen prognosis due to reduced vascularity and less delivery of chemotherapy to tumours? In our study, no significant relationship was noted for pathological responses after neoadjuvant chemotherapy, either with baseline values of functional MRI parameters or with changes in these parameters after the single cycle of bevacizumab. This may be due to a lack of statistical power in this study for subgroup analysis based on pathological response (pCR=6, near to pCR=7, PR=18, no response=2, not available=2). To our knowledge, no other study has been reported previously where one cycle of bevacizumab was given as a single agent prior to neoadjuvant chemotherapy. Further large scale studies are needed to better understand the effect (if any) of a single cycle of bevacizumab in the long term.

The results summarised in this chapter has shown that after a single cycle of bevacizumab there was a significant reduction in the DCE-MRI pharmacokinetic parameters, although with marked heterogeneity across patients. In the following chapter, we investigate whether gene expression analysis may be helpful in understanding the reasons behind the heterogeneity observed on DCE-MRI.

CHAPTER FIVE

5 Gene expression and Immuno-histochemistry analysis (Prospective study)

5.1 Introduction

Bevacizumab is a humanized monoclonal antibody to human VEGF that inhibits VEGF-mediated angiogenesis. Over the last decade, bevacizumab has become the most commonly used anti-angiogenic agent in clinical practice. In advanced breast cancer patients, although the use of bevacizumab with chemotherapy had shown improved progression-free survival (PFS), overall survival benefit has never been shown (Miller, Wang et al. 2007; Miles, Chan et al. 2010; O'Shaughnessy, Miles et al. 2010).

While bevacizumab has proven to be of limited benefit when used broadly in unselected breast cancer patients, there is increasing evidence that “specific subsets” of patients may show a better response than others (Bear, Tang et al. 2012; von Minckwitz, Eidtmann et al. 2012).

Several potential biomarkers have been proposed to predict response and define a subgroup who may benefit, including VEGFR polymorphisms and VEGF; PDGFR-b and VCAM1 expression; DLL4, VEGFC and neurolipin-1 and infiltrating myeloid cells (Schneider, Wang et al. 2008; Yang, Steinberg et al. 2008; Baar, Silverman et al. 2009; Jubb and Harris 2010; Jubb, Miller et al. 2011). However, no validated biomarkers have been identified that could guide patient selection for treatment or predict treatment efficacy with the anti-VEGF monoclonal antibody, bevacizumab.

A genome wide expression analysis performed before and after bevacizumab therapy is a way forward to improve our understanding of the mechanisms of

response or resistance to bevacizumab. This knowledge would be useful to develop patient specific biomarkers for bevacizumab therapy that could also translate into better treatment response and would be cost effective as well in long term.

As mentioned in previous chapters (Chapter-1 and Chapter-4), we have conducted a window-of-opportunity study in newly diagnosed locally advanced breast cancer patients using a single cycle of bevacizumab given before their standard neoadjuvant chemotherapy with detailed pharmacodynamic assessments using DCE-MRI, core biopsies for gene expression arrays (Affymetrix Human Exon 1.0 ST arrays) and immunohistochemistry analysis for specific markers at baseline and 2 weeks after bevacizumab.

In this chapter, the results of the gene expression analysis and immunohistochemistry analysis for some specific markers of this study are described.

5.2 Summary of procedure

As summarised in Figure-5.1, ultrasound guided core biopsies were performed at baseline and two weeks after bevacizumab by experienced radiologists. Minimum of two core biopsy samples were taken each time to ensure good quality samples. Samples were always obtained from the margin of the tumour to avoid collection of necrotic tissue. After visual inspection one sample was collected directly in RNA Later and the other one was collected on biopsy cassettes that were then immersed in formalin. RNA extraction was performed from RNA Later fixed fresh frozen core biopsy samples using the trizol-chloroform technique. After clean-up and quality checks samples were sent for gene expression analysis at the Paterson Institute for Cancer Research, Manchester. Gene expression array was performed using Affymetrix Human Exon 1.0 ST arrays, which have the advantage of using multiple probe sets for different splicing variants of each gene and provide a much greater genomic coverage than traditional arrays. Formalin fixed samples were used to make FFPE blocks and subsequent immunohistochemistry analysis using standard protocols. (For details see Chapter 2, Section 3).

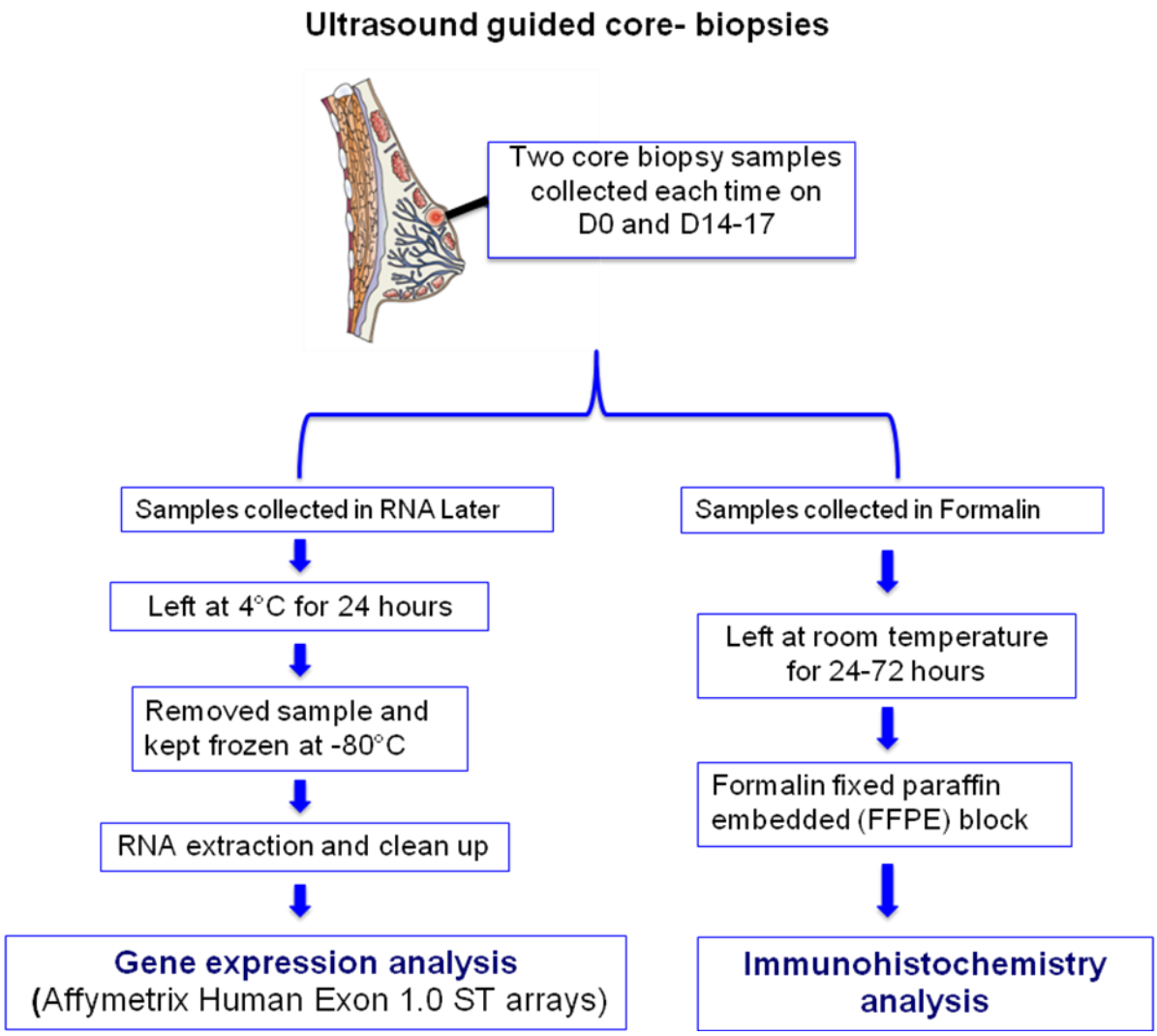

Figure-5.1: Summary of study procedure followed for gene expression and immunohistochemistry analysis.

5.3 Assessment of quantity and quality of RNA

Out of the total 47 patients recruited in this study, 36 study patients with ductal subtype had sufficient yield and good quality of RNA both pre and post bevacizumab as assessed by RNA concentrations, RNA Integrity Number (RIN) and A260/280 ratio using Nano-Drop ND-1000 spectrophotometer (Thermo Scientific, Surrey, UK) and Agilent 2100 Bioanalyzer (Agilent Technologies, Santa Clara, USA) (Figure-5.2). Along with these, there was no significant difference between pre-bevacizumab vs. post-bevacizumab RNA concentration, A260/280 ratio and RIN values (Wilcoxon-signed rank test, P=0.23, 0.23, 0.14 respectively).

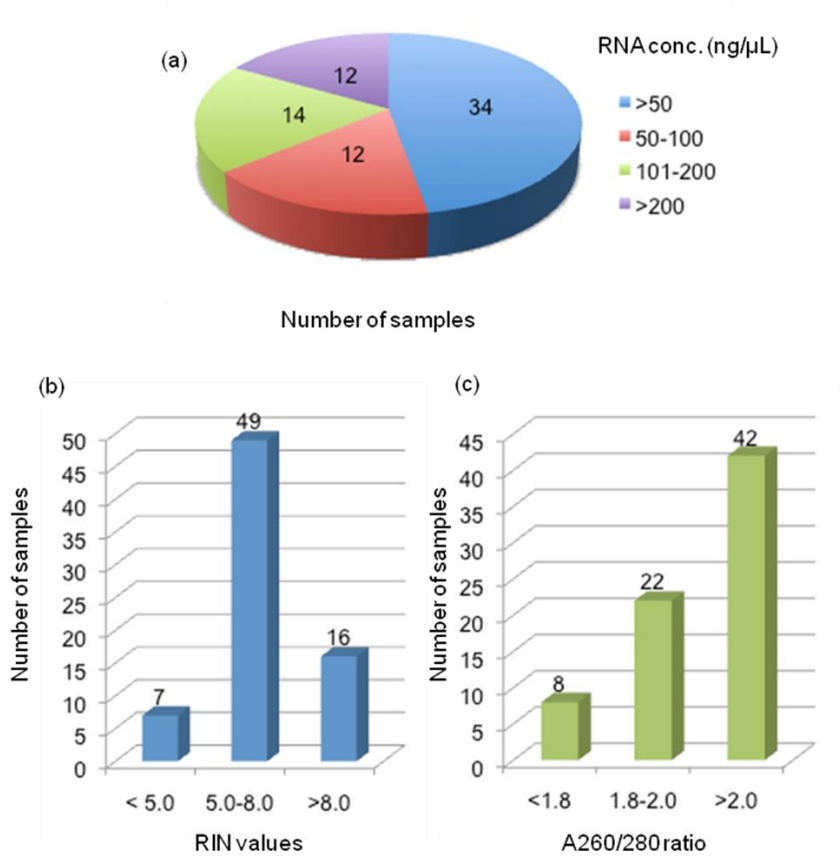

Figure-5.2: Quantity and quality of the study patient's RNA samples considering both pre and post-bevacizumab samples.

5.4 Gene expression analysis after bevacizumab

Analysis of the Affymetrix Human Exon 1.0 ST array data was performed by an experienced bioinformatician (Dr Francesca Buffa) (details of analysis steps in Chapter 2, Section 6). In summary, pre-processing, normalisation and quality checks of the data were performed. For each patient paired samples were considered (pre-bevacizumab and post-bevacizumab). Differential expression analyses before and after bevacizumab were performed both at gene level and metagene level for analysing differentially expressed genes and for phenotype/ pathway activation changes respectively. A permutation based t-test method was used which was corrected for heteroscedasticity of gene expression distributions (Tusher, Tibshirani et al. 2001). Both global and local false discovery were estimated (Tibshirani and Efron 2002). Cluster transcripts with false discovery rate <5% were extracted.

5.4.1 Differential gene expression analysis

As shown by heatmap (Figure-5.3) by using a false discovery rate (FDR) <5%, 392 genes were significantly up-regulated (Table-5.1, Appendix- 5.1), after bevacizumab and only 23 genes were significantly down-regulated (Table-5.2).

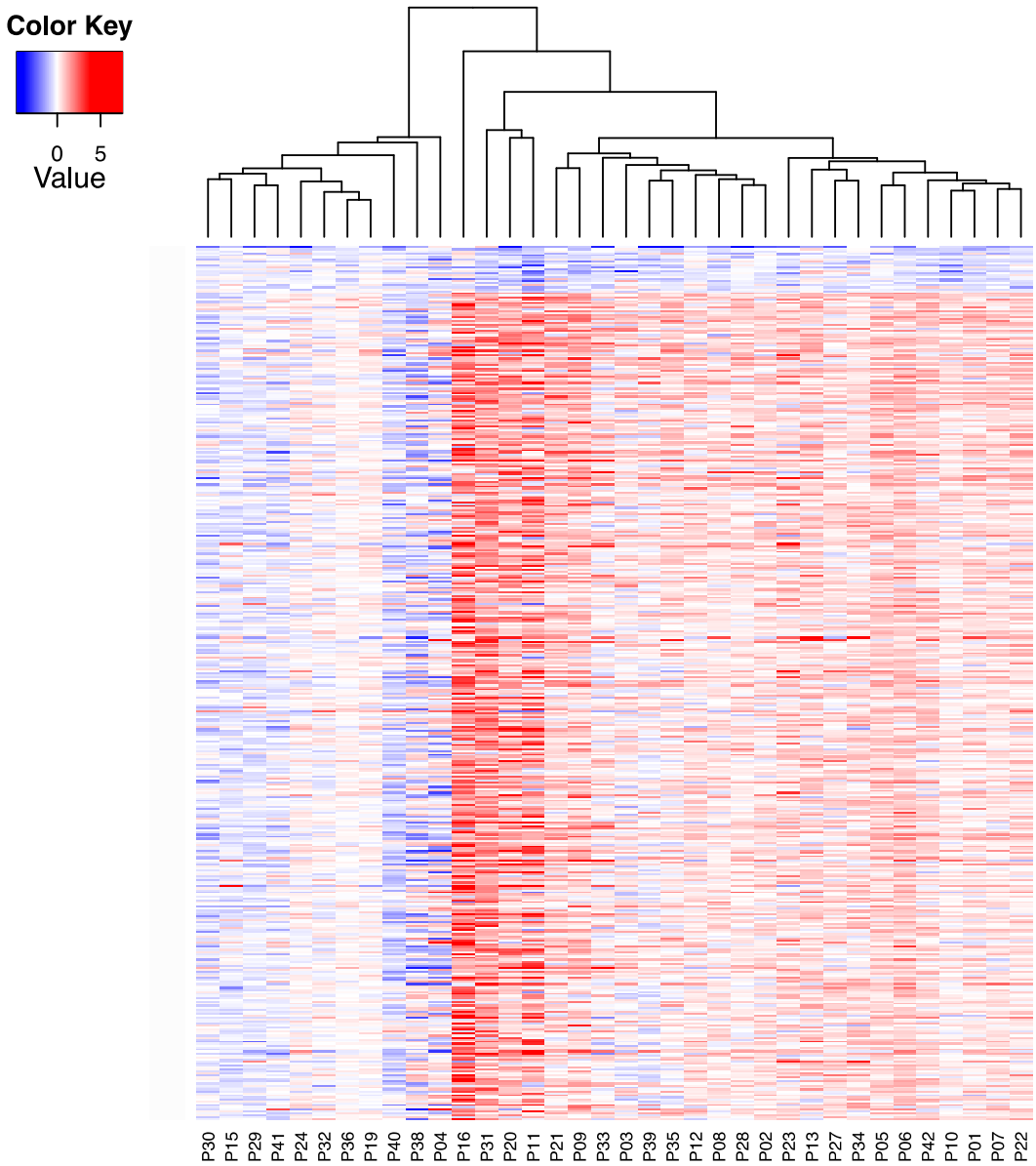

Figure-5.3: Heatmap of differentially expressed genes after bevacizumab. Each row represents a differentially expressed gene arranged by ascending order of fold change from top to bottom and each column represents fold change for single patients, red=up-regulation and blue=down-regulation, samples were visually clustered using hierarchical clustering.

Table-5.1: Top 20 genes up-regulated after bevacizumab therapy. Genes arranged by descending order of fold change

Gene Name	Gene Symbol	Fold Change	Q value	Transcript Cluster ID	Entrez Gene ID	Chr
CCL14-CCL15 read-through transcript	CCL14-CCL15	1.99	1.22	3753966	348249	17
Phosphodiesterase 3B, cGMP-inhibited	PDE3B	1.81	0.00	3321512	5140	11
Procollagen C-endopeptidase enhancer 2	PCOLCE2	1.75	3.41	2698996	26577	3
Olfactomedin 1	OLFM1	1.75	2.34	3193725	10439	9
Chemokine (C-C motif) ligand 19	CCL19	1.75	1.22	3204285	6363	9
Collectin sub-family member 12	COLEC12	1.74	0.00	3795733	81035	18
ABI family, member 3 (NESH) binding protein	ABI3BP	1.73	1.22	2686458	25890	3
HLA class II histocompatibility antigen, DQ alpha 1 chain-like	LOC100510059	1.71	2.34	2903219	100510059	6
Lymphoid-restricted membrane protein	LRMP	1.70	0.00	3408505	4033	12
Ankyrin repeat domain 29	ANKRD29	1.70	0.00	3801492	147463	18
Complement component 7	C7	1.67	2.34	2807716	730	5
Pyruvate dehydrogenase kinase, isozyme 4	PDK4	1.66	1.22	3062082	5166	7
B and T lymphocyte associated	BTLA	1.66	1.22	2688717	151888	3
Transferrin	TF	1.65	4.66	2643217	7018	3
CD28 molecule	CD28	1.65	0.00	2523801	940	2
Cytotoxic T-lymphocyte-associated protein 4	CTLA4	1.64	0.00	2523855	1493	2
B-cell scaffold protein with ankyrin repeats 1	BANK1	1.63	0.00	2737596	55024	4
Secreted frizzled-related protein 4	SFRP4	1.63	3.41	3046444	6424	7
Granzyme K (granzyme 3; tryptase II)	GZMK	1.62	0.00	2809793	3003	5

Table-5.2: Down-regulated genes after bevacizumab therapy. Genes arranged by ascending order of fold change.

Gene Name	Gene Symbol	Fold Change	Q value	Transcript Cluster ID	Entrez Gene ID	Chr
Endothelial cell-specific molecule 1	ESM1	0.31	0.00	2856995	11082	5
Exonuclease 1	EXO1	0.65	3.41	2388219	9156	1
Sulfatase 1	SULF1	0.69	3.41	3102372	23213	8
Aldo-keto reductase family 7, member A3 (aflatoxin aldehyde reductase)	AKR7A3	0.70	1.22	2399687	22977	1
Thyroid hormone receptor interactor 13	TRIP13	0.71	3.41	2798915	9319	5
Histone cluster 1, H2ae	HIST1H2AE	0.73	4.66	2899223	3012	6
G protein-coupled receptor 56	GPR56	0.73	3.41	3662808	9289	16
Selenoprotein W,1	SEPW1	0.74	1.22	3837504	6415	19
DMC1 dosage suppressor of mck1 homolog, meiosis-specific homologous recombination (yeast)	DMC1	0.74	3.41	3960685	11144	22
S100 calcium binding protein A14	S100A14	0.74	1.22	4045665	57402	1
Cyclin E1	CCNE1	0.74	3.41	3828112	898	19
Origin recognition complex, subunit 1	ORC1	0.74	4.66	2412799	4998	1
Glycerol kinase 2	GK2	0.78	4.66	2774938	2712	4
S100 calcium binding protein A16	S100A16	0.78	4.66	4045643	140576	1
Leucine rich repeat containing 41	LRRC41	0.81	3.41	2410574	10489	1
Heat shock 70kDa protein 8	HSPA8	0.82	1.22	3395416	3312	11
Interleukin enhancer binding factor 2, 45kDa	ILF2	0.82	4.66	2436155	3608	1
Progestin and adipoQ receptor family member IX	PAQR9	0.82	3.41	2699059	344838	3
Zona pellucida-such as domain containing 1	ZPLD1	0.82	3.41	2634153	131368	3
Hyalurono-glucosaminidase 2	HYAL2	0.83	3.41	2675171	8692	3
Hypothetical LOC400940	LOC400940	0.84	4.66	2468138	400940	2
MCF2 cell line derived transforming sequence-like	MCF2L	0.86	4.66	3502259	23263	13
F-box protein 6	FBXO6	0.86	3.41	2320374	26270	1

Although on visual inspection of the heatmap, there appeared to be clustering of patients in different groups, on further analysis assessing the clusters using a Bayesian information criterion (Chapter 2, Section 6), there were no significantly separated clusters that could be identified, suggesting that changes might be on a continuous rather than discrete scale.

Specific genes were also analysed in single gene analysis, which were expected to change with bevacizumab from other preclinical studies in our group e.g. carbonic anhydrase-9 (CA-9), delta like legend 4 (DLL4). For this, the stringent FDR assumption used for global analysis was relaxed.

Interestingly, as shown in the Figure-5.4, at single gene level among the up-regulated genes there were several interesting genes involved in *metabolism, immune system, cell signaling pathways, cytokines and angiogeneisis.*

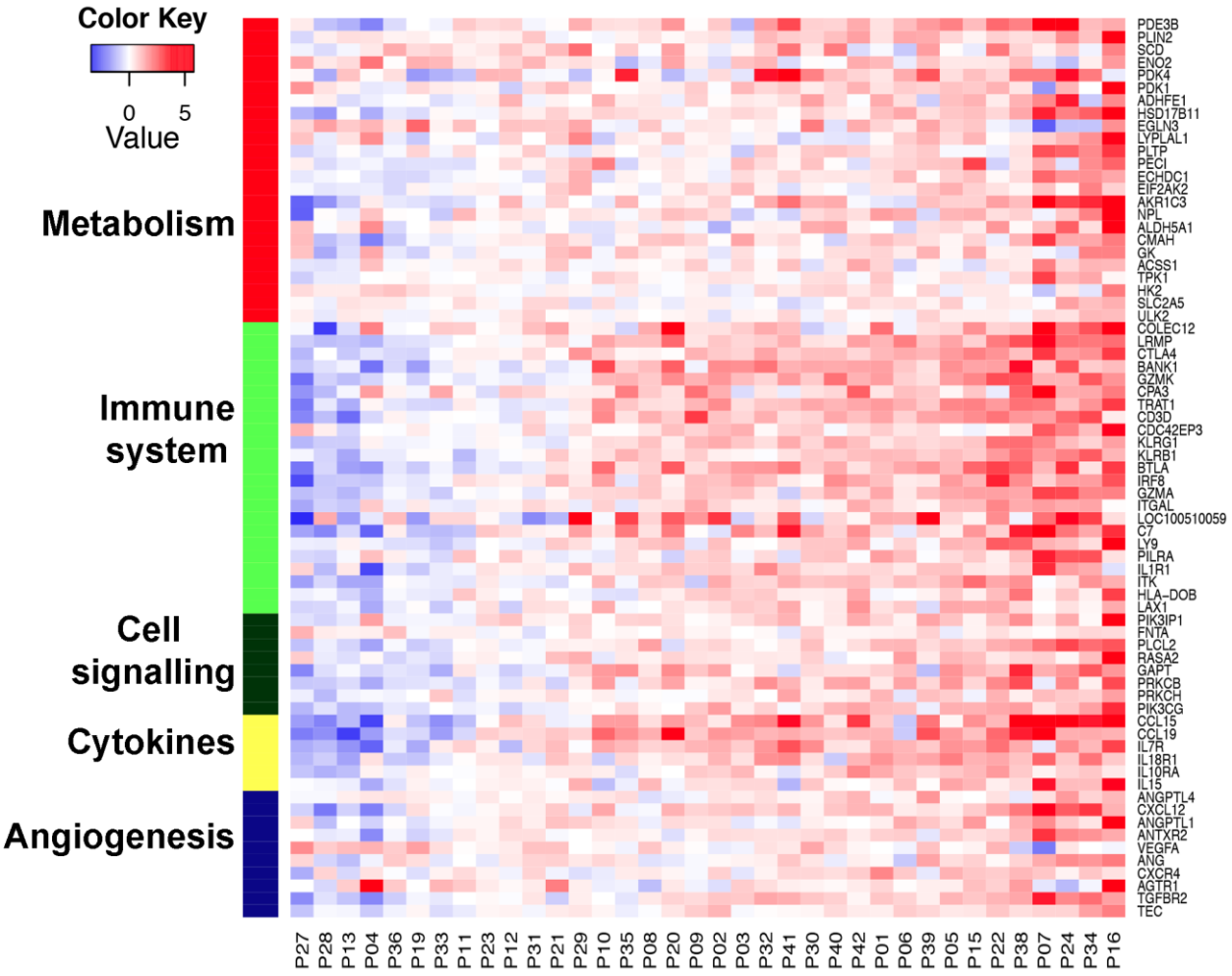

Figure-5.4: Heatmap showing Fold changes (FC) in expression of up-regulated genes involved in pathways of interest. Each column represents FC for a patient arranged by increase in median FC from left to right.

5.5 Validation by qRT-PCR

From the differentially up-regulated or down-regulated genes after bevacizumab 13 genes that were involved in significantly regulated biological processes or pathways and also known to have clinical significance, were chosen to be validated by qRT-PCR. Along with these, DLL4 and CA-9 were also considered, as significant changes in these genes were observed in response to bevacizumab in other preclinical studies in our laboratory (Details of these genes are in Table- 5.3). As mentioned previously (Chapter 2, Section

6) the same cDNA as used for gene expression work, was used for this validation experiment with qRT-PCR. House-keeping genes used were HSPCB, UBC and RPL13A and relative expression of each gene of interest was calculated (see Chapter 2, Section 6 for details).

Table- 5.3: Details of genes validated by qRT-PCR. Genes arranged in ascending order of fold change. Fold changes and Q-values are as seen by exon array analysis. Green= Downregulated; Red= Upregulated.

Gene Symbol	Gene Name	Fold Change	Q value	Transcript Cluster ID	Entrez Gene ID	Chr
ESM1	Endothelial cell-specific molecule 1	0.31	0	2856995	11082	5
SULF1	Sulfatase 1	0.69	3.41	3102372	23213	8
CCNE1	Cyclin E1	0.74	3.41	3828112	898	19
SPRY4	Sprouty homolog 4 (Drosophila)	0.76	0	2879105	81848	5
FLT1	Fms-related tyrosine kinase 1	0.77	0	3507282	2321	13
DLL4	Delta like ligand 4	0.9	N/a	7982854	54567	15
CA-9	Carbonic anhydrase 9	0.98	N/a	8155083	768	9
ANGPTL4	Angiopoietin-like 4	1.24	0	3819474	51129	19
PIK3CG	Phosphoinositide-3-kinase, catalytic, gamma polypeptide	1.29	4.66	3018309	5294	7
VEGFA	Vascular endothelial growth factor A	1.37	3.4	2908179	7422	6
PDK1	Pyruvate dehydrogenase kinase, isozyme 1	1.47	1.21	2515707	5163	2
PIK3IP1	Phosphoinositide-3-kinase interacting protein 1	1.49	0	3957790	113791	22
PPARG	Peroxisome proliferator-activated receptor gamma	1.53	3.4	2611056	5468	3
CTLA4	Cytotoxic T-lymphocyte-associated protein 4	1.64	0	2523855	1493	2
PDE3B	Phosphodiesterase 3B, cGMP-inhibited	1.81	0	3321512	5140	11

As shown by gene expression analysis, with qRT-PCR the significant down-regulation of endothelial cell specific molecule 1 (ESM1) (P<0.0001), cyclin E1 (CCNE1) (P= 0.03) and fms-related tyrosine kinase 1 (FLT1) (P= 0.001) was confirmed. Along with these genes, significant down-regulation of delta like legend 4 (DLL4) (P= 0.006) was also observed two weeks after single cycle of bevacizumab (Figure-5.5).

Significantly up-regulated genes were vascular endothelial growth factor A (VEGFA) (P= 0.01), pyruvate dehyrogenase kinase 1 (PDK1) (P= 0.002), phosphodiesterase 3B, cGMP-inhibited (PDE3B) (P= 0.05) was observed (fig-5.6).

In contrast to gene expression analysis, with qRT-PCR there was no significant change observed in sprouty homolog 4 (Drosophila) (SPRY4) (P= 0.22), sulfatase 1 (SULF1) (P=0.17), peroxisome proliferator-activated receptor gamma (PPARG) (P=0.07), angiopoietin-like 4 (ANGPTL4) (P=0.07), cytotoxic T-lymphocyte-associated protein 4 (CTLA4) (P=0.30), phosphoinositide-3-kinase, catalytic, gamma polypeptide (PIK3CG) (P=0.85). No significant change was observed in CA-9 either by gene expression analysis or by qRT-PCR (Table-5.4).

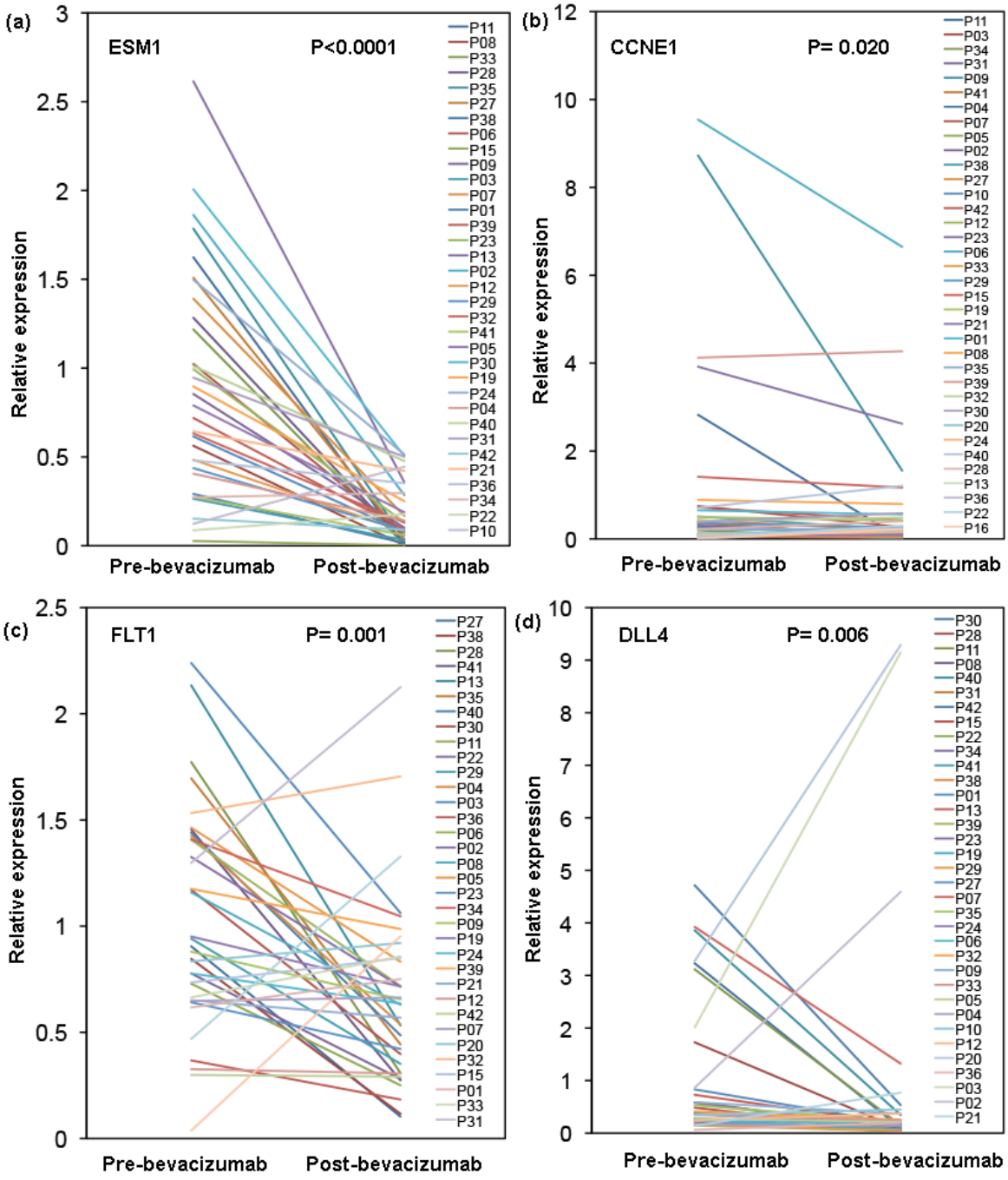

Figure-5.5: Significantly down-regulated genes two weeks after bevacizumab as validated by qRT-PCR. Plots showing patient-by-patient changes in the relative expression for (a) ESM-1 (b) CCNE1 (c) FLT-1 and (d) DLL4 (P-value, Mann-Whitney test).

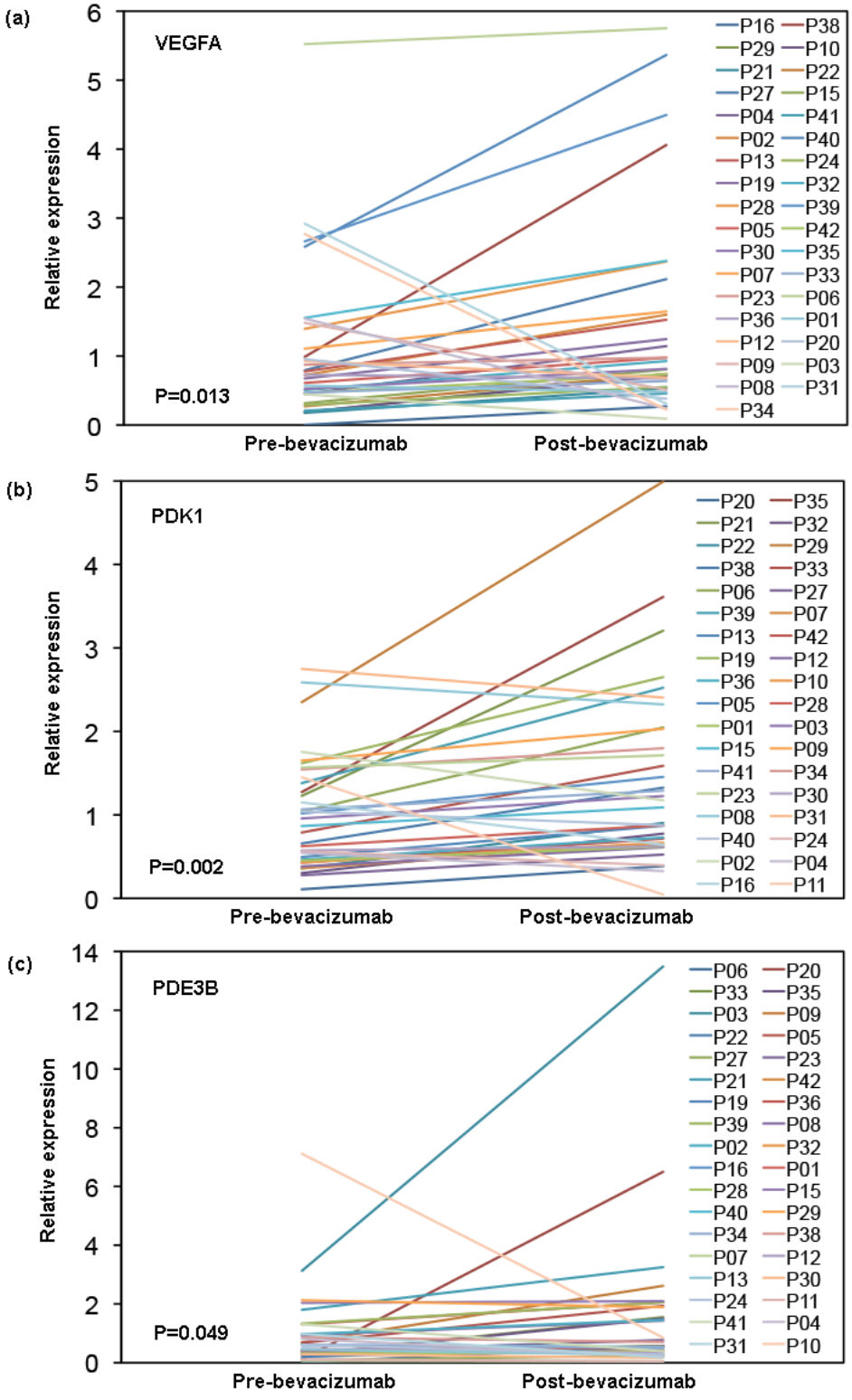

Figure-5.6: Significantly up regulated genes two weeks after bevacizumab as assessed by qRT-PCR. Plots showing patient-by-patient changes in the relative expression for (a) VEGFA (b) PDK1 and (c) PDE3B, (P-value, Mann-Whitney test).

Table-5.4: Summary of QRT-PCR analysis. Fold changes in genes as observed by qRT-PCR assessment 2 weeks after bevacizumab. (P-value, Wilcoxon signed rank test) Genes arranged in order of increasing fold change. Green= Down-regulated; Red= Up-regulated.

Gene Symbol	Gene Name	Fold Change	P-value
ESM1	**Endothelial cell-specific molecule 1**	**0.21**	**<0.0001**
CCNE1	**Cyclin E1**	**0.61**	**0.02**
FLT1	**Fms-related tyrosine kinase 1**	**0.65**	**0.00**
SPRY4	Sprouty homolog 4 (Drosophila)	0.67	0.16
DLL4	**Delta like legend 4**	**0.83**	**0.01**
SULF1	Sulfatase 1	0.85	0.17
PIK3CG	Phosphoinositide-3-kinase, catalytic, gamma polypeptide	0.95	0.85
CA-9	Carbonic anhydrase 9	1.23	0.60
VEGFA	**Vascular endothelial growth factor A**	**1.29**	**0.01**
CTLA4	Cytotoxic T-lymphocyte-associated protein 4	1.32	0.30
PIK3IP1	Phosphoinositide-3-kinase interacting protein 1	1.33	0.65
PDK1	**Pyruvate dehydrogenase kinase, isozyme 1**	**1.38**	**0.00**
PDE3B	**Phosphodiesterase 3B,cGMP-inhibited**	**1.58**	**0.05**
ANGPTL4	Angiopoietin-like 4	1.66	0.07
PPARG	Peroxisome proliferator-activated receptor gamma	1.69	0.07

By doing the further patient-by-patient analysis of exon array data similar trends were observed (Figure-5.7).

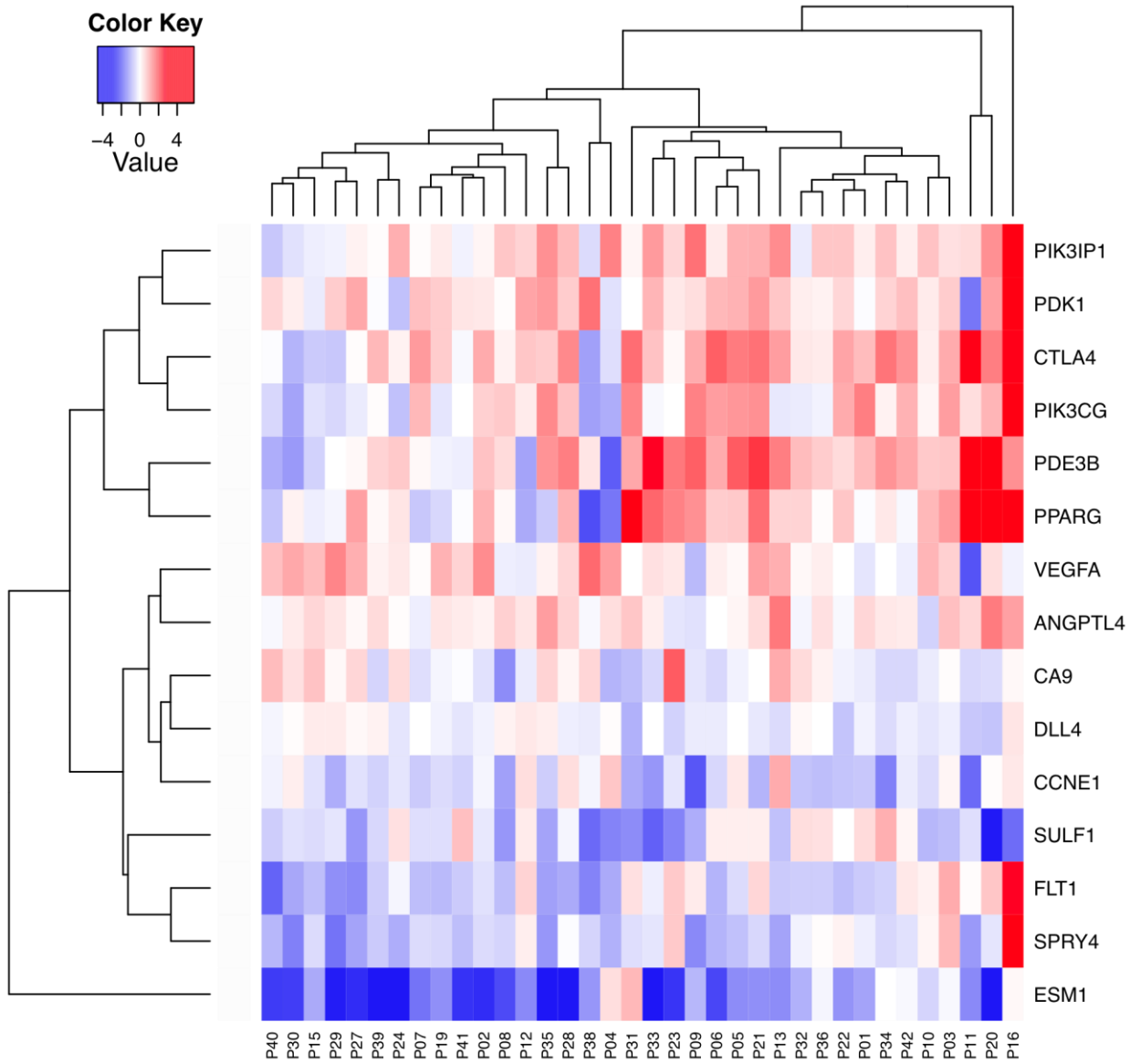

Figure-5.7: Heatmap showing high variation in expression of genes of interest after bevacizumab. Each row represents a gene and each column represents a single patient's fold change for each gene post-bevacizumab. Red= up-regulation, Blue= down-regulation.

Apart from this there was a highly significant correlation noted between the fold changes as observed by exon array and the fold changes observed by qRT-PCR that validate the exon array results (Figure-5.8).

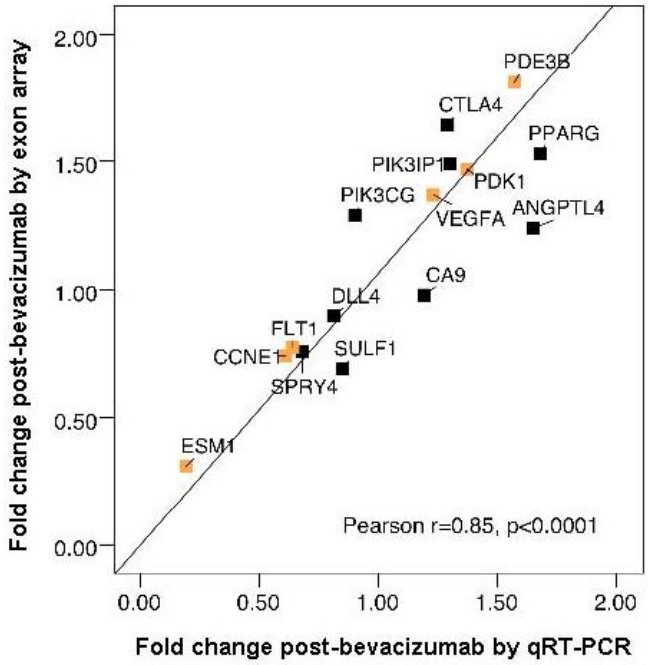

Figure-5.8: Significant correlation between fold changes in genes of interest as observed by exon array and qRT- PCR. Yellow boxes represent genes with significant changes by exon array as well as qRT-PCR analysis

5.6 Pre-bevacizumab gene expression relationship to standard clinical and pathological prognostic factors

To understand the clinical significance of up-regulation or down-regulation of genes after bevacizumab, we analyzed any difference in the baseline expression of these genes based on subgroups of patients as determined by their receptor status (ER/PR/HER2 status) (Table-5.5). The baseline expression of cyclinE1 (CCNE1), carbonic anhydrase 9 (CA-9) and pyruvate dehydrogenase kinase-1 (PDK1) were noted to be significantly higher in ER negative patients in comparison to ER positive patients (Mann-Whitney test, P= 0.001, 0.08 and 0.0001, respectively) (fig 5.9, 5.10).

Further analysis was performed between ER+PR+ (n=19) and ER+PR- (n=7) and ER-PR- (n=9) group. There was only one patient in which was ER- PR+ so it was not included in analysis.

The expression of FLTI was observed to be significantly higher in the ER+PR- group in comparison to the ER+PR+ or ER-PR- group (P=0.008, Kruskal-Wallis test) (Figure- 5.9). On the other hand, CCNE1 and PDK1 expression were significantly higher in the ER-PR- group in comparison to ER+PR+ or ER+PR- group (Kruskal-Wallis test, P=0.006 and P<0.0001, respectively) (Figure- 5.9- 5.10).

On further analysis the PDK1 expression was found to be significantly higher in the triple negative group of patients in comparison to others (P=0.03, Mann-Whitney test) (Figure- 5.10). There were no differences observed in the expression of any of these genes based on HER2 status.

Table- 5.5: Baseline expression of selected genes as a function of receptor status in breast cancer.

Green= Down-regulated; Red= Up-regulated after bevacizumab therapy.

Genes (Baseline)	ER+ vs. ER- [1*]	ER+PR+ vs. ER+PR- vs. ER-PR- [2$]	HER2+ vs. HER2 - [3*]	ER-PR-HER2- vs. others [4*]
ESM1	0.99	0.8	0.75	0.94
CCNE1	**0.001**	**0.01**	0.77	0.07
FLT1	0.66	**0.01**	0.23	0.93
SPRY4	0.30	0.26	0.1	0.75
DLL4	0.41	0.74	0.40	0.76
SULF1	0.82	0.86	0.97	0.49
PIK3CG	0.09	0.41	0.61	0.44
CA-9	**0.01**	0.06	0.25	0.65
VEGFA	0.06	0.15	0.26	1.00
CTLA4	0.70	0.64	0.98	0.49
PIK3IP1	0.17	0.18	0.77	0.91
PDK1	**0.0001**	**<0.0001**	0.09	**0.03**
PDE3B	0.28	0.53	0.47	0.10
ANGPTL4	0.06	0.05	0.91	0.36
PPARG	0.48	0.56	0.42	0.69

1. ER+ (n= 26), ER- (n= 10)
2. ER+PR+ (n= 19), ER+PR- (n=7), ER-PR- (n=9), only one patient was ER-PR+ was not included in the analysis.
3. HER2+ (n= 9), HER2- (n= 27)
4. ER-PR-HER2- (n=5), Others (n=31)

*Columns showing P-values (Mann-Whitney test)

$ Columns showing P value (Kruskal-Wallis test)

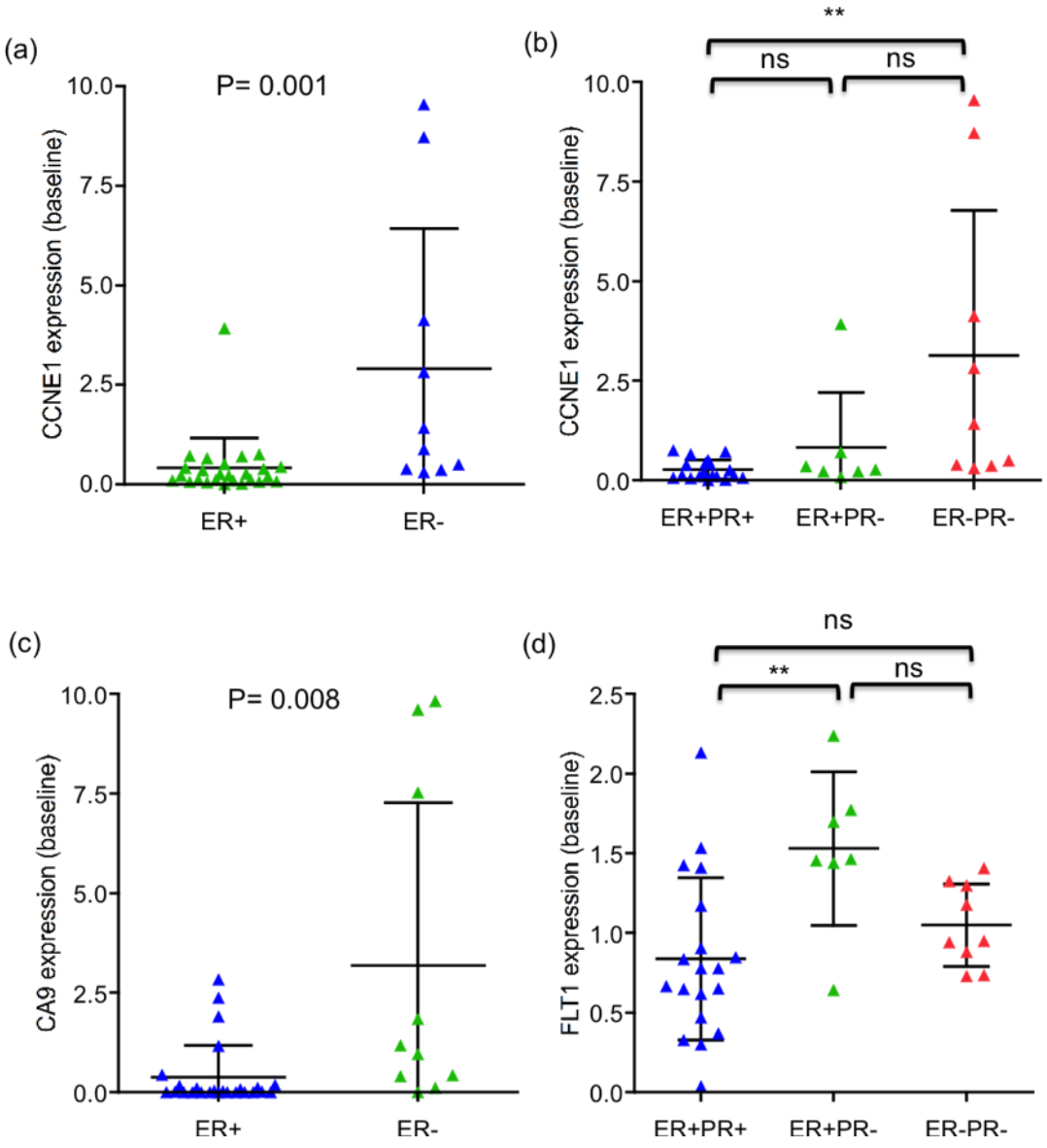

Figure-5.9: Differential expression of CCNE1, CA-9 and FLT1 at baseline in subgroups based on receptor status. Error bars represent mean±SD for each plot. For plots (a) and (c) P-value, Mann-Whitney test. For plots (b) and (d) Kruskal-Wallis test along with Dunn's multiple comparison test.
** denotes P <0.01, ns=P>0.05**.**

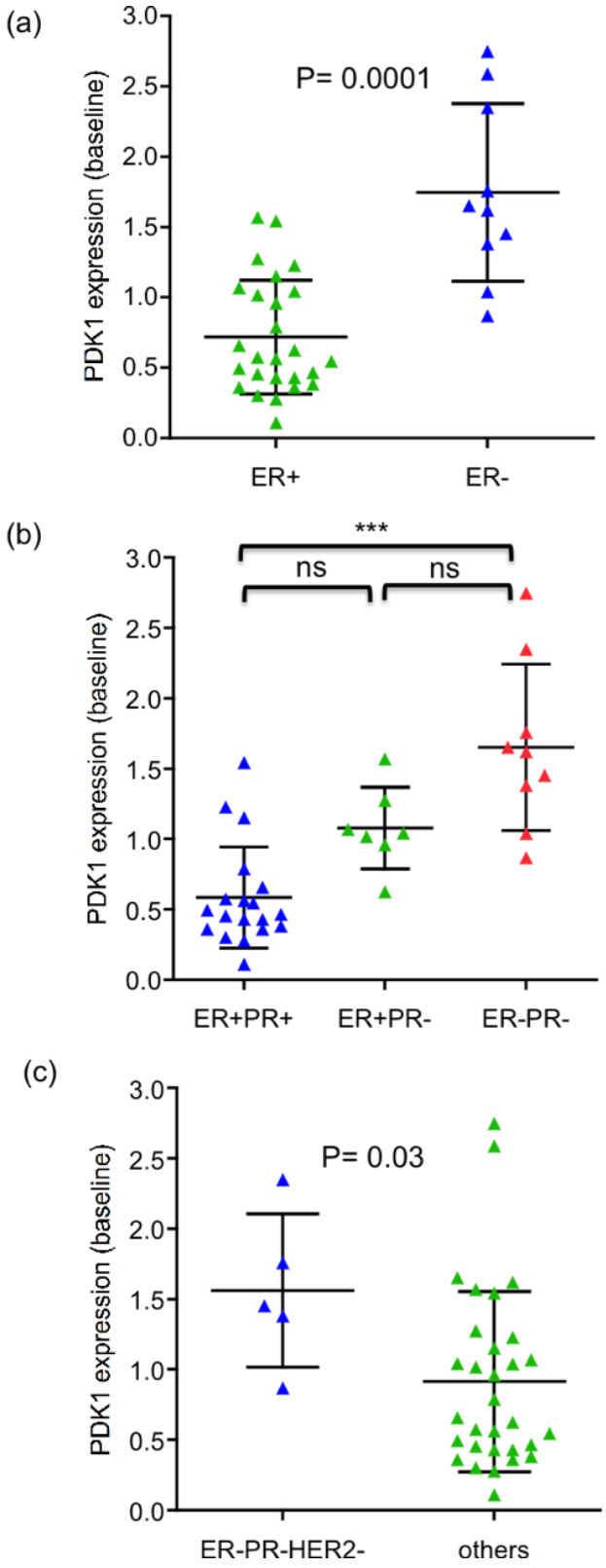

Figure-5.10: Differential expression of PDK1 at baseline in subgroups based on receptor status. Error bars represent mean±SD for each plot. For plots (a) and (c) P-value, Mann-Whitney test. For plots (b) Kruskal-Wallis test along with Dunn's multiple comparison test. *** denotes P<0.001, ns=P>0.05**.**

Further analysis was also performed to see if there was any association of the baseline expression of these genes to other prognostic factors such as grade of tumour, age of the patient and initial size of tumour at presentation (Table- 5.6).

There was no difference noted in gene expression at baseline between different grades of tumour. Similarly there was no association observed between baseline gene expressions with age of the patients at diagnosis (Table- 5.6).

There was a weak but significant positive correlation was observed between ESM1 and size of tumour i.e. bigger the tumour the greater was the ESM1 expression at baseline (Spearman r=0.44, P=0.01) (Figure- 5.11). On the other hand, there was a weakly significant negative correlation observed between CTLA4 and PIK3IP1 with size of the tumour at baseline (Spearman r=-0.34, P=0.05, r=-0.43, P=0.01 respectively). This illustrated that the bigger the tumour at baseline, the lesser was the baseline expression of CTLA4 and PIK3IP1 (Figure- 5.11).

Table-5.6: Association of baseline gene expression with clinical and pathological prognostic factors in breast cancer. Green= Down-regulated; Red= Up-regulated after bevacizumab therapy as assessed by qRT-PCR.

Baseline expression	Grade 2 vs. Grade 3[1*]	Size[$]	Age[$]
ESM1	0.35	**0.44 (0.01)**	0.11 (0.53)
CCNE1	0.08	-0.19 (0.28)	0.08 (0.63)
FLT1	0.16	0.21 (0.23)	0.05 (0.77)
SPRY4	0.85	0.03 (0.84)	0.04 (0.81)
DLL4	0.65	-0.16 (0.36)	0.07 (0.67)
SULF1	0.77	-0.02 (0.90)	0.12 (0.49)
PIK3CG	0.81	-0.17 (0.32)	-0.17 (0.35)
CA-9	0.29	0.08 (0.64)	-0.07 (0.69)
VEGFA	0.32	0.12 (0.48)	0.09 (0.62)
CTLA4	0.47	**-0.34 (0.05)**	-0.28 (0.10)
PIK3IP1	0.34	**-0.43 (0.01)**	-0.10 (0.56)
PDK1	0.39	0.07 (0.70)	0.09 (0.59)
PDE3B	0.29	-0.14 (0.42)	-0.03 (0.85)
ANGPTL4	0.70	0.02 (0.89)	0.05 (0.79)
PPARG	0.83	0.08 (0.65)	-0.01 (0.95)

1. Grade 2 (n= 15), Grade 3 (n=21)
* Columns showing P-values (Mann-Whitney test)
$ Columns showing Spearman coefficient r (P-value)

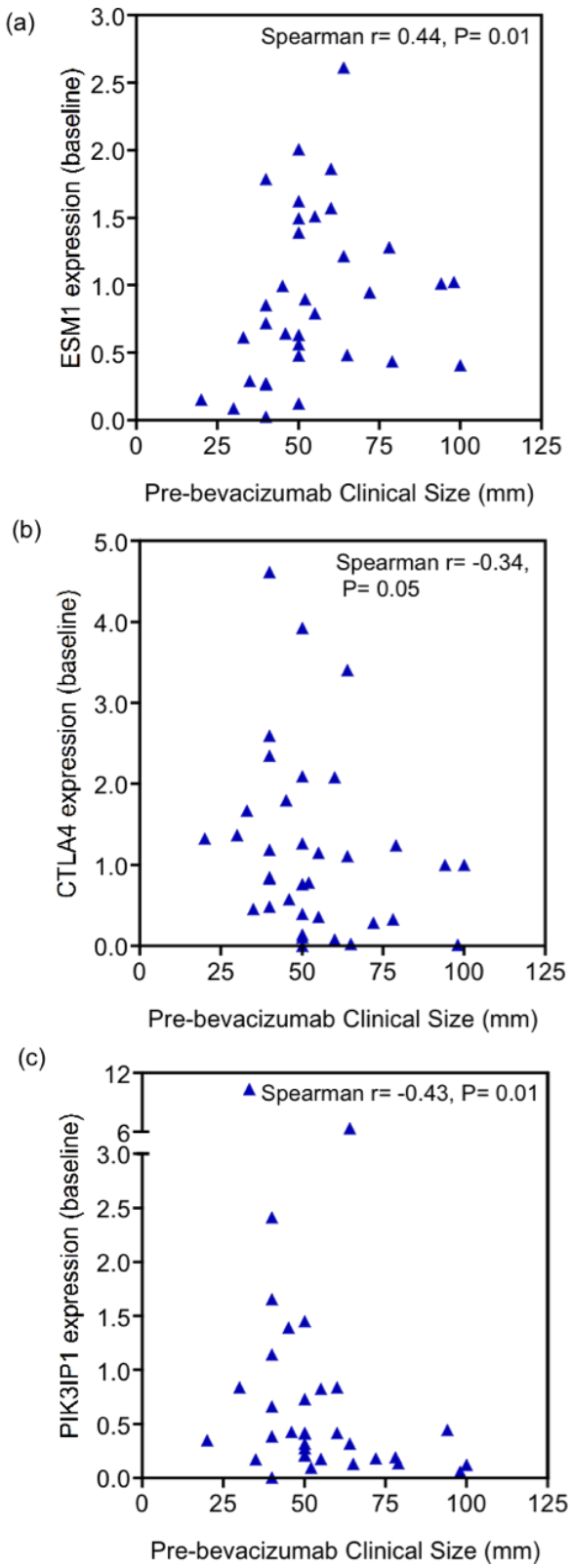

Figure-5.11: Association of gene expression at baseline with pre-bevacizumab size of tumour as assessed clinically. (a) Positive correlation of ESM1 at baseline with size of tumour, (b) Negative correlation of CTLA4 expression at baseline with size of tumour, (c) Positive correlation of PIK3IP1 with size of tumour as measured clinically.

5.7 Fold-change in genes as a function of clinical and pathological prognostic factors

Next we were interested to see if there was any difference in the fold change in subpopulations of patients based on known prognostic factors in breast cancer. There was no difference observed in the fold change of most of these genes between subpopulations based on receptor status, except the greater down-regulation of SPRTY4 in ER-PR- group of patients in comparison to ER+PR+ or ER+PR- group (Kruskal-Wallis test, P= 0.04) (Figure- 5.12).

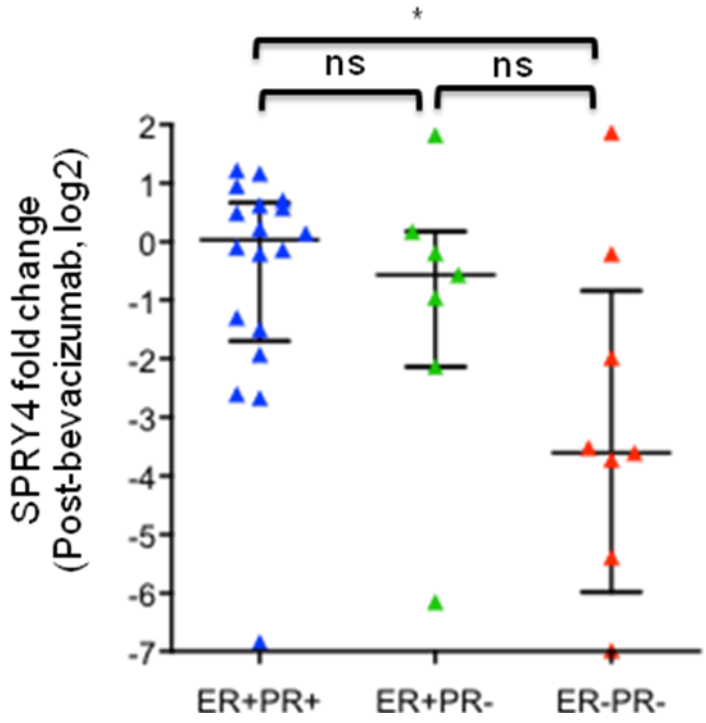

Figure-5.12: Significant down-regulation of SPRTY4 in ER-PR- in comparison to ER+PR+ and ER+PR- patients. Overall P=0.04, Kruskal-wallis test with Dunn's multiple comparison test. * denotes P<0.05, ns= P>0.05. Error bars show median± interquartile range.

Along with this, down-regulation of ESM1 was significantly greater in patients with grade 3 tumours in comparison to grade 2 tumours (Figure- 5.13). There

was no relationship observed between the fold changes in genes expression either with size or with age of patient at presentation.

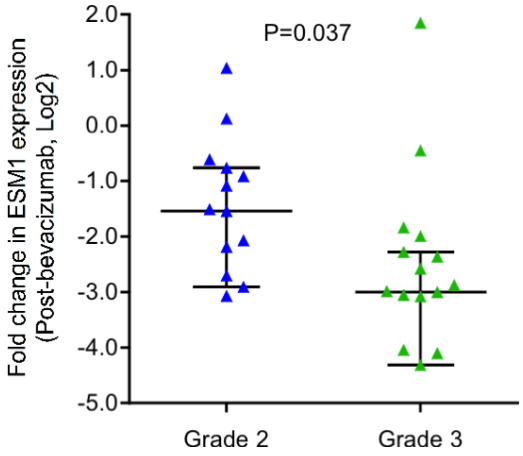

Figure-5.13: Significantly greater down-regulation of ESM1 in grade 3 patients in comparison to grade 2 patients. Error bars showing median± Interquartile range; P-value: Mann-Whitney test.

5.8 Assessment of the final pathological response after neoadjuvant chemotherapy as a function of baseline expression or fold change in expression of genes of interest

This analysis was performed to see if there was any impact of baseline values or changes in the expression of genes after bevacizumab on the final pathological responses after neoadjuvant chemotherapy.

As mentioned before (Chapter 4, Section 3), patients were classified as good pathological responders (n=13) (including PCR and near to PCR) and others (n=23) after neoadjuvant chemotherapy based on presence of viable tumour cells on histopathological examination of the tumour specimen after chemotherapy.

There was no significant difference observed in the baseline expression or fold changes in the genes in good pathological responders versus others except the CTLA4 fold change was significantly higher in good pathological responders (n=13) in comparison to others (n=23) (P=0.04, Mann-Whitney test) i.e. patients showing greater up-regulation of CTLA4 after bevacizumab showed better pathological response after chemotherapy (Figure- 5.14).

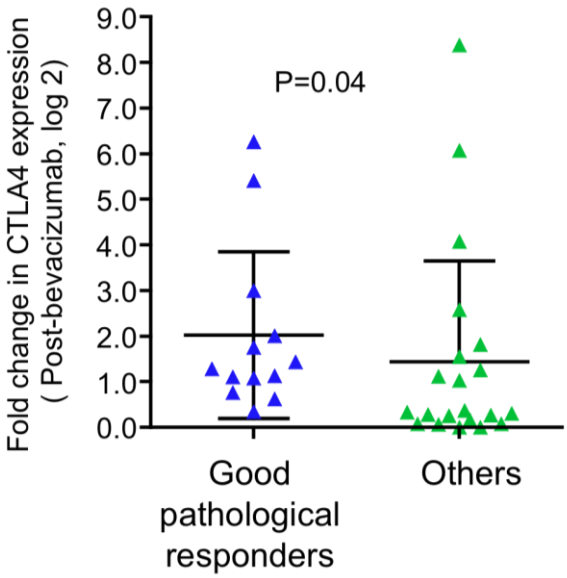

Figure-5.14: Significantly higher up-regulation of CTLA4 in good pathological responders in comparison to others. P- value, Mann-Whitney test; Error bars showing mean± SD.

5.9 Differential metagene expression analysis

A number of research groups, including our own, have previously published "metagenes" also called "signatures". These are lists of genes in involved in specific pathways and provide a means of assessing global pathway changes after bevacizumab, instead of changes in single genes. A specific breast cancer hypoxia signature (Buffa, Harris et al. 2010), proliferation signature (Desmedt, Haibe-Kains et al. 2008), angiogenesis signature (Masiero, Simoes et al. 2013) and a recently published anti-VEGF signature (Genentech Inc., South San Francisco, CA, US) (Bais, Singh et al. 2011) were used to analyze the effect of bevacizumab on these important pathways.

Considering the whole cohort of study patients (n=36) significant global down-regulation of the genes involved in the proliferation signature was noted (paired t-test: t=-2.09, P-value=0.04) but no significant change was observed in the specific breast cancer hypoxia signature (paired t-test: t= -0.20, P-value=0.84), angiogenesis signature (paired t-test: t=0.81, P-value=0.42) or anti-VEGF signature (Figure-5.15).

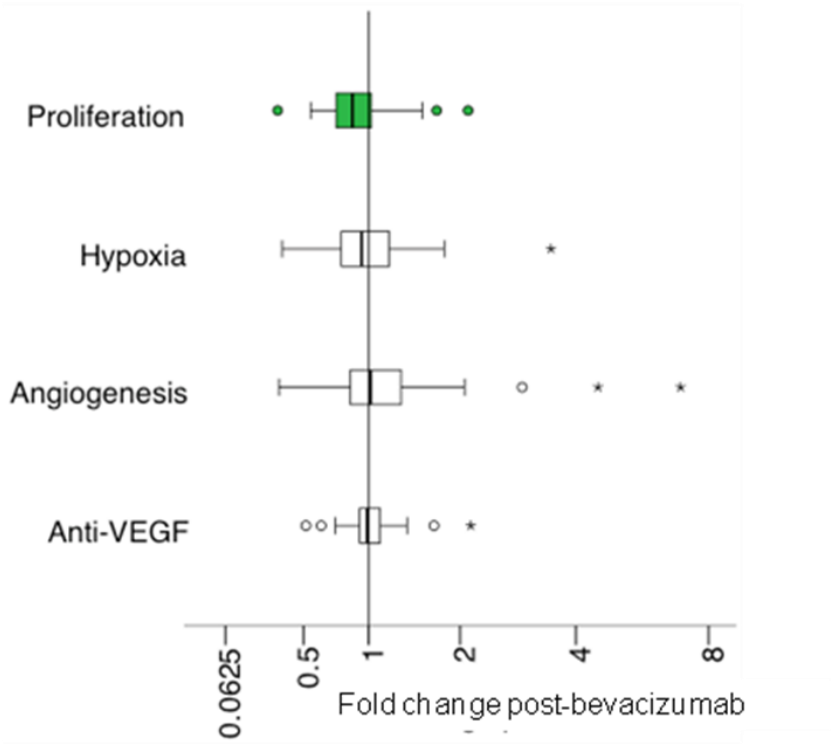

Figure-5.15: Box plot showing global changes in gene signatures post-bevacizumab. Bars depicting median±interquartile range of fold changes for each signature. X-axis showing folds changes after bevacizumab.

On further analysis, a high variability in the expression fold changes was observed for all of these signatures. In particular, expression fold changes after bevacizumab for proliferation signature ranged from 0.3-fold decrease to 2.1-fold increase and for hypoxia signature ranged from 0.4-fold decrease to 3.5-fold increase (Figure-5.16).

Similarly expression fold changes for angiogenesis signature ranged from 0.3-fold decrease to 6.9-fold increase and for anti-VEGF signature 0.5-fold decrease to 2.1-fold increase (Figure-5.17).

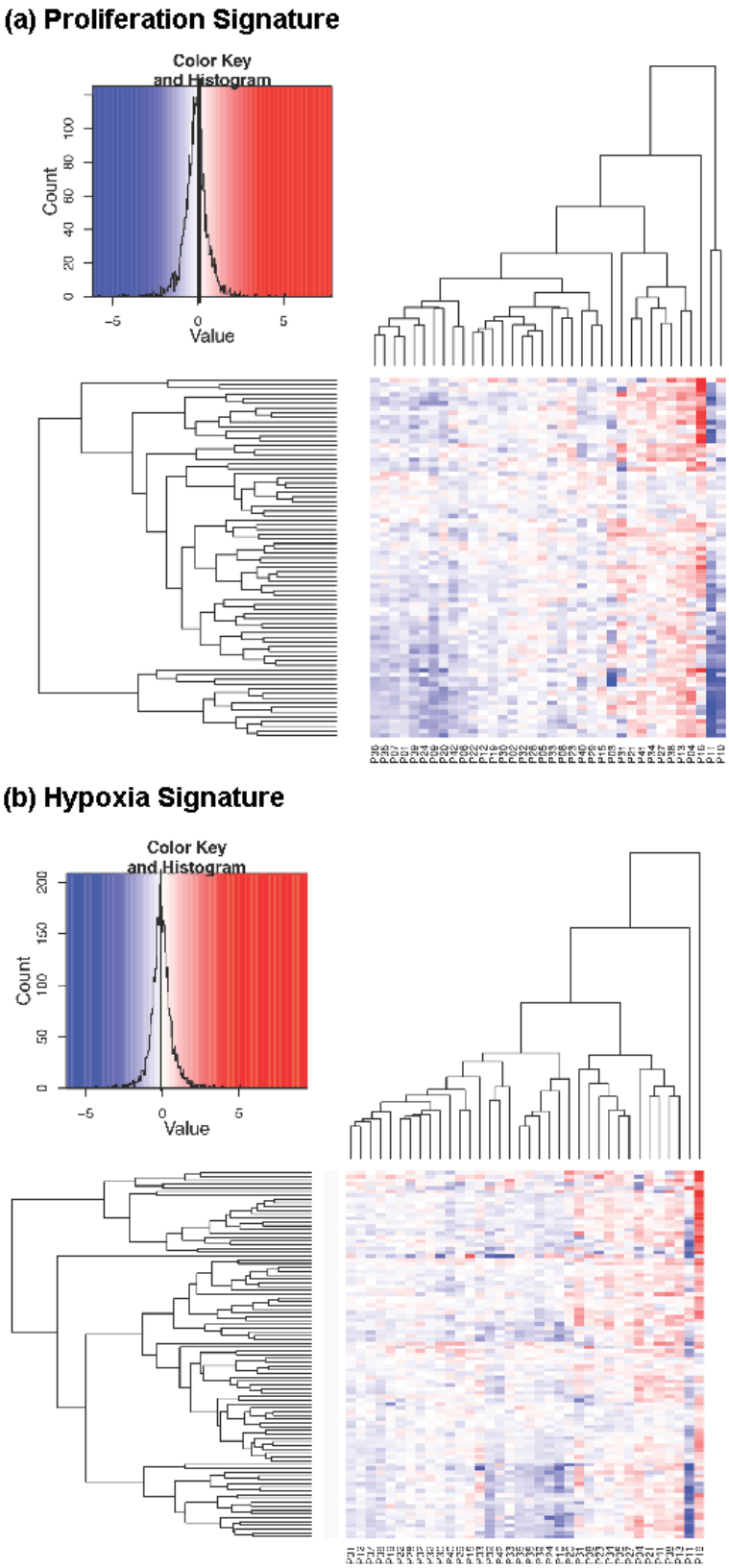

Figure-5.16: Heatmap showing high variability in genes involved in proliferation and hypoxia signatures. Each row represents a gene and each column represents single patient. Colours reflect the fold change for each gene post-bevacizumab.

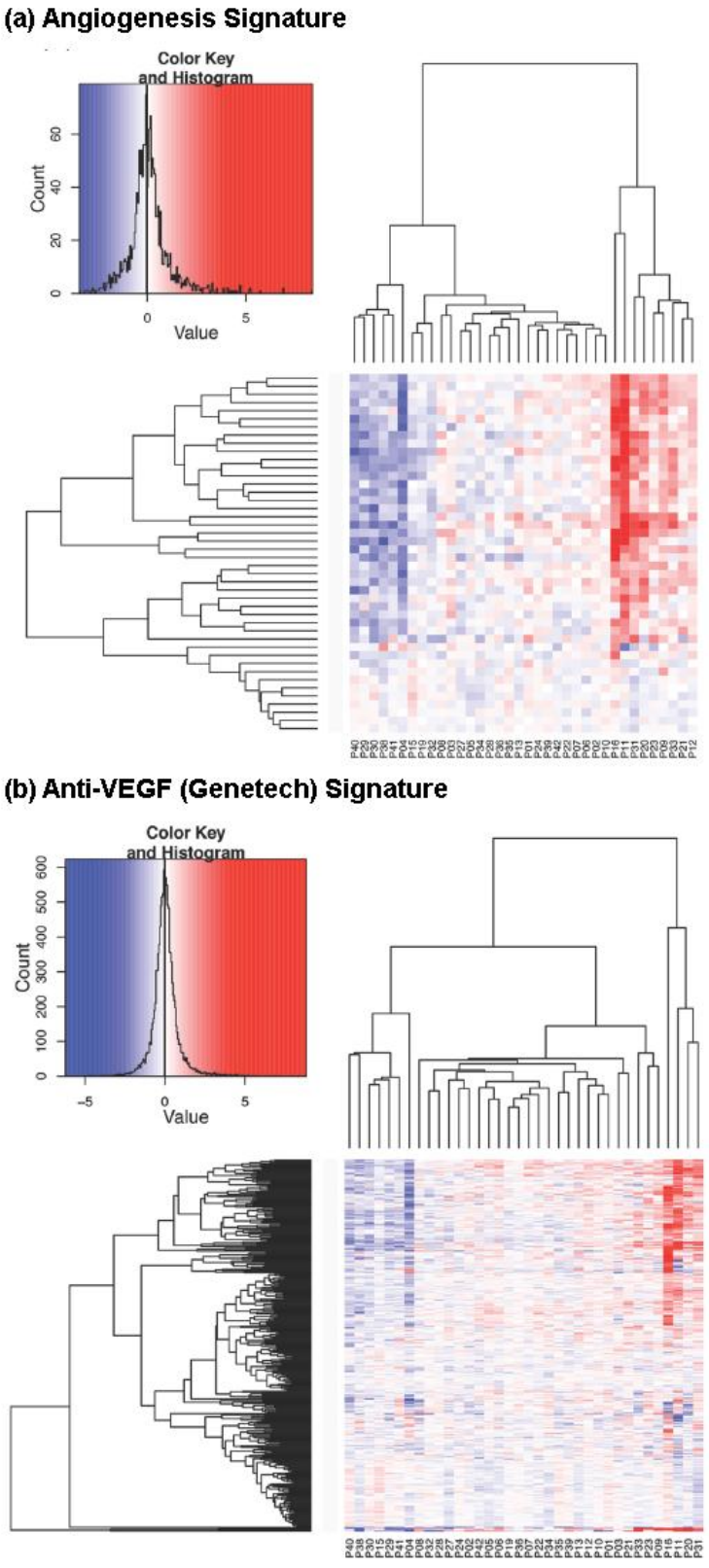

Figure-5.17: Heatmap showing high variability in genes involved in angiogenesis and anti-VEGF signature. Each row represents a gene and each column represents single patient. Colours reflect the fold change for each gene post-bevacizumab.

On further analysis, a highly significant correlation of the induction of hypoxia, as defined by the global change in hypoxia metagenes, with the induction of proliferation as defined by fold change in proliferation metagenes (Spearman r= 0.91, P < .0001) was observed (Figure-5.18). To highlight, there was no overlap of the genes in the hypoxia and proliferation metagene signatures as common genes have been excluded.

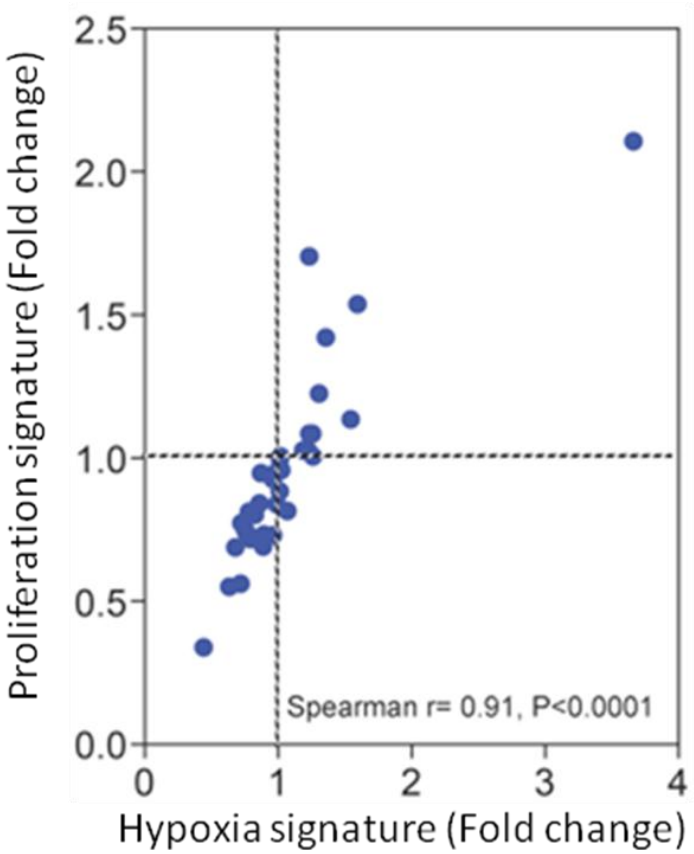

Figure-5.18: Correlation of fold change in hypoxia signature with fold change in proliferation signature after bevacizumab. X-axis and y-axis showing fold change values of respective gene signature.

Similarly, a highly significant correlation was observed between the fold change in the angiogenesis signature and the anti-VEGF signature (Spearman r=0.91, P<0.0001) (Figure- 5.19a). But there were 38 genes in common

between these two signatures, of which 29 were expressed above background in this series. Interestingly, there was significant a correlation observed between the angiogenesis signature and anti-VEGF signatures even after taking out the common genes between two signatures (Spearman r =0.55, p=0.001) (Figure- 5.19b).

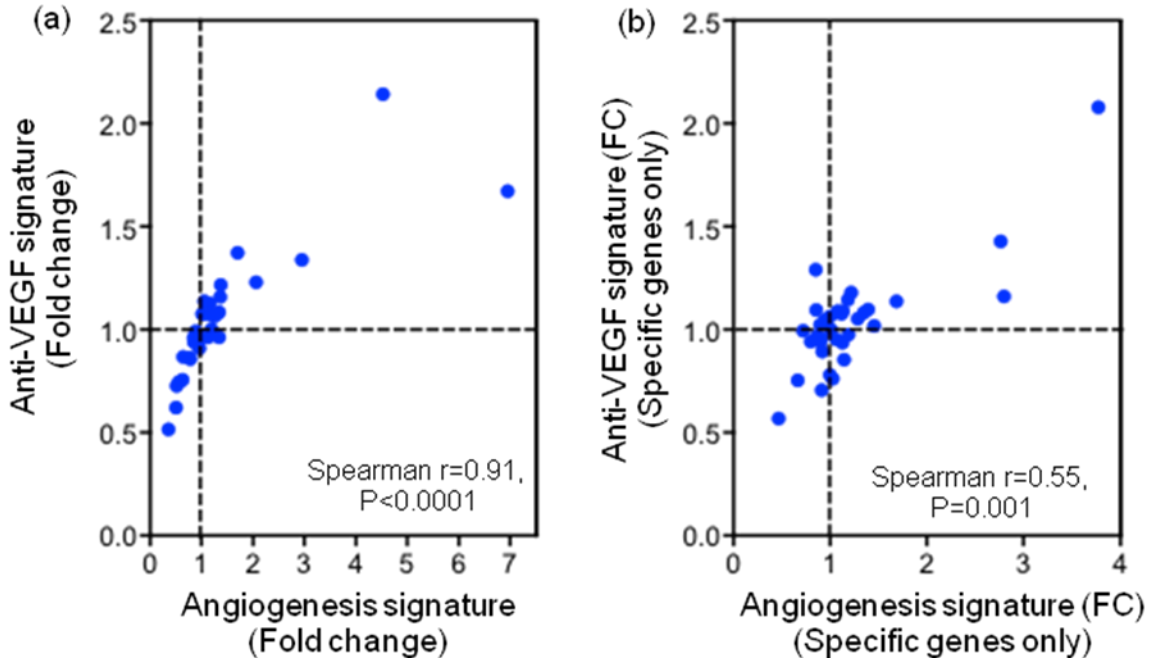

Figure-5.19: Correlation of fold change in angiogenesis signature with fold change in anti-VEGF signature after bevacizumab. X-axis and y-axis showing fold change values of respective signatures. (a) Correlation considering all the genes of both signatures; (b)Correlation considering specific genes of each signature only.

There was no significant correlation observed between fold changes in hypoxia metagenes with fold change in angiogenesis metagenes (Spearman r=-0.18, P=0.28).

5.10 Tip cell markers

Changes in tip cell specific markers recently published by del Toro (del Toro, Prahst et al. 2010) were also assessed. There was a significant down-regulation of two genes, endothelial cell-specific molecule 1 and angiopoietin 2. The other four genes including integrin beta 1, apelin, nidogen 1 and plasminogen activator urokinase receptor were down regulated, but did not reach significance level (Table-5.7).

Table-5.7: Assessment of post-bevacizumab changes in tip cell markers

Gene Title	Gene Symbol	Transcript cluster ID	Entrez. Gene ID	Paired t-test (t values)	(P-value)	Chr
Endothelial cell-specific molecule 1	**ESM1**	**2856995**	**11082**	**-1.70**	**8.99E-09**	**5**
Angiopoietin 2	**ANGPT2**	**3122489**	**285**	**-0.31**	**0.05**	**8**
Nidogen 1	NID1	2462160	4811	-0.04	0.70	1
Apelin	APLN	4021250	8862	-0.04	0.53	X
Integrin, beta 1	ITGB1	3284188	3688	-0.04	0.52	10
Plasminogen activator, urokinase receptor	PLAUR	3864551	5329	-0.01	0.90	19

5.11 Assessment of post-bevacizumab changes in genes signatures as a function of clinical and pathological prognostic factors at baseline (Pre-bevacizumab)

Further analysis was performed to see if there was any difference in changes in specific gene signature after bevacizumab in the subpopulation of breast cancer patients based on pre-bevacizumab prognostic factors e.g. receptor status (ER/ PR/ HER2), initial grade, initial size and age at presentation (Table- 5.8, 5.9). There was no significant difference in the fold changes of genes signatures in different subgroups of patients based on their receptor status at baseline (Table- 5.8).

Table-5.8: Fold changes in genes signatures as a function of receptor status at baseline.

Fold changes	ER+ vs. ER- [1*]	ER+PR+ vs. ER+PR- vs. ER-PR- [2$]	HER2+ vs. HER2 - [3*]	ER-PR-HER2- vs. others [4*]
Hypoxia	0.16	0.23	0.74	0.25
Proliferation	0.10	0.19	0.74	0.22
Angiogenesis	0.19	0.36	0.24	0.78
Anti-VEGF	0.31	0.34	0.68	0.93

1. ER+ (n= 26), ER- (n= 10)
2. ER+PR+ (n= 19), ER+PR- (n=7), ER-PR- (n=9), only one patient was ER-PR+ not included in analysis.
3. HER2+ (n= 9), HER2- (n= 27)
4. ER-PR-HER2- (n=5), Others (n=31)

*Columns showing P-values (Mann-Whitney test)
$ Columns showing P value (Kruskal-Wallis test)

However, a significant reduction in proliferation as defined by down-regulation of proliferation metagenes was observed in grade 3 patients in comparison to grade 2 patients, two weeks after a single cycle of bevacizumab (Table- 5.9, Figure- 5.20).

Table-5.9: Fold changes in genes signatures as a function of other known prognostic factors in breast cancer

Fold changes	Grade (2/3) [1*]	Size[$]	Age[$]
Hypoxia	0.06	0.09 (0.60)	-0.33 (0.05)
Proliferation	**0.03**	0.14 (0.41)	-0.25 (0.15)
Angiogenesis	0.87	0.04 (0.81)	-0.14 (0.40)
Anti-VEGF	0.8	0.08 (0.65)	-0.04 (0.82)

1. Grade 2 (n= 15), Grade 3 (n=21)
* Columns showing P-values (Mann-Whitney test)
$ Columns showing spearman coefficient r (P-value)

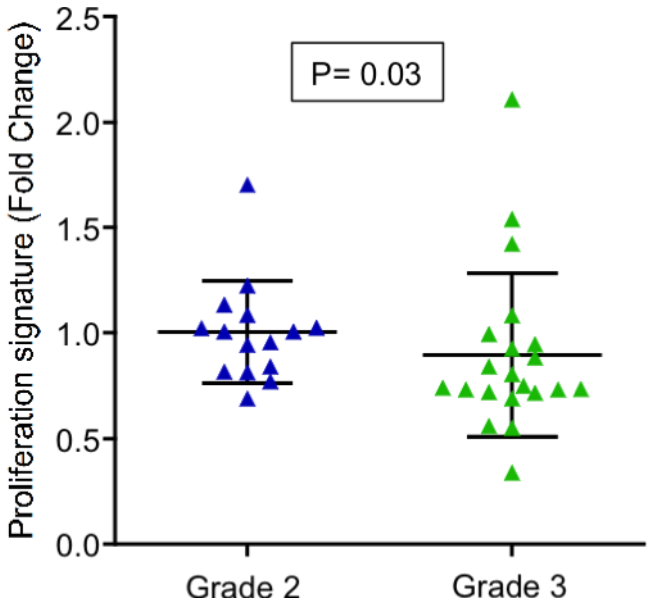

Fig-5.20: Proliferation signature fold change vs. grade. Plot showing significant down-regulation of proliferation in grade 3 (n=21) in comparison to grade 2 (n=15) after single cycle of bevacizumab. Error bars represent mean±SD.

5.12 Prognostic significance of fold changes in gene signatures

To understand the clinical impact at the end of neoadjuvant therapy due to a single cycle of bevacizumab given before the start of chemotherapy, further assessments of the relationship of fold changes in gene signatures with the pathological responses after neoadjuvant chemotherapy was performed.

As mentioned previously (in Chapter 4, Section 3) there were 13 patients who had good pathological response after neoadjuvant chemotherapy. This included 6 patients classified as complete pathological response (pCR) with no viable tumour seen either in breast or in lymph nodes and 7 patients who had only a few scattered cells in the final histological examination of either breast mass or lymph nodes after chemotherapy (classified as near to pCR). For this analysis pCR (n=6) and near to pCR (n=7) are considered as one group i.e. good pathological response (n=13).

There was no significant difference observed in terms of fold changes in different gene signatures between good pathological responders (n=13) versus others (n=23) (Table- 5.10)

Table-5.10: Prognostic significance of fold changes in gene signatures

Fold changes	Good pathological response[1]/others[2] (P-value, Mann-Whitney test)
Hypoxia	0.47
Proliferation	0.25
Angiogenesis	0.09
Anti-VEGF	0.14

1. Good pathological response: Complete/ near complete pathological response (n=13)
2. Others: Includes PR (n=19), no response (n=2), not available (n=2)

5.13 Pathways analysis of differentially expressed genes

For up-regulated genes after bevacizumab therapy, biological processes and pathways analysis were analysed using Genecodis 3.0 (Nogales-Cadenas, Carmona-Saez et al. 2009; Tabas-Madrid, Nogales-Cadenas et al. 2012)

The most significant biological processes observed were the *immune response, signal transduction, cell surface receptor signalling pathways* (Figure-5.21, Table-5.11). Among the most significant pathways from the KEGG database were *T-cell receptor signalling, cytokine-cytokine receptor signalling, haemopoietic cell lineage and cell adhesion molecules* (Figure-5.22, Table-5.12).

Similar pathways were noted using other databases e.g. PANTHER (Figure-5.23, Table-5.13), Ingenuity pathways analysis (Ingenuity® Systems, USA) and Reactome (Croft, O'Kelly et al. 2011). Pathway analysis was not performed for down-regulated genes as the number of genes (n=23) was too small to be considered for pathway analysis.

(a)

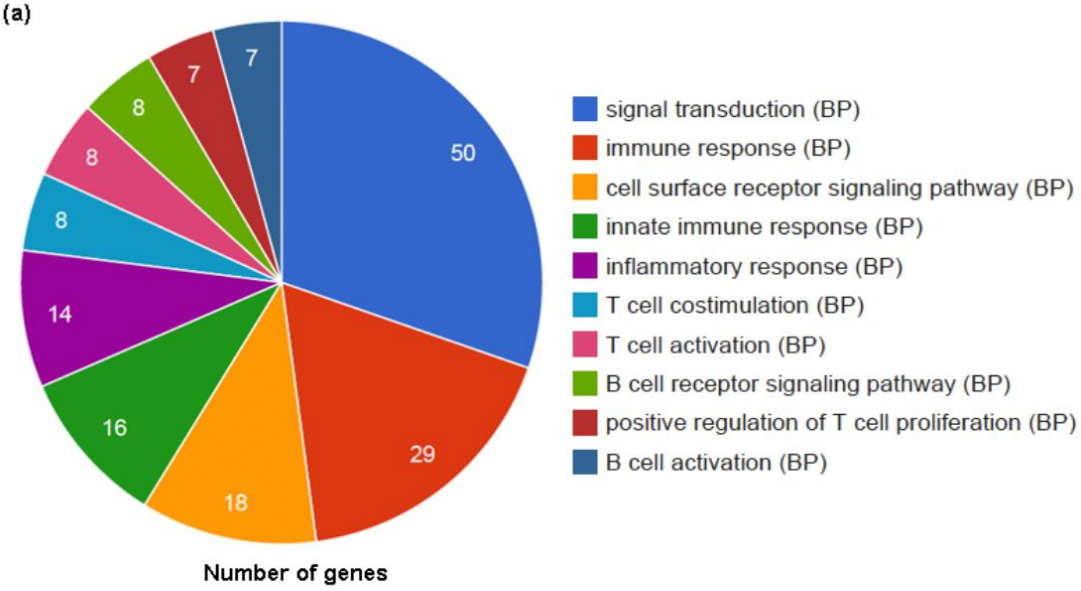

(b)

Annotations	No. of genes	Hyp*
GO:0006955: immune response (BP)	29	3.06E-13
GO:0007165: signal transduction (BP)	50	4.64E-13
GO:0007166: cell surface receptor signaling pathway (BP)	18	3.27E-10
GO:0050853: B cell receptor signaling pathway (BP)	8	5.54E-08
GO:0042113: B cell activation (BP)	7	1.80E-06
GO:0042110: T cell activation (BP)	8	1.84E-06
GO:0042102: positive regulation of T cell proliferation (BP)	7	3.61E-05
GO:0045087: innate immune response (BP)	16	6.25E-05
GO:0006954: inflammatory response (BP)	14	0.00017673
GO:0031295: T cell costimulation (BP)	8	0.00019434

Figure-5.21: Significant biological processes from up-regulated genes. (a) Pie chart showing number of genes involved in each biological process from the list of up-regulated genes. (b) Table showing annotations of each biological process arranged by order of significance. No. of genes- Number of post bevacizumab up-regulated genes involved in each biological process. Hyp*- Hypergeometric p-value corrected by FDR method.

Table-5.11: Lists of genes involved in significant biological processes. Gene symbols arranged by descending order of fold change (from left to right) after bevacizumab.

Annotations	Gene Symbols
GO:0006955: Immune response (BP)	CCL14-CCL15, CCL19, C7, CD28, CTLA4, ADAMDEC1, CD86, IL7R, IRF8, CLEC4E, RGS1, AIM2, CD96, CXCL12, GZMA, IL18R1, IL1R1, CD1C, FAS, IL18RAP, IL15, C3HC4, FTH1, P2RY14, HLA-DOB, LAX1, GPR183, CCL5, CBLB
GO:0007165: Signal transduction (BP)	CCL14-CCL15, PDE3B, TRAT1, PPARG, IL7R, RGS1, RASSF4, MFAP4, CXCL12, IQGAP2, TLR8, CDC42EP3, IL18R1, NPM1, FAM13A, SH3BP5, CD48, CD38, ARHGAP15, CD53, PRKCB, CAMK4, ARHGAP24, ARRDC3, PILRA, APBB1IP, IRS2, PAG1, ANGPTL1, IL1R1, FAS, CD226, IL18RAP, IL15, RASA2, ITGAL, ARHGAP30, LPXN, MKLN1, NCK2, LILRB4, ANGPTL4, SP110, RRAGB, HNRNPK, PRKCH, HINT1, CBLB, CALCOCO1, ULK2
GO:0007166: Cell surface receptor signalling pathway (BP)	CD28, CD3D, IL7R, LIFR, CD27, LY96, PDK1, ADRB2, KLRG1, KLRB1, CLEC2D, MS4A2, PTPRC, CD2, IL1R1, IL18RAP, CD14, CBLB

$ For full gene names please see appendix -5.1

(a)

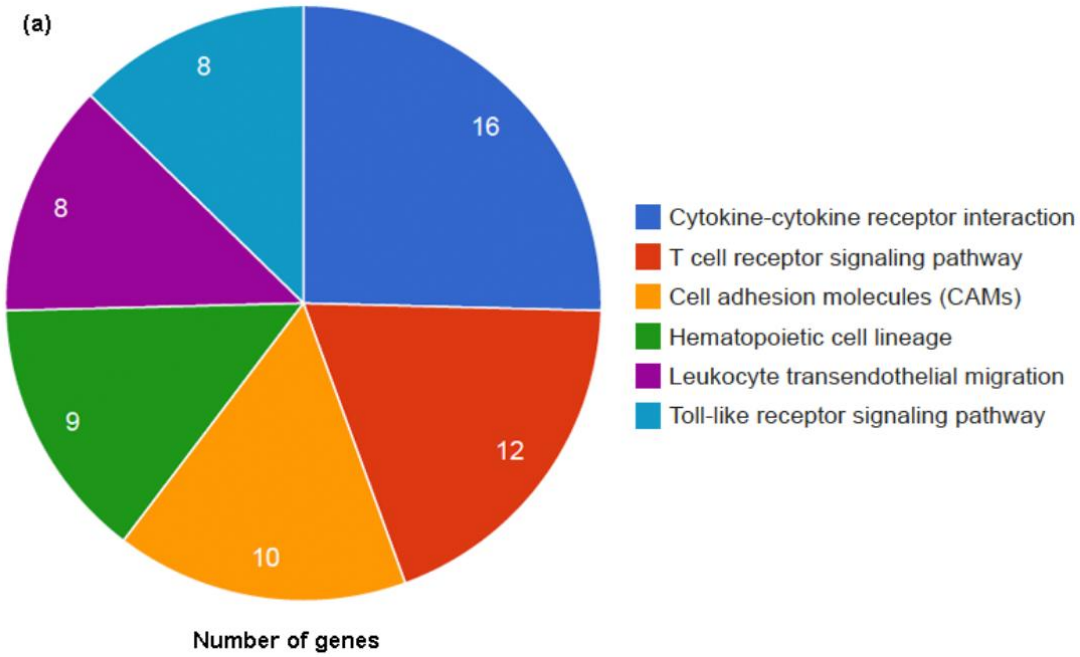

(b)

Annotations	No. of Genes	Hyp*
04660: T cell receptor signaling pathway	12	4.22E-07
04060: Cytokine-cytokine receptor interaction	16	3.03E-06
04640: Hematopoietic cell lineage	9	1.87E-05
04514: Cell adhesion molecules (CAMs)	10	4.35E-05
04620: Toll-like receptor signaling pathway	8	0.00033481
04670: Leukocyte transendothelial migration	8	0.00067186

Figure-5.22: Significant KEGG pathways from up-regulated genes. (a) Pie chart showing number of genes involved in each pathway from the list of up-regulated genes. (b) Table showing annotations of each pathway arranged by order of significance. No. of genes- Number of post bevacizumab up-regulated genes involved in each pathway. Hyp*- Hypergeometric p-value corrected by FDR method.

Table-5.12: Lists of genes involved in significant KEGG pathways. Gene symbols arranged by descending order of fold change after bevacizumab.

Annotations	Gene Symbols
(KEGG) 04660: T cell receptor signalling pathway	CD28, CTLA4, CD3D, PDK1, PTPRC, GRAP2, ITK, PPP3CC, PIK3CG, NCK2 CBLB, TEC
(KEGG) 04060: Cytokine-cytokine receptor interaction	CCL14-CCL15, CCL19, IL7R, LIFR, CD27, CXCL12, IL18R1, TGFBR2, IL1R1, FAS, IL18RAP, IL15, VEGFA, IL10RA, CXCR4, CCL5
(KEGG) 04640: Hematopoietic cell lineage	CD3D, IL7R, CR1, CD38, CD2, IL1R1, CD1C, CD14, CD37
(KEGG) 04514: Cell adhesion molecules (CAMs)	CD28, CTLA4, CD86, PTPRC, SELL, CD2, CD226, CD58, ITGAL, HLA-DOB
(KEGG) 04620: Toll-such as receptor signalling pathway	SCN7A, CD86, SPP1, LY96, TLR8, CASP8, PIK3CG, CD14
(KEGG) 04670: Leukocyte transendothelial migration	CXCL12, NCF2, PRKCB, ITGAL, ITK, RHOH, PIK3CG, CXCR4

$ For full gene names please see appendix –5.1

(a)

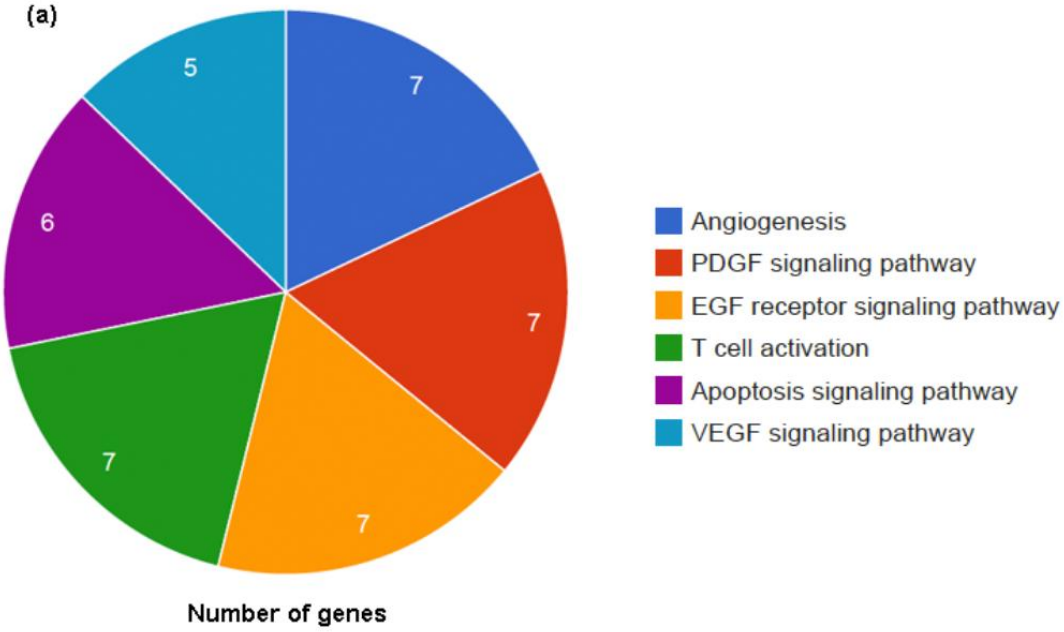

(b)

Annotations	No. of Genes	Hyp*
P00053: T cell activation	7	0.00128154
P00018: EGF receptor signaling pathway	7	0.00710977
P00047: PDGF signaling pathway	7	0.00716135
P00056: VEGF signaling pathway	5	0.00757773
P00006: Apoptosis signaling pathway	6	0.0123881
P00005: Angiogenesis	7	0.0135443

Figure-5.23: Significant PANTHER pathways from up-regulated genes. (a) Pie chart showing number of genes involved in each pathway from the list of up-regulated genes. (b) Table showing annotations of each pathway arranged by order of significance. No. of genes- Number of post bevacizumab up-regulated genes involved in each pathway. Hyp*- Hypergeometric p-value corrected by FDR method.

Table-5.13: Lists of genes involved in significant PANTHER pathways. Gene symbols arranged by descending order of fold change after bevacizumab.

Annotations	Gene Symbols
P00053: T cell activation	CD28, CD86, PTPRC, GRAP2, PPP3CC, PIK3CG, NCK2
P00018: EGF receptor signalling pathway	STAT4, PRKCB, RASA2, PIK3CG, GAB1, PRKCH, CBLB
P00047: PDGF signalling pathway	STAT4, ARHGAP15, GRAP2, RASA2, PIK3CG, NCK2, GAB1
P00056: VEGF signalling pathway	PRKCB, PIK3CG, LPXN, VEGFA, PRKCH
P00006: Apoptosis signalling pathway	PRKCB, BCL2, FAS, PIK3CG, PRKCH, EIF2AK2
P00005: Angiogenesis	PRKCB, PIK3CG, LPXN, VEGFA, NCK2, PRKCH, RBPJ

$ For full gene names please see appendix -5.1

5.14 Immunohistochemistry analysis

FFPE core biopsy specimens were collected before and two weeks after bevacizumab were used for Immunohistochemistry (IHC) work (details as in Chapter 2, Section 8). On IHC analysis, two weeks after bevacizumab, there was a significant up-regulation of hypoxia as evident by a significant increase in the percentage of tumour cells positive for carbonic anhydrase-9 (CA-9), from a mean of 3.1% to 10.6% (P=0.039) (Figure- 5.24) and percentage of tumour cells positive for HIF-1α also went up from a mean of 7.1% to 14.1% (P=0.001) (Figure- 5.25).

Along with this a significant down-regulation of proliferation and angiogenesis was observed as evident by reduction in percentage of Ki-67 positive tumour cells from a mean of 63.9% to 52.1% (P=0.006) (Figure-5.26) and reduction in the percentage of the micro-vascular area (Plasmalemma vascular associated protein (PLVAP) was used as a marker) from a mean of 0.49% to 0.31% (P=0.016) (Figure- 5.27).

There was no significant change in the vascular endothelial growth factor-A (VEGFA) (mean H-score from 132.1 to 126.3, P=0.39), vascular endothelial growth factor-C (VEGFC) (mean H-Score from 80.5 to 64.9, P=0.20) and vascular endothelial growth factor receptor (VEGFR2) both on tumour cells (mean H-score from 89.7 to 100.8, P=0.73) as well as on vessels (mean score from 1.97 to 1.90, P=0.38).

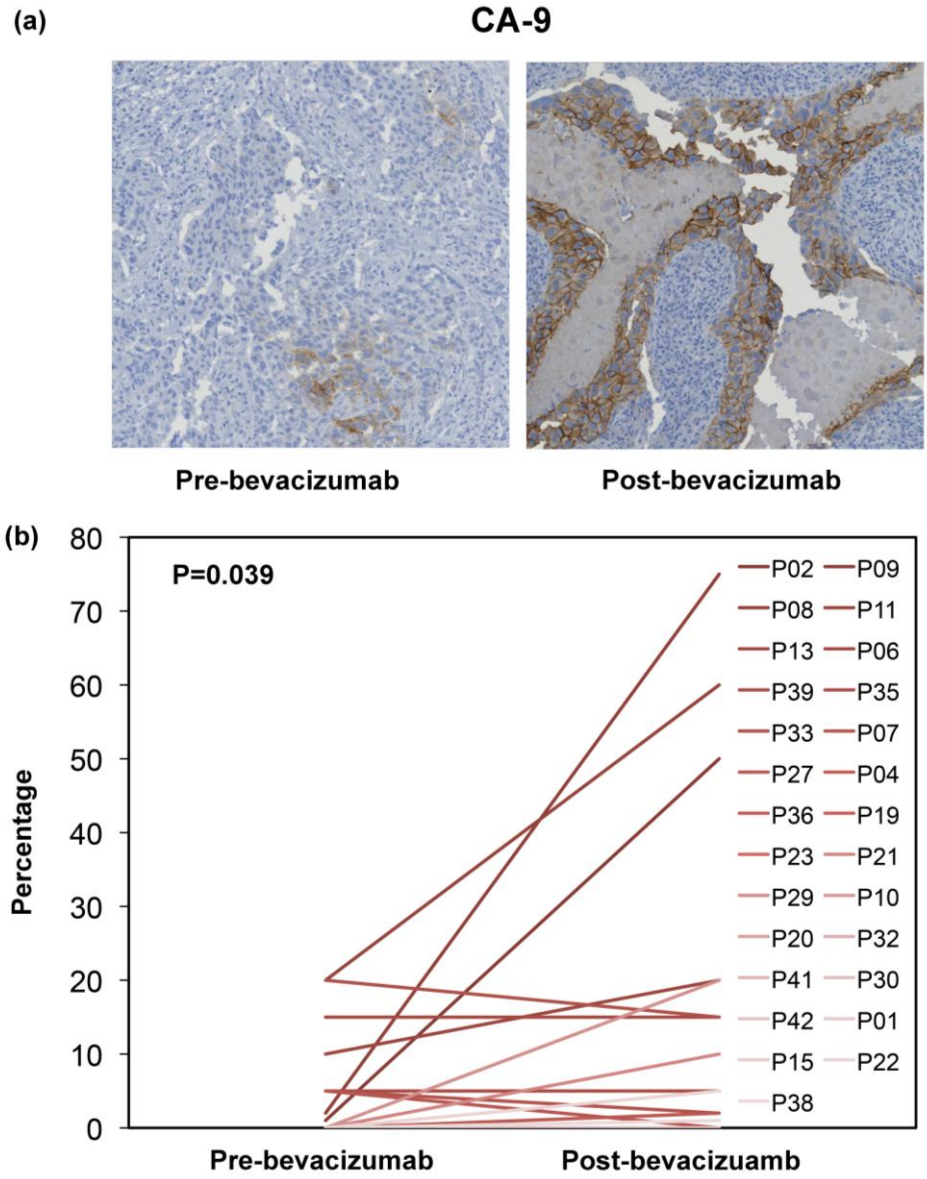

Figure-5.24: Up-regulation of carbonic anhydrase-9 in response to bevacizumab. (a) Representative sections of a core biopsy sample showing a significant increase in staining for CA-9. (b) Plot showing patient-by-patient change in CA-9 percentage in response to bevacizumab assessed after 2 weeks of therapy. Patients arranged by descending order of fold change (P-value, Wilcoxon-signed rank test).

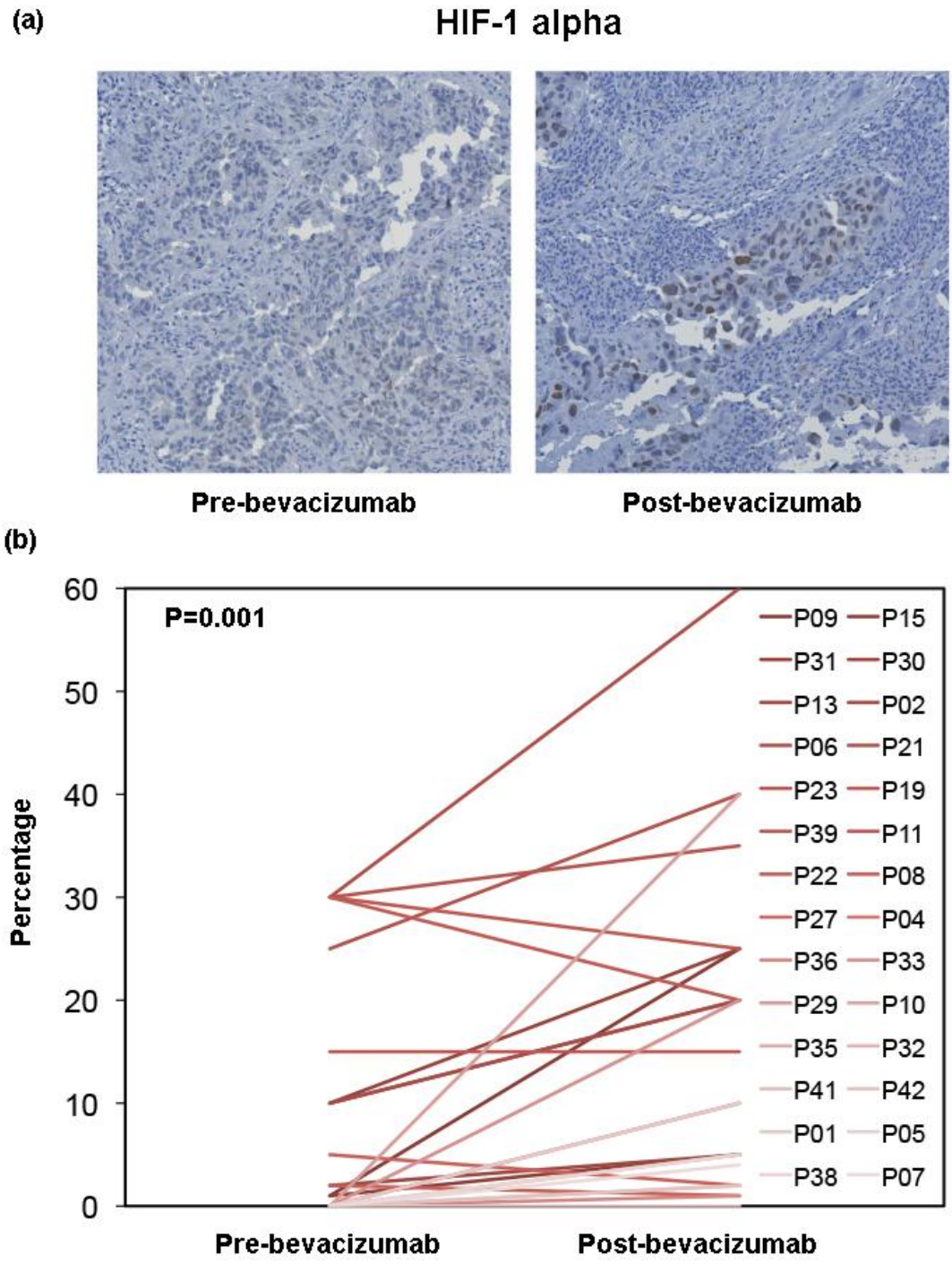

Figure-5.25: Up-regulation of hypoxia inducible factor-1 alpha in response to bevacizumab. (a) Representative sections of a core biopsy sample showing a significant increase in staining for HIF-1α, (b) Plot showing patient-by-patient change in HIF-1α percentage in response to bevacizumab assessed after 2 weeks of therapy. Patients arranged by descending order of fold change (P-value, Wilcoxon-signed rank test).

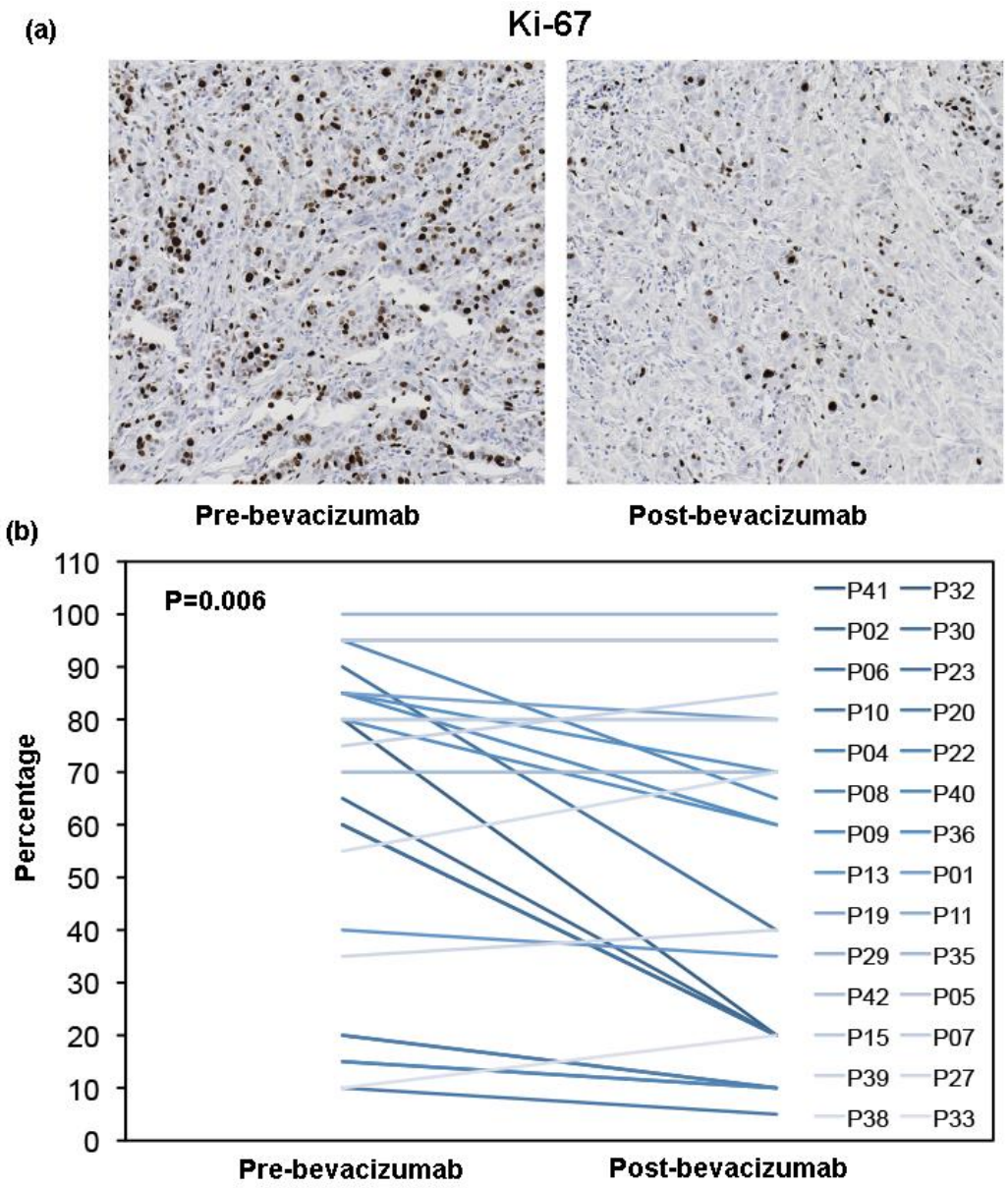

Figure-5.26: Significant down-regulation of Ki-67 in response to bevacizumab. (a) Representative sections of a core biopsy sample showing a significant reduction in staining for Ki-67, (b) Plot showing patient-by-patient change in Ki-67 percentage in response to bevacizumab assessed after 2 weeks of therapy. Patients arranged by ascending order of fold change (P-value, Wilcoxon-signed rank test).

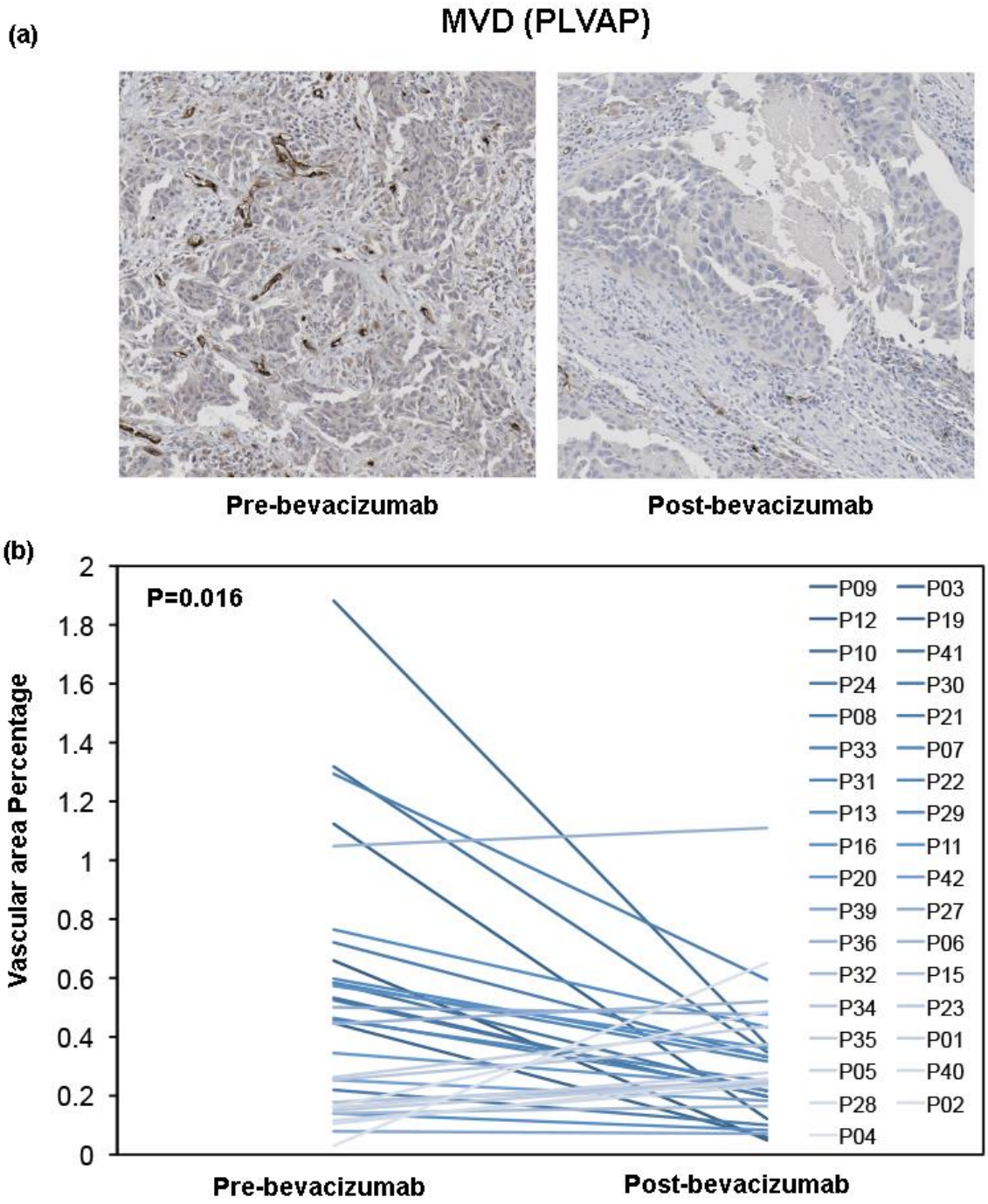

Figure-5.27: Significant down-regulation of plasmalemma vascular associated protein (PLVAP) in response to bevacizumab. (a) Representative sections of the core biopsy sample showing significant reduction in staining for PLVAP, (b) Plot showing patient-by-patient change in vascular area percentage in response to bevacizumab assessed after 2 weeks of therapy. Patients arranged by ascending order of fold change (P-value, Wilcoxon-signed rank test).

5.14.1 Absolute changes in IHC parameters as function of prognostic factors in breast cancer

The association between the absolute changes (calculated as post bevacizumab minus the pre bevacizumab value) 2 weeks after bevacizumab therapy and prognostic factors (ER, PR, HER2 status, grade, age of patient at presentation and clinical size at baseline) was assessed (Tables 5.14, 5.15).

For CA-9, absolute change was significantly higher in ER- patients (n=10) in comparison to ER+ patients (n=26) (Figure-5.28 a). This implies that the induction of hypoxia was significantly greater in ER- patients than ER+ patients. On the other hand, there was a significant down-regulation of VEGFA in ER- patients in comparison to ER+ patients at the protein level (Figure-5.28b). Furthermore, there was significant down-regulation of VEGFA in ER-PR- patients in comparison to ER+PR- patients (Kruskal-wallis test, P= 0.03, Dunn's multiple comparison test, P <0.05) but there was no significant difference between ER+PR+ vs. ER+PR- and ER+PR+ vs. ER-PR- group of patients (Figure- 5.28 c).

No significant difference was observed between the HER2+ versus HER2- groups for any of the IHC parameters analysed in this study.

Table-5.14: Relationship of absolute changes in IHC parameters after bevacizumab with receptor status at baseline.

IHC parameters	ER+ vs. ER- [1*]	ER+PR+ vs. ER+PR- vs. ER-PR- [2$]	HER2+ vs. HER2- [3*]	ER-PR-HER2- vs. others [4*]
CA-9	**0.01**	**0.04**	0.55	**0.05**
HIF1-a	0.74	0.58	0.06	0.72
Ki-67	0.96	0.65	0.67	0.24
PLVAP	0.65	0.36	0.95	0.49
VEGFA	**0.02**	**0.03**	0.35	0.10
VEGFC	0.50	0.64	0.84	0.63
KDR tumour	0.60	0.61	0.98	0.64

1. ER+ (n=26), ER- (n=10)
2. ER+PR+ (n=19), ER+PR- (n=7), ER-PR- (n=9), only one patient was ER-PR+ did not included in analysis.
3. HER2+ (n=9), HER2- (n=27)
4. ER-PR-HER2- (n=5), Others (n=31)

* Columns showing P-values (Mann-Whitney test)

$ Columns showing P value (Kruskal-Wallis test)

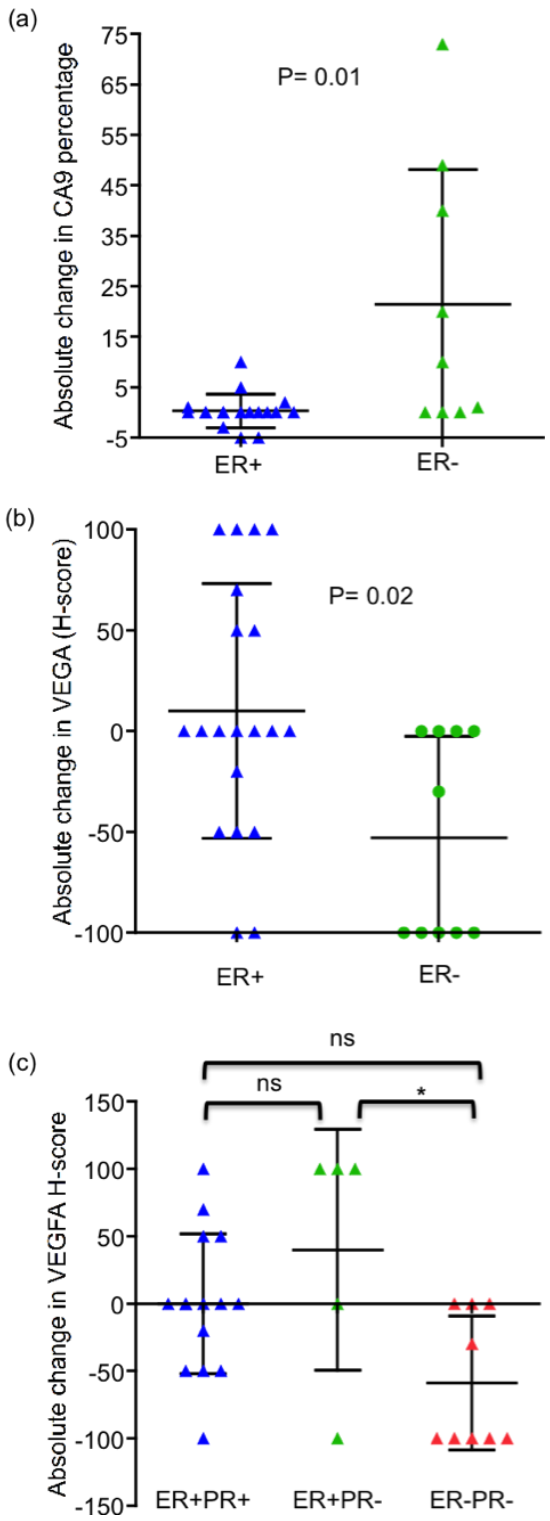

Figure-5.28: Association of absolute change in CA-9 and VEGFA with receptor status. Error bars show mean±SD for each plot; Plots (a) and (b) show P-value, Mann-Whitney test. Plot (c) show Kruskal-Wallis test along with Dunn's multiple comparison test. * Denotes P<0.05, ns = P>0.05.

Along with this there was no significant difference noted between grade 2 versus grade 3 patients for any of the IHC markers analysed. Similarly there was no significant relationship observed for tumour size and age of patient with absolute changes after bevacizumab therapy in any of the IHC parameters analysed in this study (Table- 5.15).

Table-5.15: Relationship of absolute changes in IHC parameters after bevacizumab with known prognostic factors at baseline

IHC Parameters	Grade 2 vs. Grade 3 [1*]	Size[$]	Age[$]
CA-9	0.91	-0.05 (0.79)	-0.06 (0.76)
HIF1-α	0.98	0.21 (0.22)	0.17 (0.32)
Ki-67	0.57	-0.16 (0.49)	0.15 (0.44)
PLVAP	0.45	0.11 (0.52)	-0.02 (0.93)
VEGFA	0.75	0.18 (0.35)	-0.12 (0.54)
VEGFC	0.78	-0.18 (0.35)	0.02 (0.92)
KDR tumour	0.82	-0.32 (0.09)	0.11 (0.58)

1 Grade 2 (n=15), Grade 3 (n=21)
* Columns showing P-values (Mann-Whitney test)
$ Columns showing Spearman coefficient r (P-value)

5.15 Discussion

Bevacizumab has been in clinical use for over a decade now. Several trials have been conducted initially in the metastatic setting (Miller 2003; Ramaswamy and Shapiro 2003; Miller, Chap et al. 2005; Miles 2007; Miles, Chan et al. 2010; Borson, Harker et al. 2012; Rossari, Metzger-Filho et al. 2012) and then more recently in the neoadjuvant setting to shed light on the specific group of patients most likely to show benefit to bevacizumab (Overmoyer B 2004; Wedam, Low et al. 2006; Baar, Silverman et al. 2009; Bear, Tang et al. 2012; Pierga, Petit et al. 2012; von Minckwitz, Eidtmann et al. 2012).

Several potential biomarkers of anti-VEGF therapeutic response have been proposed. However, to date, the hunt for a validated biomarker is still ongoing (Denduluri, Yang et al. 2008; Miles, de Haas et al. 2013; Jubb, Miller et al. 2011; Gyanchandani and Kim 2013; Lambrechts, Lenz et al. 2013; Sanchez-Rovira, Segui et al. 2013)

In this study, by performing a genome-wide gene expression analysis immediately before and then 2 weeks after bevacizumab mono-therapy, several key genes and molecular pathways were identified that could be useful in understanding the mechanisms governing response and resistance to bevacizumab. For example, the up-regulation of genes involved in the immune response e.g. CCL14-CCL15, CD28, CTLA4; genes involved in cancer metabolism and survival under stress e.g. PDK1, PDE3B, PDK4, PIK3CG,

EIF2AK2 and angiogenesis such as VEGFA, ANGPTL4, ANGPTL1, CXCL12 was observed in this study.

Both by exon array and by qRT-PCR analysis, at the single gene level the significant down-regulation of ESM1, CCNE1 and DLL4 was observed along with significant up-regulation of VEGFA, PDK1 and PDE3B. In addition, there were several interesting genes that changed significantly after bevacizumab therapy as assessed by exon array analysis. However, with qRT-PCR analysis these genes showed a similar trend but did not reach a level of statistical significance. This may be due to sensitivity of different techniques (exon array vs. qRT-PCR).

In this study, the significant down-regulation of ESMI was observed globally in the whole study population. ESM1 or endocan is highly specific for endothelial tip cells and has been proposed to be a marker of endothelial activation (Sarrazin, Adam et al. 2006; del Toro, Prahst et al. 2010). This gene has also been identified as one of the genes involved in the switch from dormant to angiogenic tumours (Almog, Ma et al. 2009). Endocan is highly regulated by vascular endothelial growth factor (Rennel, Mellberg et al. 2007) and is known to play an important role in neo-angiogenesis along with ang-2 (del Toro, Prahst et al. 2010). Due to these reasons endocan has been postulated as a potential biomarker to quantify the impact of an anti-VEGF treatment on the vasculature (Sarrazin S 2010). There was no difference observed in subgroups based on receptor status but a greater down-regulation of ESM1 was observed in patients with high grade tumours. This may signify a better response to

bevacizumab in this particular group of patients.

The significant down-regulation of CCNE1 previously known as cyclin E, was observed after bevacizumab therapy. CCNE1 is known to be a key regulator of the important G1/S transition of the cell cycle. High cyclin E expression has been postulated as a marker of poor clinical outcome in breast cancer and resistance to treatment (Nielsen, Arnerlov et al. 1996; Sieuwerts, Look et al. 2006; Scaltriti, Eichhorn et al. 2011). In line with other studies (Nielsen, Arnerlov et al. 1996), in this study also the high baseline expression of CCNE1 was observed in ER- patients.

Furthermore, the significant down-regulation of DLL4 was observed after bevacizumab therapy. DLL4 is an endothelial notch ligand and known to regulate angiogenesis by endothelial tip/stalk cell specification during angiogenic sprouting. Recently a number of groups have shown (Noguera-Troise, Daly et al. 2006; Li, Sainson et al. 2007; Scehnet, Jiang et al. 2007) that DLL4-notch signaling regulates tumour growth by decreasing angiogenesis but improving vascular function. Conversely, blockade of DLL4-notch signaling strikingly increases nonproductive angiogenesis which subsequently reduces tumour growth. The Harris Lab has also shown recently that DLL4-notch signalling mediates resistance to anti-VEGF agents in xenograft model (Li, Sainson et al. 2011). In a recent retrospective study in metastatic breast cancers, Jubb et al. (Jubb, Miller et al. 2011) have shown improved PFS after bevacizumab and chemotherapy in patients with a low level of DLL4 initially. In this study, there was a wide variation observed in

down-regulation of DLL4 among patients that could have important clinical implications in the long-term.

VEGFA is the most important angiogenic factor to regulate angiogenesis and levels of VEGFA have been reported to be significantly higher in breast cancers. Recent studies have shown that VEGFA amplification as assessed by FISH is a poor prognostic marker to bevacizumab along with chemotherapy in metastatic breast cancers (Schneider, Gray et al. 2013). In this study significant up-regulation of VEGFA at gene level was observed but the down-regulation of VEGFA was noted after bevacizumab at the protein level in ER- or more specifically ER-PR- patients. The discrepancy observed at gene level and protein level might be due to the reason that bevacizumab is a monoclonal antibody against VEGF that directly blocks VEGFA protein but up-regulation at the gene level might be in response to induction of hypoxia (Buffa, Harris et al. 2010) after bevacizumab monotherapy which has been observed in this study.

Similar to the retrospective study (Chapter 3) and in line with other published studies (Umemura, Yoshida et al. 2007); significant higher levels of PDK1 expression were noted in the triple negative subgroup of patients at baseline. Also after bevacizumab therapy significant up-regulation of PDK1 was observed that could contribute to resistance as PDK1 is known to be an important regulator of PI3K/AKT signalling pathway. PDK1 shunts pyruvate away from the citric acid cycle and keeps the hypoxic cell alive. Additionally, PDK1 has been shown to increase activity in hypoxic cancer cells due to the

presence of HIF-1α (Kim, Gao et al. 2007) (Kim, Tchernyshyov et al. 2006; Buffa, Harris et al. 2010).

PDE3B is known to be a critical regulator of cAMP levels that affect activation of AMP-activated protein kinase (AMPK). AMPK is known to be involved in regulating energy balance at the cellular level and is activated by stresses that deplete ATP, including glucose deprivation and hypoxia (Kahn, Alquier et al. 2005). In a recent study, PDE3B has been postulated to regulate human arterial endothelial cells and angiogenesis through Exchange protein activated by cAMP (EPAC) and PI3K encoded signals (Wilson, Baillie et al. 2011). The significant up-regulation of PDE3B observed in this study might be serving as an important escape mechanism of cancer cells to bevacizumab therapy due to up-regulation of AMPK.

A higher CA-9 level has been reported to relate to poor prognosis in breast cancer (Jubb, Buffa et al. 2010; Swietach, Hulikova et al. 2010). As reported previously by our group (Tan, Yan et al. 2009), in this study significantly higher expression of CA-9 was observed at mRNA levels at baseline in ER- breast cancers that are known to be more aggressive tumours (Sorlie, Perou et al. 2001). Following bevacizumab therapy, there was a trend towards up-regulation of CA-9 mRNA levels but it did not reach significance either by gene expression or qRT-PCR analysis. At the protein level a significant up-regulation of CA-9 was observed. CA-9 gene expression has been reported to reflect chronic hypoxia rather than acute hypoxia (Wykoff, Beasley et al. 2000); this may be the reason for the difference in CA-9 at the gene expression level

and protein level in this study.

SPRTY4 is known to be an important negative regulator of pathophysiological angiogenesis. The significant down-regulation of SPRTY4 was observed in the ER-PR- subgroup of patients after bevacizumab that may signify up-regulation of angiogenesis after bevacizumab therapy in this highly aggressive group of patients.

CTLA-4 along with CD28, are known to play critical roles in the initial activation and subsequent control of T cell mediated cellular immunity (Noel, Boise et al. 1996; Gause, Halvorson et al. 1997). The signal delivered via CTLA-4 down-regulates T cell function and inhibits excessive expansion of activated T cells (Walker and Sansom 2011). Because of its central role in restraining T-cell activation, modulation of CTLA-4–mediated T-cell inhibition holds great promise in several clinical applications (Grosso and Jure-Kunkel 2013). From the gene expression analysis in this study the up-regulation of CTLA4 was observed although the fold change did not reach statistical significance as assessed by qRT-PCR. On further analysis, the fold change in CTLA4 after bevacizumab therapy was noted to be significantly higher in responders after chemotherapy (P=0.04, Mann-Whitney test), i.e. patients showing higher up-regulation of CTLA4 after bevacizumab show better pathological response after chemotherapy. It might be a false positive result considering the marginally significant P-value on univariate analysis. Further immunohistochemistry analysis of tumours for immune related cells is needed

pre and post bevacizumab and also post chemotherapy to understand the mechanism governing this result.

By performing the gene signature analysis as well immunohistochemical analysis (IHC) a significant down-regulation of proliferation was observed after bevacizumab. There was no significant change in either the hypoxia or angiogenesis signatures considering the whole study population. However, by immunohistochemistry, a significant up-regulation of hypoxia was observed as shown by increased CA-9 and HIF1alpha. The down-regulation of angiogenesis was noted with IHC as shown by reduction in PLVAP. PLVAP was used in this study as a marker of angiogenesis as it was believed to be a component of diaphragmed endothelial fenestrations and has been suggested to be a downstream target of VEGF signaling (Strickland, Jubb et al. 2005). The observed difference noted between gene expression analysis and the IHC analysis results for hypoxia and angiogenesis changes after bevacizumab may be due to the difference in the two techniques used. Also the fact that gene signature takes into account the effect of all the genes in the signature rather than one specific marker as analysed by immunohistochemistry.

Interestingly, as we reported previously from the interim analysis of this study (Mehta, Hughes et al. 2011) the significant correlation of the fold change in hypoxia with the fold change in proliferation was observed across the whole study population. This result may have important implications for combination therapy. Of equal note there was a smaller group of patients where both tumour proliferation and hypoxia decreased after bevacizumab; one may

postulate that this group is obtaining direct benefit from the anti-VEGF agent alone. This needed to be explored further in large scale trials.

On analysing the fold changes in angiogenesis and anti-VEGF response signatures we observed that there was a subgroup of patients who had down-regulation of angiogenesis after bevacizumab therapy. This implies that in these tumours there was VEGF driven angiogenesis. However, there was a subgroup of patients in which there was up-regulation of angiogenesis after bevacizumab therapy. This implies that in these tumours angiogenesis was driven by other factors. These tumours may have active innate resistance mechanisms against bevacizumab therapy, in other words bevacizumab alone might not be beneficial in this subgroup of patients. There was no relationship observed between the fold change in hypoxia and angiogenesis gene signatures after bevacizumab.

There was no difference observed in fold changes in gene signatures in terms of hormone receptor status, size of tumour or age at presentation, except a significant down-regulation of proliferation signature and ESM1 in high-grade patients after bevacizumab therapy. This result is in agreement with recently published neoadjuvant studies showing higher rates of response in higher-grade tumours with bevacizumab in combination with chemotherapy (Bear, Tang et al. 2012; von Minckwitz, Eidtmann et al. 2012)

In summary, this study has resulted in an improved understanding of the molecular mechanisms governing response and resistance to bevacizumab

therapy. For example, downregualtion of tip cell markers ESM1, ang2, notch ligand DLL4, cell cycle regulator CCNE1 affects neoangiogenesis and tumour growth leading to hypoxia, which in turn regulates several pathways that could help tumours to survive after bevacizumab therapy. The up-regulation of immune system related pathways and up-regulation of VEGFA could lead to rebound angiogenesis at a later stage. The up-regulation of metabolic genes such as PDK1 and PDE3B could aid cell survival by switching mitochondrial metabolism to glycolysis and AMPK pathways.

This suggests that inhibition of the hypoxic adaptation to antiangiogenic therapy could enhance the bevacizumab treatment effect. For example, using bevacizumab with other targeted agents such as small molecules or antibodies which inhibit CA-9 (McIntyre, Patiar et al. 2012; Ward, Langdon et al. 2013) or using dichloroacetate, a PDK1 inhibitor, together with bevacizumab may be helpful in overcoming the development of resistance and ultimately lead to improved patient survival (Schulze and Harris 2012). In a recent clinical study metformin has been shown to downregulate PDE3B (Hadad, Iwamoto et al. 2011). Thus, combined therapy with metformin and bevacizumab might be a way forward to overcome resistance to bevacizumab. Results from an ongoing preclinical study in the Harris lab support this possibility.

Although the wide variation in gene expression after bevacizumab is noted at the single gene level, gene signature level and protein level, we were unable to identify any particular subgroup of patients showing better response. This may be due to lack of statistical power in this study to allow for detailed subgroup

analyses. The up-regulation of immune related pathways needs to be explored further to draw any inference from it. The marginally significant changes observed in this study need to be validated in further large-scale studies.

CHAPTER SIX

6 Integration of DCE-MRI and gene expression analysis (Prospective study)

6.1 Introduction

In this era of personalised medicine, the discovery of a predictive biomarker for anti-angiogenic therapy would enable clinicians to target treatment with these agents to patients who had been selected based on expression of the biomarker before treatment or at an early stage of treatment. This would potentially offer significant cost savings, as well as reduce the number of patients who experience the side effects of anti-angiogenic therapy without any of the clinical benefits. In the last decade, bevacizumab was the most commonly used anti-angiogenic agent in clinical practise. Although the search for a biomarker for bevacizumab therapy is ongoing, none is yet proven or in widespread use.

As discussed in earlier chapters, to address this issue we have conducted a window of opportunity study in which a single dose of bevacizumab was given 2 weeks prior to neoadjuvant chemotherapy in newly diagnosed breast cancer patients, with a detailed pharmacodynamic assessment using gene expression and DCE-MRI analysis before and after therapy.

In this chapter, the results of the detailed analysis using the combined approach of DCE-MRI and gene expression analysis at the single gene level, gene signature level and gene set enrichment analysis are described.
Specifically, we sought to understand:

1) Association of the change in MRI parameters after bevacizumab with the change in gene expression.

2) Association of the baseline MRI parameters with the baseline gene expression.
3) Association of the baseline gene expression with the changes in DCE-MRI parameters.
4) Association of the baseline DCE- MRI parameters with the changes in gene expression.

Aside from detailed exon array analysis, further analysis was also performed for specific genes of interest validated by qRT-PCR (as described in Chapter 5) and also for IHC parameters, in order to understand the association with MRI parameters at baseline or changes after bevacizumab.

6.2 Association of change in DCE-MRI parameters after bevacizumab with change in gene expression

6.2.1 Quantifying the effect with DCE-MRI after a single cycle of bevacizumab

To date, there are no set criteria to define response to anti-angiogenic therapy by using DCE-MRI techniques. Two approaches that could be used are:

1. Considering changes in MRI parameters as categorical variables and quantify response based on a pre-defined cut off value.

2. Considering change in MRI parameters as a continuous variable and define response qualitatively.

In this study both approaches were used for the analyses to classify the response to bevacizumab.

I. Analyses with the commonly used DCE-MRI PK parameter (median K^{trans})

Median K^{trans} is the most commonly reported parameter in the literature, and most studies have reported changes in median K^{trans} over the baseline levels and exceeding a threshold as 'vascular response' (Leach, Brindle et al. 2005). In this study, 30 percent reduction in median K^{trans} after bevacizumab was considered as a threshold to define vascular response. This criterion was decided based on published K^{trans} reproducibility statistics of DCE-MRI assessments (Galbraith, Lodge et al. 2002; Jackson, Jayson et al. 2003; O'Connor, Carano et al. 2009). By using this approach only 8 patients could be classified as non-responders, while the remaining 27 patients could be considered responders (Figure- 6.1).

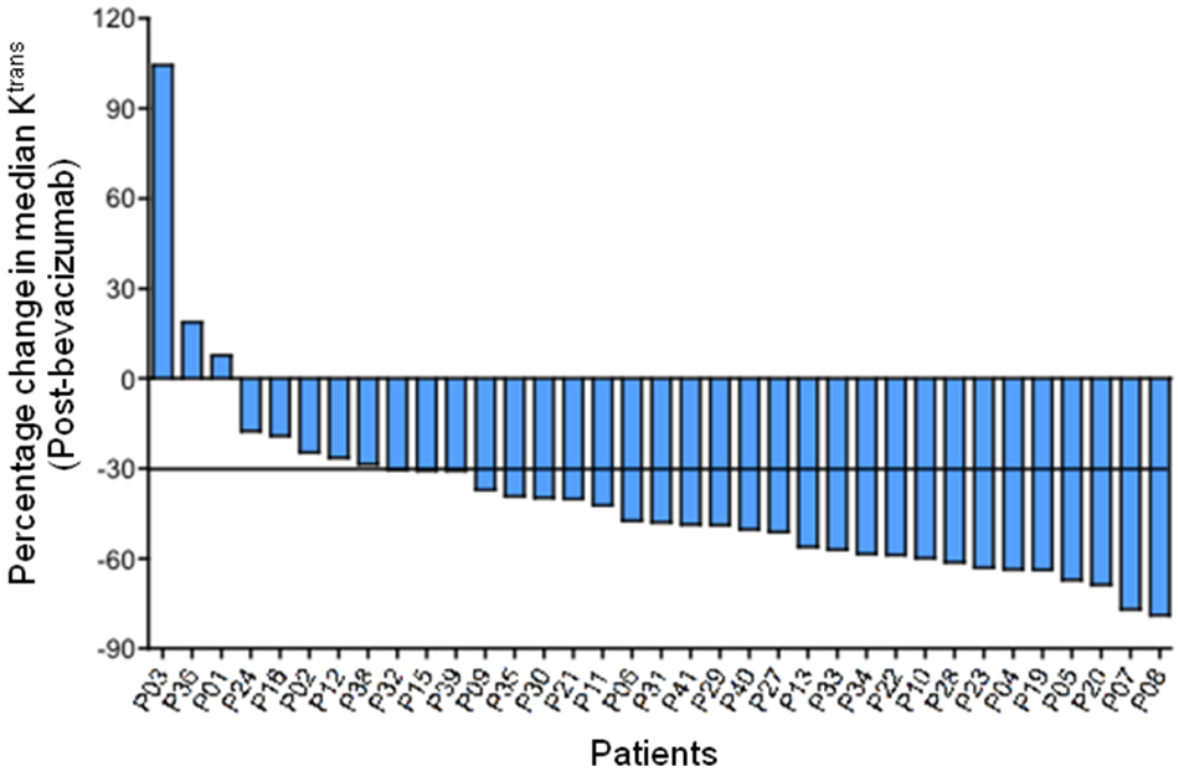

Figure-6.1: Waterfall plot showing percentage change in median K^{trans}. Based on 30% reduction as a response criterion. Non-responders (n= 8), Responders (n= 27).

Interestingly, on close observation of Figure- 6.1, a continuum of response was noted rather than the two well-defined categories. A similar trend was observed by considering absolute change in median K^{trans} (Figure- 6.2).

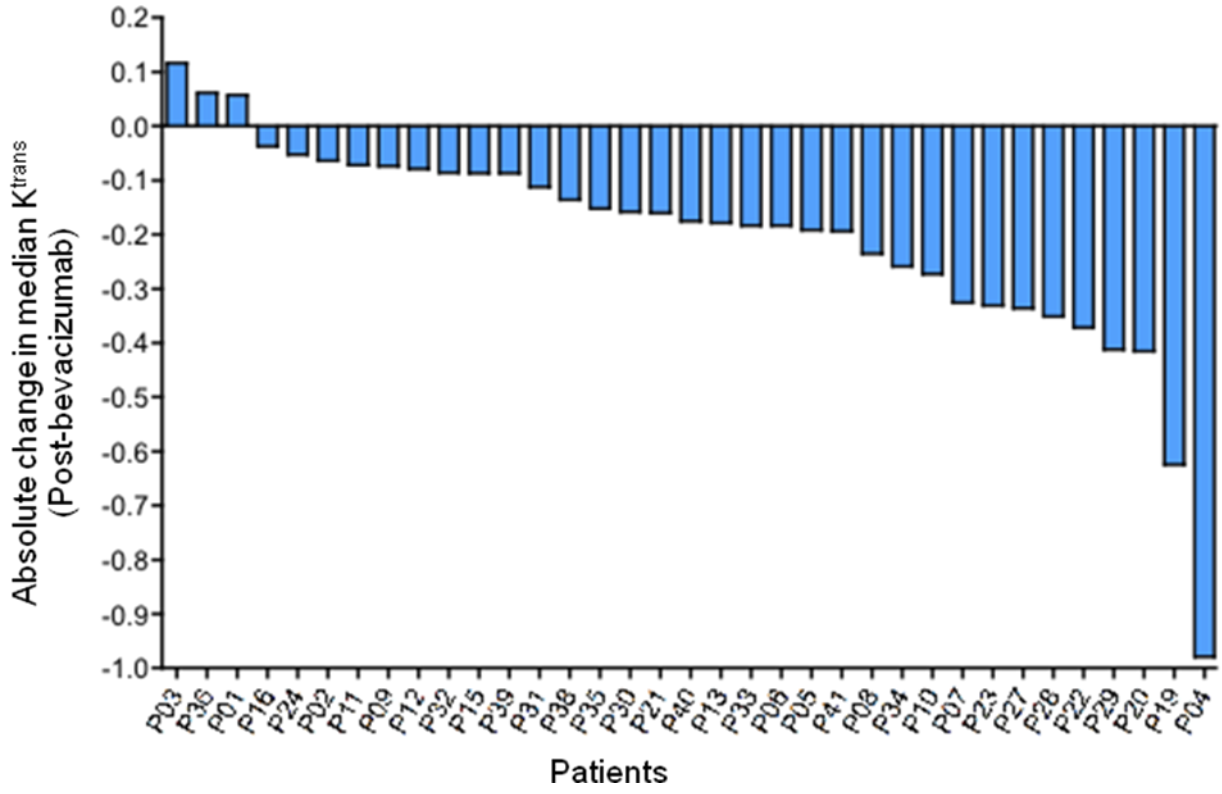

Figure-6.2: Waterfall plot showing absolute change in median K^{trans}

a) Exon array analysis considering MRI responses as categorical variable (responders vs. non-responders based on 30% reduction in median K^{trans})

As shown in above waterfall plots (Figure-6.1, 6.2) there was a high variability noted among patients in terms of changes in median K^{trans}. Gene expression analysis was done both at single gene level and the pathways/signature level to understand the molecular basis of these variabilities observed with DCE-MRI.

As mentioned before (Chapter 2, Section 6) initial pre-processing, normalisation and quality checks of the affymetrix exon array data was done. For each patient paired samples were considered (pre-bevacizumab and post-bevacizumab). Differential expression analyses before and after bevacizumab were conducted both at gene level and metagene level for analysing differentially expressed genes, and for phenotype/pathway activation changes respectively. A permutation based t-test method was used which was corrected for heteroscedasticity of gene expression distributions. Both global and local false discovery were estimated (Tibshirani and Efron 2002). Cluster transcripts with false discovery rate <5% were extracted.

Differential expression in responders versus non-responders as classified by 30% reduction in median K^{trans}

Supervised gene expression analysis was performed between responders (n=27) and non-responders (n=8) as defined by 30% reduction in median K^{trans} as response criteria. Cluster transcripts with false discovery rate <5% were extracted. There were 91 genes up-regulated (Table-6.1) and 33 genes were down-regulated (Table 6.2) among responders.

Table-6.1: Top 20 up-regulated genes after bevacizumab among patients classified as responders based on 30% reduction in median K^{trans} criteria.

Gene Name	Gene Symbol	Fold Change	Q value	Transcript Cluster ID	Entrez Gene ID	Chr
HLA class II histocompatibility antigen	LOC 100510059	2.03	2.52	2903219	100510059	6
Phosphodiesterase 3B, cGMP-inhibited	PDE3B	1.95	3.57	3321512	5140	11
Collectin sub-family member 12	COLEC12	1.89	1.96	3795733	81035	18
Chemokine (C-C motif) ligand 19	CCL19	1.88	4.55	3204285	6363	9
ABI family, member 3 (NESH) binding protein	ABI3BP	1.81	4.55	2686458	25890	3
CD3d molecule, delta (CD3-TCR complex)	CD3D	1.77	0.00	3393744	915	11
Lymphoid-restricted membrane protein	LRMP	1.76	0.00	3408505	4033	12
Regulator of G-protein signalling 13	RGS13	1.75	0.00	2372812	6003	1
Carboxypeptidase A3 (mast cell)	CPA3	1.74	0.00	2647109	1359	3
Cartilage intermediate layer protein	CILP	1.71	0.00	3629529	8483	15
Ankyrin repeat domain 29	ANKRD29	1.71	4.55	3801492	147463	18
CD27 molecule	CD27	1.69	0.00	3402506	939	12
Fas apoptotic inhibitory molecule 3	FAIM3	1.69	4.55	2452977	9214	1
B and T lymphocyte associated	BTLA	1.68	3.57	2688717	151888	3
CD28 molecule	CD28	1.67	0.00	2523801	940	2
Granzyme K (granzyme 3)	GZMK	1.67	0.00	2809793	3003	5
NEL-like 2	NELL2	1.66	2.52	3451814	4753	12
CD163 molecule	CD163	1.65	0.00	3442706	9332	12
B-cell scaffold protein with ankyrin repeats 1	BANK1	1.64	4.55	2737596	55024	4
Neuro-oncological ventral antigen 1	NOVA1	1.64	4.55	3558745	4857	14

Table-6.2: Top 20 down-regulated genes after bevacizumab among patients classified as responders based on 30% reduction in median K^{trans} criteria.

Gene Name	Gene Symbol	Fold Change	Q value	Transcript Cluster ID	Entrez Gene ID	Chr
Endothelial cell-specific molecule 1	ESM1	0.27	0.00	2856995	11082	5
Neuromedin U	NMU	0.53	4.55	2770039	10874	4
Aldo-keto reductase family 7, member A3 (aflatoxin aldehyde reductase)	AKR7A3	0.64	0.00	2399687	22977	1
Sprouty homolog 4 (Drosophila)	SPRY4	0.65	0.00	2879105	81848	5
ATP-binding cassette, sub-family C (CFTR/MRP)	ABCC11	0.65	1.96	3690470	85320	16
Sulfatase 1	SULF1	0.66	2.52	3102372	23213	8
Ectodermal-neural cortex 1 (with BTB-like domain)	ENC1	0.68	2.52	2862696	8507	5
Exonuclease 1	EXO1	0.68	3.57	2388219	9156	1
Origin recognition complex, subunit 1	ORC1	0.69	1.96	2412799	4998	1
Guanylate cyclase 1, soluble, alpha 3	GUCY1A3	0.69	2.52	2748830	2982	4
Fms-related tyrosine kinase 1	FLT1	0.69	0.00	3507282	2321	13
Cyclin E1	CCNE1	0.70	2.52	3828112	898	19
S100 calcium binding protein A14	S100A14	0.71	2.52	4045665	57402	1
Inhibin, beta A	INHBA	0.71	4.55	3047581	3624	7
Glycerol kinase 2	GK2	0.72	0.00	2774938	2712	4
Podocalyxin-like	PODXL	0.73	4.55	3073013	5420	7
Nucleolar protein 4	NOL4	0.74	3.57	3803628	8715	18
Selenoprotein W, 1	SEPW1	0.75	2.52	3837504	6415	19
Hydrolethalus syndrome 1	HYLS1	0.76	4.55	3354879	219844	11
Solute carrier family 25 (mitochondrial carrier; adenine nucleotide translocator), member 31	SLC25A31	0.78	2.52	2742919	83447	4

But, 89/91 genes were common between genes up-regulated by bevacizumab considering the whole patient population (n=36) and genes up-regulated in responders (n=27). Similarly, 14/33 genes were common between the genes down-regulated after bevacizumab in the whole patient population (n=36) and genes down-regulated in responders (n=27) (Figure- 6.3).

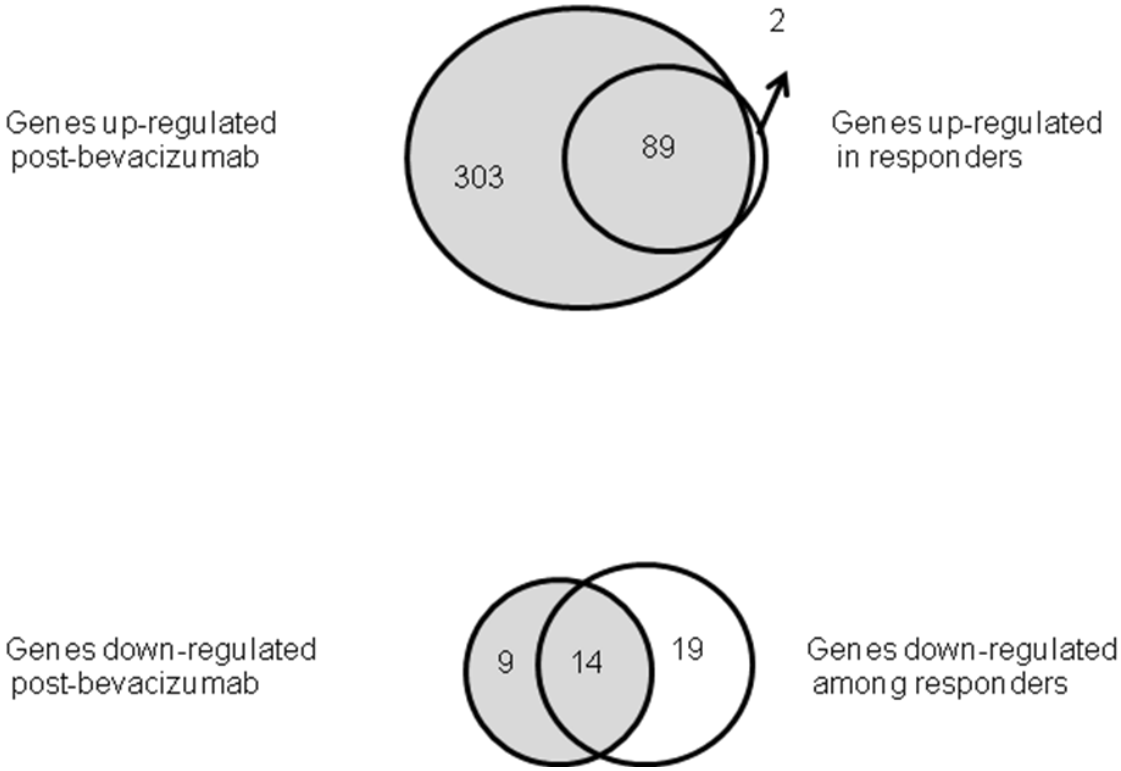

Figure-6.3: Venn- diagram showing number of genes up-regulated or down-regulated after bevacizumab. In study patient population (n=36) versus in patients classified as responders based on 30% reduction median K^{trans} (n=27).

Furthermore, these genes were tested by conducting an interaction analysis (i.e. the analysis of difference in fold change) between responders and non-responders but there was nothing significant when a multiple test correction was done, indicating either these groups were no different or we did not have enough power to distinguish them.

Difference in gene signature fold changes after bevacizumab in responders vs. non-responders (based on 30 % reduction in median K^{trans})

Further analysis was done to see whether there were any differences in fold change of gene signatures amongst responder (n=27) and non-responder groups of patients (n= 8) based on 30% reduction in median K^{trans} two weeks after a single cycle of bevacizumab. The fold change in metagenes for hypoxia, proliferation, angiogenesis and anti-VEGF signatures were considered for this analysis.

There was no significant difference observed between responders and non-responders in terms of fold change in metagenes for hypoxia, proliferation, angiogenesis and anti-VEGF (Table- 6.3)

Table-6.3: Difference between the fold changes in gene-signatures in responders versus non-responders

Gene Signatures (Fold-change)	**Responders (N=27) vs. Non-responders (N=8)** (P-value, Mann-Whitney test)
Hypoxia	0.89
Proliferation	0.53
Angiogenesis	0.20
Anti-VEGF	0.28

b) Exon array analysis compared to percentage or absolute change in median K^{trans} as a continuous variable

As shown in Figures 6.1 and 6.2, there was a continuum of response observed rather than two well defined categories, both in percentage change as well as absolute change of median K^{trans}. Further analysis was conducted considering both of these parameters as continuous variables to see if there was any association of fold change in the global expression of genes at single gene level and metagene level with the absolute/percentage change in median K^{trans}. Furthermore, gene set analyses was done to see pathways/ signatures whose changes after bevacizumab were significantly positively correlated with absolute change in median $K^{trans.}$ Gene sets considered were BioCarta pathway (http://www.biocarta.com/genes/index.asp) and relevant breast cancer related signatures such as proliferation (Desmedt, Haibe-Kains et al. 2008), hypoxia (Buffa, Harris et al. 2010), angiogenesis (Masiero, Simoes et al. 2013), anti-VEGF (Bais, Singh et al. 2011). For these analyses 1000 permutations were considered.

Correlation analysis of differential gene expression with percentage change or absolute change in median K^{trans}

To understand if there was any association of increase or decrease in expression of a particular gene with the absolute or percentage change in median K^{trans}, a correlation analysis was done using a parametric approach.

After multiple test correction (FDR<0.05), there were only two genes, whose fold changes were negatively correlated with percentage change in median K^{trans} i.e. increase in expression of these genes was observed in patients having maximum percentage reduction in median K^{trans} (Table 6.4). However, no gene was positively correlated with percentage change in median K^{trans}.

Table-6.4: Association of post- bevacizumab fold changes in gene expression with percentage change in median K^{trans}

Gene Symbol	Gene Name	Correlation Coefficient	Q value	Transcript Cluster ID	Entrez Gene ID	Chromosome
VANGL1	Vang-like 1 (van gogh, Drosophila)	-0.72	0	2353283	81839	1
TDRD5	Tudor domain containing 5	-0.65	0	2369680	163589	1

Considering the association of absolute change in median K^{trans} with the fold changes in genes, there was only one gene whose fold change showed a positive association with median K^{trans} absolute change (i.e. maximum reduction in gene expression of T-cell leukaemia homeobox 3 (TLX3) was noted in patients having maximum reduction in absolute value of median K^{trans}) (Table-6.5). There was no gene whose fold change in expression showed a negative association with absolute change in median K^{trans} after bevacizumab.

Table-6.5: Association of post- bevacizumab fold changes in gene expression with percentage change in median K^{trans}

Gene Symbol	Gene Name	Correlation coefficient	Q value	Transcript Cluster ID	Entrez Gene ID	Chromosome
TLX3	T-cell leukaemia homeobox 3	0.74	0	2840574	30012	5

Correlation of percentage or absolute change in median K^{trans} with fold changes in gene signatures after bevacizumab.

There was no significant association noted between percentage changes or absolute changes in median K^{trans} with fold changes in hypoxia signatures, proliferation signature and anti-VEGF gene signature (Table 6.6). However, the fold change in angiogenesis signature was weakly positively correlated with absolute change in median K^{trans} (Spearman r= 0.35, P= 0.04) i.e. maximum reduction in angiogenesis related genes was seen in patients showing higher reduction in median K^{trans} values (Figure- 6.4), this relationship does not exist when analysing percentage change in median K^{trans} versus fold change in angiogenesis signature.

Table-6.6: Association of post-bevacizumab fold changes in gene signatures with percentage or absolute change in median K^{trans}.
Columns showing spearman coefficient r (P-value).

Gene Signatures (Fold Change)	Percentage change in median K^{trans}	Absolute change in median K^{trans}
Hypoxia	-0.10 (0.55)	-0.19 (0.27)
Proliferation	-0.04 (0.80)	-0.14 (0.43)
Angiogenesis	0.01 (0.54)	**0.35 (0.04)**
Anti-VEGF	0.12 (0.49)	0.30 (0.08)

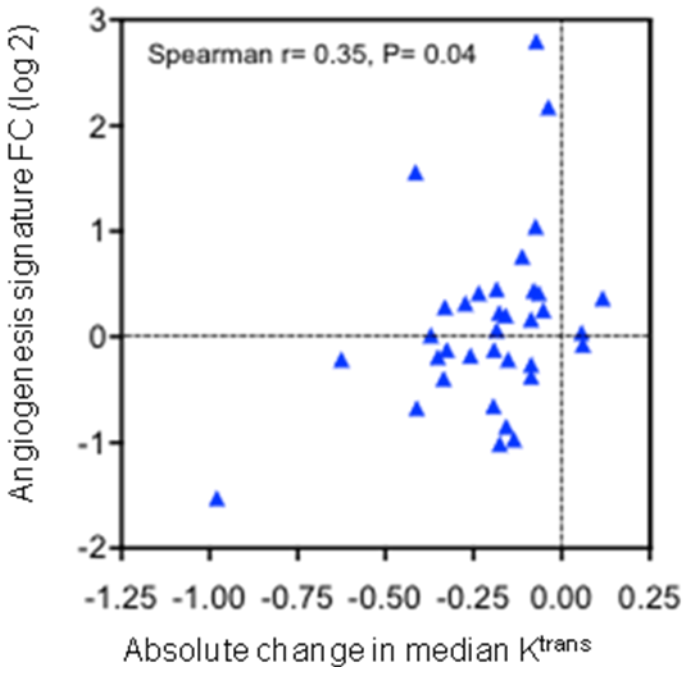

Figure-6.4: Association of absolute change in median K^{trans} with the fold change in angiogenesis signature.

Furthermore, by using gene set enrichment analysis, there were 20 gene sets observed whose global expression changes after bevacizumab were significantly positively correlated with percentage change in median K^{trans} i.e. there was maximum reduction observed in expression of genes related to

these gene sets in patients having maximum percentage reduction in median K^{trans} (Table- 6.7).

Table-6.7: Gene-sets whose post-bevacizumab expression changes showing positive correlation with percentage change in median K^{trans}.

Gene set Name (Biocarta Pathway)	Biocarta Pathway Description	Score	FDR
TOB1	Role of Tob in T-cell activation	5.01	0.01
COMP	Complement Pathway	4.45	0.04
CSK	Activation of Csk by cAMP-dependent Protein Kinase Inhibits Signalling through the T Cell Receptor	4.11	0.04
TCR	T Cell Receptor Signalling Pathway	4.08	0.00
VIP	Neuropeptides Vasoactive intestinal peptide (VIP) and PACAP inhibit the apoptosis of activated T cells	3.91	0.00
FCER1	Fc Epsilon Receptor I Signalling in Mast Cells	3.52	0.01
PPARA	Mechanism of Gene Regulation by Peroxisome Proliferators via peroxisome proliferator-activated receptor alpha(PPARa)	3.42	0.00
GPCR	Signalling Pathway from G-Protein Families	3.40	0.00
HDAC	Control of skeletal myogenesis by Histone deacetylases (HDAC) & calcium/calmodulin-dependent kinase (CaMK)	2.99	0.00
CALCINEURIN	Effects of calcineurin in Keratinocyte Differentiation	2.96	0.00
CCR5	C-C chemokine receptor type 5 (CCR5) Signalling in Macrophage	2.77	0.00
EIF4	Regulation of eukaryotic translation initiation factor 4 (eIF4e) and p70 S6 Kinase	2.72	0.00
SPRY	Sprouty regulation of tyrosine kinase signals	2.51	0.02
NFAT	NFAT and Hypertrophy of the heart	2.39	0.00
ECM	Erk and PI-3 Kinase Are Necessary for Collagen Binding	2.28	0.00
CXCR4	C-X-C chemokine receptor type 4 (CXCR4) signalling pathways	2.20	0.01
MET	Signalling of Hepatocyte Growth Factor Receptor	2.20	0.03
GH	Growth Hormone Signalling Pathway	1.96	0.03
CREB	Transcription factor CREB (cAMP response element-binding protein) and its extracellular signals	1.79	0.04

Score represents enrichment score of gene set on GSEA.

However, only 3 gene sets were positively correlated to absolute change in median K^{trans} (Table-6.8). There was no gene sets observed that showed negative association with absolute or percentage change in median K^{trans}.

Table-6.8: Gene-sets whose post-bevacizumab expression changes showing positive correlation with absolute change in median K^{trans}.

Gene set name	Pathway Description	Score	FDR
Anti VEGF	Anti VEGF response (Genentech)	15.03	0
PAR1	Thrombin signalling and protease-activated receptors	3.39	0
NFAT	Nuclear factor of activated T-cells (NFAT) and Hypertrophy of the heart	2.10	0

I. Is total K^{trans} a better parameter to analyse response than median K^{trans}?

As shown by Figures 4.9-4.13, (Chapter 4) there was a high variability noted in voxel by voxel basis in K^{trans}. By analysing median, the effect of heterogeneity seen might get masked as two tumours having very different K^{trans} distribution might have the same median K^{trans} .

To address this issue we analysed total K^{trans}, which is the summation of K^{trans} of all the voxels of tumour as assessed by DCE-MRI. This gives an estimate of the total target presented for modification by bevacizumab, is likely to be more variable and more likely to show heterogeneity of response. It is a major variable ignored in most data sets and papers.

As mentioned before (Chapter 4) a significant reduction in total K^{trans} was observed globally considering the whole population of 35 patients. Similar to median K^{trans} there was a wide variation observed in absolute change of total K^{trans} after bevacizumab therapy (Figure-6.5).

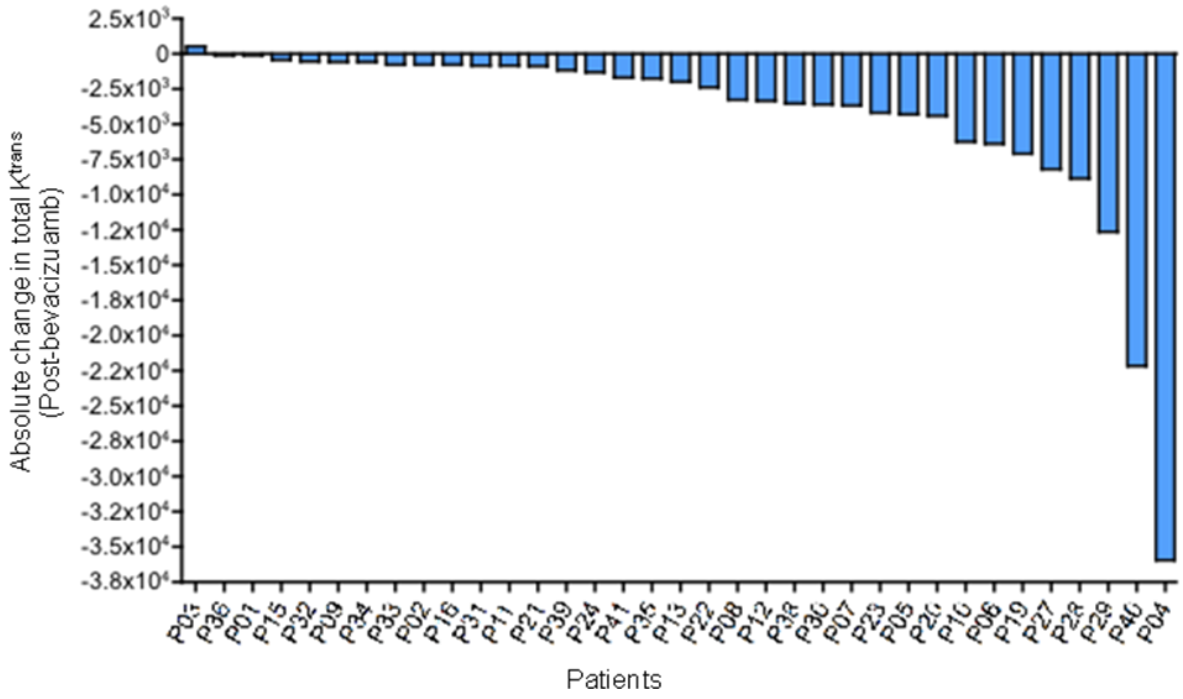

Figure-6.5: Waterfall plot showing post-bevacizumab absolute change in total K^{trans} among patients.

a) Exon array analysis considering absolute change in total K^{trans} as continuous variable.

Similar to analysis using absolute change in median K^{trans} as continuous variable (mentioned above) this analysis was done to see if there was any association of fold changes in the global expression of genes at single gene level or at metagene level, with the absolute change in total K^{trans} considering it as a continuous variable.

Correlation analysis of post-bevacizumab differential gene expression versus absolute change in total K^{trans}

Global gene expression analysis was performed to see the genes whose fold change was correlated with the absolute change in total $K^{trans.}$ There were 471 genes (Table-6.9) that were positively correlated with absolute change in total K^{trans} i.e. maximum reduction in gene expression of these genes in patients showing maximum reduction in total K^{trans}. On the other hand, there was no significant gene that was negatively correlated.

Table-6.9: Top 20 genes whose fold change after bevacizumab was positively correlated with absolute change in total K^{trans}

Gene Symbol	Gene Name	Correlation	Q value	Transcript Cluster ID	Entrez Gene ID	Chr
PARM1	Prostate androgen-regulated mucin-like protein 1	0.66	1.40	2731636	25849	4
ADAM7	ADAM metallopeptidase domain 7	0.65	1.40	3090326	8756	8
STARD13	StAR-related lipid transfer (START) domain containing 13	0.63	1.40	3508898	90627	13
EYS	Eyes shut homolog (Drosophila)	0.62	1.40	2959596	346007	6
CMTM7	CKLF-like MARVEL transmembrane domain containing 7	0.62	1.40	2615938	112616	3
PTGS2	Prostaglandin-endoperoxide synthase 2	0.61	1.40	2448382	5743	1
ATP10D	ATPase, class V, type 10D	0.60	1.40	2726072	57205	4
PRKCA	Protein kinase C, alpha	0.60	1.40	3731826	5578	17
SOSTDC1	Sclerostin domain containing 1	0.60	1.40	3039671	25928	7
HIST1H2AG	Histone cluster 1, H2ag	0.60	1.40	2899756	8969	6
RCAN2	Regulator of calcineurin 2	0.59	1.40	2955691	10231	6
MYLK	Myosin light chain kinase	0.59	1.40	2692447	4638	3
CPXM1	Carboxypeptidase X (M14 family) member1	0.58	1.40	3895118	56265	20
GCNT2	Glucosaminyl (N-acetyl) transferase 2	0.58	1.40	2894573	2651	6
RELN	Reelin	0.58	1.40	3065740	5649	7
NPR1	Natriuretic peptide receptor A	0.58	1.40	2359780	4881	1
PAGE1	P antigen family, member 1 (prostate associated)	0.58	1.40	4008078	8712	X
TRPC1	Transient receptor potential cation channel, subfamily C, member 1	0.58	1.40	2645951	7220	3
MAGEB18	Melanoma antigen family B, 18	0.58	1.40	3972339	286514	X
CASQ2	Calsequestrin 2 (cardiac muscle)	0.58	1.40	2429556	845	1

Association of absolute change in total K^{trans} with fold change in gene signature

There was no significant association noted between absolute changes in total K^{trans} with fold changes in hypoxia or proliferation genes signatures but absolute change in total K^{trans} was significantly positively correlated with fold changes in angiogenesis and anti-VEGF signatures (Table- 6.10, Figure- 6.6). This signifies that two weeks after bevacizumab, maximum reduction in angiogenesis (as depicted by fold change in angiogenesis/ anti-VEGF signatures) was noted in patients who had maximum reduction total K^{trans}.

Table-6.10: Association of absolute change in total K^{trans} with fold changes in gene signatures. Column showing Spearman r (P-value).

Gene signatures (Fold change)	**Absolute change in total K^{trans}**
Hypoxia	0.007 (0.97)
Proliferation	0.006 (0.97)
Angiogenesis	**0.40 (0.02)**
Anti-VEGF	**0.39 (0.02)**

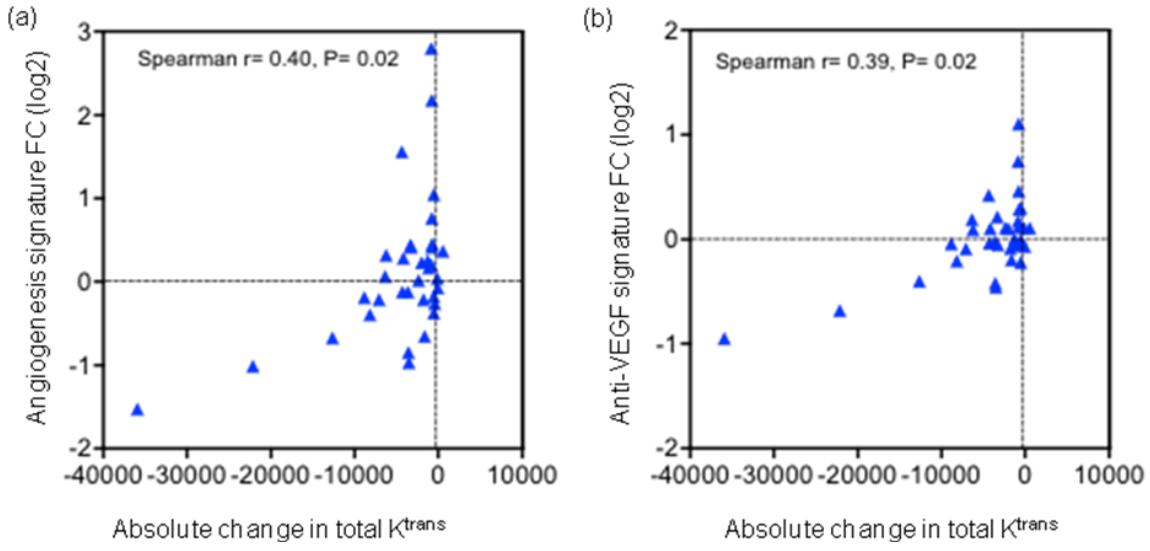

Figure-6.6: Association of absolute change in total K^{trans} with fold change in angiogenesis and anti-VEGF signature.

By using gene set enrichment analysis, there were 39 gene sets observed whose global expression changes after bevacizumab were significantly positively correlated with absolute change in total K^{trans} i.e. there was maximum reduction observed in expression of genes related to these gene sets in patients having maximum absolute reduction in total K^{trans} (Figure- 6.7, Table-6.11).

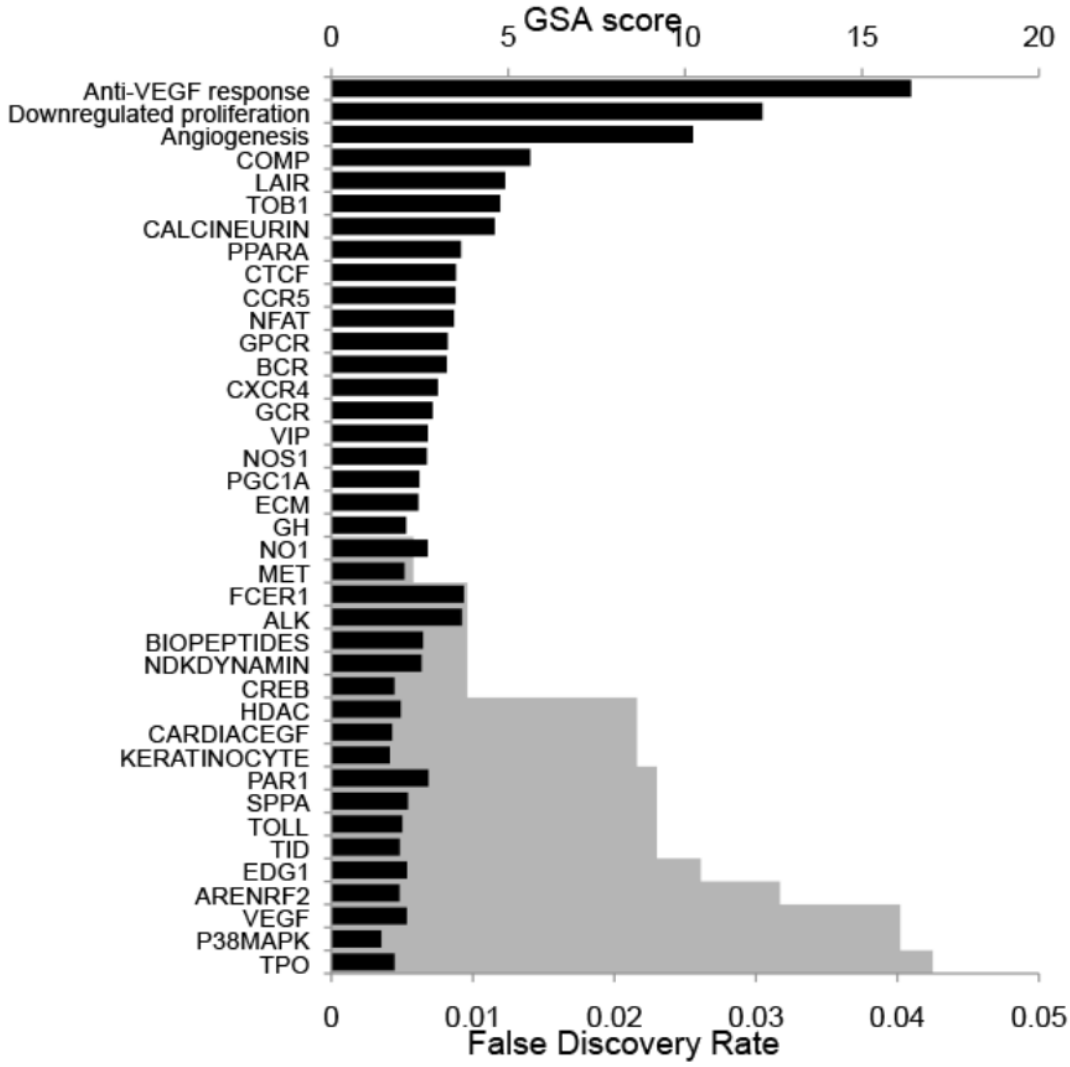

Figure-6.7: Gene sets whose expression changes after bevacizumab is significantly positively correlated with absolute change in total K^{trans}.

Table-6.11: Pathways/signatures whose expression changes after bevacizumab are significantly positively correlated with absolute change in total K^{trans}.

Gene set name	Pathway/ Signature Description	Score	FDR
Anti-VEGF response	Anti-VEGF (Genentech)	16.39	0.00
Down-regulated proliferation	Proliferation signature	12.19	0.00
Angiogenesis	Angiogenesis signature	10.23	0.00
COMP	Complement pathway	5.62	0.00
LAIR	Cells and molecules involved in local acute inflammatory response	4.91	0.00
TOB1	Role of Tob in T-cell activation	4.78	0.00
CALCINEURIN	Effects of calcineurin in keratinocyte Differentiation	4.62	0.00
PPARA	Mechanism of gene regulation by peroxisome proliferators via peroxisome proliferator-activated receptor alpha (PPARα)	3.67	0.00
CTCF	CCCTC-binding factor (CTCF): First multivalent nuclear factor	3.52	0.00
CCR5	C-C chemokine receptor type 5 (CCR5) signalling in macrophage	3.51	0.00
TCR	T cell receptor signalling pathway	3.47	0.00
NFAT	Nuclear factor of activated T-cells (NFAT) and hypertrophy of the heart	3.47	0.00
GPCR	Signalling pathway from G-protein families	3.29	0.00
BCR	B cell antigen receptor (BCR) signalling pathway	3.27	0.00
CXCR4	C-X-C chemokine receptor type 4 (CXCR4) signalling pathways	3.01	0.00
GCR	Corticosteroids and cardioprotection	2.86	0.00
VIP	Neuropeptides vasoactive intestinal peptide (VIP) and PACAP inhibit the apoptosis of activated T cells	2.73	0.00
NOS1	Nitric oxide signalling pathway	2.70	0.00
PGC1A	Regulation of peroxisome proliferator-activated receptor gamma coactivator-1 alpha	2.49	0.00
ECM	Erk and PI-3 kinase are necessary for collagen binding in corneal epithelia	2.46	0.00
GH	Growth hormone signalling pathway	2.11	0.00
NO1	Actions of nitric oxide in the heart	2.72	0.01
MET	Signalling of hepatocyte growth factor receptor	2.07	0.01
FCER1	Fc epsilon receptor I signalling in mast cells	3.75	0.01
ALK	Activin receptor-like kinase (ALK) in cardiac myocytes	3.69	0.01
BIOPEPTIDES	Bioactive peptide induced signalling pathway	2.59	0.01

NDKDYNAMIN	Endocytotic role of nucleoside diphosphate kinase (NDK), phosphins and dynamin	2.55	0.01
CREB	Transcription factor CREB (cAMP response element-binding protein) and its extracellular signals	1.78	0.01
HDAC	Control of skeletal myogenesis by histone deacetylase (HDAC) & calcium/calmodulin-dependent kinase (CaMK)	1.96	0.02
CARDIACEGF	Role of EGF receptor transactivation by G-protein coupled receptor (GPCRs) in cardiac hypertrophy	1.72	0.02
KERATINOCYTE	Keratinocyte differentiation	1.66	0.02
PAR1	Thrombin signalling and protease-activated receptor	2.75	0.02
SPPA	Aspirin blocks signalling pathway involved in platelet activation	2.17	0.02
TOLL	Toll-like receptor pathway	2.01	0.02
TID	Chaperones modulate interferon signalling pathway	1.93	0.02
EDG1	Phospholipids as signalling intermediaries	2.14	0.03
ARENRF2	Oxidative stress induced gene expression via Nrf2 (Nuclear factor erythroid 2-related factor 2)	1.93	0.03
ERK5	Extracellular signal-regulated protein kinase 5 (*ERK5*)	1.48	0.03
VEGF	VEGF, hypoxia, angiogenesis pathway	2.14	0.04
P38MAPK	p38 MAPK signalling pathway	1.42	0.04
TPO	Thrombopoietin signalling pathway	1.79	0.04

6.3 Association of baseline DCE-MRI parameters with baseline gene expression

Exon array analysis was done to find out the genes, or gene-sets whose pre-bevacizumab expression was correlated to baseline values of DCE-MRI parameters. Median K^{trans} and total K^{trans} were considered for these analyses.

6.3.1 Baseline single gene expression vs. baseline median K^{trans}

There were 262 genes, which were positively correlated to median K^{trans} i.e. higher gene expression in patients with higher median K^{trans} (Table- 6.12). On the other hand, 191 genes were negatively correlated to median K^{trans} i.e. higher the expression of these genes lower is the value of median K^{trans} at baseline (Table-6.13)

Table-6.12: Top 20 genes whose baseline expression was positively correlated to baseline median K^{trans}

Gene Symbol	Gene Name	Corr	Q value	Transcript Cluster ID	Entrez Gene ID	Chr
TMEM67	Transmembrane protein 67	0.69	1.10	3107242	91147	8
LOC81691	Exonuclease NEF-sp	0.67	1.10	3651509	81691	16
PRLR	Prolactin receptor	0.67	1.10	2853102	5618	5
CREB3L4	cAMP responsive element binding protein 3-like 4	0.66	1.10	2359993	148327	1
FAM84B	Family with sequence similarity 84, member B	0.65	1.10	3152558	157638	8
NPNT	Nephronectin	0.65	1.10	2738378	255743	4
ATAT1	Alpha tubulin acetyltransferase 1	0.64	1.10	2901841	79969	6
PKIB	Protein kinase (cAMP-dependent, catalytic) inhibitor beta	0.63	1.10	2923868	5570	6
PSMG2	Proteasome assembly chaperone 2	0.63	1.10	3799542	56984	18
BUB3	Budding uninhibited by benzimidazoles 3 homolog (yeast)	0.62	1.10	3268669	9184	10
TRIM45	Tripartite motif-containing 45	0.62	1.10	2430126	80263	1
INTS8	Integrator complex subunit 8	0.62	1.10	3107661	55656	8
POMT2	Protein-O-mannosyltransferase 2	0.62	1.10	3572982	29954	14
UBR7	Ubiquitin protein ligase E3 component n-recognin 7	0.62	1.10	3549220	55148	14
TRMT12	tRNA methyltransferase 12 homolog	0.62	1.10	3114600	55039	8
XPNPEP3	X-prolyl aminopeptidase 3,	0.62	1.10	3946510	63929	22
ARFIP2	ADP-ribosylation factor interacting protein 2	0.62	1.10	3360941	23647	11
KIAA1598	KIAA1598	0.61	1.10	3308489	57698	10
PHF20L1	PHD finger protein 20-like 1	0.61	1.10	3116535	51105	8
NEK5	NIMA (never in mitosis gene a)-related kinase 5	0.61	1.10	3514804	341676	13

Table-6.13: Top 20 genes whose baseline expression was negatively correlated to baseline median K^{trans}

Gene Symbol	Gene Name	Corr	Q value	Transcript Cluster ID	Entrez Gene ID	Chr
MRAS	Muscle RAS oncogene homolog	-0.75	0.00	2644565	22808	3
CLEC3B	C-type lectin domain family 3, member B	-0.73	0.00	2620448	7123	3
SLCO3A1	Solute carrier organic anion transporter family, member 3A1	-0.66	1.10	3608787	28232	15
HLA-E	Major histocompatibility complex, class I, E	-0.64	1.10	2901620	3133	6
DNASE1L3	Deoxyribonuclease I-like 3	-0.64	1.10	2678298	1776	3
GIMAP8	GTPase, IMAP family member 8	-0.63	1.10	3031466	155038	7
S100B	S100 calcium binding protein B	-0.63	1.10	3935486	6285	21
FREM1	FRAS1 related extracellular matrix 1	-0.63	1.10	3199511	158326	9
CD209	CD209 molecule	-0.63	1.10	3848540	30835	19
EFEMP1	EGF-containing fibulin-like extracellular matrix protein 1	-0.63	1.10	2554018	2202	2
TSHZ2	Teashirt zinc finger homeobox 2	-0.63	1.10	3889419	128553	20
CARD6	Caspase recruitment domain family, member 6	-0.63	1.10	2807686	84674	5
XCR1	Chemokine (C motif) receptor 1	-0.62	1.10	2672075	2829	3
TRIM22	Tripartite motif-containing 22	-0.62	1.10	3318443	10346	11
ENPP2	Ectonucleotide pyrophosphatase/phospho diesterase 2	-0.62	1.10	3150579	5168	8
SERPING1	Serpin peptidase inhibitor, clade G (C1 inhibitor), member 1	-0.62	1.10	3331355	710	11
HOXA4	Homeobox A4	-0.62	1.10	3042816	3201	7
CD34	CD34 molecule	-0.61	1.10	2453307	947	1
APLNR	Apelin receptor	-0.61	1.10	3373630	187	11
INPP1	Inositol polyphosphate-1-phosphatase	-0.61	1.10	2520113	3628	2

6.3.2 Baseline single gene expression vs. baseline total K^{trans}

By considering FDR of 0.05 there was no significantly positively correlated gene to total K^{trans} and only one gene that was negatively correlated with total K^{trans} at baseline (Table- 6.14) i.e. the lower the expression of ras homolog family member A (RHOA) the higher is the value of total K^{trans}.

Table-6.14: Association of baseline gene expression with baseline total K^{trans}

Gene Symbol	Gene Name	Correlation coefficient	Q value	Transcript Cluster ID	Entrez Gene ID	Chromo some
RHOA	Ras homolog family member A	-0.71	0	2674242 (2674397)	387	3

6.3.3 Baseline gene set enrichment analysis versus baseline DCE-MRI parameters

Surprisingly, there were no gene-sets whose expression at baseline was significantly positively or negatively correlated to baseline median K^{trans}, but there were two gene sets which were negatively correlated and one positively correlated to the baseline total K^{trans} (Table- 6.15)

Table-6.15: Association of baseline expression of gene-sets with baseline total K^{trans}

Gene-set Name	Pathway Description	Score	FDR
IL2	Interleukin-2 (IL-2) signalling pathway	-2.83	0.07
IL2RB	IL-2 Receptor beta chain in T cell activation pathway	-2.18	0.07
PPARA	Mechanism of gene regulation by peroxisome proliferators via peroxisome proliferator-activated receptor alpha (PPARα)	2.82	0

In other words, for patients with lower total K^{trans} at baseline the expression of genes related to interleukin-2 (IL-2) signalling pathway (http://www.biocarta com/pathfiles/h_il2Pathway.asp) and IL-2 receptor beta chain in T-cell activation pathway (http://www.biocarta.com/pathfiles/h_il2rbPathway.asp) was higher and the expression of genes related to peroxisome proliferator-activated receptor alpha (PPARα) pathway (http://www.biocarta.com/pathfiles/ h_pparaPathway.asp) was lower.

6.4 Association of baseline gene expression with change in DCE-MRI parameters after bevacizumab

The analyses were done to investigate an association of expression of genes/ gene sets at baseline with the changes in DCE-MRI PK parameters (absolute change in median K^{trans} and total K^{trans}) after bevacizumab treatment.

6.4.1 Single gene analysis versus absolute change in median K^{trans}

There was only one gene whose baseline expression had shown significant negative correlation to absolute change in median K^{trans}. In other words higher the baseline expression of paraneoplastic antigen like 5 (PNMA5) greater would be the absolute reduction in median K^{trans}. On the other hand, there were two genes whose baseline expression was positively correlated with absolute change in median K^{trans} after bevacizumab (Table- 6.16) i.e. higher the baseline expression of T-cell leukaemia homeobox3 (TLX3) and melanoma antigen family B, 18 (MAGEB18) smaller would be the absolute reduction in median K^{trans} after bevacizumab.

Table-6.16: Association of baseline gene expression with absolute change in median K^{trans}

Gene Symbol	Gene Name	Correlation	Q value	Transcript Cluster ID	Entrez Gene ID	Chromosome
PNMA5	Paraneoplastic antigen like 5	-0.71	0	4026346	114824	X
TLX3	T-cell leukaemia homeobox3	0.74	0	2840574	30012	5
MAGEB18	Melanoma antigen family B, 18	0.63	0	3972339	286514	X

6.4.2 Single gene analysis versus absolute change in total K^{trans}

After the multiple test corrections (FDR <0.05), the baseline expression of only one gene had shown positive correlation with absolute change in total K^{trans}. In other words, the lower the baseline expression of RHOA, the greater was the reduction in total K^{trans} (Table-6.17). Furthermore, no gene at baseline had shown a negative association with absolute change in total K^{trans}.

Table-6.17: Association of baseline gene expression with absolute change in total K^{trans}

Gene Symbol	Gene Name	Correlation	Q value	Transcript Cluster ID	Entrez Gene ID	Chromosome
RHOA	Ras homolog family member A	0.71	0	2674242 (2674397)	387	3

6.4.3 Association of gene sets at baseline with changes in DCE-MRI PK parameters

By doing gene set enrichment analysis, none of the gene sets at baseline were negatively correlated to absolute change in median K^{trans} but interestingly, there were four gene sets/ pathways whose expression at baseline shows positive correlation with absolute change in median K^{trans} i.e. the lower the gene expression, the greater was the absolute reduction in median K^{trans} noted two weeks after bevacizumab treatment (Table-6.18).

Table-6.18: Association of gene sets at baseline to absolute change in median K^{trans}

Gene-set Name	Pathways description	Score	FDR
CSK	Activation of csk by cAMP-dependent protein kinase inhibits signaling through the T cell receptor	4.95	0.03
TCR	T cell receptor signaling pathway	3.68	0
IL2	Interleukin 2 (IL2) signalling pathway	2.79	0.03
IL2RB	IL-2 receptor beta chain in T cell activation pathway	2.48	0

Similarly, there were no gene sets whose expression at baseline had negative correlation with absolute change in total K^{trans} but there was only one gene set at baseline that had positive correlation with the absolute change in total K^{trans} i.e. the lower the gene expression of the genes involved in interleukin-2 signalling pathway at baseline, the greater was the reduction in total K^{trans}, two weeks after bevacizumab treatment (Table-6.19).

Table-6.19: Association of gene sets at baseline with absolute change in Total K^{trans}

Gene-set Name	Pathways description	Score	FDR
IL2	Interleukin 2 (IL2) signalling pathway	2.921	0

6.5 Association of baseline DCE-MRI parameters with change in gene expression after bevacizumab

The analyses were done to assess any association of changes in expression of genes/ gene sets after bevacizumab with the baseline DCE-MRI PK parameters (median K^{trans} and total K^{trans}) to detect the predictive value (if any) of the baseline DCE-MRI parameters.

6.5.1 Association of baseline DCE-MRI parameters with changes in gene expression after bevacizumab (single genes)

By using a FDR of < 0.05, there were 6 genes for which fold change in expression after bevacizumab was significantly positively correlated with baseline median K^{trans} (Table -6.20). In other words, there was up-regulation of these genes in patients having higher value of median K^{trans} at baseline.

Table-6.20: Genes showing positive correlation between baseline median K^{trans} and fold change in their expression after bevacizumab

Gene symbol	Gene name	Correlation	Q value	Transcript cluster ID	Entrez gene ID	Chr
PNMA5	Paraneoplastic Ma antigen family member 5	0.72	0	4026346	114824	X
BCAS1	Breast carcinoma amplified sequence 1	0.67	0	3910360	8537	20
TMED3	Transmembrane emp24 protein transport domain containing 3	0.66	0	3603687	23423	15
MORC2	MORC family CW-type zinc finger 2	0.66	0	3957589	22880	22
SYT4	Synaptotagmin IV	0.65	0	3805614	6860	18
OR10G9	Olfactory receptor, family 10, subfamily G, member9	0.64	0	3353876	219870	11

On the other hand, there were 110 genes whose fold change in expression after bevacizumab was significantly negatively correlated with baseline median K^{trans} (Table-6.21). In other words, there was up-regulation of these genes in patients having lower value of median K^{trans} at baseline.

Table-6.21: Top 10 genes whose fold change in expression after bevacizumab is negatively correlated with baseline median K^{trans}

Gene symbol	Gene name	Correlation	Q value	Transcript cluster ID retrieved	Entrez gene ID	Chr
EYS	Eyes shut homolog (Drosophila)	-0.71	0.00	2959596	346007	6
TLX3	T-cell leukaemia homeobox 3	-0.64	4.25	2840574	30012	5
MAGEB18	Melanoma antigen family B, 18	-0.63	4.25	3972339	286514	X
GUCY1B3	Guanylate cyclase 1, soluble, beta 3	-0.63	4.25	2748923	2983	4
HENMT1	HEN1 methyltransferase homolog 1 (Arabidopsis)	-0.62	4.25	2426676	113802	1
DCBLD2	discoidin, CUB and LCCL domain containing 2	-0.62	4.25	2686023	131566	3
OR5P3	Olfactory receptor, family 5, subfamily P, member 3	-0.61	4.25	3361504	120066	11
NES	Nestin	-0.61	4.25	2438411	10763	1
CASQ2	Calsequestrin 2 (cardiac muscle)	-0.61	4.25	2429556	845	1
PTPLA	Protein tyrosine phosphatase-like (proline instead of catalytic arginine), member A	-0.61	4.25	3279982	9200	10

By analysing the relationship of fold change in gene expression with total K^{trans} at baseline, there were 1081 genes whose fold change in expression after bevacizumab was significantly negatively correlated to baseline total K^{trans} (Table-6.22). In other words, there was up-regulation of these genes after bevacizumab in patients having lower value of total K^{trans} at baseline.

Table-6.22: Top 20 genes whose fold change in expression after bevacizumab is negatively correlated with baseline total K^{trans}

Gene symbol	Gene name	Corr	Q value	Transcript cluster ID	Entrez gene ID	Chr
TK2	Thymidine kinase 2, mitochondrial	-0.80	0.00	3695107	7084	16
EMR2	Egf-like module containing, mucin-like, hormone receptor-like 2	-0.78	0.00	3822657	30817	19
TPM2	Tropomyosin 2 (beta)	-0.76	0.00	3204721	7169	9
DLC1	Deleted in liver cancer 1	-0.73	0.00	3125116	10395	8
JAM3	Junctional adhesion molecule 3	-0.72	0.00	3357237	83700	11
LDHB	Lactate dehydrogenase B	-0.71	0.00	3446868	3945	12
ADD3	Adducin 3 (gamma)	-0.71	0.00	3263555	120	10
ZNF462	Zinc finger protein 462	-0.71	0.00	3183604	58499	9
NNMT	Nicotinamide N-methyltransferase	-0.70	0.00	3349858	4837	11
DCBLD2	Discoidin, CUB and LCCL domain containing 2	-0.70	0.00	2686023	131566	3
HENMT1	HEN1 methyltransferase homolog 1 (Arabidopsis)	-0.69	0.00	2426676	113802	1
SEMA6D	Sema domain, transmembrane domain (TM), and cytoplasmic domain, (semaphorin) 6D	-0.69	0.00	3592755	80031	15
TBC1D4	TBC1 domain family, member 4	-0.69	0.00	3518086	9882	13
ADAMTS18	ADAM metallopeptidase with thrombospondin type 1 motif, 18	-0.69	0.00	3700158	170692	16
ANXA2	Annexin A2	-0.69	0.00	3627248	302	15
HIF1A	Hypoxia inducible factor 1, alpha subunit	-0.69	0.00	3539070	30917	14
SGPP1	Sphingosine-1-phosphate phosphatase 1	-0.69	0.00	3568108	81537	14
PRNP	Prion protein	-0.68	0.00	3874751	5621	20
LNX1	Ligand of numb-protein X 1, E3 ubiquitin protein ligase	-0.68	0.00	2727226	84708	4
MBNL2	Muscleblind-like splicing regulator 2	-0.68	0.00	3497586	10150	13

6.5.2 Association of baseline MRI parameters with fold changes in gene signature

This analysis was done to see if there was any association of baseline median K^{trans} or total K^{trans} with the fold changes in four gene signatures only considered for this research work. There was no association observed with hypoxia or proliferation signatures but significant negative association was noted between baseline median as well as total K^{trans} to fold changes in angiogenesis and anti-VEGF signatures (Table- 6.23). This signifies that the higher the value of median K^{trans} or total K^{trans} the more would be the reduction in angiogenesis as observed by down regulation of angiogenesis and anti-VEGF signatures (Figure- 6.8).

Table-6.23: Association of baseline MRI parameters with fold changes in gene signature. Column showing Spearman r (P-value)

Gene signatures (Fold changes)	Baseline median K^{trans}	Baseline total K^{trans}
Hypoxia	0.09 (0.60)	-0.05 (0.76)
Proliferation	0.07 (0.67)	-0.01 (0.95)
Angiogenesis	**-0.53 (0.001)**	**-0.40 (0.02)**
Anti-VEGF	**-0.42 (0.01)**	**-0.42 (0.01)**

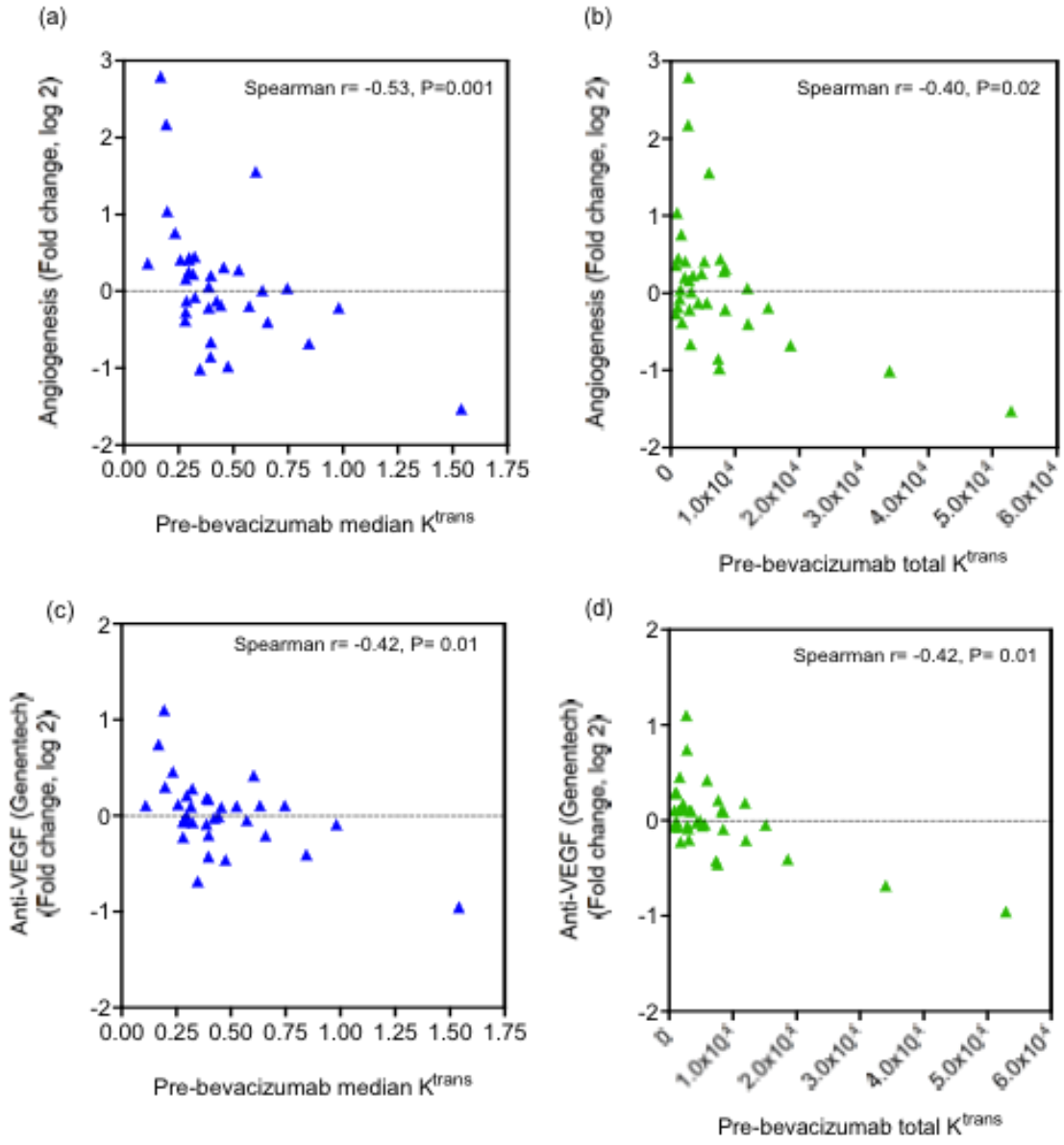

Figure-6.8: Association of baseline median/ total K^{trans} with fold changes in angiogenesis and anti-VEGF signature

6.5.3 Association of baseline median/ total K^{trans} with fold changes in gene sets after bevacizumab.

Furthermore, on gene set enrichment analysis, by considering FDR≤0.01, there were 11 pathways/ signatures whose fold change after bevacizumab were negatively correlated with the baseline median K^{trans} i.e. patients with higher median K^{trans} at baseline showed maximum reduction in expression (or down-regulation) of genes related to these pathways/ signatures after a single cycle of bevacizumab. (Table- 6.24)

Table-6.24: Pathways/ Signatures whose expression changes after bevacizumab are significantly negatively correlated with baseline median K^{trans}

Gene set name	Pathway/ Signature description	Score	FDR
Anti-VEGF response	Anti-VEGF response (Genentech)	-15.71	0.00
Proliferation BC down-regulation	Proliferation breast cancer	-10.92	0.00
Angiogenesis	Angiogenesis	-10.87	0.00
COMP	Complement Pathway	-5.01	0.00
PAR1	Thrombin signalling and protease-activated receptors	-3.67	0.00
PPARA	Mechanism of gene regulation by peroxisome proliferators via peroxisome proliferator-activated receptor alpha (PPARα)	-2.82	0.01
NO1	Actions of nitric oxide in the heart	-2.77	0.01
GPCR	Signalling pathway from G-protein families	-2.41	0.01
EDG1	Phospholipids as signalling intermediaries	-2.40	0.01
NFAT	Nuclear factor of activated T-cells (NFAT) and hypertrophy of the heart	-2.25	0.01
ECM	Erk and PI-3 kinase are necessary for collagen binding in corneal epithelia	-1.80	0.01

On the other hand, there were 29 gene sets whose global expression change after bevacizumab was significantly negatively correlated with baseline total K^{trans} i.e. patients with higher total K^{trans} at baseline showed maximum reduction in expression (or down-regulation) of genes related to these pathways/ signatures after single cycle of bevacizumab (Figure- 6.9, Table- 6.25).

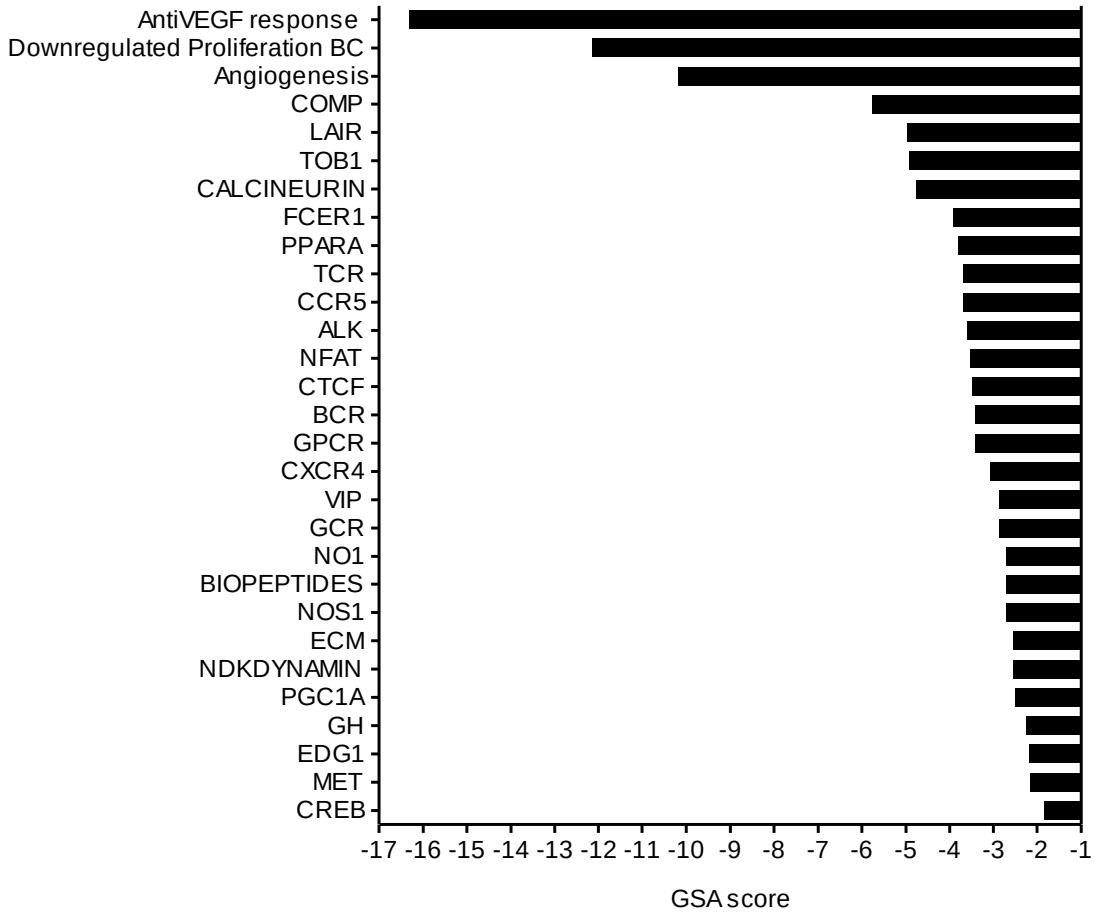

Fig-6.9: Gene sets whose fold change after bevacizumab were negatively correlated to baseline total K^{trans}.

Table-6.25: Pathways/ signatures whose expression changes after bevacizumab were significantly negatively correlated with baseline total K^{trans}

Gene set name	Pathway/ signature description	Score	FDR
AntiVEGF response	Anti-VEGF (Genentech)	-16.31	0.00
Down-regulated Proliferation BC	Proliferation signature breast cancer	-12.14	0.00
Angiogenesis	Angiogenesis signature	-10.18	0.00
COMP	Complement pathway	-5.76	0.00
LAIR	Cells and molecules involved in local acute inflammatory response	-4.97	0.00
TOB1	Role of Tob in T-cell activation	-4.93	0.00
CALCINEURIN	Effects of calcineurin in keratinocyte differentiation	-4.77	0.00
FCER1	Fc epsilon receptor I signalling in mast cells	-3.92	0.00
PPARA	Mechanism of gene regulation by peroxisome proliferators via peroxisome proliferator-activated receptor (PPARa(alpha)	-3.81	0.00
TCR	T cell receptor signalling pathway	-3.70	0.00
CCR5	C-C chemokine receptor type 5 (CCR5) signalling in macrophage	-3.69	0.00
ALK	Activin receptor-like kinase (ALK) in cardiac myocytes	-3.61	0.01
NFAT	Nuclear factor of activated T-cells (NFAT) and hypertrophy of the heart	-3.54	0.00
CTCF	CCCTC-binding factor (CTCF): first multivalent nuclear factor	-3.49	0.00
BCR	B cell antigen receptor (BCR) signalling pathway	-3.43	0.00
GPCR	Signalling pathway from G-protein families	-3.42	0.00
CXCR4	C-X-C chemokine receptor type 4 (CXCR4) signalling pathways	-3.08	0.00
VIP	Neuropeptides vasoactive intestinal peptide (VIP) and PACAP inhibit the apoptosis of activated T cells	-2.88	0.00
GCR	Corticosteroids and cardioprotection	-2.87	0.01
NO1	Actions of nitric oxide in the heart	-2.72	0.00
BIOPEPTIDES	Bioactive peptide induced signalling pathway	-2.70	0.01
NOS1	Nitric oxide signalling pathway	-2.69	0.01
ECM	Erk and PI-3 kinase are necessary for collagen binding in corneal epithelia	-2.54	0.00
NDKDYNAMIN	Endocytotic role of nucleoside diphosphate kinase (NDK), phosphins and dynamin	-2.53	0.01
PGC1A	Regulation of peroxisome proliferator-activated receptor gamma coactivator-1 alpha	-2.49	0.01
GH	Growth hormone signalling pathway	-2.24	0.01
EDG1	Phospholipids as signalling intermediaries	-2.18	0.01
MET	Signalling of hepatocyte growth factor receptor	-2.16	0.00
CREB	Transcription factor CREB (cAMP response element-binding protein) and its extracellular signals	-1.84	0.00

6.6 Association of genes validated by qRT-PCR with DCE-MRI parameters

As mentioned previously (Chapter 2 and Chapter 6), there were 15 genes that were validated by qRT-PCR from the global expression analysis of genes significantly changing after bevacizumab. We were interested to find out if there was any association of these genes with DCE-MRI parameters, either at baseline or after bevacizumab. DCE-MRI pharmacokinetic parameters, median K^{trans} and total K^{trans} were considered for these analyses. As total K^{trans} is dependent on tumour volume, association of genes with tumour volume as assessed by MRI was also considered.

6.6.1 Baseline gene expression of genes of interest versus baseline DCE-MRI parameters

There was no association observed between baseline expression of most of these genes with any of the MRI parameters analysed (Table-6.26). However, interestingly, there was significant negative correlation of angiopoietin-related protein 4 (ANGPTL4) with baseline median K^{trans} i.e. the higher the value of median K^{trans}, the lower the expression of ANGPTL4 (Figure-6.10a). Also, there was a significant but weak negative correlation of phosphoinositide-3-kinase interacting protein 1 (PIK3IP1) with total K^{trans}. Similarly there was a weakly significant negative correlation observed between phosphatidylinositol-4,5-bisphosphate 3-kinase catalytic subunit gamma (PIK3CG) and baseline total K^{trans} i.e. the higher the value of total K^{trans} at baseline, the lower is the expression of PIK3IP1 (Figure- 6.10b) and PIK3CG. Along with these, there was significant negative correlation observed between baseline expression of

cytotoxic T-Lymphocyte Antigen 4 (CTLA4) and baseline tumour volume as well as baseline total K^{trans} (Figure- 6.10 c, d).

Table-6.26: Association of baseline expression of Genes with baseline MRI parameters. Columns show spearman r (P-value). Genes arranged by ascending order of fold changes as observed by qRT-PCR analysis.

Genes*	Median K^{trans}	Total K^{trans}	Tumour volume
ESM1	-0.13 (0.47)	0.17 (0.33)	0.28 (0.11)
CCNE1	-0.03 (0.85)	0.14 (0.44)	0.13 (0.44)
FLT1	-0.10 (0.59)	0.10 (0.56)	0.15 (0.40)
SPRY4	-0.28 (0.11)	-0.17 (0.33)	-0.11 (0.54)
DLL4	-0.18 (0.32)	-0.18 (0.30)	-0.07 (0.68)
SULF1	0.08 (0.64)	-0.05 (0.76)	-0.21 (0.24)
PIK3CG	-0.25 (0.15)	-0.35 (0.05)	-0.33 (0.06)
CA-9	-0.18 (0.31)	-0.07 (0.68)	-0.03 (0.88)
VEGFA	-0.13 (0.44)	0.07 (0.70)	0.12 (0.49)
CTLA4	-0.17 (0.35)	**-0.46 (0.006)**	**-0.45 (0.007)**
PIK3IP1	-0.17 (0.33)	**-0.39 (0.02)**	-0.31 (0.07)
PDK1	-0.29 (0.09)	-0.16 (0.36)	-0.06 (0.75)
PDE3B	-0.22 (0.21)	-0.23 (0.18)	-0.16 (0.36)
ANGPTL4	**-0.46 (0.005)**	-0.05 (0.77)	0.16 (0.37)
PPARG	-0.02 (0.90)	-0.05 (0.80)	0.04 (0.81)

*Genes in green= down-regulated; Genes in red= up-regulated after bevacizumab as assessed by qRT-PCR

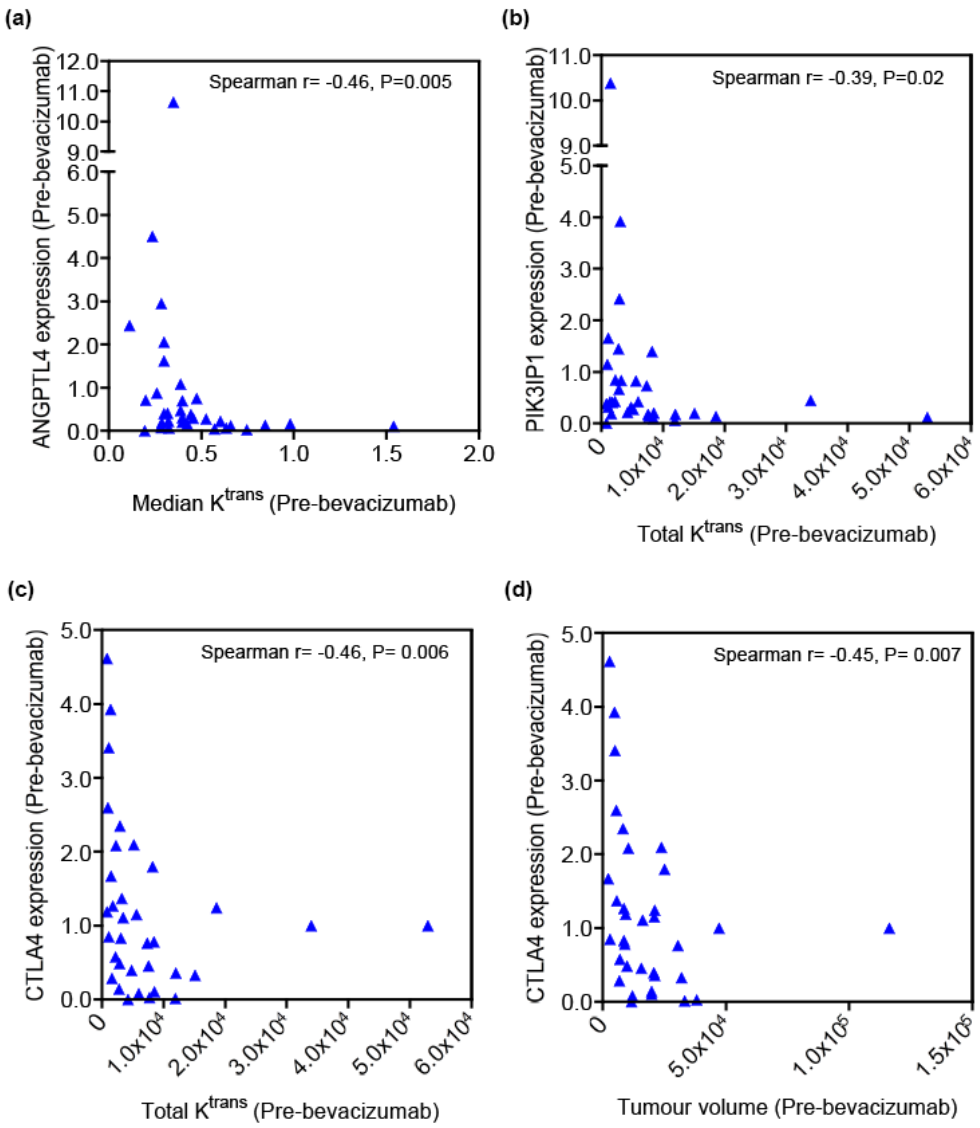

Figure-6.10: Association of baseline gene expression with baseline MRI parameters. (a) Significant negative correlation of baseline Angiopoietin-related protein 4 (ANGPTL4) with baseline median K^{trans}. (b) Weakly significant negative correlation of baseline phosphoinositide-3-kinase interacting protein 1 (PIK3IP1) with baseline total K^{trans}. (c) Significant negative correlation of baseline expression of cytotoxic T-Lymphocyte antigen 4 (CTLA4) with baseline total K^{trans} (d) Significant negative correlation of baseline expression of cytotoxic T-Lymphocyte antigen 4 (CTLA4) with baseline tumour volume.

6.6.2 Baseline gene expression of genes of interest versus changes in MRI parameters

This analysis was done to see if there was any association of baseline expression of these genes with changes in MRI parameters after bevacizumab. In other words, we were interested to see if any of these genes at baseline had any predictive value of MRI responses as assessed by absolute changes in DCE-MRI parameters. There was no significant relationship observed between most of these genes at baseline and absolute changes in MRI parameters (Table- 6.27)

Table-6.27: Association of baseline expression of Genes with absolute changes in MRI parameters. Column showing spearman r (P-value). Genes arranged by ascending order of fold changes as observed by qRT-PCR analysis

Genes*	Absolute change in Median K^{trans}	Absolute change in Total K^{trans}	Absolute change in Tumour volume
ESM1	0.03 (0.86)	-0.19 (0.28)	-0.12 (0.50)
CCNE1	-0.04 (0.84)	-0.15 (0.39)	0.07 (0.68)
FLT1	-0.15 (0.38)	-0.15 (0.39)	-0.07 (0.67)
SPRY4	0.20 (0.24)	0.14 (0.42)	-0.16 (0.35)
DLL4	0.14 (0.43)	0.12 (0.49)	0.06 (0.72)
SULF1	-0.11 (0.53)	0.00 (0.10)	-0.05 (0.78)
PIK3CG	0.13 (0.48)	0.30 (0.08)	0.32 (0.07)
CA-9	0.01 (0.94)	0.04 (0.83)	0.14 (0.42)
VEGFA	0.00 (0.98)	-0.10 (0.55)	0.02 (0.91)
CTLA4	0.22 (0.20)	**0.46 (0.006)**	**0.38 (0.03)**
PIK3IP1	0.26 (0.14)	**0.39 (0.02)**	**0.44 (0.01)**
PDK1	0.08 (0.64)	0.11 (0.53)	**0.37 (0.03)**
PDE3B	0.25 (0.14)	0.26 (0.13)	0.22 (0.21)
ANGPTL4	0.26 (0.13)	0.05 (0.76)	-0.04 (0.82)
PPARG	0.10 (0.56)	0.07 (0.68)	-0.17 (0.34)

*Genes in green= down-regulated; Genes in red= up-regulated after bevacizumab as assessed by qRT-PCR

There was significant positive correlation observed between baseline CTLA4 and PIK3IP1 expression with absolute change in tumour volume as well as absolute change in total K^{trans}. That signifies that higher is the expression of CTLA4 and PIK3IP1 lesser is the reduction in tumour volume and total K^{trans} after bevacizumab (Figure- 6.11).

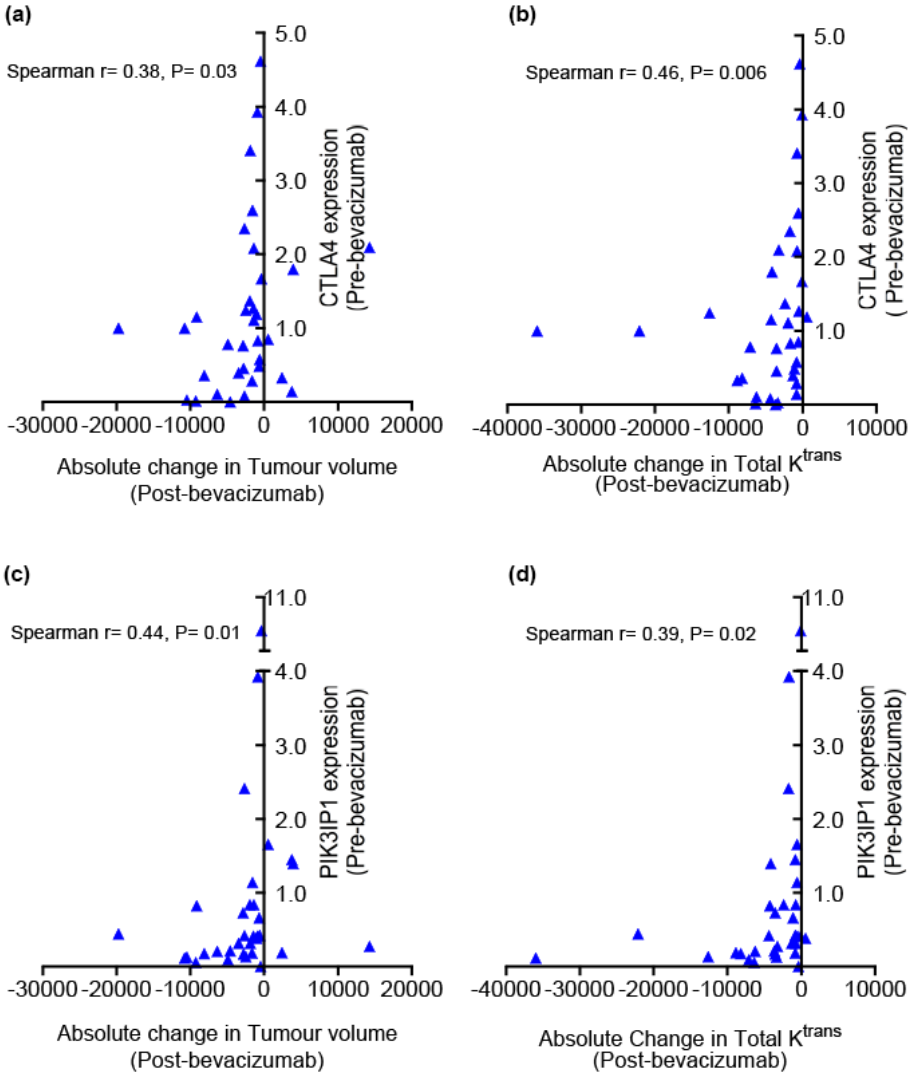

Figure-6.11: Association of baseline CTLA4 and PIK3IP1 with absolute change in tumour volume and total K^{trans} after bevacizumab. (a,b) Positive correlation of baseline cytotoxic T-Lymphocyte Antigen 4 (CTLA4) expression to absolute change in tumour volume and total K^{trans}; (c,d) Positive correlation of baseline phosphoinositide-3-kinase interacting protein 1 (PIK3IP1) expression to absolute change in tumour volume and total K^{trans}.

There was significant positive correlation observed between the baseline PDK1 versus absolute change in tumour volume as measured by MRI two weeks after bevacizumab i.e. the higher the baseline expression of PDK1, the lower was the reduction in tumour volume as assessed by MRI (Figure- 6.12).

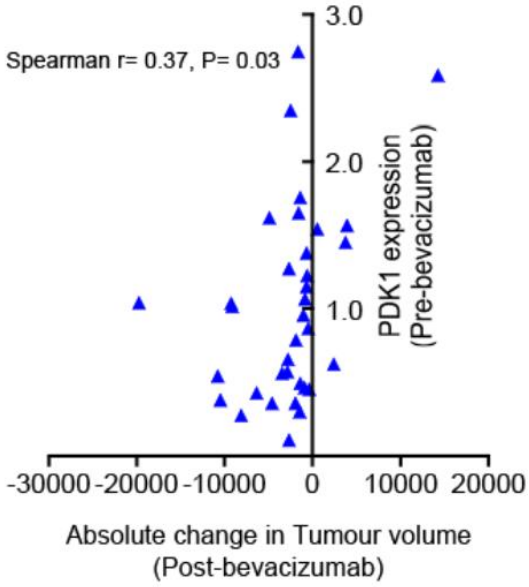

Figure-6.12: Baseline PDK1 versus absolute change in tumour volume after bevacizumab. Significant positive correlation observed between the baseline PDK1 versus absolute change in tumour volume after bevacizumab.

6.6.3 Correlation of fold change in the expression of genes of interest with changes in MRI parameters after bevacizumab

Next we were interested to see how the fold changes in these genes related to changes observed in DCE-MRI parameters (Table- 6.28).

There was a significant positive correlation observed between fold change in fms-related tyrosine kinase 1 (FLT1) and absolute change in total K^{trans} i.e. the higher the down-regulaton of FLT1, the higher was the absolute reduction in

total K^{trans} (Figure- 6.13a). On the other hand, there were negative correlations observed between fold changes in Delta like legend 4 (DLL4) and PIK3IP1 with absolute change in volume. This signified that the higher the down- regulation of DLL4, the lesser was the absolute reduction in tumour volume (Figure- 6.13b). There was a wide variation noted in the fold changes of PIK3IP1 expression after bevacizumab. The patients who had down-regulation of PIK3IP1 had lesser reduction in tumour volume. On the other hand, patients showing up-regulation of PIK3IP1 had higher reduction in tumour volume (Figure- 6.13c).

Table-6.28: Association of fold change in gene expression with changes in MRI Parameters after bevacizumab. Columns showing Spearman correlation coefficient r (P- value). Genes arranged by ascending order of fold changes as observed by qRT-PCR analysis

Gene expression (Fold change)	Absolute change in median K^{trans}	Absolute change in total K^{trans}	Absolute change in tumour vol.
ESM1	-0.13 (0.48)	-0.06 (0.76)	-0.25 (0.14)
CCNE1	-0.06 (0.73)	-0.13 (0.48)	0.05 (0.78)
FLT1	0.22 (0.20)	**0.38 (0.03)**	0.09 (0.62)
SPRY4	0.02 (0.92)	-0.03 (0.08)	0.13 (0.46)
DLL4	0.08 (0.67)	0.09 (0.60)	**-0.33 (0.05)**
SULF1	0.21 (0.22)	0.26 (0.12)	0.11 (0.53)
PIK3CG	-0.14 (0.45)	-0.16 (0.37)	-0.15 (0.42)
CA-9	-0.27 (0.13)	-0.32 (0.06)	-0.24 (0.17)
VEGFA	-0.19 (0.29)	-0.31 (0.07)	-0.26 (0.14)
CTLA4	-0.18 (0.32)	-0.07 (0.71)	0.10 (0.59)
PIK3IP1	-0.27 (0.12)	-0.32 (0.06)	**-0.41 (0.02)**
PDK1	-0.29 (0.09)	-0.12 (0.48)	-0.21 (0.24)
PDE3B	-0.04 (0.83)	0.11 (0.53)	0.04 (0.82)
ANGPTL4	0.08 (0.65)	0.10 (0.56)	0.13 (0.44)
PPARG	0.05 (0.77)	0.28 (0.11)	0.32 (0.07)

*Genes in green= down-regulated; Genes in red= up-regulated after bevacizumab as assessed by qRT-PCR

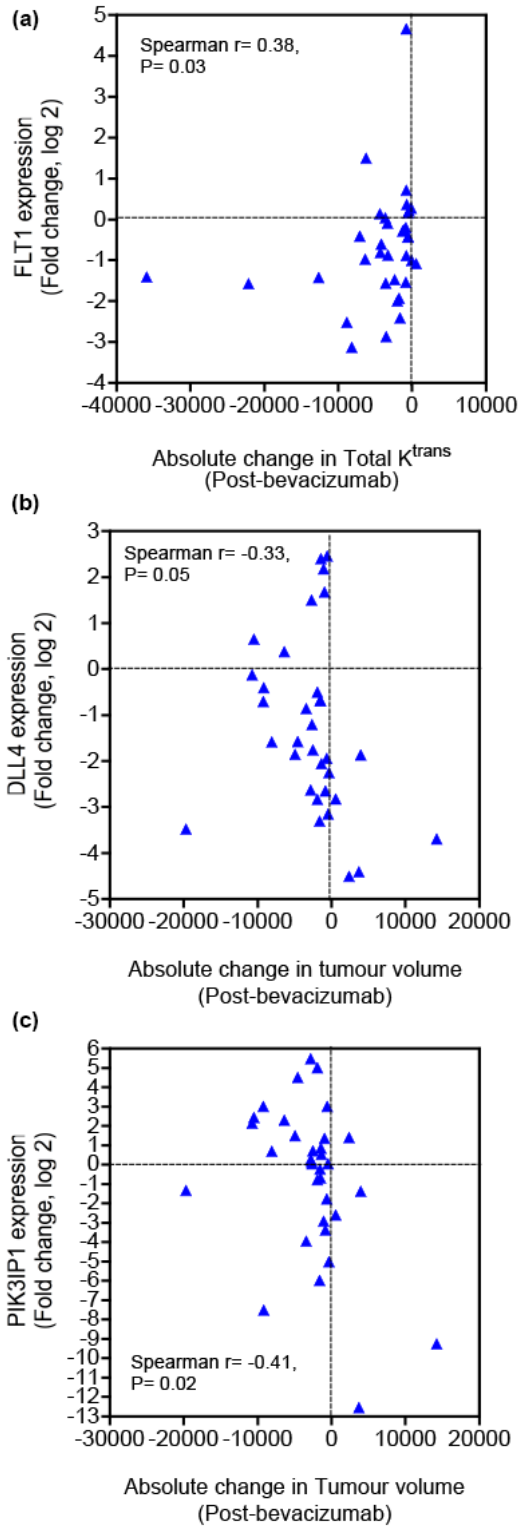

Figure-6.13: Association of fold changes in genes with absolute change in MRI parameters. (a) Significant positive correlation observed between fold change in fms-related tyrosine kinase 1 (FLT1) and absolute change in total K^{trans}, (b) negative correlation observed between fold changes in delta like legend 4 (DLL4) and absolute change in tumour volume; (c) negative correlation observed between fold changes in PIK3IP1 and absolute change in tumour volume.

6.6.4 Association of baseline MRI parameters with fold changes in genes of interest after bevacizumab

As mentioned above there were significant association observed between expression of certain genes and MRI parameters at baseline, this analysis was done to see if the baseline MRI parameters could predict fold changes in the genes significantly changed after bevacizumab.

As shown below in Table- 6.29, baseline median K^{trans}, total K^{trans} and tumour volume were significantly related to fold changes in some genes. Specifically, there was a significant negative association between baseline tumour volume and total K^{trans} with the fold change in FLT1 after bevacizumab i.e. the higher the tumour volume/ total K^{trans} at baseline, the more was the down regulation of FLT1 (Figure- 6.14a,b). There was a wide variation observed in carbonic anhydrase (CA-9) fold change after bevacizumab. As shown in Figure- 6.14c, there was a positive correlation between baseline total K^{trans} and CA-9 fold change after bevacizumab. This signifies that patients with higher total K^{trans} show up regulation of CA-9 after bevacizumab. Similarly, there was significant positive correlation between baseline total K^{trans} and fold change in VEGFA, indicating that the higher the value of total K^{trans}, the higher was the up regulation of VEGFA after bevacizumab (Figure- 6.14d).

As mentioned before, there was a wide variation observed in fold changes of PIK3IP1 after bevacizumab. Interestingly, there was a significant positive correlation between baseline median K^{trans} and fold change in PIK3IP1. This highlights that patients with higher baseline median K^{trans} had up regulation of PIK3IP1, patients with lower median K^{trans} at baseline had significant down

regulation of PIK3IP1 (Figure-6.14e). There was a weak but significant positive correlation observed between baseline median K^{trans} and fold change in PDK1 i.e. higher the baseline median K^{trans} more was the up-regulation of PDK1 after bevacizumab (Figure- 6.14f).

Table-6.29: Association of baseline MRI with fold changes in genes after bevacizumab. Columns showing spearman correlation coefficient r (P- value). Genes arranged by ascending order of fold changes as observed by qRT-PCR analysis

Gene expression* (Fold change)	Baseline median K^{trans}	Baseline total K^{trans}	Baseline tumour volume
ESM1	0.20 (0.25)	0.06 (0.73)	-0.09 (0.60)
CCNE1	0.21 (0.23)	0.18 (0.31)	0.05 (0.76)
FLT1	-0.25 (0.15)	**-0.40 (0.02)**	**-0.36 (0.03)**
SPRY4	0.17 (0.34)	0.13 (0.45)	0.14 (0.43)
DLL4	-0.006 (0.97)	-0.09 (0.62)	-0.10 (0.55)
SULF1	0.10 (0.58)	-0.24 (0.16)	-0.26 (0.13)
PIK3CG	0.25 (0.16)	0.10 (0.57)	-0.03 (0.88)
CA-9	0.28 (0.11)	**0.34 (0.05)**	0.19 (0.29)
VEGFA	0.25 (0.15)	**0.35 (0.04)**	0.18 (0.30)
CTLA4	0.05 (0.76)	-0.02 (0.91)	-0.09 (0.62)
PIK3IP1	**0.39 (0.02)**	0.31 (0.07)	0.14 (0.44)
PDK1	**0.36 (0.03)**	0.06 (0.73)	-0.23 (0.17)
PDE3B	-0.01 (0.94)	-0.18 (0.30)	-0.22 (0.20)
ANGPTL4	0.11 (0.53)	-0.09 (0.61)	-0.22 (0.21)
PPARG	-0.20 (0.26)	-0.32 (0.07)	-0.26 (0.13)

*Genes in green= down-regulated; Genes in red= up-regulated after bevacizumab as assessed by qRT-PCR

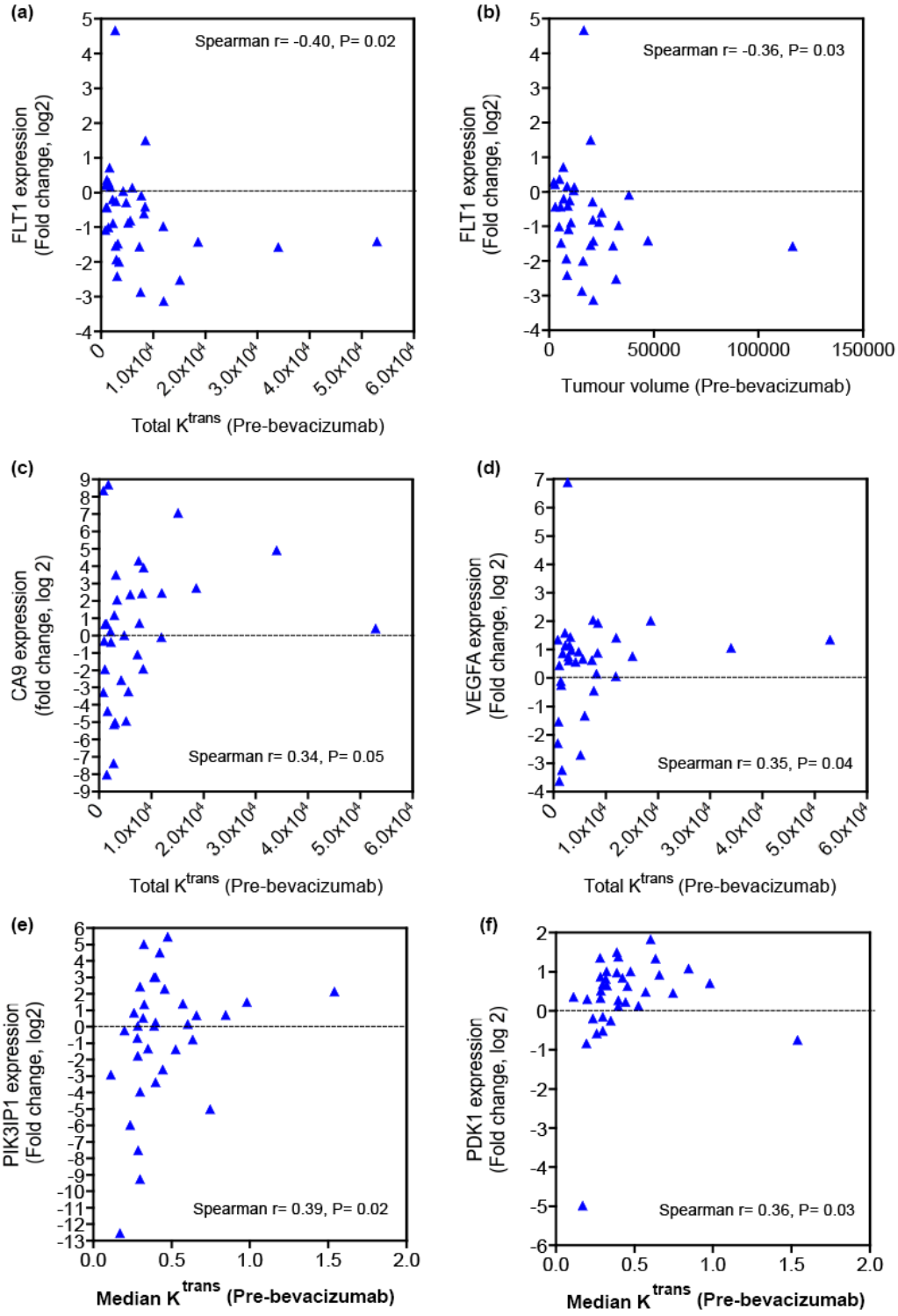

Figure-6.14: Association of baseline MRI parameters with fold changes in genes after bevacizumab. (a,b) Significant negative correlation between baseline total K^{trans} and tumour volume with the fold change in FLT1 after bevacizumab; (c) Significant positive correlation between baseline total K^{trans} and CA-9 fold change after bevacizumab; (d) significant positive correlation between baseline total K^{trans} and fold change in VEGFA after bevacizumab; (e) significant positive correlation between baseline median K^{trans} and fold change in PIK3IP1; (f) Significant positive correlation observed between baseline median K^{trans} and fold change in PDK1.

Interestingly, on further analysis there was a very significant positive relationship observed between fold changes in CA-9 versus fold changes in VEGFA (spearman r=0.51, P= 0.002). As expected, this relationship existed even after taking out the extreme outliers (n=3) of CA-9 fold change (Spearman r=0.50, P= 0.004) indicating that breast tumours with higher values of baseline total K^{trans} when treated with bevacizumab, had hypoxia driven up-regulation of VEGFA gene (Figure- 6.15).

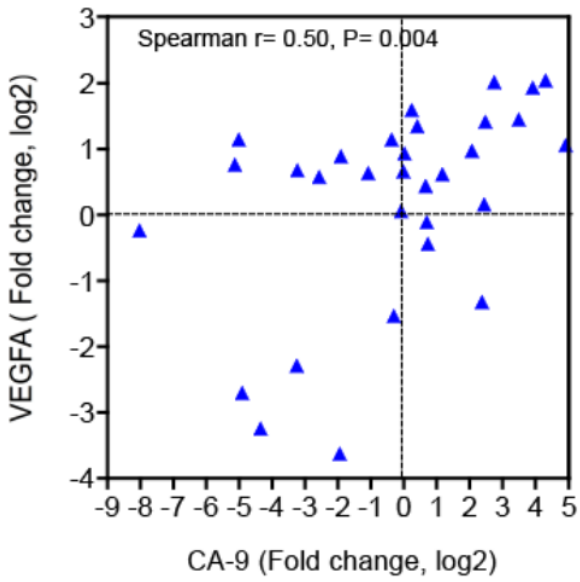

Figure-6.15: Significant positive correlation between CA-9 fold change with VEGFA fold change after bevacizumab.

6.7 Association of IHC markers with DCE- MRI parameters

As mentioned in chapter 5, on immunohistochemistry analysis considering all patients there was a significant down-regulation of proliferation and angiogenesis along with significant up-regulation of hypoxia. But there were no changes in VEGFA, VEGFC and VEGFR2 (KDR) tumour (see Chapter 5 for details). Further on, we were interested to see how the IHC parameters were related to DCE-MRI both at baseline as well changes after bevacizumab.

There was no significant relationship observed between baseline expression of HIF1a, proliferation marker (Ki67), angiogenesis (PLVAP, VEGFA, VEGFC, KDR tumour) markers with MRI parameters both at baseline as well as changes in MRI parameters after bevacizumab treatment except there was significant positive correlation observed between CA-9 and total K^{trans} at baseline (Table- 6.30, 6.31).

Table-6.30: Association of baseline expression (IHC) versus baseline MRI parameters.
Columns show Spearman correlation coefficient r (P- value).

Baseline Expression (IHC)	Baseline Median K^{trans}	Baseline Total K^{trans}	Baseline Tumour volume
CA-9	0.39 (0.18)	**0.62 (0.02)**	0.37 (0.22)
HIF 1a	0.08 (0.76)	0.36 (0.17)	0.37 (0.15)
Ki67	-0.27 (0.14)	-0.15 (0.44)	-0.04 (0.82)
PLVAP	0.04 (0.84)	-0.17 (0.34)	-0.27 (0.12)
VEGFA	0.25 (0.21)	0.12 (0.53)	-0.01 (0.96)
VEGFC	0.22 (0.40)	0.26 (0.32)	0.25 (0.33)
KDR tumour	0.29 (0.19)	0.25 (0.27)	0.15 (0.52)

Table- 6.31: Association of baseline expression (IHC) versus changes in MRI parameters.
Columns show Spearman correlation coefficient r (P- value).

Baseline Expression (IHC)	Absolute change in Median K^{trans}	Absolute change in Total K^{trans}	Absolute change in Tumour Volume
CA-9	-0.31 (0.30)	-0.50 (0.08)	-0.13 (0.67)
HIF 1a	-0.04 (0.90)	-0.30 (0.27)	0.11 (0.67)
Ki67	0.30 (0.11)	0.16 (0.40)	0.26 (0.17)
PLVAP	0.04 (0.83)	0.15 (0.40)	-0.08 (0.65)
VEGFA	-0.12 (0.53)	-0.08 (0.67)	-0.13 (0.50)
VEGFC	-0.23 (0.38)	-0.19 (0.47)	0.20 (0.44)
KDR tumour	-0.18 (0.41)	-0.20 (0.38)	-0.22 (0.33)

6.8 Discussion

The search for reliable biomarkers of response to anti-VEGF therapy has been ongoing over the last decade without any success to date. Over 20,000 breast cancer patients have been randomized to receive bevacizumab in various clinical trials and there is a pressing need to find reliable biomarkers. As discussed in previous Chapters, this window of opportunity study has shown a high variability of response as assessed with either DCE-MRI or gene expression analysis. In this Chapter, several interesting correlations between the two techniques have been shown, that could be useful in understanding the molecular mechanisms governing response, which in turn could assist in the development of reliable biomarkers of anti-angiogenic therapy.

As there were many analyses performed with the exon array data, if the number of genes deemed significant, was too small at the single gene level it has not been discussed further, due to high statistical variability and the difficulty in making reliable inferences from such data. Instead, gene set enrichment analysis was considered in order to provide more statistical power to the analyses and to provide potentially clinically useful information. All the single genes analysed by qRT-PCR were considered for correlative analysis as they are known to be the part of important molecular pathways (as discussed in Chapter 5) known to play vital roles in angiogenesis.

There are no set criteria to define response by use of DCE-MRI techniques. Most studies have reported changes in DCE-MRI parameters such as median

K^{trans} or k_{ep} with use of bevacizumab but there were no cut off points defined for response classification of patients.

In this study the response based on the change in median K^{trans} (the most commonly used parameter) was defined in two different ways - as a categorical variable and as a continuous variable. Based on previously published reproducibility studies and more recent advances in DCE-MRI techniques (Galbraith, Lodge et al. 2002; Jackson, Jayson et al. 2003; O'Connor, Carano et al. 2009), a 30% reduction in median K^{trans} was agreed as the response threshold for the categorical analysis. By performing exon array analysis using 30% reduction in median K^{trans} after bevacizumab as the response criterion to stratify patients, there were no differences in gene expression changes between the responder vs. non-responder groups. This result highlighted the point made in Chapter 4 that there was a continuum of response rather than two well defined groups, or alternatively that a 30% reduction in median K^{trans} was not the right cut off to define responders/ non-responders to bevacizumab.

As discussed in Chapter 4, marked heterogeneity was observed in vascularity/perfusion of tumours as assessed by MRI parameters and there was a significant reduction in tumour volume in a subset of patients analysed. In view of these, a new measure termed total K^{trans} - the summation of K^{trans} values over all voxels in the tumour ROI - was analysed at baseline as well as two weeks after bevacizumab treatment. This gives an estimate of the total vascular target available for modification by bevacizumab, and is likely to be

more variable and more likely to show heterogeneity of response. It is a major variable ignored in most data sets and papers.

By performing gene expression analysis using the change in median K^{trans} as a continuous variable, several interesting gene sets were found to be positively correlated and that are known to be involved in important biological processes e.g. gene sets involved in *inflammatory pathways* such as role of Tob in T-cell activation (TOB1), T cell receptor signalling pathway (TCR); *cell surface receptor signalling* such as C-X-C chemokine receptor type 4 (CXCR4)(Yan, Jene et al. 2011); *metabolism* e.g. peroxisome proliferators via peroxisome proliferator-activated receptor alpha (PPARα)(Lamers, Schubert-Zsilavecz et al. 2012) and *angiogenesis* e.g. Sprouty regulation of tyrosine kinase signals (SPRY) as well as the angiogenesis gene signature (Masiero, Simoes et al. 2013).

On consideration of the absolute change in total K^{trans} as a continuous variable, the differential gene profile was much stronger at the single gene level. With this gene set enrichment analysis a similar profile was noted as observed with the change in median K^{trans} but with a higher number of gene sets, such as a positive correlation with angiogenesis and anti-VEGF signatures, immune related pathways, and cell signalling pathways. There was a positive correlation noted with the down-regulated proliferation signature (Desmedt, Haibe-Kains et al. 2008), i.e. those patients showing maximum reduction in total K^{trans} having maximum reduction over down-regulated proliferation signature. Although this sounds paradoxical, based on our results as

discussed in Chapter 5 (down-regulation of proliferation both by exon array as well as by immunohistochemistry), on further exploration, this signature consisted of genes related to the *wnt/ b-catenin pathway* e.g. secreted frizzled-related protein 4 (SFRP4), wingless-type MMTV integration site family, member 5A (WNT5A), frizzled-related protein (FRZB), FZD4); *transforming growth factor beta (TGFb) pathways* such as transforming growth factor, beta 3 (TGFBR3), FBJ murine osteosarcoma viral oncogene homolog (FOS), follistatin (FST) and *angiogenesis pathways* such as sprouty homolog 1 (SPRY1), sprouty homolog 2 (SPRY2), aquaporin 1 (AQP1). In other words, the maximum down-regulation of genes related to Wnt, TGFb and angiogenesis pathways was seen in patients having maximum reduction in total K^{trans}. These pathways are known to play an important role in angiogenesis (Blobe, Schiemann et al. 2000; Dufourcq, Leroux et al. 2008; Parmalee and Kitajewski 2008; Zerlin, Julius et al. 2008)

The analysis of baseline MRI using median K^{trans} vs. baseline gene expression revealed a high number of positively correlated genes. However, the clinical significance of most of these was not known and there were no gene sets that came as positive or negatively correlated to baseline median K^{trans}.

Similarly by considering total baseline K^{trans} only one gene i.e. Ras homolog family member A (RHOA) was significantly correlated at baseline, but with the gene set enrichment analysis, interleukin-2 (IL-2) signalling pathway and IL-2 receptor beta chain in T cell activation pathway (IL2RB) showed a negative correlation, although this did not reach the level of statistical significance. The

interleukins are known to play a key role the immune signalling pathway that is required for the activation, proliferation, and survival of T cells (Nelson 2004). Also there was a positive correlation of baseline total K^{trans} with PPAR-alpha, a transcription factor that is known as a major regulator of lipid metabolism in the liver. Activation of PPAR-alpha under stress promotes uptake, utilization, and catabolism of fatty acids by up-regulation of genes involved in fatty acid transport, fatty binding and activation, and peroxisomal and mitochondrial fatty acid β-oxidation (van Raalte, Li et al. 2004). PPARA has also been found in human breast cancer cell lines, where its activation has been associated with increased proliferation (Suchanek, May et al. 2002). The association of breast cancer and genetic variants of PPARA (PPARA polymorphism rs4253760) has been reported (Golembesky, Gammon et al. 2008)

On analysing the association of baseline gene expression with changes in DCE-MRI parameters, we observed that lower expression of genes involved in T cell receptor signalling and interleukin signalling pathways, the greater the absolute reduction in median K^{trans} after bevacizumab treatment. Similar results were found with change in total K^{trans}. The role of immune related pathways has been reported previously in regulating angiogenesis (Rofstad, Gaustad et al. 2010; Andre, Dieci et al. 2013) but the exact impact of these observations in the context of antiangiogenic therapy responses needs to be explored further.

To see whether baseline DCE-MRI parameters predict changes in gene sets after bevacizumab therapy, we noted that patients with high values of baseline DCE-MRI parameters (median K^{trans} and total K^{trans}) show greater down-

regulation of the angiogenesis related gene signature. However in patients with lower values at baseline, there was actually up-regulation of angiogenesis, which again highlights that bevacizumab could be useful in the subset of patients having high values of median/ total K^{trans} at baseline. A similar effect was observed for immune related pathways (TOB1) and metabolic pathways (PPARA).

Further analyses were performed considering specific genes from the different pathways showing changes after bevacizumab therapy (as shown in Chapter 5). By considering baseline expression as analysed by qRT-PCR vs. baseline values of DCE-MRI parameters we noted that the lower the value of median K^{trans} / total K^{trans}, the higher the expression of angiopoietin-related protein 4 (ANGPTL4). ANGPTL4 is known to be induced under hypoxic (low oxygen) conditions in endothelial and cancer cells.

Similarly, the lower the value of total K^{trans} at baseline, the higher the expression of phosphoinositide-3-kinase interacting protein 1 (PIK3IP1) at baseline. PIK3IP1 is a negative regulator of PI3K (He, Zhu et al. 2008). PI3K signalling is known to be involved in the homeostasis of lipid and glucose metabolism. It gives an insight into the mechanisms regulating cell survival under hypoxic condition as seen by low values of median/total K^{trans}; these in turn may be responsible for resistance to bevacizumab therapy.

We also observed that lower total K^{trans} was associated with higher CTLA4 expression at baseline. CTLA4 is known to play an important role in T-cell

regulation (Walker and Sansom 2011). On analyses of baseline gene expression vs. changes in MRI parameters after bevacizumab we observed the higher baseline expression of immune related genes (CTLA4) and metabolic genes (PIK3IP1) was associated with lower reduction in tumour volume and total K^{trans} after bevacizumab.

In addition, higher levels of PDK1 at baseline were found to be associated with a lower reduction in tumour volume after bevacizumab. PDK1 is an important regulator of the switch from mitochondrial metabolism to glycolysis and helps cells survive under hypoxic conditions (Kim, Tchernyshyov et al. 2006). As discussed in Chapter 5 we also noticed up-regulation of PDK1 after bevacizumab therapy. This further validates our suggestion concerning the use of combination therapy such as dichloroacetate to overcome resistance seen with bevacizumab. This needs to be explored further in preclinical and clinical trials.

On analysing the change in gene expression vs. change in MRI parameters we noted that the higher absolute reduction in total K^{trans} was associated with greater down-regulation of VEGF regulated genes such as FLT1.

As mentioned earlier in Chapter 5, there was a wide variation noted in expression of CA-9 after bevacizumab both at the gene level as well as the protein level. On further analysis, higher baseline total K^{trans} was positively correlated with the fold change in CA-9 and VEGFA. This signifies that there was a hypoxia induced VEGFA up-regulation in patients. In other words

tumours with high baseline K^{trans} showed maximum reduction in K^{trans} after bevacizumab and the resultant hypoxia induces further escape mechanisms such as immune responses, metabolic changes (Finlay, Rosenzweig et al. 2012) that might lead to resistance in the long term. Thus, using a combination therapy such as anti-CA-9 agents or dichloroacetate may be a way forward to overcome this resistance.

CHAPTER SEVEN

7 Clinical implications and Future directions

This study met the objectives and gave valuable insight into the molecular mechanisms governing response and resistance to anti-angiogenic therapy. As summarised below the results of this study could have very important clinical implications. The imaging and molecular biomarkers proposed in this study could be helpful for identifying breast cancer patients for anti-angiogenic therapy and developing agents to overcome resistance.

The retrospective study showed that:

- Quantitative and physiologically relevant information can be extracted from diagnostic low temporal resolution DCE-MRI scans routinely used in clinical practice.

- Good quality RNA can be extracted from archived FFPE samples. Detailed genomic analyses of these samples would be useful in understanding the tumour biology and potentially in the development of biomarkers for personalized therapy in breast cancer.

- The higher median k_{ep} values may reflect the rapid return of contrast medium into the vasculature that may render the tumour more hypoxic leading to hypoxia induced adaptation by post-translational and transcriptional changes that promote cell survival and metastasis. The detailed genomic analysis conducted in this study, highlighted an important biological correlation of median k_{ep} with cell survival pathways. This suggested median k_{ep} could serve as a potential non-invasive biomarker for hypoxia.

The prospective window of opportunity study demonstrated that:

- There was a continuum of response rather than the well defined categories as assessed by DCE-MRI analyses.

- Anti-angiogenic therapy could be beneficial only for highly vascular tumours at baseline, as the maximum reduction was observed in tumours with higher baseline values of DCE-MRI parameters.

- Analysing total K^{trans} along with median K^{trans} could be more informative as it gives an estimate of the total target presented for modification by bevacizumab.

- This study suggested certain genes that could serve as the biomarkers of response to bevacizumab such as ESM1, CCNE1 and DLL4. Along with genes such as PDK1, PDE3B as markers of resistance on repeated biopsy after a single cycle of bevacizumab. This could have important clinical implication in terms of decision making regarding continuation of therapy with bevacizumab.

- Greater down-regulation of proliferation and ESM1 was observed in patients with high-grade tumours signifying that bevacizumab could be beneficial for this subgroup of patients.

- The significant correlation observed between hypoxia and proliferation

fold change may have important clinical implications for combination therapy. This implies that with bevacizumab therapy there was a subgroup of patients in which there was induction of hypoxia and hypoxia driven up-regulation of growth factors, which results in increased proliferation. For this particular subgroup bevacizumab alone might not be beneficial. Of equal note is the smaller group of patients where both tumour proliferation and hypoxia decrease after bevacizumab; one may postulate that this group is obtaining direct benefit of the agent alone.

- The subgroup of patients showing down-regulation of angiogenesis after bevacizumab therapy implies that in these tumours, there is VEGF driven angiogenesis. Of further note a subgroup of patient observed in which there was up-regulation of angiogenesis after bevacizumab therapy that implies that in those tumours the angiogenesis is driven by other factors also and they have active innate resistance mechanisms against bevacizumab therapy, in other words bevacizumab alone may not beneficial in this subgroup of patients.

- Similar to the retrospective study a strong positive correlation was observed between baseline DCE-MRI parameters with baseline expression of genes related to immune pathways. The clinical implication of this should be explored further.

- The lower baseline expression of genes involved in T cell receptor signalling, interleukin signalling pathways the greater was the absolute reduction observed in median K^{trans}/ total K^{trans}, two weeks after the single cycle of bevacizumab treatment. This information could be helpful in selecting patients based on baseline biopsy results.

- The patients with high values of baseline DCE-MRI parameters (median K^{trans} and total K^{trans}) show greater down-regulation of the angiogenesis related gene signature as well as immune signalling pathways. However in patients with lower values at baseline, there was up-regulation of angiogenesis, which again highlighted that bevacizumab could be useful in the subset of patients having high values of median/ total K^{trans} at baseline.

- The positive association of baseline higher total K^{trans} with up-regulation of CA-9 and VEGFA observed at gene level may be related to rebound angiogenesis. The inhibition of the hypoxia driven adaptive mechanisms to antiangiogenic therapy could enhance bevacizumab treatment effect. Using bevacizumab in combination with the other targeted agents such as small molecules or antibodies that inhibit CA-9 or dichloroacetate, a PDK1 inhibitor or metformin might be a way forward to overcome resistance to bevacizumab. This needed to be explored further by conducting preclinical and clinical studies.

- The strong up-regulation of immune response related pathways observed after bevacizumab therapy needs to be explored further by immunohistochemistry analysis to decide the clinical implications.

List of Publications

- Mehta S, Hughes NP et al: Assessing early therapeutic response to bevacizumab in primary breast cancer using magnetic resonance imaging and gene expression profiles. J Natl Cancer Inst Monogr 2011;43:71–74

- Azam F, Mehta S, Harris A Mechanisms of resistance to antiangiogenesis therapy. Eur J Cancer. 2010 May; 46(8):1323-32.

References

1. American College of Radiology. Breast imaging reporting and data system atlas (BI-RADS atlas). (2003). Reston, VA, American College of Radiology.
2. Abdueva, D., M. Wing, et al. (2010). "Quantitative expression profiling in formalin-fixed paraffin-embedded samples by affymetrix microarrays." J Mol Diagn 12(4): 409-417.
3. Ah-See, M. L., A. Makris, et al. (2008). "Early changes in functional dynamic magnetic resonance imaging predict for pathologic response to neoadjuvant chemotherapy in primary breast cancer." Clin Cancer Res 14(20): 6580-6589.
4. Ali, H. R., S. J. Dawson, et al. (2011). "Cancer stem cell markers in breast cancer: pathological, clinical and prognostic significance." Breast Cancer Res 13(6): R118.
5. Almog, N., L. Ma, et al. (2009). "Transcriptional switch of dormant tumours to fast-growing angiogenic phenotype." Cancer Res 69(3): 836-844.
6. Andre, F., M. V. Dieci, et al. (2013). "Molecular Pathways: Involvement of Immune Pathways in the Therapeutic Response and Outcome in Breast Cancer." Clin Cancer Res 19(1): 28-33.
7. Arpino, G., H. Weiss, et al. (2005). "Oestrogen receptor-positive, progesterone receptor-negative breast cancer: association with growth factor receptor expression and tamoxifen resistance." J Natl Cancer Inst 97(17): 1254-1261.
8. Baar, J., P. Silverman, et al. (2009). "A vasculature-targeting regimen of preoperative docetaxel with or without bevacizumab for locally advanced breast cancer: impact on angiogenic biomarkers." Clin Cancer Res 15(10): 3583-3590.
9. Baeriswyl, V. and G. Christofori (2009). "The angiogenic switch in carcinogenesis." Semin Cancer Biol 19(5): 329-337.
10. Bais, C., M. Singh,J. Kaminker, M. Brauer (2011). BIOLOGICAL MARKERS FOR MONITORING PATIENT RESPONSE TO VEGF ANTAGONISTS. United States, Genentech, Inc. (South San Francisco, CA, US).
11. Banerjee, S., M. Dowsett, et al. (2007). "Mechanisms of disease: angiogenesis and the management of breast cancer." Nature clinical practice. Oncology 4(9): 536-550.
12. Barnett, A. G., J. C. van der Pols, et al. (2005). "Regression to the mean: what it is and how to deal with it." Int J Epidemiol 34(1): 215-220.
13. Bear, H. D., G. Tang, et al. (2012). "Bevacizumab added to neoadjuvant chemotherapy for breast cancer." N Engl J Med 366(4): 310-320.
14. Benson, J. R. and I. Jatoi (2012). "The global breast cancer burden." Future Oncol 8(6): 697-702.
15. Berry, D. A., K. A. Cronin, et al. (2005). "Effect of screening and adjuvant therapy on mortality from breast cancer." N Engl J Med 353(17): 1784-1792.
16. Blobe, G. C., W. P. Schiemann, et al. (2000). "Role of transforming growth factor beta in human disease." N Engl J Med 342(18): 1350-1358.
17. Boddy, J. L., S. B. Fox, et al. (2005). "The androgen receptor is significantly associated with vascular endothelial growth factor and hypoxia sensing via hypoxia-inducible factors HIF-1a, HIF-2a, and the prolyl hydroxylases in human prostate cancer." Clin Cancer Res 11(21): 7658-7663.
18. Borson, R., G. Harker, et al. (2012). "Phase II study of gemcitabine and bevacizumab as first-line treatment in taxane-pretreated, HER2-negative,

locally recurrent or metastatic breast cancer." Clin Breast Cancer 12(5): 322-330.
19. Brufsky, A. M., S. Hurvitz, et al. (2011). "RIBBON-2: a randomized, double-blind, placebo-controlled, phase III trial evaluating the efficacy and safety of bevacizumab in combination with chemotherapy for second-line treatment of human epidermal growth factor receptor 2-negative metastatic breast cancer." J Clin Oncol 29(32): 4286-4293.
20. Buckley, D. L., P. J. Drew, et al. (1997). "Microvessel density of invasive breast cancer assessed by dynamic Gd-DTPA enhanced MRI." J Magn Reson Imaging 7(3): 461-464.
21. Budczies, J., W. Weichert, et al. (2011). "Genome-wide gene expression profiling of formalin-fixed paraffin-embedded breast cancer core biopsies using microarrays." J Histochem Cytochem 59(2): 146-157.
22. Masiero, M.,F.C. Simoes, et al.(2013). "A core human primary tumour angiogenesis signature identifies the endothelial orphan receptor ELTD1 as a key regulator of angiogenesis." Cancer Cell 24(2): 229-241.
23. Buffa, F. M., C. Camps, et al. (2011). "microRNA-associated progression pathways and potential therapeutic targets identified by integrated mRNA and microRNA expression profiling in breast cancer." Cancer Res 71(17): 5635-5645.
24. Buffa, F. M., A. L. Harris, et al. (2010). "Large meta-analysis of multiple cancers reveals a common, compact and highly prognostic hypoxia metagene." Br J Cancer 102(2): 428-435.
25. Carmeliet, P. and R. K. Jain (2000). "Angiogenesis in cancer and other diseases." Nature 407(6801): 249-257.
26. Casanovas, O., D. J. Hicklin, et al. (2005). "Drug resistance by evasion of antiangiogenic targeting of VEGF signaling in late-stage pancreatic islet tumours." Cancer Cell 8(4): 299-309.
27. Chang, J. C., A. Makris, et al. (2008). "Gene expression patterns in formalin-fixed, paraffin-embedded core biopsies predict docetaxel chemosensitivity in breast cancer patients." Breast Cancer Res Treat 108(2): 233-240.
28. Chen, J. H., B. Feig, et al. (2008). "MRI evaluation of pathologically complete response and residual tumours in breast cancer after neoadjuvant chemotherapy." Cancer 112(1): 17-26.
29. Chen, J. H., R. S. Mehta, et al. (2007). "Magnetic resonance imaging in predicting pathological response of triple negative breast cancer following neoadjuvant chemotherapy." J Clin Oncol 25(35): 5667-5669.
30. Choyke, P. L., A. J. Dwyer, et al. (2003). "Functional tumour imaging with dynamic contrast-enhanced magnetic resonance imaging." J Magn Reson Imaging 17(5): 509-520.
31. Chu, J. S., W. J. Lee, et al. (1995). "Correlation between tumour angiogenesis and metastasis in breast cancer." J Formos Med Assoc 94(7): 373-378.
32. Costouros, N. G., D. Lorang, et al. (2002). "Microarray gene expression analysis of murine tumour heterogeneity defined by dynamic contrast-enhanced MRI." Mol Imaging 1(3): 301-308.
33. Coudry, R. A., S. I. Meireles, et al. (2007). "Successful application of microarray technology to microdissected formalin-fixed, paraffin-embedded tissue." J Mol Diagn 9(1): 70-79.

34. Croft, D., G. O'Kelly, et al. (2011). "Reactome: a database of reactions, pathways and biological processes." Nucleic Acids Res 39(Database issue): D691-697.
35. Cui, X., R. Schiff, et al. (2005). "Biology of progesterone receptor loss in breast cancer and its implications for endocrine therapy." J Clin Oncol 23(30): 7721-7735.
36. Daniel, A. R., C. R. Hagan, et al. (2011). "Progesterone receptor action: defining a role in breast cancer." Expert Rev Endocrinol Metab 6(3): 359-369.
37. Degani, H., D. M. Chetrit, et al. (2003). "Magnetic resonance imaging of tumour vasculature." Thrombosis and haemostasis 89(1): 25-33.
38. del Toro, R., C. Prahst, et al. (2010). "Identification and functional analysis of endothelial tip cell-enriched genes." Blood 116(19): 4025-4033.
39. Denduluri, N., S. X. Yang, et al. (2007). "Circulating biomarkers of bevacizumab activity in patients with breast cancer." Cancer Biology & Therapy 7(epub: 21Nov 2007).
40. Denduluri, N., S. X. Yang, et al. (2008). "Circulating biomarkers of bevacizumab activity in patients with breast cancer." Cancer Biol Ther 7(1): 15-20.
41. Desmedt, C., B. Haibe-Kains, et al. (2008). "Biological processes associated with breast cancer clinical outcome depend on the molecular subtypes." Clin Cancer Res 14(16): 5158-5165.
42. Dey, S., F. Tameire, et al. (2013). "PERK-ing up autophagy during MYC-induced tumourigenesis." Autophagy 9(4).
43. Diehn, M., C. Nardini, et al. (2008). "Identification of noninvasive imaging surrogates for brain tumour gene-expression modules." Proc Natl Acad Sci U S A 105(13): 5213-5218.
44. Dongfeng, H., M. Daqing, et al. (2012). "Dynamic breast magnetic resonance imaging: pretreatment prediction of tumour response to neoadjuvant chemotherapy." Clin Breast Cancer 12(2): 94-101.
45. Dufourcq, P., L. Leroux, et al. (2008). "Regulation of endothelial cell cytoskeletal reorganization by a secreted frizzled-related protein-1 and frizzled 4- and frizzled 7-dependent pathway: role in neovessel formation." Am J Pathol 172(1): 37-49.
46. Eisenhauer, E. A., P. Therasse, et al. (2009). "New response evaluation criteria in solid tumours: revised RECIST guideline (version 1.1)." Eur J Cancer 45(2): 228-247.
47. Ellis, L. M., L. Rosen, et al. (2006). "Overview of anti-VEGF therapy and angiogenesis Part 1: Angiogenesis inhibition in solid tumour malignancies." Clinical advances in hematology & oncology : H&O 4(1).
48. Erguvan-Dogan, B., G. J. Whitman, et al. (2006). "BI-RADS-MRI: a primer." AJR Am J Roentgenol 187(2): W152-160.
49. Eroles, P., A. Bosch, et al. (2012). "Molecular biology in breast cancer: intrinsic subtypes and signaling pathways." Cancer Treat Rev 38(6): 698-707.
50. Ferrara, N. (2010). "Role of myeloid cells in vascular endothelial growth factor-independent tumour angiogenesis." Curr Opin Hematol 17(3): 219-224.
51. Ferrara, N. and T. Davis-Smyth (1997). "The biology of vascular endothelial growth factor." Endocr Rev 18(1): 4-25.
52. Ferrara, N., K. Houck, et al. (1992). "Molecular and biological properties of the vascular endothelial growth factor family of proteins." Endocr Rev 13(1): 18-32.

53. Finlay, D. K., E. Rosenzweig, et al. (2012). "PDK1 regulation of mTOR and hypoxia-inducible factor 1 integrate metabolism and migration of CD8+ T cells." J Exp Med 209(13): 2441-2453.
54. Fischer, C., M. Mazzone, et al. (2008). "FLT1 and its ligands VEGFB and PlGF: drug targets for anti-angiogenic therapy?" Nat Rev Cancer 8(12): 942-956.
55. Fodor, I. K., G. G. Hutchins, et al. (2012). "Prognostic and predictive significance of proliferation in 867 colorectal cancers." J Clin Pathol 65(11): 989-995.
56. Folkman, J. (1971). "Tumour angiogenesis: therapeutic implications." N Engl J Med 285(21): 1182-1186.
57. Fox, S. B., R. D. Leek, et al. (1997). "Association of tumour angiogenesis with bone marrow micrometastases in breast cancer patients." J Natl Cancer Inst 89(14): 1044-1049.
58. Fritz-Hansen, T., E. Rostrup, et al. (1996). "Measurement of the arterial concentration of Gd-DTPA using MRI: a step toward quantitative perfusion imaging." Magn Reson Med 36(2): 225-231.
59. Furman, H. E., F. Kelcz, et al. (2002). "Magnetic resonance imaging of breast cancer angiogenesis: a review." Journal of experimental & clinical cancer research : CR 21(3 Suppl): 47-54.
60. Galbraith, S. M., M. A. Lodge, et al. (2002). "Reproducibility of dynamic contrast-enhanced MRI in human muscle and tumours: comparison of quantitative and semi-quantitative analysis." NMR Biomed 15(2): 132-142.
61. Gasparini, G. (2000). "Prognostic value of vascular endothelial growth factor in breast cancer." Oncologist 5 Suppl 1: 37-44.
62. Gasparini, G. and A. L. Harris (1995). "Clinical importance of the determination of tumour angiogenesis in breast carcinoma: much more than a new prognostic tool." J Clin Oncol 13(3): 765-782.
63. Gause, W. C., M. J. Halvorson, et al. (1997). "The function of costimulatory molecules and the development of IL-4-producing T cells." Immunol Today 18(3): 115-120.
64. Generali, D., A. Berruti, et al. (2006). "Hypoxia-Inducible Factor-1{alpha} Expression Predicts a Poor Response to Primary Chemoendocrine Therapy and Disease-Free Survival in Primary Human Breast Cancer." Clin Cancer Res 12(15): 4562-4568.
65. Generali, D., A. Berruti, et al. (2011). "Molecular oncology and the neoadjuvant setting: the perfect blend for treatment personalization and clinical trial design." J Natl Cancer Inst Monogr 2011(43): 67-70.
66. Gerber, H. P. and N. Ferrara (2005). "Pharmacology and pharmacodynamics of bevacizumab as monotherapy or in combination with cytotoxic therapy in preclinical studies." Cancer Res 65(3): 671-680.
67. Gianni, L., M. Zambetti, et al. (2005). "Gene expression profiles in paraffin-embedded core biopsy tissue predict response to chemotherapy in women with locally advanced breast cancer." J Clin Oncol 23(29): 7265-7277.
68. Globocan (2008). Cancer Fact Sheet. Retrieved 13/04/2013, from http://globocan.iarc.fr/factsheet.asp.
69. Golembesky, A. K., M. D. Gammon, et al. (2008). "Peroxisome proliferator-activated receptor-alpha (PPARA) genetic polymorphisms and breast cancer risk: a Long Island ancillary study." Carcinogenesis 29(10): 1944-1949.

70. Grosso, J. F. and M. N. Jure-Kunkel (2013). "CTLA-4 blockade in tumour models: an overview of preclinical and translational research." Cancer Immun 13: 5.
71. Gyanchandani, R. and S. Kim (2013). "Predictive Biomarkers to Anti-VEGF Therapy: Progress toward an Elusive Goal." Clin Cancer Res.
72. Hadad, S., T. Iwamoto, et al. (2011). "Evidence for biological effects of metformin in operable breast cancer: a pre-operative, window-of-opportunity, randomized trial." Breast Cancer Res Treat 128(3): 783-794.
73. Hall, B. A., T. Y. Kim, et al. (2012). "Serum and glucocorticoid-regulated kinase 1 (SGK1) activation in breast cancer: requirement for mTORC1 activity associates with ER-alpha expression." Breast Cancer Res Treat 135(2): 469-479.
74. Harris, L. K. and M. Westwood (2012). "Biology and significance of signalling pathways activated by IGF-II." Growth Factors 30(1): 1-12.
75. Hayes, C., A. R. Padhani, et al. (2002). "Assessing changes in tumour vascular function using dynamic contrast-enhanced magnetic resonance imaging." NMR Biomed 15(2): 154-163.
76. He, X., Z. Zhu, et al. (2008). "PIK3IP1, a negative regulator of PI3K, suppresses the development of hepatocellular carcinoma." Cancer Res 68(14): 5591-5598.
77. Hicklin, D. J. and L. M. Ellis (2005). "Role of the vascular endothelial growth factor pathway in tumour growth and angiogenesis." J Clin Oncol 23(5): 1011-1027.
78. Ignoffo, R. J. (2004). "Overview of bevacizumab: a new cancer therapeutic strategy targeting vascular endothelial growth factor." American journal of health-system pharmacy : AJHP : official journalof the American Society of Health-System Pharmacists 61(Suppl 5): S21-26.
79. Ikeda, O., R. Nishimura, et al. (2004). "Evaluation of tumour angiogenesis using dynamic enhanced magnetic resonance imaging: comparison of plasma vascular endothelial growth factor, hemodynamic, and pharmacokinetic parameters." Acta radiologica (Stockholm Sweden : 1987) 45(4): 446-452.
80. Irizarry, R. A., S. L. Ooi, et al. (2003). "Use of mixture models in a microarray-based screening procedure for detecting differentially represented yeast mutants." Stat Appl Genet Mol Biol 2: Article1.
81. Jackson, A., G. C. Jayson, et al. (2003). "Reproducibility of quantitative dynamic contrast-enhanced MRI in newly presenting glioma." Br J Radiol 76(903): 153-162.
82. Jain, R. K. (2005). "Normalization of Tumour Vasculature: An Emerging Concept in Antiangiogenic Therapy." Science 307(5706): 58-62.
83. Jayson GC, d. H. S., Delmar P (2011). "Evaluationof plasma VEGFA as a potential predictive pan-tumour biomarker for bevacizumab." Proceedings of the 2011 European Multidisciplinary Cancer Congress, Stockholm, Sweden (abstr 804)
84. Jubb, A. M., F. M. Buffa, et al. (2010). "Assessment of tumour hypoxia for prediction of response to therapy and cancer prognosis." J Cell Mol Med 14(1-2): 18-29.
85. Jubb, A. M. and A. L. Harris (2010). "Biomarkers to predict the clinical efficacy of bevacizumab in cancer." Lancet Oncol 11(12): 1172-1183.

86. Jubb, A. M., K. D. Miller, et al. (2011). "Impact of exploratory biomarkers on the treatment effect of bevacizumab in metastatic breast cancer." Clin Cancer Res 17(2): 372-381.
87. Kahn, B. B., T. Alquier, et al. (2005). "AMP-activated protein kinase: ancient energy gauge provides clues to modern understanding of metabolism." Cell Metab 1(1): 15-25.
88. Karrison, T. G., M. L. Maitland, et al. (2007). "Design of phase II cancer trials using a continuous endpoint of change in tumour size: application to a study of sorafenib and erlotinib in non small-cell lung cancer." J Natl Cancer Inst 99(19): 1455-1461.
89. Khodarev, N. N., B. Roizman, et al. (2012). "Molecular pathways: interferon/stat1 pathway: role in the tumour resistance to genotoxic stress and aggressive growth." Clin Cancer Res 18(11): 3015-3021.
90. Kibriya, M. G., F. Jasmine, et al. (2010). "Analyses and interpretation of whole-genome gene expression from formalin-fixed paraffin-embedded tissue: an illustration with breast cancer tissues." BMC Genomics 11: 622.
91. Kim, J. W., P. Gao, et al. (2007). "Hypoxia-inducible factor 1 and dysregulated c-Myc cooperatively induce vascular endothelial growth factor and metabolic switches hexokinase 2 and pyruvate dehydrogenase kinase 1." Mol Cell Biol 27(21): 7381-7393.
92. Kim, J. W., I. Tchernyshyov, et al. (2006). "HIF-1-mediated expression of pyruvate dehydrogenase kinase: a metabolic switch required for cellular adaptation to hypoxia." Cell Metab 3(3): 177-185.
93. Kolacinska, A., W. Fendler, et al. (2012). "Gene expression and pathologic response to neoadjuvant chemotherapy in breast cancer." Mol Biol Rep 39(7): 7435-7441.
94. Koo, H. R., N. Cho, et al. (2012). "Correlation of perfusion parameters on dynamic contrast-enhanced MRI with prognostic factors and subtypes of breast cancers." J Magn Reson Imaging 36(1): 145-151.
95. Kowanetz, M. and N. Ferrara (2006). "Vascular endothelial growth factor signaling pathways: therapeutic perspective." Clin Cancer Res 12(17): 5018-5022.
96. Kuo, M. D., J. Gollub, et al. (2007). "Radiogenomic analysis to identify imaging phenotypes associated with drug response gene expression programs in hepatocellular carcinoma." J Vasc Interv Radiol 18(7): 821-831.
97. Lambrechts, D., H. J. Lenz, et al. (2013). "Markers of Response for the Antiangiogenic Agent Bevacizumab." J Clin Oncol 31(9): 1219-1230.
98. Lamers, C., M. Schubert-Zsilavecz, et al. (2012). "Therapeutic modulators of peroxisome proliferator-activated receptors (PPAR): a patent review (2008-present)." Expert Opin Ther Pat 22(7): 803-841.
99. Leach, M. O. (2001). "Application of magnetic resonance imaging to angiogenesis in breast cancer." Breast cancer research : BCR 3(1): 22-27.
100. Leach, M. O., K. M. Brindle, et al. (2005). "The assessment of antiangiogenic and antivascular therapies in early-stage clinical trials using magnetic resonance imaging: issues and recommendations." Br J Cancer 92(9): 1599-1610.
101. Levin, P. B. a. B., Ed. (2008). World Cancer report, International Agency for Research on Cancer, World Health Organization

102. Li, J. L., R. C. Sainson, et al. (2011). "DLL4-Notch signaling mediates tumour resistance to anti-VEGF therapy in vivo." Cancer Res 71(18): 6073-6083.
103. Li, J. L., R. C. Sainson, et al. (2007). "Delta-like 4 Notch ligand regulates tumour angiogenesis, improves tumour vascular function, and promotes tumour growth in vivo." Cancer Res 67(23): 11244-11253.
104. Li, S. P., A. Makris, et al. (2011). "Use of dynamic contrast-enhanced MR imaging to predict survival in patients with primary breast cancer undergoing neoadjuvant chemotherapy." Radiology 260(1): 68-78.
105. Li, S. P. and A. R. Padhani (2012). "Tumour response assessments with diffusion and perfusion MRI." J Magn Reson Imaging 35(4): 745-763.
106. Li, S. P., A. R. Padhani, et al. (2011). "Vascular characterisation of triple negative breast carcinomas using dynamic MRI." Eur Radiol 21(7): 1364-1373.
107. Loncaster, J. A., A. L. Harris, et al. (2001). "Carbonic anhydrase (CA IX) expression, a potential new intrinsic marker of hypoxia: correlations with tumour oxygen measurements and prognosis in locally advanced carcinoma of the cervix." Cancer Res 61(17): 6394-6399.
108. Lu, R., M. Kujawski, et al. (2012). "Tumour angiogenesis mediated by myeloid cells is negatively regulated by CEACAM1." Cancer Res 72(9): 2239-2250.
109. Marinovich, M. L., F. Sardanelli, et al. (2012). "Early prediction of pathologic response to neoadjuvant therapy in breast cancer: Systematic review of the accuracy of MRI." Breast 21(5): 669-677.
110. McIntyre, A., S. Patiar, et al. (2012). "Carbonic anhydrase IX promotes tumour growth and necrosis in vivo and inhibition enhances anti-VEGF therapy." Clin Cancer Res 18(11): 3100-3111.
111. Mehta, S., N. P. Hughes, et al. (2011). "Assessing early therapeutic response to bevacizumab in primary breast cancer using magnetic resonance imaging and gene expression profiles." J Natl Cancer Inst Monogr 2011(43): 71-74.
112. Miles, D. (2007). "Bevacizumab in first-line treatment of metastatic breast cancer: a viewpoint by David Miles." Drugs 67(12): 1800-1801.
113. Miles, D. W., A. Chan, et al. (2010). "Phase III study of bevacizumab plus docetaxel compared with placebo plus docetaxel for the first-line treatment of human epidermal growth factor receptor 2-negative metastatic breast cancer." J Clin Oncol 28(20): 3239-3247.
114. Miles, D. W., S. L. de Haas, et al. (2013). "Biomarker results from the AVADO phase 3 trial of first-line bevacizumab plus docetaxel for HER2-negative metastatic breast cancer." Br J Cancer 108(5): 1052-1060.
115. Miller, K., M. Wang, et al. (2007). "Paclitaxel plus bevacizumab versus paclitaxel alone for metastatic breast cancer." N Engl J Med 357(26): 2666-2676.
116. Miller, K. D. (2003). "E2100: a phase III trial of paclitaxel versus paclitaxel/bevacizumab for metastatic breast cancer." Clinical breast cancer 3(6): 421-422.
117. Miller, K. D., L. I. Chap, et al. (2005). "Randomized phase III trial of capecitabine compared with bevacizumab plus capecitabine in patients with previously treated metastatic breast cancer." Journal of Clinical Oncology 23(4): 792-799.
118. Mortimer, J., H. B. Zonder, et al. (2012). "Lessons learned from the bevacizumab experience." Cancer Control 19(4): 309-316.

119. Nelson, B. H. (2004). "IL-2, regulatory T cells, and tolerance." J Immunol 172(7): 3983-3988.
120. Neufeld, G., O. Kessler, et al. (2002). "The interaction of Neuropilin-1 and Neuropilin-2 with tyrosine-kinase receptors for VEGF." Adv Exp Med Biol 515: 81-90.
121. Nielsen, N. H., C. Arnerlov, et al. (1996). "Cyclin E overexpression, a negative prognostic factor in breast cancer with strong correlation to ooOestrogen receptor status." Br J Cancer 74(6): 874-880.
122. Njiaju, U. O., E. R. Gamazon, et al. (2012). "Whole-genome studies identify solute carrier transporters in cellular susceptibility to paclitaxel." Pharmacogenet Genomics 22(7): 498-507.
123. Noel, P. J., L. H. Boise, et al. (1996). "Regulation of T cell activation by CD28 and CTLA4." Adv Exp Med Biol 406: 209-217.
124. Nogales-Cadenas, R., P. Carmona-Saez, et al. (2009). "GeneCodis: interpreting gene lists through enrichment analysis and integration of diverse biological information." Nucleic Acids Res 37(Web Server issue): W317-322.
125. Noguera-Troise, I., C. Daly, et al. (2006). "Blockade of DLL4 inhibits tumour growth by promoting non-productive angiogenesis." Nature 444(7122): 1032-1037.
126. O'Connor, J. P., R. A. Carano, et al. (2009). "Quantifying antivascular effects of monoclonal antibodies to vascular endothelial growth factor: insights from imaging." Clin Cancer Res 15(21): 6674-6682.
127. O'Connor, J. P., A. Jackson, et al. (2007). "DCE-MRI biomarkers in the clinical evaluation of antiangiogenic and vascular disrupting agents." Br J Cancer 96(2): 189-195.
128. O'Connor, J. P., A. Jackson, et al. (2012). "Dynamic contrast-enhanced MRI in clinical trials of antivascular therapies." Nat Rev Clin Oncol 9(3): 167-177.
129. O'Connor, J. P. and G. C. Jayson (2012). "Do imaging biomarkers relate to outcome in patients treated with VEGF inhibitors?" Clin Cancer Res 18(24): 6588-6598.
130. O'Connor, J. P., G. C. Jayson, et al. (2007). "Enhancing fraction predicts clinical outcome following first-line chemotherapy in patients with epithelial ovarian carcinoma." Clin Cancer Res 13(20): 6130-6135.
131. O'Shaughnessy, J., D. Miles, et al. (2010). "A meta-analysis of overall survival data from three randomized trials of bevacizumab (BV) and first-line chemotherapy as treatment for patients with metastatic breast cancer (MBC)." ASCO Meeting Abstracts 28(15_suppl): 1005.
132. Overmoyer B, S. P., Leeming R, Shenk R, Lyons J, Jesberger J, Hartman P, Dumadag L, Chen H. (2004). "Phase II trial of neoadjuvant docetaxel with or without bevacizumab in patients with locally advanced breast cancer [SABCS, poster presentation]." Breast Cancer Res Treat 88(S106).
133. Padhani, A. R., G. Liu, et al. (2009). "Diffusion-weighted magnetic resonance imaging as a cancer biomarker: consensus and recommendations." Neoplasia 11(2): 102-125.
134. Parmalee, N. L. and J. Kitajewski (2008). "Wnt signaling in angiogenesis." Curr Drug Targets 9(7): 558-564.
135. Pastorekova, S., Z. Zavadova, et al. (1992). "A novel quasi-viral agent, MaTu, is a two-component system." Virology 187(2): 620-626.
136. Patiar, S. and A. L. Harris (2006). "Role of hypoxia-inducible factor-1alpha as a cancer therapy target." Endocr Relat Cancer 13 Suppl 1: S61-75.

137. Penland, S. K., T. O. Keku, et al. (2007). "RNA expression analysis of formalin-fixed paraffin-embedded tumours." Lab Invest 87(4): 383-391.
138. Perou, C. M., T. Sorlie, et al. (2000). "Molecular portraits of human breast tumours." Nature 406(6797): 747-752.
139. Pickles, M. D., D. J. Manton, et al. (2009). "Prognostic value of pre-treatment DCE-MRI parameters in predicting disease free and overall survival for breast cancer patients undergoing neoadjuvant chemotherapy." Eur J Radiol 71(3): 498-505.
140. Pierga, J. Y., T. Petit, et al. (2012). "Neoadjuvant bevacizumab, trastuzumab, and chemotherapy for primary inflammatory HER2-positive breast cancer (BEVERLY-2): an open-label, single-arm phase 2 study." Lancet Oncol 13(4): 375-384.
141. Pinheiro, C., A. Albergaria, et al. (2010). "Monocarboxylate transporter 1 is up-regulated in basal-like breast carcinoma." Histopathology 56(7): 860-867.
142. Pinheiro, C., B. Sousa, et al. (2011). "GLUT1 and CAIX expression profiles in breast cancer correlate with adverse prognostic factors and MCT1 overexpression." Histol Histopathol 26(10): 1279-1286.
143. Polyak, K. (2011). "Heterogeneity in breast cancer." J Clin Invest 121(10): 3786-3788.
144. Prat, A., J. S. Parker, et al. (2010). "Phenotypic and molecular characterization of the claudin-low intrinsic subtype of breast cancer." Breast Cancer Res 12(5): R68.
145. Prat, A. and C. M. Perou (2011). "Deconstructing the molecular portraits of breast cancer." Mol Oncol 5(1): 5-23.
146. Quesada, A. R., M. A. Medina, et al. (2007). "Playing only one instrument may be not enough: limitations and future of the antiangiogenic treatment of cancer." Bioessays 29(11): 1159-1168.
147. Raatschen, H. J., G. H. Simon, et al. (2008). "Vascular permeability during antiangiogenesis treatment: MR imaging assay results as biomarker for subsequent tumour growth in rats." Radiology 247(2): 391-399.
148. Ramaswamy, B. and C. L. Shapiro (2003). "Phase II trial of bevacizumab in combination with docetaxel in women with advanced breast cancer." Clinical breast cancer 4(4): 292-294.
149. Rapisarda, A. and G. Melillo (2012). "Role of the VEGF/VEGFR axis in cancer biology and therapy." Adv Cancer Res 114: 237-267.
150. Rennel, E., S. Mellberg, et al. (2007). "Endocan is a VEGFA and PI3K regulated gene with increased expression in human renal cancer." Exp Cell Res 313(7): 1285-1294.
151. Ribeiro-Silva, A., H. Zhang, et al. (2007). "RNA extraction from ten year old formalin-fixed paraffin-embedded breast cancer samples: a comparison of column purification and magnetic bead-based technologies." BMC Mol Biol 8: 118.
152. Robert, N. J., V. Dieras, et al. (2011). "RIBBON-1: randomized, double-blind, placebo-controlled, phase III trial of chemotherapy with or without bevacizumab for first-line treatment of human epidermal growth factor receptor 2-negative, locally recurrent or metastatic breast cancer." J Clin Oncol 29(10): 1252-1260.
153. Rofstad, E. K., J. V. Gaustad, et al. (2010). "Tumours exposed to acute cyclic hypoxic stress show enhanced angiogenesis, perfusion and metastatic dissemination." Int J Cancer.

154. Rossari, J. R., O. Metzger-Filho, et al. (2012). "Bevacizumab and Breast Cancer: A Meta-Analysis of First-Line Phase III Studies and a Critical Reappraisal of Available Evidence." J Oncol 2012: 417673.
155. Rutman, A. M. and M. D. Kuo (2009). "Radiogenomics: creating a link between molecular diagnostics and diagnostic imaging." Eur J Radiol 70(2): 232-241.
156. Rzymski, T., M. Milani, et al. (2009). "Role of ATF4 in regulation of autophagy and resistance to drugs and hypoxia." Cell Cycle 8(23): 3838-3847.
157. Sadi, A. M., D. Y. Wang, et al. (2011). "Clinical relevance of DNA microarray analyses using archival formalin-fixed paraffin-embedded breast cancer specimens." BMC Cancer 11: 253:251-213.
158. Sanchez-Rovira, P., M. A. Segui, et al. (2013). "Bevacizumab plus preoperative chemotherapy in operable HER2 negative breast cancer: biomarkers and pathologic response." Clin Transl Oncol.
159. Sarrazin, S., E. Adam, et al. (2006). "Endocan or endothelial cell specific molecule-1 (ESM-1): a potential novel endothelial cell marker and a new target for cancer therapy." Biochim Biophys Acta 1765(1): 25-37.
160. Sarrazin S, M. C., Delmas D, Lassalle P, Delehedde M (2010). "Endocan as a Biomarker of Endothelial Dysfunction in Cancer." J Cancer Sci Ther 2: 047-052.
161. Scaltriti, M., P. J. Eichhorn, et al. (2011). "Cyclin E amplification/overexpression is a mechanism of trastuzumab resistance in HER2+ breast cancer patients." Proc Natl Acad Sci U S A 108(9): 3761-3766.
162. Scehnet, J. S., W. Jiang, et al. (2007). "Inhibition of DLL4-mediated signaling induces proliferation of immature vessels and results in poor tissue perfusion." Blood 109(11): 4753-4760.
163. Schneider, B. P., R. J. Gray, et al. (2013). "Prognostic and Predictive Value of Tumour Vascular Endothelial Growth Factor Gene Amplification in Metastatic Breast Cancer Treated with Paclitaxel with and without Bevacizumab; Results from ECOG 2100 Trial." Clin Cancer Res.
164. Schneider, B. P. and K. D. Miller (2005). "Angiogenesis of breast cancer." Journal of Clinical Oncology 23(8): 1782-1790.
165. Schneider, B. P., F. Shen, et al. (2012). "Pharmacogenetic biomarkers for the prediction of response to antiangiogenic treatment." Lancet Oncol 13(10): e427-436.
166. Schneider, B. P., M. Wang, et al. (2008). "Association of vascular endothelial growth factor and vascular endothelial growth factor receptor-2 genetic polymorphisms with outcome in a trial of paclitaxel compared with paclitaxel plus bevacizumab in advanced breast cancer: ECOG 2100." J Clin Oncol 26(28): 4672-4678.
167. Schulze, A. and A. L. Harris (2012). "How cancer metabolism is tuned for proliferation and vulnerable to disruption." Nature 491(7424): 364-373.
168. Shibuya, M. (2006). "Vascular endothelial growth factor receptor-1 (VEGFR-1/Flt-1): a dual regulator for angiogenesis." Angiogenesis 9(4): 225-230; discussion 231.
169. Shipitsin, M., L. L. Campbell, et al. (2007). "Molecular definition of breast tumour heterogeneity." Cancer Cell 11(3): 259-273.
170. Shojaei, F., X. Wu, et al. (2007). "Bv8 regulates myeloid-cell-dependent tumour angiogenesis." Nature 450(7171): 825-831.

171. Sieuwerts, A. M., M. P. Look, et al. (2006). "Which cyclin E prevails as prognostic marker for breast cancer? Results from a retrospective study involving 635 lymph node-negative breast cancer patients." Clin Cancer Res 12(11 Pt 1): 3319-3328.
172. Singletary, S. E., C. Allred, et al. (2002). "Revision of the American Joint Committee on Cancer staging system for breast cancer." J Clin Oncol 20(17): 3628-3636.
173. Smith, I. E., J. Y. Pierga, et al. (2010). "First-line bevacizumab plus taxane-based chemotherapy for locally recurrent or metastatic breast cancer: safety and efficacy in an open-label study in 2251 patients." Ann Oncol.
174. Smith, N. R., D. Baker, et al. (2010). "Vascular endothelial growth factor receptors VEGFR-2 and VEGFR-3 are localized primarily to the vasculature in human primary solid cancers." Clin Cancer Res 16(14): 3548-3561.
175. Sorlie, T., C. M. Perou, et al. (2001). "Gene expression patterns of breast carcinomas distinguish tumour subclasses with clinical implications." Proc Natl Acad Sci U S A 98(19): 10869-10874.
176. Storey, J. D. and R. Tibshirani (2003). "Statistical significance for genomewide studies." Proc Natl Acad Sci U S A 100(16): 9440-9445.
177. Straver, M. E., A. M. Glas, et al. (2010). "The 70-gene signature as a response predictor for neoadjuvant chemotherapy in breast cancer." Breast Cancer Res Treat 119(3): 551-558.
178. Strickland, L. A., A. M. Jubb, et al. (2005). "Plasmalemmal vesicle-associated protein (PLVAP) is expressed by tumour endothelium and is up-regulated by vascular endothelial growth factor-A (VEGF)." J Pathol 206(4): 466-475.
179. Su, M. Y., Y. C. Cheung, et al. (2003). "Correlation of dynamic contrast enhancement MRI parameters with microvessel density and VEGF for assessment of angiogenesis in breast cancer." Journal of magnetic resonance imaging : JMRI 18(4): 467-477.
180. Subramanian, A., P. Tamayo, et al. (2005). "Gene set enrichment analysis: a knowledge-based approach for interpreting genome-wide expression profiles." Proc Natl Acad Sci U S A 102(43): 15545-15550.
181. Suchanek, K. M., F. J. May, et al. (2002). "Peroxisome proliferator-activated receptor alpha in the human breast cancer cell lines MCF-7 and MDA-MB-231." Mol Carcinog 34(4): 165-171.
182. Sutendra, G., P. Dromparis, et al. (2012). "Mitochondrial activation by inhibition of PDKII suppresses HIF1a signaling and angiogenesis in cancer." Oncogene.
183. Swietach, P., A. Hulikova, et al. (2010). "New insights into the physiological role of carbonic anhydrase IX in tumour pH regulation." Oncogene 29(50): 6509-6521.
184. Tabas-Madrid, D., R. Nogales-Cadenas, et al. (2012). "GeneCodis3: a non-redundant and modular enrichment analysis tool for functional genomics." Nucleic Acids Res 40(Web Server issue): W478-483.
185. Tan, E. Y., M. Yan, et al. (2009). "The key hypoxia regulated gene CAIX is up-regulated in basal-like breast tumours and is associated with resistance to chemotherapy." Br J Cancer 100(2): 405-411.
186. Tavassoli, P. D. F. A. (2003). World Health Organization: Tumours of the Breast and Female Genital Organs. Oxford(Oxfordshire), Oxford University Press.

187. Thukral, A., D. M. Thomasson, et al. (2007). "Inflammatory breast cancer: dynamic contrast-enhanced MR in patients receiving bevacizumab--initial experience." Radiology 244(3): 727-735.
188. Tibshirani, R. J. and B. Efron (2002). "Pre-validation and inference in microarrays." Stat Appl Genet Mol Biol 1: Article1.
189. Tofts, P. S., G. Brix, et al. (1999). "Estimating kinetic parameters from dynamic contrast-enhanced T(1)-weighted MRI of a diffusable tracer: standardized quantities and symbols." J Magn Reson Imaging 10(3): 223-232.
190. Tolaney SM, D. D., Boucher Y (2012). "Aphase II study of preoperative (preop) bevacizumab (bev) followed by dose-dense (dd) doxorubicin (A)/ cyclophosphamide (C)/paclitaxel (T) in combination with bev in HER2-negative operable breast cancer(BC)." J Clin Oncol 30(55s): (suppl; abstr 1026).
191. Tong, R. T., Y. Boucher, et al. (2004). "Vascular normalization by vascular endothelial growth factor receptor 2 blockade induces a pressure gradient across the vasculature and improves drug penetration in tumours." Cancer Res 64(11): 3731-3736.
192. Tozaki, M. (2004). "Interpretation of breast MRI: correlation of kinetic and morphological parameters with pathological findings." Magn Reson Med Sci 3(4): 189-197.
193. Tsavachidou-Fenner, D., N. Tannir, et al. (2010). "Gene and protein expression markers of response to combined antiangiogenic and epidermal growth factor targeted therapy in renal cell carcinoma." Ann Oncol 21(8): 1599-1606.
194. Tse, G. M., B. Chaiwun, et al. (2007). "Magnetic resonance imaging of breast lesions--a pathologic correlation." Breast Cancer Res Treat 103(1): 1-10.
195. Turkbey, B., D. Thomasson, et al. (2009). "The role of dynamic contrast-enhanced MRI in cancer diagnosis and treatment." Diagn Interv Radiol.
196. Turley, H., P. A. Scott, et al. (1998). "Expression of VEGF in routinely fixed material using a new monoclonal antibody VG1." J Pathol 186(3): 313-318.
197. Tusher, V. G., R. Tibshirani, et al. (2001). "Significance analysis of microarrays applied to the ionizing radiation response." Proc Natl Acad Sci U S A 98(9): 5116-5121.
198. Umemura, S., S. Yoshida, et al. (2007). "Increased phosphorylation of Akt in triple-negative breast cancers." Cancer Sci 98(12): 1889-1892.
199. van 't Veer, L. J., H. Dai, et al. (2002). "Gene expression profiling predicts clinical outcome of breast cancer." Nature 415(6871): 530-536.
200. van Raalte, D. H., M. Li, et al. (2004). "Peroxisome proliferator-activated receptor (PPAR)-alpha: a pharmacological target with a promising future." Pharm Res 21(9): 1531-1538.
201. von Minckwitz, G., H. Eidtmann, et al. (2012). "Neoadjuvant chemotherapy and bevacizumab for HER2-negative breast cancer." N Engl J Med 366(4): 299-309.
202. Walker, L. S. and D. M. Sansom (2011). "The emerging role of CTLA4 as a cell-extrinsic regulator of T cell responses." Nat Rev Immunol 11(12): 852-863.
203. Walker-Samuel, S., M. O. Leach, et al. (2006). "Evaluation of response to treatment using DCE-MRI: the relationship between initial area under the gadolinium curve (IAUGC) and quantitative pharmacokinetic analysis." Phys Med Biol 51(14): 3593-3602.

204. Ward, C., S. P. Langdon, et al. (2013). "New strategies for targeting the hypoxic tumour microenvironment in breast cancer." Cancer Treat Rev 39(2): 171-179.
205. Wedam, S. B., J. A. Low, et al. (2006). "Antiangiogenic and Antitumour Effects of Bevacizumab in Patients With Inflammatory and Locally Advanced Breast Cancer." J Clin Oncol 24(5): 769-777.
206. Wee, N. K., D. C. Weinstein, et al. (2013). "The mammalian copper transporters CTR1 and CTR2 and their roles in development and disease." Int J Biochem Cell Biol 45(5): 960-963.
207. Weidner, N., J. Folkman, et al. (1992). "Tumour angiogenesis: a new significant and independent prognostic indicator in early-stage breast carcinoma." J Natl Cancer Inst 84(24): 1875-1887.
208. Weidner, N., J. P. Semple, et al. (1991). "Tumour angiogenesis and metastasis--correlation in invasive breast carcinoma." N Engl J Med 324(1): 1-8.
209. Wilson, L. S., G. S. Baillie, et al. (2011). "A phosphodiesterase 3B-based signaling complex integrates exchange protein activated by cAMP 1 and phosphatidylinositol 3-kinase signals in human arterial endothelial cells." J Biol Chem 286(18): 16285-16296.
210. Wu, J. M. and C. A. Staton (2012). "Anti-angiogenic drug discovery: lessons from the past and thoughts for the future." Expert Opin Drug Discov 7(8): 723-743.
211. Wu JZ, I. R., MacDonald J (2002). gcrma: Background Adjustment Using Sequence Information. R package version 2.20.0.
212. Wykoff, C. C., N. J. Beasley, et al. (2000). "Hypoxia-inducible expression of tumour-associated carbonic anhydrases." Cancer Res 60(24): 7075-7083.
213. Yamamoto, S., D. D. Maki, et al. (2012). "Radiogenomic analysis of breast cancer using MRI: a preliminary study to define the landscape." AJR Am J Roentgenol 199(3): 654-663.
214. Yan, M., N. Jene, et al. (2011). "Recruitment of regulatory T cells is correlated with hypoxia-induced CXCR4 expression, and is associated with poor prognosis in basal-like breast cancers." Breast Cancer Res 13(2): R47.
215. Yang, S. X., S. M. Steinberg, et al. (2008). "Gene expression profile and angiogenic marker correlates with response to neoadjuvant bevacizumab followed by bevacizumab plus chemotherapy in breast cancer." Clin Cancer Res 14(18): 5893-5899.
216. Zembutsu, H., Y. Suzuki, et al. (2009). "Predicting response to docetaxel neoadjuvant chemotherapy for advanced breast cancers through genome-wide gene expression profiling." Int J Oncol 34(2): 361-370.
217. Zerlin, M., M. A. Julius, et al. (2008). "Wnt/Frizzled signaling in angiogenesis." Angiogenesis 11(1): 63-69.
218. Zhang, T., R. Ramakrishnan, et al. (1996). "BIRCH: an efficient data clustering method for very large databases." SIGMOD Rec. 25(2): 103-114.

Appendix 3.1

Genes positively correlated with median k_{ep} at baseline (Retrospective study)

S No	Gene Symbol	Gene Title	Numerator(r)	q-value(%)	Chromosomal Location	Entrez Gene
1	SLC31A2	solute carrier family 31 (copper transporters) member 2	0.62	0.00	chr9q31-q32	1318
2	IGF2R	insulin-like growth factor 2 receptor	0.58	0.00	chr6q26	3482
3	UBE2J1	ubiquitin-conjugating enzyme E2 J1 (UBC6 homolog yeast)	0.55	0.00	chr6q15	51465
4	MTO1	mitochondrial translation optimization 1 homolog (S. cerevisiae)	0.54	0.00	chr6q13	25821
5	BCLAF1	BCL2-associated transcription factor 1	0.54	0.00	chr6q22-q23	9774
6	TRAPPC10	trafficking protein particle complex 10	0.54	0.00	chr21q22.3	7109
7	CALR	calreticulin	0.53	0.00	chr19p13.3-p13.2	811
8	LGMN	legumain	0.53	0.00	chr14q32.1	5641
9	SGK1	serum/glucocorticoid regulated kinase 1	0.52	0.72	chr6q23	6446
10	NUS1	nuclear undecaprenyl pyrophosphate synthase 1 homolog (S. cerevisiae)	0.52	0.72	chr6q22.1	116150
11	EIF2S1	eukaryotic translation initiation factor 2 subunit 1 alpha 35kDa	0.51	0.72	chr14q23.3	1965
12	HDAC2	histone deacetylase 2	0.51	0.72	chr6q21	3066
13	ASCC3	activating signal cointegrator 1 complex subunit 3	0.51	0.72	chr6q16	10973
14	RIPK2	receptor-interacting serine-threonine kinase 2	0.51	0.72	chr8q21	8767
15	TRMT11	tRNA methyltransferase 11 homolog (S. cerevisiae)	0.50	0.72	chr6q11.1-q22.33	60487
16	MTHFD1L	methylenetetrahydrofolate dehydrogenase (NADP+ dependent) 1-like	0.50	0.72	chr6q25.1	25902
17	RNF8	ring finger protein 8	0.50	0.72	chr6p21.3	9025
18	LYN	v-yes-1 Yamaguchi sarcoma viral related oncogene homolog	0.49	0.72	chr8q13	4067
19	RPF2	ribosome production factor 2 homolog (S. cerevisiae)	0.49	0.72	chr6q21	84154
20	CDT1	Chromatin licensing and DNA replication factor 1	0.49	0.72	chr16q24.3	81620
21	ZNF462	zinc finger protein 462	0.49	0.72	chr9q31.2	58499
22	NUP43	nucleoporin 43kDa	0.48	0.72	chr6q25.1	348995
23	GTF3C6	general transcription factor IIIC polypeptide 6 alpha 35kDa	0.48	0.72	chr6q21	112495
24	BTG3	BTG family member 3	0.48	0.72	chr21q21.1	10950
25	MSN	moesin	0.48	0.72	chrXq11.1	4478
26	GCA	grancalcin EF-hand calcium binding protein	0.48	0.72	chr2q24.2	25801
27	C6orf115	chromosome 6 open reading frame 115	0.48	0.72	chr6q24.1	58527
28	RRP1B	ribosomal RNA processing 1 homolog B (S. cerevisiae)	0.48	0.72	chr21q22.3	23076
29	GLRX	glutaredoxin (thioltransferase)	0.48	0.72	chr5q14	2745
30	FAM26F	family with sequence similarity 26 member F	0.48	0.72	chr6q22.1	441168
31	NUS1	nuclear undecaprenyl pyrophosphate synthase 1 homolog (S. cerevisiae) /// nuclear undecaprenyl pyrophosphate synthase 1 homolog (S. cerevisiae) pseudogene 3	0.48	0.72	chr13q12	11049
32	ELK4	ELK4 ETS-domain protein (SRF accessory protein 1)	0.47	0.72	chr1q32	2005
33	TRIM38	tripartite motif-containing 38	0.47	0.72	chr6p21.3	10475
34	LTV1	LTV1 homolog (S. cerevisiae)	0.47	0.72	chr6q24.2	84946
35	MANEA	mannosidase endo-alpha	0.47	0.72	chr6q16.1	79694
36	DTX3L	deltex 3-like (Drosophila)	0.47	0.72	chr3q21.1	151636
37	TMEM123	transmembrane protein 123	0.47	0.72	chr11q22.1	114908
38	ATP2C1	ATPase Ca++ transporting type 2C member 1	0.47	0.72	chr3q22.1	27032
39	IFNAR2	interferon (alpha beta and omega) receptor 2	0.47	0.72	chr21q22.1|21q22.11	3455
40	CD58	CD58 molecule	0.47	0.72	chr1p13	965
41	PPPDE2	PPPDE peptidase domain containing 2	0.47	0.72	chr22q13.2	27351
42	AK4	adenylate kinase 4	0.47	0.72	chr1p31.3	205

Genes positively correlated with median k_{ep} at baseline (Retrospective study)

S No	Gene Symbol	Gene Title	Numerator(r)	q-value(%)	Chromosomal Location	Entrez Gene
43	BRP44L	brain protein 44-like	0.47	0.72	chr6q27	51660
44	ILF2	interleukin enhancer binding factor 2 45kDa	0.47	0.72	chr1q21.3	3608
45	GLIPR2	GLI pathogenesis-related 2	0.47	0.72	chr9p13.3	152007
46	MTSS1L	metastasis suppressor 1-like	0.46	0.72	chr16q22.1	92154
47	FAM111B	family with sequence similarity 111 member B	0.46	0.72	chr11q12.1	374393
48	DCBLD1	discoidin CUB and LCCL domain containing 1	0.46	0.72	chr6q22.1	285761
49	HLA-A	major histocompatibility complex class I A	0.46	0.72	chr6p21.3	3105
50	LOC100190939	hypothetical LOC100190939	0.46	0.72	chr13q14.13	100190939
51	DEK	DEK oncogene	0.46	0.72	chr6p22.3	7913
52	PDK1	pyruvate dehydrogenase kinase isozyme 1	0.46	0.72	chr2q31.1	5163
53	FBXO5	F-box protein 5	0.46	0.72	chr6q25.2	26271
54	C9orf95	chromosome 9 open reading frame 95	0.46	0.72	chr9q21.13	54981
55	USP31	ubiquitin specific peptidase 31	0.46	0.72	chr16p12.2	57478
56	PDK3	pyruvate dehydrogenase kinase isozyme 3	0.45	0.72	chrXp22.11	5165
57	LY75	lymphocyte antigen 75	0.45	0.72	chr2q24	4065
58	MPZL2	myelin protein zero-like 2	0.45	0.72	chr11q24	10205
59	IL6R	interleukin 6 receptor	0.45	0.72	chr1q21	3570
60	PRIM2	primase DNA polypeptide 2 (58kDa)	0.45	0.72	chr6p12-p11.1	5558
61	AIDA	axin interactor dorsalization associated	0.45	0.72	chr1q41	64853
62	ATP13A3	ATPase type 13A3	0.45	0.72	chr3q29	79572
63	MUTED	muted homolog (mouse) /// thioredoxin domain containing 5 (endoplasmic reticulum)	0.45	0.72	chr6p24.3	63915
64	PTPN14	protein tyrosine phosphatase non-receptor type 14	0.45	0.72	chr1q32.2	5784
65	GNPTAB	N-acetylglucosamine-1-phosphate transferase alpha and beta subunits	0.45	0.72	chr12q23.2	79158
66	TLR2	toll-like receptor 2	0.45	0.72	chr4q32	7097
67	PIK3AP1	phosphoinositide-3-kinase adaptor protein 1	0.45	0.72	chr10q24.1	118788
68	GK	glycerol kinase	0.45	0.72	chrXp21.3	2710
69	LTF	lactotransferrin	0.45	0.72	chr3p21.31	4057
70	C16orf61	chromosome 16 open reading frame 61	0.45	1.06	chr16q23.2	56942
71	PRPS2	phosphoribosyl pyrophosphate synthetase 2	0.44	1.06	chrXp22.3-p22.2	5634
72	MCM3AP-AS	MCM3AP antisense RNA (non-protein coding)	0.44	1.06	chr21q22.3	114044
73	C19orf2	Chromosome 19 open reading frame 2	0.44	1.06	chr19q12	8725
74	SOD2	Superoxide dismutase 2 mitochondrial	0.44	1.06	chr6q25.3	6648
75	FOXK1	forkhead box K1	0.44	1.06	chr7p22.1	221937
76	RARS2	arginyl-tRNA synthetase 2 mitochondrial	0.44	1.06	chr6q16.1	57038
77	ZNF146	zinc finger protein 146	0.44	1.06	chr19q13.1	7705
78	NMI	N-myc (and STAT) interactor	0.44	1.06	chr2q23	9111
79	FCF1	FCF1 small subunit (SSU) processome component homolog (S. cerevisiae) /// rRNA-processing protein FCF1 homolog /// mitogen-activated protein kinase 1 interacting protein 1-like	0.44	1.06	chr14q22.3	100507758
80	NCOA7	nuclear receptor coactivator 7	0.44	1.06	chr6q22.32	135112
81	APTX	aprataxin	0.44	1.06	chr9p13.3	54840
82	MNDA	myeloid cell nuclear differentiation antigen	0.44	1.06	chr1q22	4332
83	MYO10	myosin X	0.44	1.06	chr5p15.1-p14.3	4651
84	PERP	PERP TP53 apoptosis effector	0.44	1.06	chr6q24	64065
85	PLSCR1	phospholipid scramblase 1	0.44	1.06	chr3q23	5359
86	PAPOLA	poly(A) polymerase alpha	0.44	1.06	chr14q32.31	10914
87	RAB27A	RAB27A member RAS oncogene family	0.44	1.06	chr15q15-q21.1	5873
88	DEPDC1	DEP domain containing 1	0.43	1.06	chr1p31.2	55635

Genes positively correlated with median k_{ep} at baseline (Retrospective study)

S No	Gene Symbol	Gene Title	Numerator(r)	q-value(%)	Chromosomal Location	Entrez Gene
89	PTPLB	protein tyrosine phosphatase-like (proline instead of catalytic arginine) member b	0.43	1.06	chr3q21.1	201562
90	C14orf2	chromosome 14 open reading frame 2	0.43	1.06	chr14q32.33	9556
91	OPTN	optineurin	0.43	1.06	chr10p13	10133
92	DAPK1	death-associated protein kinase 1	0.43	1.06	chr9q34.1	1612
93	ORC6	origin recognition complex subunit 6	0.43	1.06	chr16q12	23594
94	LYZ	lysozyme	0.43	1.06	chr12q15	4069
95	HLA-C	major histocompatibility complex class I C	0.43	1.06	chr6p21.3	3107
96	HLA-DQA1	major histocompatibility complex class II DQ alpha 1 /// major histocompatibility complex class II DQ alpha 2	0.43	1.06	chr6p21.3	3117
97	FAM46A	family with sequence similarity 46 member A	0.43	1.06	chr6q14	55603
98	CCR1	chemokine (C-C motif) receptor 1	0.43	1.06	chr3p21	1230
99	HECA	headcase homolog (Drosophila)	0.43	1.06	chr6q23-q24	51696
100	RAD1	RAD1 homolog (S. pombe)	0.43	1.06	chr5p13.2	5810
101	ZBTB33	zinc finger and BTB domain containing 33	0.43	1.06	chrXq23	10009
102	OBFC2A	oligonucleotide/oligosaccharide-binding fold containing 2A	0.43	1.06	chr2q32.3	64859
103	CREG1	cellular repressor of E1A-stimulated genes 1	0.43	1.06	chr1q24	8804
104	HMGN3	high mobility group nucleosomal binding domain 3	0.43	1.06	chr6q14.1	9324
105	LPIN1	lipin 1	0.43	1.06	chr2p25.1	23175
106	PRNP	prion protein	0.42	1.06	chr20p13	5621
107	DIP2A	DIP2 disco-interacting protein 2 homolog A (Drosophila)	0.42	1.06	chr21q22.3	23181
108	GNB4	guanine nucleotide binding protein (G protein) beta polypeptide 4	0.42	1.06	chr3q26.33	59345
109	DNAJA1	DnaJ (Hsp40) homolog subfamily A member 1	0.42	1.06	chr9p13.3	3301
110	RHEB	Ras homolog enriched in brain	0.42	1.06	chr7q36	6009
111	MRPL9	mitochondrial ribosomal protein L9	0.42	1.06	chr1q21	65005
112	ESYT2	extended synaptotagmin-like protein 2	0.42	1.06	chr7q36.3	57488
113	B2M	beta-2-microglobulin	0.42	1.06	chr15q21-q22.2	567
114	UGGT1	UDP-glucose glycoprotein glucosyltransferase 1	0.42	1.06	chr2q14.3	56886
115	CCDC99	coiled-coil domain containing 99	0.42	1.06	chr5q35.1	54908
116	B3GALNT2	beta-13-N-acetylgalactosaminyltransferase 2	0.42	1.06	chr1q42.3	148789
117	PFKP	phosphofructokinase platelet	0.42	1.06	chr10p15.3-p15.2	5214
118	SLC7A1	solute carrier family 7 (cationic amino acid transporter y+ system) member 1	0.42	1.06	chr13q12-q14	6541
119	ACTR3	ARP3 actin-related protein 3 homolog (yeast)	0.42	1.06	chr2q14.1	10096
120	CD44	CD44 molecule (Indian blood group)	0.42	1.06	chr11p13	960
121	IFNGR1	interferon gamma receptor 1	0.42	1.06	chr6q23.3	3459
122	STK17A	serine/threonine kinase 17a	0.42	1.06	chr7p13	9263
123	UCHL3	ubiquitin carboxyl-terminal esterase L3 (ubiquitin thiolesterase)	0.42	1.06	chr13q22.2	7347
124	CENPW	centromere protein W	0.42	1.06	chr6q22.32	387103
125	ANP32E	acidic (leucine-rich) nuclear phosphoprotein 32 family member E	0.42	1.06	chr1q21.2	81611
126	PCNA	proliferating cell nuclear antigen	0.42	1.06	chr20pter-p12	5111
127	DLAT	dihydrolipoamide S-acetyltransferase	0.42	1.06	chr11q23.1	1737
128	F11R	F11 receptor	0.42	1.06	chr1q21.2-q21.3	50848
129	CRY1	cryptochrome 1 (photolyase-like)	0.42	1.06	chr12q23-q24.1	1407
130	ERI1	exoribonuclease 1	0.42	1.06	chr8p23.1	90459
131	TRIM14	tripartite motif-containing 14	0.42	1.06	chr9q22.33	9830
132	ADCY7	adenylate cyclase 7	0.42	1.06	chr16q12.1	113
133	C9orf72	chromosome 9 open reading frame 72	0.42	1.06	chr9p21.2	203228
134	LOC283508	hypothetical protein LOC283508	0.42	1.99	chr13q13.3	283508

Genes positively correlated with median k_{ep} at baseline (Retrospective study)

S No	Gene Symbol	Gene Title	Numerator(r)	q-value(%)	Chromosomal Location	Entrez Gene
135	HIF1A	hypoxia inducible factor 1 alpha subunit (basic helix-loop-helix transcription factor)	0.42	1.99	chr14q23.2	3091
136	VTA1	Vps20-associated 1 homolog (S. cerevisiae)	0.42	1.99	chr6q24.1	51534
137	KHDRBS3	KH domain containing RNA binding signal transduction associated 3	0.41	1.99	chr8q24.2	10656
138	TANK	TRAF family member-associated NFKB activator	0.41	1.99	chr2q24-q31	10010
139	RWDD1	RWD domain containing 1	0.41	1.99	chr6q13-q22.33	51389
140	SYK	spleen tyrosine kinase	0.41	1.99	chr9q22	6850
141	ERH	enhancer of rudimentary homolog (Drosophila)	0.41	1.99	chr14q24.1|7q34	2079
142	E2F3	E2F transcription factor 3	0.41	1.99	chr6p22	1871
143	HBS1L	HBS1-like (S. cerevisiae)	0.41	1.99	chr6q23.3	10767
144	CHAF1A	chromatin assembly factor 1 subunit A (p150)	0.41	1.99	chr19p13.3	10036
145	VASH2	vasohibin 2	0.41	1.99	chr1q32.3	79805
146	CARD16	caspase recruitment domain family member 16 /// caspase 1 apoptosis-related cysteine peptidase (interleukin 1 beta convertase)	0.41	1.99	chr11q23	114769
147	OAT	ornithine aminotransferase	0.41	1.99	chr10q26	4942
148	CLEC7A	C-type lectin domain family 7 member A	0.41	1.99	chr12p13.2	64581
149	HSPA13	heat shock protein 70kDa family member 13	0.41	1.99	chr21q11.1|21q11	6782
150	SAMSN1	SAM domain SH3 domain and nuclear localization signals 1	0.41	1.99	chr21q11	64092
151	ATF6	activating transcription factor 6	0.41	1.99	chr1q22-q23	22926
152	CEP170	centrosomal protein 170kDa	0.41	1.99	chr1q44	9859
153	RARRES1	retinoic acid receptor responder (tazarotene induced) 1	0.41	1.99	chr3q25.32	5918
154	CBR3	carbonyl reductase 3	0.41	1.99	chr21q22.2	874
155	HYOU1	hypoxia up-regulated 1	0.41	1.99	chr11q23.1-q23.3	10525
156	ARHGAP18	Rho GTPase activating protein 18	0.41	1.99	chr6q22.33	93663
157	GBP2	guanylate binding protein 2 interferon-inducible	0.41	1.99	chr1p22.2	2634
158	U2AF1	U2 small nuclear RNA auxiliary factor 1	0.41	1.99	chr21q22.3	7307
159	STAT1	signal transducer and activator of transcription 1 91kDa	0.41	1.99	chr2q32.2	6772
160	SENP6	SUMO1/sentrin specific peptidase 6	0.41	1.99	chr6q13-q14.3	26054
161	PM20D2	peptidase M20 domain containing 2	0.41	1.99	chr6q15	135293
162	BRIX1	BRX1 biogenesis of ribosomes homolog (S. cerevisiae)	0.41	1.99	chr5p13.2	55299
163	SCARF1	scavenger receptor class F member 1	0.41	1.99	chr17p13.3	8578
164	AQP3	aquaporin 3 (Gill blood group)	0.41	1.99	chr9p13	360
165	SRPK1	SRSF protein kinase 1	0.41	1.99	chr6p21.31	6732
166	FCER1G	Fc fragment of IgE high affinity I receptor for; gamma polypeptide	0.41	1.99	chr1q23	2207
167	HMMR	hyaluronan-mediated motility receptor (RHAMM)	0.41	1.99	chr5q33.2-qter	3161
168	EBP	emopamil binding protein (sterol isomerase)	0.41	1.99	chrXp11.23-p11.22	10682
169	NOM1	nucleolar protein with MIF4G domain 1	0.41	1.99	chr7q36.3	64434
170	ZNF695	zinc finger protein 695	0.41	1.99	chr1q44	57116
171	SPIN4	spindlin family member 4	0.41	1.99	chrXq11.1	139886
172	PCDHB2	protocadherin beta 2	0.41	1.99	chr5q31	56133
173	CRYAB	crystallin alpha B	0.41	1.99	chr11q22.3-q23.1	1410
174	CDC40	cell division cycle 40 homolog (S. cerevisiae)	0.41	1.99	chr6q21	51362
175	CSTB	cystatin B (stefin B)	0.41	1.99	chr21q22.3	1476
176	UBE2D1	ubiquitin-conjugating enzyme E2D 1 (UBC4/5 homolog yeast)	0.41	1.99	chr10q21.1	7321
177	CTSC	cathepsin C	0.41	1.99	chr11q14.2	1075
178	BEX2	brain expressed X-linked 2	0.40	1.99	chrXq22	84707

Genes positively correlated with median k_{ep} at baseline (Retrospective study)

S No	Gene Symbol	Gene Title	Numerator(r)	q-value(%)	Chromosomal Location	Entrez Gene
179	RASSF4	Ras association (RalGDS/AF-6) domain family member 4	0.40	1.99	chr10q11.21	83937
180	TOMM5	translocase of outer mitochondrial membrane 5 homolog (yeast)	0.40	1.99	chr9p13.2	401505
181	PDXK	pyridoxal (pyridoxine vitamin B6) kinase	0.40	1.99	chr21q22.3	8566
182	IVNS1ABP	influenza virus NS1A binding protein	0.40	1.99	chr1q25.1-q31.1	10625
183	B4GALT1	UDP-Gal:betaGlcNAc beta 14-galactosyltransferase polypeptide 1	0.40	1.99	chr9p13	2683
184	MED4	mediator complex subunit 4	0.40	1.99	chr13q14.2	29079
185	SLC9A6	solute carrier family 9 (sodium/hydrogen exchanger) member 6	0.40	1.99	chrXq26.3	10479
186	C12orf4	chromosome 12 open reading frame 4	0.40	1.99	chr12p13.3	57102
187	HLA-DRB1	major histocompatibility complex class II DR beta 1 /// major histocompatibility complex class II DR beta 4	0.40	1.99	chr6p21.3	3123
188	NLRC5	NLR family CARD domain containing 5	0.40	1.99	chr16q13	84166
189	AKIRIN2	akirin 2	0.40	1.99	chr6q15	55122
190	HCP5	HLA complex P5	0.40	1.99	chr6p21.3	10866
191	C9orf40	chromosome 9 open reading frame 40	0.40	1.99	chr9q21.13	55071
192	RAP2A	RAP2A member of RAS oncogene family	0.40	1.99	chr13q34	5911
193	CDC25B	cell division cycle 25 homolog B (S. pombe)	0.40	1.99	chr20p13	994
194	SCO2	SCO cytochrome oxidase deficient homolog 2 (yeast)	0.40	1.99	chr22q13.33	9997
195	IFIH1	interferon induced with helicase C domain 1	0.40	1.99	chr2q24	64135
196	PPA1	pyrophosphatase (inorganic) 1	0.40	1.99	chr10q11.1-q24	5464
197	PCMT1	protein-L-isoaspartate (D-aspartate) O-methyltransferase	0.40	1.99	chr6q24-q25	5110
198	SLC16A1	solute carrier family 16 member 1 (monocarboxylic acid transporter 1)	0.40	1.99	chr1p12	6566
199	CA13	carbonic anhydrase XIII	0.40	1.99	chr8q21.2	377677
200	AMD1	adenosylmethionine decarboxylase 1	0.40	1.99	chr6q21	262
201	KARS	lysyl-tRNA synthetase	0.40	1.99	chr16q23.1	3735
202	CSDA	cold shock domain protein A	0.40	1.99	chr12p13.1	8531
203	LBR	lamin B receptor	0.40	1.99	chr1q42.1	3930
204	ZNF267	zinc finger protein 267	0.40	1.99	chr16p11.2	10308
205	SR140	U2-associated SR140 protein	0.40	1.99	chr3q23	23350
206	TOR3A	torsin family 3 member A	0.40	1.99	chr1q25.2	64222
207	HSF2	heat shock transcription factor 2	0.40	1.99	chr6q22.31	3298
208	MDN1	MDN1 midasin homolog (yeast)	0.40	1.99	chr6q15	23195
209	YOD1	YOD1 OTU deubiquinating enzyme 1 homolog (S. cerevisiae)	0.40	1.99	chr1q32.2	55432
210	LOC441454	prothymosin alpha pseudogene	0.40	1.99	chr9q22.33	441454
211	RSU1	Ras suppressor protein 1	0.40	1.99	chr10p13	6251
212	ZDHHC20	zinc finger DHHC-type containing 20	0.40	1.99	chr13q12.11	253832
213	ERAP1	endoplasmic reticulum aminopeptidase 1	0.40	1.99	chr5q15	51752
214	ZNF22	zinc finger protein 22 (KOX 15)	0.40	1.99	chr10q11	7570
215	DDX21	DEAD (Asp-Glu-Ala-Asp) box polypeptide 21	0.40	1.99	chr10q21	9188
216	CBL	Cas-Br-M (murine) ecotropic retroviral transforming sequence	0.40	1.99	chr11q23.3	867
217	RNASET2	ribonuclease T2	0.40	1.99	chr6q27	8635
218	SDHD	succinate dehydrogenase complex subunit D integral membrane protein	0.40	1.99	chr11q23	6392
219	MLKL	mixed lineage kinase domain-like	0.39	1.99	chr16q23.1	197259
220	CMPK2	cytidine monophosphate (UMP-CMP) kinase 2 mitochondrial	0.39	1.99	chr2p25.2	129607
221	CDC37L1	cell division cycle 37 homolog (S. cerevisiae)-like 1	0.39	1.99	chr9p24.1	55664
222	DYNC1H1	dynein cytoplasmic 1 heavy chain 1	0.39	1.99	chr14q32.3-qter|14q32	1778
223	CXorf38	chromosome X open reading frame 38	0.39	1.99	chrXp11.4	159013
224	KIAA1826	KIAA1826	0.39	1.99	chr11q22	84437

Genes positively correlated with median k_{ep} at baseline (Retrospective study)

S No	Gene Symbol	Gene Title	Numerator(r)	q-value(%)	Chromosomal Location	Entrez Gene
225	OSBPL3	oxysterol binding protein-like 3	0.39	1.99	chr7p15	26031
226	ASF1A	ASF1 anti-silencing function 1 homolog A (S. cerevisiae)	0.39	1.99	chr6q22.31	25842
227	MFSD1	major facilitator superfamily domain containing 1	0.39	1.99	chr3q25.32	64747
228	HLA-DRA	major histocompatibility complex class II DR alpha	0.39	1.99	chr6p21.3	3122
229	MCTS1	malignant T cell amplified sequence 1	0.39	1.99	chrXq24	28985
230	ELL2	elongation factor RNA polymerase II 2	0.39	1.99	chr5q15	22936
231	SLC35B3	solute carrier family 35 member B3	0.39	1.99	chr6p24.3	51000
232	CBFB	core-binding factor beta subunit	0.39	1.99	chr16q22.1	865
233	POLR1D	polymerase (RNA) I polypeptide D 16kDa	0.39	1.99	chr13q12.2	51082
234	LRRC58	leucine rich repeat containing 58	0.39	1.99	chr3q13.33	116064
235	UBAP2	ubiquitin associated protein 2	0.39	2.27	chr9p13.3	55833
236	EIF2AK2	eukaryotic translation initiation factor 2-alpha kinase 2	0.39	2.27	chr2p22-p21	5610
237	MARCH7	membrane-associated ring finger (C3HC4) 7	0.39	2.27	chr2q24.2	64844
238	NFX1	nuclear transcription factor X-box binding 1	0.39	2.27	chr9p13.3	4799
239	RAD51AP1	RAD51 associated protein 1	0.39	2.27	chr12p13.2-p13.1	10635
240	IFI44	interferon-induced protein 44	0.39	2.27	chr1p31.1	10561
241	C21orf91	chromosome 21 open reading frame 91	0.39	2.27	chr21q21.1	54149
242	PTAR1	protein prenyltransferase alpha subunit repeat containing 1	0.39	2.27	chr9q21.12	375743
243	FKBP11	FK506 binding protein 11 19 kDa	0.39	2.27	chr12q13.12	51303
244	SDCBP	syndecan binding protein (syntenin)	0.39	2.27	chr8q12	6386
245	SLC31A1	solute carrier family 31 (copper transporters) member 1	0.39	2.27	chr9q31-q32	1317
246	SEC63	SEC63 homolog (S. cerevisiae)	0.39	2.27	chr6q21	11231
247	CCDC14	coiled-coil domain containing 14	0.39	2.27	chr3q21.1	64770
248	G3BP1	GTPase activating protein (SH3 domain) binding protein 1	0.39	2.27	chr5q33.1	10146
249	HPRT1	hypoxanthine phosphoribosyltransferase 1	0.39	2.27	chrXq26.1	3251
250	TARS	threonyl-tRNA synthetase	0.39	2.27	chr5p13.2	6897
251	MFSD6	major facilitator superfamily domain containing 6	0.39	2.27	chr2q32.2	54842
252	GART	phosphoribosylglycinamide formyltransferase phosphoribosylglycinamide synthetase phosphoribosylaminoimidazole synthetase	0.39	2.27	chr21q22.1|21q22.11	2618
253	RCAN1	regulator of calcineurin 1	0.39	2.27	chr21q22.1-q22.2|21q22.12	1827
254	MRPL18	mitochondrial ribosomal protein L18	0.39	2.27	chr6q25.3	29074
255	GTF2H5	general transcription factor IIH polypeptide 5	0.39	2.27	chr6q25.3	404672
256	MCFD2	multiple coagulation factor deficiency 2	0.39	2.27	chr2p21	90411
257	ATP5L	ATP synthase H+ transporting mitochondrial Fo complex subunit G	0.39	2.27	chr11q23.3	10632
258	HLA-B	major histocompatibility complex class I B	0.39	2.27	chr6p21.3	3106
259	ATR	ataxia telangiectasia and Rad3 related	0.39	2.27	chr3q22-q24	545
260	FMNL2	formin-like 2	0.38	2.27	chr2q23.3	114793
261	SCPEP1	serine carboxypeptidase 1	0.38	2.27	chr17q22	59342
262	ADAMDEC1	ADAM-like decysin 1	0.38	2.27	chr8p21.2	27299
263	MTHFD1	methylenetetrahydrofolate dehydrogenase (NADP+ dependent) 1 methenyltetrahydrofolate cyclohydrolase formyltetrahydrofolate synthetase	0.38	2.27	chr14q24	4522
264	CLTA	clathrin light chain A	0.38	2.27	chr9p13	1211
265	LOC650794	hypothetical LOC650794	0.38	2.27	chr13q12.11	650794
266	ZNF410	zinc finger protein 410	0.38	2.27	chr14q24.3	57862
267	SERBP1	SERPINE1 mRNA binding protein 1	0.38	2.27	chr1p31	26135

Genes positively correlated with median k_{ep} at baseline (Retrospective study)

S No	Gene Symbol	Gene Title	Numerator(r)	q-value(%)	Chromosomal Location	Entrez Gene
268	VRK1	vaccinia related kinase 1	0.38	2.27	chr14q32	7443
269	ITGA6	integrin alpha 6	0.38	2.27	chr2q31.1	3655
270	TLE1	transducin-like enhancer of split 1 (E(sp1) homolog Drosophila)	0.38	2.27	chr9q21.32	7088
271	EIF2AK1	eukaryotic translation initiation factor 2-alpha kinase 1	0.38	2.27	chr7p22	27102
272	C11orf75	chromosome 11 open reading frame 75	0.38	2.27	chr11q21	56935
273	NCK1	NCK adaptor protein 1	0.38	2.27	chr3q21	4690
274	INTS7	integrator complex subunit 7	0.38	2.27	chr1p36.13-q42.3	25896
275	HAUS6	HAUS augmin-like complex subunit 6	0.38	2.27	chr9p22.1	54801
276	TMX2	thioredoxin-related transmembrane protein 2	0.38	2.27	chr11cen-q22.3	51075
277	C1orf96	chromosome 1 open reading frame 96	0.38	2.27	chr1q42.13	126731
278	R3HDM1	R3H domain containing 1	0.38	2.27	chr2q21.3	23518
279	DIMT1L	DIM1 dimethyladenosine transferase 1-like (S. cerevisiae)	0.38	2.27	chr5q12.1	27292
280	FDPS	farnesyl diphosphate synthase	0.38	2.27	chr1q22	2224
281	SIM2	single-minded homolog 2 (Drosophila)	0.38	2.27	chr21q22.2|21q22.13	6493
282	STX6	syntaxin 6	0.38	2.27	chr1q25.3	10228
283	WDR89	WD repeat domain 89	0.38	2.27	chr14q23.2	112840
284	LOC100509231	ovostatin homolog 2-like /// ovostatin homolog 2-like /// ovostatin 2	0.38	2.27	chr12p11.21	100509231
285	ALDH1A3	aldehyde dehydrogenase 1 family member A3	0.38	2.27	chr15q26.3	220
286	IQGAP3	IQ motif containing GTPase activating protein 3	0.38	2.27	chr1q21.3	128239
287	EDEM3	ER degradation enhancer mannosidase alpha-like 3	0.38	2.27	chr1q25	80267
288	SSFA2	sperm specific antigen 2	0.38	2.27	chr2q31.3	6744
289	PRDX6	peroxiredoxin 6	0.38	2.27	chr1q25.1	9588
290	RASA2	RAS p21 protein activator 2	0.38	2.27	chr3q22-q23	5922
291	KYNU	kynureninase (L-kynurenine hydrolase)	0.38	2.27	chr2q22.2	8942
292	HEBP2	heme binding protein 2	0.38	2.27	chr6q24	23593
293	COMMD2	COMM domain containing 2	0.38	2.27	chr3q25.1	51122
294	CENPN	centromere protein N	0.38	2.27	chr16q23.2	55839
295	PPP2R5E	protein phosphatase 2 regulatory subunit B' epsilon isoform	0.38	2.27	chr14q23.1	5529
296	SGMS1	sphingomyelin synthase 1	0.38	2.27	chr10q11.2	259230
297	BID	BH3 interacting domain death agonist	0.38	2.27	chr22q11.1	637
298	TGS1	trimethylguanosine synthase 1	0.38	2.27	chr8q11	96764
299	RNF146	ring finger protein 146	0.38	2.71	chr6q22.1-q22.33	81847
300	CD163	CD163 molecule	0.38	2.71	chr12p13.3	9332
301	CCT6A	chaperonin containing TCP1 subunit 6A (zeta 1)	0.38	2.71	chr7p11.2	908
302	RBM17	RNA binding motif protein 17	0.38	2.71	chr10p15.1	84991
303	FANCD2	Fanconi anemia complementation group D2	0.38	2.71	chr3p26	2177
304	PEA15	phosphoprotein enriched in astrocytes 15	0.38	2.71	chr1q21.1	8682
305	CLNS1A	chloride channel nucleotide-sensitive 1A	0.38	2.71	chr11q13.5-q14	1207
306	FANCB	Fanconi anemia complementation group B	0.38	2.71	chrXp22.2	2187
307	IL21R	interleukin 21 receptor	0.38	2.71	chr16p11	50615
308	SEC61B	Sec61 beta subunit	0.38	2.71	chr9q22.32-q31.3	10952
309	LITAF	lipopolysaccharide-induced TNF factor	0.38	2.71	chr16p13.13	9516
310	MAX	MYC associated factor X	0.38	2.71	chr14q23	4149
311	FLJ31958	hypothetical LOC143153	0.38	2.71	chr10q11.23	143153
312	CP	ceruloplasmin (ferroxidase)	0.38	2.71	chr3q23-q25	1356
313	PSMB1	proteasome (prosome macropain) subunit beta type 1	0.38	2.71	chr6q27	5689
314	HLA-E	major histocompatibility complex class I E	0.38	2.71	chr6p21.3	3133
315	SLC17A5	solute carrier family 17 (anion/sugar transporter) member 5	0.38	2.71	chr6q14-q15	26503
316	ENSA	endosulfine alpha	0.38	2.71	chr1q21.3	2029
317	DSCR3	Down syndrome critical region gene 3	0.38	2.71	chr21q22.2	10311

Genes positively correlated with median k_{ep} at baseline (Retrospective study)

S No	Gene Symbol	Gene Title	Numerator(r)	q-value(%)	Chromosomal Location	Entrez Gene
318	IFI16	interferon gamma-inducible protein 16	0.38	2.71	chr1q22	3428
319	NAA50	N(alpha)-acetyltransferase 50 NatE catalytic subunit	0.37	2.71	chr3q13.2	80218
320	EPHB2	EPH receptor B2	0.37	2.71	chr1p36.1-p35	2048
321	SGOL2	shugoshin-like 2 (S. pombe)	0.37	2.71	chr2q33.1	151246
322	CHMP5	chromatin modifying protein 5	0.37	2.71	chr9p13.3	51510
323	ATP11B	ATPase class VI type 11B	0.37	2.71	chr3q27	23200
324	C1orf107	chromosome 1 open reading frame 107	0.37	2.71	chr1q32.2	27042
325	APOL3	apolipoprotein L 3	0.37	2.71	chr22q13.1	80833
326	KDM5A	lysine (K)-specific demethylase 5A	0.37	2.71	chr12p11	5927
327	VCP	valosin-containing protein	0.37	2.71	chr9p13.3	7415
328	SFT2D1	SFT2 domain containing 1	0.37	2.71	chr6q27	113402

Appendix 5.1

Genes upregulated after bevacizumab therapy (Prospective study)

S No	Gene Symbol	Gene Name	Fold Change	Q value	Transcript Cluster ID	Entrez Gene ID	Chromosome
1	CCL14-CCL15	CCL14-CCL15 read-through transcript	1.989	1.220	3753966	348249	17
2	PDE3B	phosphodiesterase 3B, cGMP-inhibited	1.813	0.000	3321512	5140	11
3	PCOLCE2	procollagen C-endopeptidase enhancer 2	1.754	3.409	2698996	26577	3
4	OLFM1	olfactomedin 1	1.753	2.340	3193725	10439	9
5	CCL19	chemokine (C-C motif) ligand 19	1.748	1.220	3204285	6363	9
6	COLEC12	collectin sub-family member 12	1.736	0.000	3795733	81035	18
7	ABI3BP	ABI family, member 3 (NESH) binding protein	1.731	1.220	2686458	25890	3
8	LOC100510059	HLA class II histocompatibility antigen, DQ alpha 1 chain-like	1.705	2.340	2903219	100510059	6
9	LRMP	lymphoid-restricted membrane protein	1.701	0.000	3408505	4033	12
10	ANKRD29	ankyrin repeat domain 29	1.699	0.000	3801492	147463	18
11	C7	complement component 7	1.673	2.340	2807716	730	5
12	PDK4	pyruvate dehydrogenase kinase, isozyme 4	1.662	1.220	3062082	5166	7
13	BTLA	B and T lymphocyte associated	1.656	1.220	2688717	151888	3
14	TF /// SRPRB	transferrin /// signal recognition particle receptor, B subunit	1.651	4.663	2643217	7018 /// 58477	3
15	CD28	CD28 molecule	1.646	0.000	2523801	940	2
16	CTLA4	cytotoxic T-lymphocyte-associated protein 4	1.645	0.000	2523855	1493	2
17	BANK1	B-cell scaffold protein with ankyrin repeats 1	1.632	0.000	2737596	55024	4
18	SFRP4	secreted frizzled-related protein 4	1.631	3.409	3046444	6424	7
19	GZMK	granzyme K (granzyme 3; tryptase II)	1.625	0.000	2809793	3003	5
20	FAIM3	Fas apoptotic inhibitory molecule 3	1.617	1.220	2452977	9214	1
21	CPA3	carboxypeptidase A3 (mast cell)	1.614	0.000	2647109	1359	3
22	ABCD2	ATP-binding cassette, sub-family D (ALD), member 2	1.612	3.409	3450861	225	12
23	STAT4	signal transducer and activator of transcription 4	1.610	2.340	2592356	6775	2
24	TRAT1	T cell receptor associated transmembrane adaptor 1	1.609	0.000	2635349	50852	3
25	SLC19A3	solute carrier family 19, member 3	1.605	4.663	2602403	80704	2
26	CD3D	CD3d molecule, delta (CD3-TCR complex)	1.599	0.000	3393744	915	11
27	CILP	cartilage intermediate layer protein, nucleotide pyrophosphohydrolase	1.591	0.000	3629529	8483	15
28	PZP	pregnancy-zone protein	1.589	0.000	3443464	5858	12
29	ABCA6	ATP-binding cassette, sub-family A (ABC1), member 6	1.583	3.409	3768791	23460	17
30	RBP7	retinol binding protein 7, cellular	1.582	2.340	2319550	116362	1
31	SCN7A	sodium channel, voltage-gated, type VII, alpha	1.577	0.000	2585476	6332	2
32	PARP15	poly (ADP-ribose) polymerase family, member 15	1.577	1.220	2638988	165631	3
33	RGS13	regulator of G-protein signaling 13	1.572	0.000	2372812	6003	1
34	ADAMDEC1	ADAM-like, decysin 1	1.552	1.220	3090294	27299	8
35	CLEC9A	C-type lectin domain family 9, member A	1.548	1.220	3404567	283420	12
36	CD86	CD86 molecule	1.541	4.663	2638789	942	3
37	PPARG	peroxisome proliferator-activated receptor gamma	1.533	3.409	2611056	5468	3
38	SPP1	secreted phosphoprotein 1	1.531	3.409	2735027	6696	4
39	ABCB5	ATP-binding cassette, sub-family B (MDR/TAP), member 5	1.530	3.409	2991995	340273	7
40	IL7R	interleukin 7 receptor	1.528	1.220	2806468	3575	5
41	FAM65B	family with sequence similarity 65, member B	1.524	0.000	2945741	9750	6
42	FAT4	FAT tumor suppressor homolog 4 (Drosophila)	1.523	4.663	2742581	79633	4
43	IRF8	interferon regulatory factor 8	1.516	1.220	3672489	3394	16
44	LIFR	leukemia inhibitory factor receptor alpha	1.513	3.409	2854092	3977	5
45	CD163	CD163 molecule	1.512	1.220	3442706	9332	12
46	MMRN1	multimerin 1	1.512	4.663	2735759	22915	4
47	NOVA1	neuro-oncological ventral antigen 1	1.510	2.340	3558745	4857	14
48	IKZF3	IKAROS family zinc finger 3 (Aiolos)	1.507	0.000	3755862	22806	17
49	SH2D1A	SH2 domain containing 1A	1.506	1.220	3989826	4068	X
50	AKR1C3	aldo-keto reductase family 1, member C3 (3-alpha hydroxysteroid dehydrogenase, type II)	1.506	4.663	3233049	8644	10
51	CLEC4E	C-type lectin domain family 4, member E	1.505	1.220	3443183	26253	12
52	RGS1	regulator of G-protein signaling 1	1.505	4.663	2372781	5996	1
53	SOCS2	suppressor of cytokine signaling 2	1.499	4.663	3426257	8835	12
54	PIK3IP1	phosphoinositide-3-kinase interacting protein 1	1.496	0.000	3957790	113791	22
55	CD27 /// LOC678655	CD27 molecule /// hypothetical locus LOC678655	1.495	0.000	3402506	939 /// 678655	12
56	LY96	lymphocyte antigen 96	1.493	4.663	3103523	23643	8
57	PLIN2	perilipin 2	1.492	0.000	3200648	123	9
58	SEPP1	selenoprotein P, plasma, 1	1.490	1.220	2855285	6414	5

Genes upregulated after bevacizumab therapy (Prospective study)

S No	Gene Symbol	Gene Name	Fold Change	Q value	Transcript Cluster ID	Entrez Gene ID	Chromosome
59	HSD17B11	hydroxysteroid (17-beta) dehydrogenase 11	1.490	2.340	2777070	51170	4
60	AIM2	absent in melanoma 2	1.487	0.000	2439554	9447	1
61	SAMSN1 /// LOC388813	SAM domain, SH3 domain and nuclear localization signals 1 /// uncharacterized protein ENSP00000383407-like	1.484	0.000	3925473	64092 /// 388813	21
62	IRF4	interferon regulatory factor 4	1.477	2.340	2891341	3662	6
63	CD96	CD96 molecule	1.474	2.340	2635741	10225	3
64	CCDC69	coiled-coil domain containing 69	1.472	1.220	2881860	26112	5
65	PDK1	pyruvate dehydrogenase kinase, isozyme 1	1.471	1.220	2515707	5163	2
66	RASSF4	Ras association (RalGDS/AF-6) domain family member 4	1.471	3.409	3244488	83937	10
67	SLAMF7	SLAM family member 7	1.470	4.663	2363202	57823	1
68	MFAP4	microfibrillar-associated protein 4	1.470	2.340	3748798	4239	17
69	VNN2	vanin 2	1.469	2.340	2974635	8875	6
70	CXCL12	chemokine (C-X-C motif) ligand 12	1.468	2.340	3286602	6387	10
71	GZMA	granzyme A (granzyme 1, cytotoxic T-lymphocyte-associated serine esterase 3)	1.467	1.220	2809810	3001	5
72	ADRB2	adrenergic, beta-2-, receptor, surface	1.466	3.409	2834743	154	5
73	C5orf41	chromosome 5 open reading frame 41	1.464	1.220	2841491	153222	5
74	DPP4	dipeptidyl-peptidase 4	1.459	3.409	2584018	1803	2
75	IQGAP2	IQ motif containing GTPase activating protein 2	1.455	0.000	2816298	10788	5
76	TLR8	toll-like receptor 8	1.455	3.409	3969115	51311	X
77	SCD	stearoyl-CoA desaturase (delta-9-desaturase)	1.451	0.000	3260586	6319	10
78	GIMAP5 /// GIMAP1	GTPase, IMAP family member 5 /// GTPase, IMAP family member 1	1.448	4.663	3031573	55340 /// 170575	7
79	NELL2	NEL-like 2 (chicken)	1.448	4.663	3451814	4753	12
80	SLC22A3	solute carrier family 22 (extraneuronal monoamine transporter), member 3	1.447	1.220	2934521	6581	6
81	CDC42EP3	CDC42 effector protein (Rho GTPase binding) 3	1.443	0.000	2548617	10602	2
82	HELQ	helicase, POLQ-like	1.440	2.340	2776026	113510	4
83	KLRG1	killer cell lectin-like receptor subfamily G, member 1	1.439	0.000	3404030	10219	12
84	KLRB1	killer cell lectin-like receptor subfamily B, member 1	1.438	0.000	3443804	3820	12
85	KLHL6	kelch-like 6 (Drosophila)	1.438	1.220	2708066	89857	3
86	IL18R1	interleukin 18 receptor 1	1.437	1.220	2497119	8809	2
87	STEAP1 /// MGC87042	six transmembrane epithelial antigen of the prostate 1 /// STEAP family protein MGC87042	1.436	2.340	3011838	26872 /// 256227	7
88	TNMD	tenomodulin	1.435	3.409	3984445	64102	X
89	CLEC2D /// NPM1	C-type lectin domain family 2, member D /// nucleophosmin (nucleolar phosphoprotein B23, numatrin)	1.434	0.000	3404436	29121 /// 4869	12
90	POLR2J4 /// CCDC146	polymerase (RNA) II (DNA directed) polypeptide J4, pseudogene /// coiled-coil domain containing 146	1.431	4.663	3009838	84820 /// 57639	7
91	NPM1 /// LMBRD1	nucleophosmin (nucleolar phosphoprotein B23, numatrin) /// LMBR1 domain containing 1	1.429	4.663	2960010	4869 /// 55788	6
92	FAM13A	family with sequence similarity 13, member A	1.429	4.663	2777487	10144	4
93	CR1	complement component (3b/4b) receptor 1 (Knops blood group)	1.429	3.409	2377332	1378	1
94	SH3BP5	SH3-domain binding protein 5 (BTK-associated)	1.429	4.663	2664209	9467	3
95	DOCK11	dedicator of cytokinesis 11	1.427	2.340	3988435	139818	X
96	LY9	lymphocyte antigen 9	1.426	2.340	2363248	4063	1
97	CD48	CD48 molecule	1.425	3.409	2440354	962	1
98	ZC3H6	zinc finger CCCH-type containing 6	1.425	0.000	2500722	376940	2
99	SNRPN	small nuclear ribonucleoprotein polypeptide N	1.424	1.220	3584728	6638	15
100	ATP8A1	ATPase, aminophospholipid transporter (APLT), class I, type 8A, member 1	1.423	1.220	2767378	10396	4
101	SRPX	sushi-repeat-containing protein, X-linked	1.422	4.663	4004853	8406	X
102	DDIT4	DNA-damage-inducible transcript 4	1.422	2.340	3251393	54541	10
103	LARP6	La ribonucleoprotein domain family, member 6	1.419	3.409	3631498	55323	15
104	FRMD4A	FERM domain containing 4A	1.417	3.409	3278401	55691	10
105	KCNA3	potassium voltage-gated channel, shaker-related subfamily, member 3	1.415	3.409	2427619	3738	1
106	CD38	CD38 molecule	1.415	2.340	2719656	952	4
107	RGS18	regulator of G-protein signaling 18	1.413	3.409	2372719	64407	1
108	AGTR1	angiotensin II receptor, type 1	1.412	4.663	2647015	185	3
109	ARHGAP15	Rho GTPase activating protein 15	1.411	3.409	2508611	55843	2

Genes upregulated after bevacizumab therapy (Prospective study)

S No	Gene Symbol	Gene Name	Fold Change	Q value	Transcript Cluster ID	Entrez Gene ID	Chromosome
110	CD53	CD53 molecule	1.411	0.000	2351572	963	1
111	SLAMF6	SLAM family member 6	1.410	1.220	2440258	114836	1
112	TRAF3IP3	TRAF3 interacting protein 3	1.406	1.220	2378121	80342	1
113	FUCA1	fucosidase, alpha-L- 1, tissue	1.405	3.409	2401643	2517	1
114	MS4A2	membrane-spanning 4-domains, subfamily A, member 2 (Fc fragment of IgE, high affinity I, receptor for; beta polypeptide)	1.403	1.220	3332276	2206	11
115	TMEM38B	transmembrane protein 38B	1.400	2.340	3183364	55151	9
116	DHRS9	dehydrogenase/reductase (SDR family) member 9	1.399	3.409	2514304	10170	2
117	BHMT2 /// BHMT	betaine--homocysteine S-methyltransferase 2 /// betaine--homocysteine S-methyltransferase	1.399	3.409	2817212	23743 /// 635	5
118	GAPT	GRB2-binding adaptor protein, transmembrane	1.397	3.409	2810764	202309	5
119	C5orf45 /// SQSTM1	chromosome 5 open reading frame 45 /// sequestosome 1	1.395	1.220	2890292	51149 /// 8878	5
120	NCF2	neutrophil cytosolic factor 2	1.393	2.340	2447414	4688	1
121	PTPRC	protein tyrosine phosphatase, receptor type, C	1.390	3.409	2373842	5788	1
122	CCDC84	coiled-coil domain containing 84	1.390	4.663	3351768	338657	11
123	RNASE6	ribonuclease, RNase A family, k6	1.389	2.340	3527662	6039	14
124	TRAV20 /// TRAC /// TRAJ17	T cell receptor alpha variable 20 /// T cell receptor alpha constant /// T cell receptor alpha joining 17	1.389	4.663	3528172	28663 /// 28755 /// 28738	14
125	MS4A4A	membrane-spanning 4-domains, subfamily A, member 4	1.388	3.409	3332298	51338	11
126	PRKCB	protein kinase C, beta	1.387	3.409	3653123	5579	16
127	CAMK4	calcium/calmodulin-dependent protein kinase IV	1.386	2.340	2823880	814	5
128	ARHGAP24	Rho GTPase activating protein 24	1.383	2.340	2734421	83478	4
129	ARRDC3	arrestin domain containing 3	1.382	4.663	2866704	57561	5
130	CD52	CD52 molecule	1.382	1.220	2326463	1043	1
131	RNASE1	ribonuclease, RNase A family, 1 (pancreatic)	1.382	2.340	3555675	6035	14
132	FAM133B /// BICC1 /// LOC728066 /// LOC728640	family with sequence similarity 133, member B /// bicaudal C homolog 1 (Drosophila) /// family with sequence similarity 133, member B pseudogene /// family with sequence similarity 133, member B pseudogene	1.380	3.409	3247818	257415 /// 80114 /// 728066 /// 728640	10
133	PLCL2	phospholipase C-like 2	1.380	2.340	2612813	23228	3
134	CLIP4	CAP-GLY domain containing linker protein family, member 4	1.378	2.340	2475407	79745	2
135	PILRA /// PILRB	paired immunoglobin-like type 2 receptor alpha /// paired immunoglobin-like type 2 receptor beta	1.378	2.340	3015519	29992 /// 29990	7
136	SETDB2	SET domain, bifurcated 2	1.377	4.663	3489418	83852	13
137	C9orf95	chromosome 9 open reading frame 95	1.374	1.220	3210179	54981	9
138	SNX2	sorting nexin 2	1.374	1.220	2826295	6643	5
139	TNFAIP8	tumor necrosis factor, alpha-induced protein 8	1.374	2.340	2825629	25816	5
140	SP140 /// SP140L	SP140 nuclear body protein /// SP140 nuclear body protein-like	1.373	2.340	2531233	11262 /// 93349	2
141	APBB1IP	amyloid beta (A4) precursor protein-binding, family B, member 1 interacting protein	1.372	4.663	3239760	54518	10
142	SELL	selectin L	1.372	3.409	2443450	6402	1
143	ENO2	enolase 2 (gamma, neuronal)	1.372	0.000	3403015	2026	12
144	NPL	N-acetylneuraminate pyruvate lyase (dihydrodipicolinate synthase)	1.371	4.663	2370926	80896	1
145	SMNDC1	survival motor neuron domain containing 1	1.371	2.340	3306519	10285	10
146	CCDC80	coiled-coil domain containing 80	1.370	3.409	2688813	151887	3
147	PLEKHH1 /// PIGH	pleckstrin homology domain containing, family H (with MyTH4 domain) member 1 /// phosphatidylinositol glycan anchor biosynthesis, class H	1.368	1.220	3569339	57475 /// 5283	14
148	IRS2	insulin receptor substrate 2	1.367	0.000	3525234	8660	13
149	EGLN3	egl nine homolog 3 (C. elegans)	1.366	2.340	3560403	112399	14
150	ADHFE1	alcohol dehydrogenase, iron containing, 1	1.365	1.220	3101629	137872	8
151	N4BP2L1	NEDD4 binding protein 2-like 1	1.365	3.409	3508644	90634	13
152	CD2	CD2 molecule	1.365	3.409	2353669	914	1
153	CEP110	centrosomal protein 110kDa	1.365	3.409	3187577	11064	9
154	GRAP2	GRB2-related adaptor protein 2	1.364	1.220	3946095	9402	22
155	BCL2	B-cell CLL/lymphoma 2	1.363	4.663	3811339	596	18
156	EID3	EP300 interacting inhibitor of differentiation 3	1.361	4.663	3429555	493861	12

Genes upregulated after bevacizumab therapy (Prospective study)

S No	Gene Symbol	Gene Name	Fold Change	Q value	Transcript Cluster ID	Entrez Gene ID	Chromosome
157	EWSR1 /// FLI1	Ewing sarcoma breakpoint region 1 /// Friend leukemia virus integration 1	1.358	4.663	3355733	2130 /// 2313	11
158	BTK	Bruton agammaglobulinemia tyrosine kinase	1.357	2.340	4015709	695	X
159	C7orf31	chromosome 7 open reading frame 31	1.357	1.220	3042012	136895	7
160	GGTA1	glycoprotein, alpha-galactosyltransferase 1 pseudogene	1.354	4.663	3223967	2681	9
161	ANKRD37 /// UFSP2	ankyrin repeat domain 37 /// UFM1-specific peptidase 2	1.353	0.000	2754673	353322 /// 55325	4
162	ZNF540	zinc finger protein 540	1.353	1.220	3831975	163255	19
163	PAG1	phosphoprotein associated with glycosphingolipid microdomains 1	1.352	0.000	3142217	55824	8
164	ABCA1	ATP-binding cassette, sub-family A (ABC1), member 1	1.352	1.220	3218528	19	9
165	LOC648740 /// AMY1A /// AMY1B /// AMY1C /// AMY2B /// AMY2A	actin, beta pseudogene /// amylase, alpha 1A (salivary) /// amylase, alpha 1B (salivary) /// amylase, alpha 1C (salivary) /// amylase, alpha 2B (pancreatic) /// amylase, alpha 2A (pancreatic)	1.351	1.220	2349402	648740 /// 276 /// 277 /// 278 /// 280 /// 279	1
166	KIAA1109	KIAA1109	1.351	4.663	2741901	84162	4
167	SLC18A2	solute carrier family 18 (vesicular monoamine), member 2	1.351	0.000	3266279	6571	10
168	ANGPTL1	angiopoietin-like 1	1.351	3.409	2445982	9068	1
169	TGFBR2	transforming growth factor, beta receptor II (70/80kDa)	1.349	4.663	2615360	7048	3
170	ANKRD44	ankyrin repeat domain 44	1.348	4.663	2593464	91526	2
171	PPWD1	peptidylprolyl isomerase domain and WD repeat containing 1	1.347	2.340	2812273	23398	5
172	IL1R1	interleukin 1 receptor, type I	1.346	3.409	2496962	3554	2
173	C1orf38	chromosome 1 open reading frame 38	1.345	3.409	2327283	9473	1
174	PYHIN1	pyrin and HIN domain family, member 1	1.344	2.340	2362351	149628	1
175	CD1C	CD1c molecule	1.343	3.409	2362201	911	1
176	TMEM220 /// MAGOH2	transmembrane protein 220 /// mago-nashi homolog 2, proliferation-associated (Drosophila)	1.342	3.409	3745525	388335 /// 548332	17
177	FAS /// STAMBPL1	Fas (TNF receptor superfamily, member 6) /// STAM binding protein-like 1	1.339	3.409	3257031	355 /// 57559	10
178	CD226	CD226 molecule	1.338	3.409	3812385	10666	18
179	SNHG12 /// SNORA61 /// SNORA16A /// SNORA44	small nucleolar RNA host gene 12 (non-protein coding) /// small nucleolar RNA, H/ACA box 61 /// small nucleolar RNA, H/ACA box 16A /// small nucleolar RNA, H/ACA box 44	1.338	2.340	2403557	85028 /// 677838 /// 692073 /// 677825	1
180	HESX1	HESX homeobox 1	1.336	2.340	2677902	8820	3
181	AGTPBP1	ATP/GTP binding protein 1	1.333	3.409	3212728	23287	9
182	HCLS1	hematopoietic cell-specific Lyn substrate 1	1.333	1.220	2691668	3059	3
183	CYTH4	cytohesin 4	1.330	2.340	3944690	27128	22
184	IL18RAP	interleukin 18 receptor accessory protein	1.330	3.409	2497161	8807	2
185	CYP1B1	cytochrome P450, family 1, subfamily B, polypeptide 1	1.329	2.340	2548699	1545	2
186	FOXN3	forkhead box N3	1.329	1.220	3575567	1112	14
187	LRRFIP1	leucine rich repeat (in FLII) interacting protein 1	1.328	1.220	2534456	9208	2
188	CELF2	CUGBP, Elav-like family member 2	1.328	4.663	3234760	10659	10
189	IL15	interleukin 15	1.327	4.663	2745288	3600	4
190	FIP1L1 /// PDGFRA	FIP1 like 1 (S. cerevisiae) /// platelet-derived growth factor receptor, alpha polypeptide	1.327	2.340	2727226	81608 /// 5156	4
191	NCOA7	nuclear receptor coactivator 7	1.327	4.663	2924514	135112	6
192	RASA2	RAS p21 protein activator 2	1.326	2.340	2645579	5922	3
193	MTMR10 /// FAN1	myotubularin related protein 10 /// FANCD2/FANCI-associated nuclease 1	1.325	3.409	3615985	54893 /// 22909	15
194	LYPLAL1	lysophospholipase-like 1	1.324	3.409	2380785	127018	1
195	LYRM7	Lyrm7 homolog (mouse)	1.324	3.409	2828135	90624	5
196	PLTP /// CTSA	phospholipid transfer protein /// cathepsin A	1.324	3.409	3907524	5360 /// 5476	20
197	ANAPC5	anaphase promoting complex subunit 5	1.324	3.409	3474937	51433	12
198	EPM2A	epilepsy, progressive myoclonus type 2A, Lafora disease (laforin)	1.323	1.220	2977949	7957	6
199	CD58	CD58 molecule	1.322	3.409	2429842	965	1
200	RPGR	retinitis pigmentosa GTPase regulator	1.322	3.409	4004878	6103	X
201	ALDH5A1	aldehyde dehydrogenase 5 family, member A1	1.322	4.663	2898499	7915	6
202	C6orf97	chromosome 6 open reading frame 97	1.321	4.663	2931700	80129	6
203	ABCG1	ATP-binding cassette, sub-family G (WHITE), member 1	1.320	0.000	3922444	9619	21

Genes upregulated after bevacizumab therapy (Prospective study)

S No	Gene Symbol	Gene Name	Fold Change	Q value	Transcript Cluster ID	Entrez Gene ID	Chromosome
204	C1GALT1	core 1 synthase, glycoprotein-N-acetylgalactosamine 3-beta-galactosyltransferase, 1	1.318	2.340	2989435	56913	7
205	ITGAL	integrin, alpha L (antigen CD11A (p180), lymphocyte function-associated antigen 1; alpha polypeptide)	1.318	1.220	3656223	3683	16
206	ZNF30	zinc finger protein 30	1.317	4.663	3829964	90075	19
207	PRELID2 /// GRXCR2	PRELI domain containing 2 /// glutaredoxin, cysteine rich 2	1.316	0.000	2879739	153768 /// 643226	5
208	FCRL3	Fc receptor-like 3	1.313	4.663	2439001	115352	1
209	ITK	IL2-inducible T-cell kinase	1.311	4.663	2837232	3702	5
210	PECI /// C6orf201 /// FNBP1L	peroxisomal D3,D2-enoyl-CoA isomerase /// chromosome 6 open reading frame 201 /// formin binding protein 1-like	1.309	3.409	2892800	10455 /// 404220 /// 54874	6
211	DOCK2 /// DOCK5	dedicator of cytokinesis 2 /// dedicator of cytokinesis 5	1.307	4.663	2840036	1794 /// 80005	5
212	RNASET2	ribonuclease T2	1.305	1.220	2984884	8635	6
213	RNF13	ring finger protein 13	1.302	1.220	2647458	11342	3
214	ANKRA2	ankyrin repeat, family A (RFXANK-like), 2	1.302	4.663	2862380	57763	5
215	MTERFD2	MTERF domain containing 2	1.302	4.663	2607020	130916	2
216	RHOH	ras homolog gene family, member H	1.301	2.340	2724671	399	4
217	CMAH	cytidine monophosphate-N-acetylneuraminic acid hydroxylase (CMP-N-acetylneuraminate monooxygenase) pseudogene	1.301	4.663	2945882	8418	6
218	GSTM2 /// GSTM4 /// GSTM1	glutathione S-transferase mu 2 (muscle) /// glutathione S-transferase mu 4 /// glutathione S-transferase mu 1	1.300	4.663	2350952	2946 /// 2948 /// 2944	1
219	WIPF1	WAS/WASL interacting protein family, member 1	1.299	4.663	2587841	7456	2
220	COQ10A	coenzyme Q10 homolog A (S. cerevisiae)	1.299	2.340	3417531	93058	12
221	TOX	thymocyte selection-associated high mobility group box	1.299	3.409	3136888	9760	8
222	AP1S2 /// LOC653653	adaptor-related protein complex 1, sigma 2 subunit /// adaptor-related protein complex 1, sigma 2 subunit pseudogene	1.298	2.340	4000704	8905 /// 653653	X
223	CNOT6L	CCR4-NOT transcription complex, subunit 6-like	1.298	1.220	2774565	246175	4
224	PRO1768	PRO1768	1.297	4.663	3548050	29018	14
225	EPB41L4A /// NCRNA00219 /// SNORA13	erythrocyte membrane protein band 4.1 like 4A /// non-protein coding RNA 219 /// small nucleolar RNA, H/ACA box 13	1.295	1.220	2824089	64097 /// 114915 /// 654322	5
226	CASP8	caspase 8, apoptosis-related cysteine peptidase	1.295	4.663	2522728	841	2
227	LOC100129195 /// ZSCAN16	hypothetical LOC100129195 /// zinc finger and SCAN domain containing 16	1.294	3.409	2900269	100129195 /// 80345	6
228	CAPRIN2	caprin family member 2	1.293	2.340	3449368	65981	12
229	PPP3CC	protein phosphatase 3, catalytic subunit, gamma isozyme	1.293	2.340	3089401	5533	8
230	ARHGAP30	Rho GTPase activating protein 30	1.293	0.000	2440549	257106	1
231	PIK3CG	phosphoinositide-3-kinase, catalytic, gamma polypeptide	1.293	4.663	3018309	5294	7
232	ZNF354C	zinc finger protein 354C	1.292	3.409	2843935	30832	5
233	C17orf48	chromosome 17 open reading frame 48	1.292	3.409	3710277	56985	17
234	RALGAPA1	Ral GTPase activating protein, alpha subunit 1 (catalytic)	1.291	4.663	3561110	253959	14
235	P2RY10	purinergic receptor P2Y, G-protein coupled, 10	1.290	3.409	3982560	27334	X
236	DNAJC19	DnaJ (Hsp40) homolog, subfamily C, member 19	1.289	4.663	2707359	131118	3
237	TRDMT1	tRNA aspartic acid methyltransferase 1	1.289	3.409	3279857	1787	10
238	ANTXR2	anthrax toxin receptor 2	1.288	3.409	2774971	118429	4
239	Mar-01	membrane-associated ring finger (C3HC4) 1	1.288	2.340	2792166	55016	4
240	RARRES2	retinoic acid receptor responder (tazarotene induced) 2	1.288	4.663	3079005	5919	7
241	BHLHE41	basic helix-loop-helix family, member e41	1.288	4.663	3448088	79365	12
242	AZI2	5-azacytidine induced 2	1.286	1.220	2667181	64343	3
243	HNRNPM	heterogeneous nuclear ribonucleoprotein M	1.286	4.663	3819584	4670	19
244	ZNF721 /// ABCA11P	zinc finger protein 721 /// ATP-binding cassette, sub-family A (ABC1), member 11 (pseudogene)	1.285	2.340	2756404	170960 /// 79963	4
245	CLEC2B	C-type lectin domain family 2, member B	1.284	4.663	3443891	9976	12
246	ZNF449	zinc finger protein 449	1.283	3.409	3991992	203523	X
247	RABGAP1L	RAB GTPase activating protein 1-like	1.282	2.340	2367963	9910	1
248	KDM3A	lysine (K)-specific demethylase 3A	1.282	1.220	2492064	55818	2
249	EVI2B	ecotropic viral integration site 2B	1.280	2.340	3752258	2124	17

Genes upregulated after bevacizumab therapy (Prospective study)

S No	Gene Symbol	Gene Name	Fold Change	Q value	Transcript Cluster ID	Entrez Gene ID	Chromosome
250	MAN1A1	mannosidase, alpha, class 1A, member 1	1.280	4.663	2971801	4121	6
251	BMP2K /// PAQR3	BMP2 inducible kinase /// progestin and adipoQ receptor family member III	1.279	2.340	2732942	55589 /// 152559	4
252	LPXN	leupaxin	1.278	3.409	3374402	9404	11
253	DHX36	DEAH (Asp-Glu-Ala-His) box polypeptide 36	1.277	4.663	2701595	170506	3
254	PNRC1	proline-rich nuclear receptor coactivator 1	1.273	1.220	2916716	10957	6
255	VEGFA	vascular endothelial growth factor A	1.272	3.409	2908179	7422	6
256	SP100	SP100 nuclear antigen	1.270	2.340	2531377	6672	2
257	SLC38A6	solute carrier family 38, member 6	1.269	4.663	3538789	145389	14
258	XRN1	5'-3' exoribonuclease 1	1.268	4.663	2698738	54464	3
259	ANG /// RNASE4	angiogenin, ribonuclease, RNase A family, 5 /// ribonuclease, RNase A family, 4	1.268	3.409	3527597	283 /// 6038	14
260	C14orf145	chromosome 14 open reading frame 145	1.267	4.663	3573994	145508	14
261	CHIC2	cysteine-rich hydrophobic domain 2	1.267	4.663	2769539	26511	4
262	TBRG1 /// SIAE	transforming growth factor beta regulator 1 /// sialic acid acetylesterase	1.267	3.409	3354174	84897 /// 54414	11
263	ZNF334 /// LOC100240726	zinc finger protein 334 /// makorin ring finger protein 1 pseudogene	1.266	2.340	3907934	55713 /// 100240726	20
264	ST3GAL5	ST3 beta-galactoside alpha-2,3-sialyltransferase 5	1.266	3.409	2562529	8869	2
265	CCDC53	coiled-coil domain containing 53	1.266	4.663	3468225	51019	12
266	KIAA0748	KIAA0748	1.265	4.663	3456955	9840	12
267	FCRL1	Fc receptor-like 1	1.264	4.663	2439101	115350	1
268	ZNF141	zinc finger protein 141	1.263	2.340	2713950	7700	4
269	IL10RA	interleukin 10 receptor, alpha	1.263	2.340	3351166	3587	11
270	ECHDC1	enoyl CoA hydratase domain containing 1	1.263	3.409	2973168	55862	6
271	ANKAR /// OSGEPL1	ankyrin and armadillo repeat containing /// O-sialoglycoprotein endopeptidase-like 1	1.262	3.409	2591906	150709 /// 64172	2
272	SEPT6	septin 6	1.262	2.340	4019486	23157	X
273	HSPBAP1	HSPB (heat shock 27kDa) associated protein 1	1.262	2.340	2692136	79663	3
274	ARL4C	ADP-ribosylation factor-like 4C	1.261	2.340	2604390	10123	2
275	SP140 /// SP140L	SP140 nuclear body protein /// SP140 nuclear body protein-like	1.261	3.409	2531310	11262 /// 93349	2
276	ELL	elongation factor RNA polymerase II	1.261	3.409	3855011	8178	19
277	TBC1D19	TBC1 domain family, member 19	1.260	4.663	2722291	55296	4
278	ALS2CR8	amyotrophic lateral sclerosis 2 (juvenile) chromosome region, candidate 8	1.260	1.220	2523419	79800	2
279	CD14	CD14 molecule	1.260	4.663	2878437	929	5
280	FTH1	ferritin, heavy polypeptide 1	1.260	2.340	3375648	2495	11
281	TBC1D8 /// RPL31	TBC1 domain family, member 8 (with GRAM domain) /// ribosomal protein L31	1.259	3.409	2496536	11138 /// 6160	2
282	MKLN1	muskelin 1, intracellular mediator containing kelch motifs	1.258	3.409	3024275	4289	7
283	NCK2	NCK adaptor protein 2	1.257	4.663	2498143	8440	2
284	CCNL1	cyclin L1	1.257	3.409	2702307	57018	3
285	LILRB4 /// LILRB5	leukocyte immunoglobulin-like receptor, subfamily B (with TM and ITIM domains), member 4 /// leukocyte immunoglobulin-like receptor, subfamily B (with TM and ITIM domains), member 5	1.256	1.220	3841621	11006 /// 10990	19
286	GATAD1	GATA zinc finger domain containing 1	1.256	4.663	3012633	57798	7
287	P2RY14	purinergic receptor P2Y, G-protein coupled, 14	1.254	4.663	2701033	9934	3
288	MBNL1	muscleblind-like (Drosophila)	1.254	2.340	2648141	4154	3
289	HLA-DOB /// TAP2	major histocompatibility complex, class II, DO beta /// transporter 2, ATP-binding cassette, sub-family B (MDR/TAP)	1.254	4.663	2950145	3112 /// 6891	6
290	GK /// CKS1B	glycerol kinase /// CDC28 protein kinase regulatory subunit 1B	1.253	4.663	3972929	2710 /// 1163	X
291	SMAP2	small ArfGAP2	1.252	3.409	2331857	64744	1
292	C1orf114	chromosome 1 open reading frame 114	1.252	4.663	2443305	57821	1
293	SPATA7	spermatogenesis associated 7	1.252	3.409	3547500	55812	14
294	NR1D2	nuclear receptor subfamily 1, group D, member 2	1.251	1.220	2614142	9975	3
295	CEP120 /// KRT8	centrosomal protein 120kDa /// keratin 8	1.251	1.220	2873168	153241 /// 3856	5
296	KPNA5	karyopherin alpha 5 (importin alpha 6)	1.251	3.409	2922840	3841	6
297	ZNF187	zinc finger protein 187	1.250	3.409	2900423	7741	6
298	ANGPTL4	angiopoietin-like 4	1.248	0.000	3819474	51129	19
299	TRMT11	tRNA methyltransferase 11 homolog (S. cerevisiae)	1.248	2.340	2924619	60487	6
300	C4orf3	chromosome 4 open reading frame 3	1.247	3.409	2783473	401152	4
301	CLK4	CDC-like kinase 4	1.246	4.663	2889698	57396	5
302	EBAG9	estrogen receptor binding site associated, antigen, 9	1.246	4.663	3111695	9166	8
303	CENPV	centromere protein V	1.246	2.340	3747199	201161	17
304	SP110	SP110 nuclear body protein	1.245	1.220	2603051	3431	2

Genes upregulated after bevacizumab therapy (Prospective study)

S No	Gene Symbol	Gene Name	Fold Change	Q value	Transcript Cluster ID	Entrez Gene ID	Chromosome
305	HBP1 /// LOC100506312 /// COG5	HMG-box transcription factor 1 /// hypothetical LOC100506312 /// component of oligomeric golgi complex 5	1.245	3.409	3018420	26959 /// 100506312 /// 10466	7
306	BOD1L	biorientation of chromosomes in cell division 1-like	1.244	3.409	2761321	259282	4
307	ZNF718	zinc finger protein 718	1.244	4.663	2713837	255403	4
308	C9orf156	chromosome 9 open reading frame 156	1.241	2.340	3216931	51531	9
309	DEF6	differentially expressed in FDCP 6 homolog (mouse)	1.241	3.409	2904563	50619	6
310	RAB20	RAB20, member RAS oncogene family	1.241	2.340	3525498	55647	13
311	RRAGB	Ras-related GTP binding B	1.240	3.409	3978819	10325	X
312	CXCR4	chemokine (C-X-C motif) receptor 4	1.240	3.409	2578028	7852	2
313	KLHL3	kelch-like 3 (Drosophila)	1.239	4.663	2877028	26249	5
314	C2orf64	chromosome 2 open reading frame 64	1.237	4.663	2566383	493753	2
315	C5orf53	chromosome 5 open reading frame 53	1.237	4.663	2831591	492311	5
316	USP33	ubiquitin specific peptidase 33	1.236	3.409	2419113	23032	1
317	ZNF624 /// SRSF6	zinc finger protein 624 /// serine/arginine-rich splicing factor 6	1.236	4.663	3747324	57547 /// 6431	17
318	EIF4G2 /// SNORD97	eukaryotic translation initiation factor 4 gamma, 2 /// small nucleolar RNA, C/D box 97	1.234	3.409	3362774	1982 /// 692223	11
319	ZNF224	zinc finger protein 224	1.233	1.220	3835418	7767	19
320	STK17B	serine/threonine kinase 17b	1.233	1.220	2593159	9262	2
321	LAX1	lymphocyte transmembrane adaptor 1	1.233	4.663	2375795	54900	1
322	FBXO11	F-box protein 11	1.233	3.409	2552153	80204	2
323	ORMDL1	ORM1-like 1 (S. cerevisiae)	1.230	2.340	2591942	94101	2
324	GPR183	G protein-coupled receptor 183	1.230	4.663	3522662	1880	13
325	RPS13	ribosomal protein S13	1.230	2.340	3364736	6207	11
326	RHOU	ras homolog gene family, member U	1.230	3.409	2384401	58480	1
327	NR2C1 /// FGD6	nuclear receptor subfamily 2, group C, member 1 /// FYVE, RhoGEF and PH domain containing 6	1.230	4.663	3466318	7181 /// 55785	12
328	OXNAD1	oxidoreductase NAD-binding domain containing 1	1.229	2.340	2612625	92106	3
329	PLAG1	pleiomorphic adenoma gene 1	1.229	2.340	3136178	5324	8
330	ZMYM6 /// LOC653160 /// LOC100130633	zinc finger, MYM-type 6 /// hypothetical LOC653160 /// hypothetical protein LOC100130633	1.228	3.409	2405992	9204 /// 653160 /// 100130633	1
331	CCL5	chemokine (C-C motif) ligand 5	1.228	2.340	3753860	6352	17
332	MYST2	MYST histone acetyltransferase 2	1.228	2.340	3725802	11143	17
333	REC8	REC8 homolog (yeast)	1.227	2.340	3529725	9985	14
334	SNX13	sorting nexin 13	1.226	4.663	3040073	23161	7
335	THEM4	thioesterase superfamily member 4	1.223	3.409	2435347	117145	1
336	ZNF395 /// FBXO16	zinc finger protein 395 /// F-box protein 16	1.222	3.409	3129304	55893 /// 157574	8
337	C7orf49	chromosome 7 open reading frame 49	1.221	4.663	3074101	78996	7
338	CCT6B	chaperonin containing TCP1, subunit 6B (zeta 2)	1.220	4.663	3753288	10693	17
339	CERK	ceramide kinase	1.220	3.409	3964154	64781	22
340	GAB1	GRB2-associated binding protein 1	1.217	4.663	2745547	2549	4
341	HNRNPK /// MIR7-1	heterogeneous nuclear ribonucleoprotein K /// microRNA 7-1	1.216	4.663	3212321	3190 /// 407043	9
342	PRKCH	protein kinase C, eta	1.216	3.409	3538893	5583	14
343	EIF5 /// SNORA28	eukaryotic translation initiation factor 5 /// small nucleolar RNA, H/ACA box 28	1.215	4.663	3553607	1983 /// 677811	14
344	ACSS1	acyl-CoA synthetase short-chain family member 1	1.215	4.663	3901696	84532	20
345	ALG13	asparagine-linked glycosylation 13 homolog (S. cerevisiae)	1.215	4.663	3987446	79868	X
346	DDX18	DEAD (Asp-Glu-Ala-Asp) box polypeptide 18	1.213	4.663	2502300	8886	2
347	C6orf162 /// C6orf164	chromosome 6 open reading frame 162 /// chromosome 6 open reading frame 164	1.212	3.409	2916246	57150 /// 63914	6
348	JMY	junction mediating and regulatory protein, p53 cofactor	1.212	4.663	2817291	133746	5
349	EIF2AK2	eukaryotic translation initiation factor 2-alpha kinase 2	1.210	3.409	2548402	5610	2
350	NSL1	NSL1, MIND kinetochore complex component, homolog (S. cerevisiae)	1.209	4.663	2454838	25936	1
351	LOC256021 /// BTG1	hypothetical protein LOC256021 /// B-cell translocation gene 1, anti-proliferative	1.209	3.409	3465409	256021 /// 694	12
352	CCDC93	coiled-coil domain containing 93	1.209	4.663	2572595	54520	2
353	EZH1	enhancer of zeste homolog 1 (Drosophila)	1.209	1.220	3758078	2145	17
354	ARMC8	armadillo repeat containing 8	1.209	4.663	2644461	25852	3
355	TXNIP	thioredoxin interacting protein	1.209	4.663	2356115	10628	1
356	TMOD1 /// TSTD2	tropomodulin 1 /// thiosulfate sulfurtransferase (rhodanese)-like domain containing 2	1.207	2.340	3216860	7111 /// 158427	9

Genes upregulated after bevacizumab therapy (Prospective study)

S No	Gene Symbol	Gene Name	Fold Change	Q value	Transcript Cluster ID	Entrez Gene ID	Chromosome
357	TPK1	thiamin pyrophosphokinase 1	1.207	4.663	3077766	27010	7
358	SEPT10	septin 10	1.206	4.663	2569908	151011	2
359	HNRPDL	heterogeneous nuclear ribonucleoprotein D-like	1.205	3.409	2775562	9987	4
360	NGLY1	N-glycanase 1	1.205	4.663	2666566	55768	3
361	HINT1	histidine triad nucleotide binding protein 1	1.205	4.663	2874688	3094	5
362	CBLB	Cas-Br-M (murine) ecotropic retroviral transforming sequence b	1.203	3.409	2687255	868	3
363	TEC	tec protein tyrosine kinase	1.203	4.663	2768396	7006	4
364	MLL	myeloid/lymphoid or mixed-lineage leukemia (trithorax homolog, Drosophila)	1.203	2.340	3351461	4297	11
365	BBX	bobby sox homolog (Drosophila)	1.202	4.663	2634965	56987	3
366	SECISBP2	SECIS binding protein 2	1.202	4.663	3178611	79048	9
367	NSMCE2	non-SMC element 2, MMS21 homolog (S. cerevisiae)	1.201	4.663	3114878	286053	8
368	SLC25A36	solute carrier family 25, member 36	1.198	3.409	2645275	55186	3
369	MSL3	male-specific lethal 3 homolog (Drosophila)	1.197	3.409	3968833	10943	X
370	MSH5 /// C6orf26	mutS homolog 5 (E. coli) /// chromosome 6 open reading frame 26	1.197	4.663	2902633	4439 /// 401251	6
371	KIAA1324L	KIAA1324-like	1.195	4.663	3059942	222223	7
372	SGK3 /// C8orf44	serum/glucocorticoid regulated kinase family, member 3 /// chromosome 8 open reading frame 44	1.194	4.663	3101765	23678 /// 56260	8
373	RPS3A	ribosomal protein S3A	1.194	3.409	3255509	6189	10
374	ZNF354A /// ZNF879 /// ZNF354B	zinc finger protein 354A /// zinc finger protein 879 /// zinc finger protein 354B	1.194	4.663	2843804	6940 /// 345462 /// 117608	5
375	CALCOCO1	calcium binding and coiled-coil domain 1	1.193	3.409	3456353	57658	12
376	ENY2	enhancer of yellow 2 homolog (Drosophila)	1.191	4.663	3111530	56943	8
377	ZNF880	zinc finger protein 880	1.188	4.663	3840194	400713	19
378	HK2	hexokinase 2	1.183	4.663	2489545	3099	2
379	PAPD4	PAP associated domain containing 4	1.181	4.663	2817386	167153	5
380	FNTA	farnesyltransferase, CAAX box, alpha	1.178	1.220	3096448	2339	8
381	CYP2R1	cytochrome P450, family 2, subfamily R, polypeptide 1	1.175	4.663	3364095	120227	11
382	AHSA2	AHA1, activator of heat shock 90kDa protein ATPase homolog 2 (yeast)	1.174	4.663	2484552	130872	2
383	CD37	CD37 molecule	1.171	2.340	3838385	951	19
384	CYTH1	cytohesin 1	1.170	4.663	3772525	9267	17
385	SLC2A5	solute carrier family 2 (facilitated glucose/fructose transporter), member 5	1.170	4.663	2395564	6518	1
386	USP53	ubiquitin specific peptidase 53	1.169	4.663	2741236	54532	4
387	MLL5	myeloid/lymphoid or mixed-lineage leukemia 5 (trithorax homolog, Drosophila)	1.168	1.220	3017547	55904	7
388	SIGLEC6	sialic acid binding Ig-like lectin 6	1.168	4.663	3869097	946	19
389	TNFAIP8L2	tumor necrosis factor, alpha-induced protein 8-like 2	1.167	3.409	2358736	79626	1
390	C22orf39 /// HIRA	chromosome 22 open reading frame 39 /// HIR histone cell cycle regulation defective homolog A (S. cerevisiae)	1.155	4.663	3952703	128977 /// 7290	22
391	ULK2	unc-51-like kinase 2 (C. elegans)	1.138	4.663	3749010	9706	17
392	RBPJ	recombination signal binding protein for immunoglobulin kappa J region	1.120	3.409	2722151	3516	4